University of Alberta
Department of Civil &
Environmental Engineering

Structural Engineering Report No. 67

Inelastic Analysis of Prestressed Concrete Secondary Containments

by

D.W. Murray

L. Chitnuyanondh

C. Wong

K.Y. Rijub-Agha

July, 1978

University of Alberta

Department of Civil Engineering

INELASTIC ANALYSIS OF PRESTRESSED CONCRETE SECONDARY CONTAINMENTS

by

D.W. Murray

L. Chitnuyanondh

C. Wong

and

K.Y. Rijub-Agha

A Technical Report to the
Atomic Energy Control Board
Nuclear Plant Licensing Directorate
P.O. Box 1046
Ottawa, Canada K1P 5S9

July 1978

Acknowledgements

The authors wish to acknowledge the cooperation of the following agencies which provided technical information and/or financial support for the overall study.

The Atomic Energy Control Board

Atomic Energy of Canada, Limited

Hydro-Québec

Canatom Limited

Ontario Hydro

Disclaimer

The interpretation of the technical data and any opinions or conclusions arising in this report are those of the authors only and do not necessarily reflect those of the cooperating agencies.

Note on Final Report

A preliminary version of this report, without the results of the computer runs on the U. of A. test structure, was provided to the Atomic Energy Control Board in December, 1977. The writing of this report spanned a period of 9 months during which improvements to analytical technique were continually being made and new experimental data was being accumulated. This process is not yet complete. Therefore, this report does not reflect the final state of development of concepts or comparisons to be expected from the project.

Abstract

This report develops an elastic-plastic constitutive model for the simulation of stress-strain response of concrete under any biaxial combination of compressive and/or tensile stresses. The predictions of the constitutive model are compared to the results of Kupfer, Hilsdorf and Rüsch (19). An effective tensile stress-strain curve is obtained indirectly from experimental results of a test on a large scale prestressed concrete wall segment. These concrete properties are then utilized in predicting the response of a second test and the results compared with the experiment.

Modifications to the BOSOR5 program, in order to incorporate the new constitutive relation into it, are described. Techniques of modelling structures in order to perform inelastic analysis of thin shell axisymmetric prestressed concrete secondary containments are investigated. The results of inelastic BOSOR5 analyses of two different models of the University of Alberta Test Structure are presented. The predicted deterioration of the structure and the limit states associated with its behavior are determined and discussed. It is concluded that the technique is a practical one which can be used for the inelastic analysis of Gentilly-type containment structures.

Table of Contents

List of Tables

List of Figures

Notation

Special Symbols

$\{\ \}$	=	a column vector
$<\ >$	=	a row vector
$[\ ]$	=	a matrix
$(\dot{})$	=	a total derivative with respect to time $(d/d\tau)$
$(\ )'$	=	a total derivative with respect to the independent variable
$(\bar{})$	=	an equivalent (strain) quantity
∂	=	partial differentiation symbol
Δ	=	an increment
d	=	ordinary differentiation symbol

Superscripts and Subscripts

1,2	=	subscripts indicating orthogonal directions or a sequence of points
c	=	subscript indicating "compression" or "concrete"
s	=	subscript indicating "steel"
T	=	superscript indicating "tangent"
E	=	superscript indicating "elastic"
eff	=	subscript indicating "effective"
P	=	superscript indicating "plastic"
+	=	superscript indicating evaluation for $\sigma_2 = 0^+$
-	=	superscript indicating evaluation for $\sigma_2 = 0^-$
o,0	=	superscript indicating "initial" value
u	=	superscript indicating "ultimate" value
	=	subscript indicating uniaxial

Roman Letter Symbols

A	=	function defined in Eq. 2.3.23c
A1, A2, A3	=	a sequence of subincrement stress points
A_c, A_s	=	area of concrete and steel, respectively
B	=	the magnitude of {B} (Eq. 2.2.12b)
{B}	=	the gradient vector of F (Eq. 2.2.12a)
B1, B2	=	components of {B}; a sequence of subincrement stress points
[C]	=	matrix relating $\{\varepsilon^P\}$ and $\{\varepsilon\}$ (Eq. 2.2.16)
C1, C2, C3	=	a sequence of subincrement stress points
C11, C12, C21, C22	=	elements of the matrix [C]
[D]	=	the linear elastic stiffness matrix (Eq. 2.2.15)
D1, D2, D3	=	a sequence of subincrement stress points
D11, D12, D21, D22	=	elements of the matrix [D]
$[D_{EP}]$	=	the elastic-plastic stiffness matrix (Eq. 2.2.17b)
DOT	=	the dot product $\langle \Delta\sigma \rangle$ {B}
E	=	the initial elastic modulus
E1, E2	=	a sequence of subincrement stress points
E_c	=	initial elastic modulus of concrete
E_s	=	initial elastic modulus of steel
E^T	=	a tangent modulus
F( )	=	the yield function
F_1, F_2, F_3	=	the value of F at points 1, 2 and 3
F^+, F^-	=	the function F for $\sigma_2 = 0^+$ and $\sigma_2 = 0^-$, respectively

$\langle \partial F/\partial \sigma \rangle$	=	the gradient of F ($= \langle \frac{\partial F}{\partial \sigma_1}, \frac{\partial F}{\partial \sigma_2} \rangle$)
f'_c	=	28 day compressive strength of 6 x 12 cylinder
f'_t	=	tensile strength by Brazilian concrete test
f''_t	=	maximum tensile strength in segment
g, g'	=	the compressive strain hardening function and its derivative, respectively
h, h'	=	the tensile strain hardening function and its derivative, respectively
I	=	the identity matrix
L	=	length of segment
M1, M_1	=	moment per unit width caused by stresses in direction 1
M2, M_2	=	moment per unit width caused by stresses in direction 2
$\{m\}$, m_1, m_2	=	a unit vector and its components
N1, N_1	=	membrane force in direction 1
N2, N_2	=	membrane force in direction 2
$\{n\}^+$, $\{n\}^-$	=	unit normals to F^+ and F^-, respectively
P	=	total axial load on segment
P_c	=	effective load carried by concrete
P_s	=	effective load carried by steel
p_c	=	nondimensionalized concrete load (P_c/P)
p_s	=	nondimensionalized steel load (P_s/P)
t	=	current time
X1, X2	=	generic notation for a sequence of subincrement stress points

Greek Letter Symbols

α	=	compression decomposition parameter (Eq. 2.2.6a)
β_1, β_2	=	tension decomposition parameters (Eqs. 2.2.6b, c)
γ	=	the determinant of [D] (Eq. 2.3.23d)
ε	=	strain
$\{\varepsilon\}$, ε_1, ε_2	=	the vector of total principal strains and its components
$\{\varepsilon^E\}$	=	the vector of elastic principal strains
$\{\varepsilon^P\}$	=	the vector of plastic principal strains
ε_s	=	steel strain
ε_i^P	=	break point plastic strains (Fig. 2.5a)
ε_u^P, ε_{u1}^P, ε_{u2}^P	=	uniaxial plastic strains (Fig. 2.5a)
$\bar{\varepsilon}^P$	=	the equivalent plastic strain (Eq. 2.2.5)
$\{\dot{\varepsilon}\}$	=	the vector of total principal strain rates
$\dot{\theta}$	=	a scalar constant (Eq. 2.2.10)
λ	=	compressive equivalent plastic strain (Eq. 2.2.8a)
μ	=	Bushnell's fraction to reach the yield curve
μ_1, μ_2	=	tensile equivalent plastic strains in directions 1 and 2 (eqs. 2.2.8b, c)
ν	=	elastic Poisson's ratio
$\{\sigma\}$, σ_1, σ_2	=	the vector of principal stresses and its components
σ_i	=	break point stresses (Fig. 2.5a)
σ_c	=	the current yield stress in compression
σ_c^o, σ_c^u	=	the initial and ultimate compressive yield stresses
σ_t^o, σ_t^u	=	the initial and ultimate tensile yield stresses
σ_{t1}, σ_{t2}	=	current tensile yield stresses in directions 1 and 2
τ	=	a time-like variable

1. Introduction

1.1 Background to Report

This report is the third technical report resulting from a continuing program of analytical development, sponsored by the Atomic Energy Control Board of Canada, to investigate the overpressure response of nuclear containment structures. The prototype building for the study is the Gentilly-2 Nuclear Power Station Reactor Building [4], which is considered to be representative of containment buildings to house 600 MW CANDU-PHW type nuclear reactors.

The first report in this series [12, 13], entitled 'An Elastic Stress Analysis of a Gentilly Type Containment Structure', contains a description of the prototype building and outlines the objectives of the overall study. The structural analyses of Refs. 12 and 13 were carried out employing the BOSOR4 computer code [8, 9]. This code is a versatile program, based on an energy finite-difference displacement model, which is generally available for use, and is specifically designed to handle complex problems in shells of revolution.

The second report in this series [25], entitled 'A Classical Flexibility Analysis for Gentilly Type Containment Structures', develops a simple classical shell analysis code which essentially confirms the results in Refs. 12 and 13. Unreported finite element studies of axi-symmetric behavior, carried out on SAP IV [6], also indicate that the results of Refs. 12 and 13 are substantially correct and form a reasonable basis on which to estimate first cracking pressures. Ref. 25 contains plots of these estimated cracking pressures.

In studying the response of containment structures to overpressures, 'first cracking' represents the initiation of significant nonlinear behavior. Determination of response beyond crack initiation requires nonlinear analysis. The present report describes some of the work currently underway at the University of Alberta with the ultimate objective of developing analytical capabilities for the prediction of nonlinear response of Gentilly type structures up to their collapse conditions. It will become apparent that the concept of crack initiation at a specific load level is an oversimplistic approach.

1.2 Methodology and Objective of Report

In attempting the nonlinear analysis of any structure it is necessary to make a number of decisions with respect to the analytical technique to be employed. The two most fundamental decisions are: (a) the basic mechanics for the analytical model and, (b) whether to adapt and employ an existing available computer code or whether to develop a new program. To some extent these decisions are interdependent.

At the time the decisions were made (early 1976) it was the opinion of the investigators that it would be less costly and time consuming to adapt an existing available computer code rather than to develop their own. The choice of available codes at that time was rather limited. MARC [3] was available on a proprietory basis. It would, therefore, be difficult to modify. NONSAP [5] was freely available but had less technical support. Both of these codes theoretically handle nonlinear finite element analysis for two-dimensional or three-dimensional structures. In addition, MARC had an axisymmetric thin-shell element and a particular form of reinforced concrete modelling. BOSOR5 [10, 11]

which is an extension of BOSOR4 to handle nonlinear metal plasticity and creep strains for axisymmetric shells, had recently become available.

It was the judgement of the investigators that two-dimensional (axisymmetric) or three-dimensional finite element nonlinear analyses of the entire structure would be excessively expensive. In view of the geometry of the structure it was their judgement that an axisymmetric thin shell approach would be adequate to determine fundamental response and that finite element studies could be confined to localized regions once the overall response had been determined.

The primary problem in the nonlinear analysis of concrete structures is adequate characterization of the material behavior. Hence, a fundamental aspect of the current investigation is to explore material characterizations of concrete which will allow adequate correlation of predictive analytical capability with experimental observations. In order to permit the maximum flexibility with respect to adjustment of the material characterization it was decided to opt for a nonproprietary code. The investigators selected BOSOR5 [10, 11] as the code which appeared to be most suitable for their purposes.

The BOSOR5 code is described briefly in Appendix A. The code was developed for the analysis of layered, thin shell, metallic structures and, as such, the nonlinear constitutive relationship was based on a von-Mises flow theory of metal plasticity. In order to adapt this code to the analysis of prestressed concrete structures it was necessary to develop an elastic-plastic flow theory characterization of concrete.

The objectives of this report are to describe the elastic-plastic flow theory characterization of concrete which has been developed; to illustrate the capability of this characterization to simulate the

behavior of prestressed concrete wall segment tests; to describe a technique for modelling Gentilly type structures; and to present BOSOR5 predictions of the nonlinear behavior of a prestressed concrete test structure which is currently under construction in the I.F. Morrison Structural Laboratory at the University of Alberta and will be tested sometime in the fall of 1978.

This report should be regarded as a progress report whose basic objective is to illustrate methodology and capability. In particular, it should be noted that the experimental program is not complete at the time of writing (the results of only three of 14 proposed wall segment tests are processed to obtain comparisons with the material characterization), and that consequently the material characterization is not yet complete. In addition, material characterizations other than elastic-plastic characterizations are under study and will be reported elsewhere.

1.3 Structure of Report

The report begins with a very brief rationale for the elastic-plastic constitutive modelling of concrete in Sect. 2.1. The fundamentals of the theory are presented in Sect. 2.2 and techniques of implementation are discussed in Sect. 2.3. Functional forms of failure and yield surfaces developed by the authors, and comparisons of BOSOR5 results, based on these assumed forms, with the data of Ref. 19 are presented in Sect. 2.4. Comparisons with wall segment tests carried out at the University of Alberta are contained in Sect. 2.5. The basis for the constitutive theory and verification against test observations are,

therefore, contained in Chapter 2.

Chapter 3 discusses problems associated with the analytical modelling of the laboratory test structure and examines the prediction of behavior of the test structure on the basis of the theory developed in Chapter 2. Experience with this first model indicated that an improved modelling technique could be employed and therefore a second model was developed. The results of this second analysis are presented in Chapter 4. The report concludes with a brief review in Chapter 5.

2. Development and Application of Constitutive Theory

2.1 Rationale for Constitutive Relationship

Overpressures in Gentilly type nuclear containments produce a situation in which a thin shell structure is subjected to internal pressure. The containment structure then becomes analagous to a thin shell pressure vessel in which the predominant effect is a state of membrane tension. Although compatibility moments are significant in the initial stages of loading, and will certainly be important in determining 'first cracking' conditions, the significance of such moments was expected to be much more subdued at later stages in the progression of the structure towards collapse. Significant leakage will probably occur only in those areas where the compressive stress block has effectively disappeared, and ultimate failure may occur in a purely tensile manner. (The possibilities of 'failure' associated with penetrations, and brittle behavior associated with shearing phenomena, are not considered herein). Thus, in order to predict the behavior of the structure up to the point of ultimate failure it is necessary to model the tensile response of thin (two-dimensional) prestressed structural segments, herein called 'wall segments'.

Accurate prediction of the behavior of wall segments in tension is a somewhat unusual structural engineering problem since concrete structures are normally intended to function primarily in compression and/or flexure. In structures where a steel liner is provided to ensure leak tightness, an estimation of ultimate strength and failure mode is all that is required. An estimate of ultimate

strength can be obtained by ignoring the tensile strength of the concrete or, at least, ignoring the tensile strength of the concrete after cracking ('tension cut-off' analysis).

For unlined concrete structures, or structures in which a plastic liner of limited ductility is installed, a tension cut-off analysis will probably yield an adequate estimate of ultimate strength but is likely to greatly overestimate the tensile strains and thus the leakage characteristics of the structure. This may lead to erroneous conclusions about a containment since it is possible that, because of leakage, an effective upper limit to the internal pressure may be developed prior to attaining structural collapse conditions. Since the integrity of the containment depends on the progression of failure in the concrete, it is desirable to have a reliable technique for the prediction of the response of wall segments subjected to tensile membrane forces. The technique should be adequate to predict the probable strains in the structure and assess the effects of these strains on the redistribution of forces and leakage characteristics.

A simple engineering approach to the prediction of the tensile behavior of a wall segment is illustrated in Table 2.1. (The properties are similar to those of Segment 1 which will be the subject of more extensive analysis in Sect. 2.5.4). The critical points computed in Table 2.1 are the basis of the segment load-strain plot in Fig. 2.1. Ignoring biaxial effects, assuming concrete has a tensile strength of 450 psi and that the prestressing steel is stressed to 153 ksi prior to external load application, the cracking load (P_{cr}), the yield load for the reinforcing steel (P_{sy}), and the ultimate load (P_{fy}) are computed in

Table 2.1 along with the associated strains. The behavior is computed for the simple material properties illustrated in the sketch in Table 2.1 and, although oversimplified, are adequate for the purposes of illustrating behavior.

The predicted response of the segment is plotted as the solid line in Fig. 2.1. The tension cut-off analysis predicts a strain of 0.31×10^{-3} at cracking (point a), at which time the concrete loses its capacity to resist stress so that all load is transferred to the steel and an abrupt increase in strain, to 1.60×10^{-3} (point b), occurs. Thereafter the stiffness of the section is that provided by the steel only, until the reinforcing yields (point c), after which only the stiffness of the prestressing tendons remain. The tendons yield at a load of 576 kips (point d) and extension occurs to failure.

The tension cut-off analysis predicts an abrupt increase in strains, by a factor of approximately 6, at the 'cracking load'. However, this extensibility is not observed in the laboratory and it is simple to demonstrate that such behavior should not be expected. A prismatic specimen, with a single reinforcing bar, subjected to an axial tension is illustrated in Fig. 2.2a. Equilibrium, from the free-body diagram of Fig. 2.2b, requires that

$$P = P_c + P_s \tag{2.1.1}$$

where the notation is as shown in Fig. 2.2b. Dividing by P, Eq. 2.1.1 may be expressed as

$$p_c + p_s = 1 \tag{2.1.2}$$

where p_c and p_s are the fraction of the total load carried by the concrete and steel, respectively, and are illustrated in Fig. 2.2c.

Assume now that a crack occurs at section A-A. Then p_c reduces to zero at this location. However bond stress is developed between the concrete and steel which prevents the effective stress in the concrete from reducing to zero along the entire length of the specimen. In fact the entire load is carried by the steel at the location of the crack only, and the strain associated with the maximum steel stress occurs only over a very short length of the bar. The shaded area in Fig. 2.2c indicates the distribution of the shift of load from concrete to steel that takes place upon the formation of the crack. The average strain in the specimen is

$$\varepsilon_{AVG} = \int_L \varepsilon_s \, dx/L << \frac{P}{A_s E_s} \tag{2.1.3}$$

where ε_s is the 'true' strain in the steel at any point and E_s is the modulus of elasticity of the steel.

The actual extensibility of the specimen may be simulated by defining an average steel stress which produces the average strain arising from Eq. 2.1.3. Thus an 'effective' load carried by the steel may be determined as

$$(P_s)_{eff} = E_s A_s \varepsilon_{AVG} \tag{2.1.4}$$

and the remainder of the load may be considered to be carried by the concrete. Therefore

$$(P_c)_{eff} = P - (P_s)_{eff} \tag{2.1.5}$$

which leads to the concept of an 'effective' stress in the concrete

$$(\sigma_c)_{eff} = (P_c)_{eff}/A_c \tag{2.1.6}$$

Alternatively, if it is possible to determine the relationship between the effective stress in the concrete and the average strain, the effective stress in the steel may be computed.

The concept of retaining an effective stiffness in the concrete is necessary if accurate predictions of deformations are to be made for membrane tension states in prestressed concrete wall segments. The effective stiffness of the concrete is reduced, of course, as more and more cracks form and ultimately the stiffening effect of the concrete disappears as the internal force becomes almost totally transferred to the steel. The effective stress-strain curve for concrete may, therefore, be expected to appear somewhat as shown in Fig. 2.2d where the declining portion is in part fictitious but leads to a reasonable prediction of overall strains as explained above. The result of this is that the behavior of the wall segment illustrated in Fig. 2.1 may be expected to resemble that shown by the dot-dash line rather than that indicated by the tension cut-off analysis.

The actual response of a wall segment is considerably more complex than that described in association with the simple model of Fig. 2.1. Cracks when initially formed may not penetrate through the section. Furthermore there is evidence to show [16] that the tensile stress-strain curve of unreinforced concrete also resembles that illus-

trated in Fig. 2.2d and that nonlinearities are due to the formation of microcracks throughout the medium. It is apparent that if one is to simulate such behavior, a nonlinear tensile response with a degrading stiffness is required. This may be simulated with a pseudo-elastic constitutive relationship but the investigators have chosen herein to attempt an elastic-plastic strain softening model because the BOSOR5 code, and other generally available computer codes, have the capability of treating a flow theory of plasticity.

The remainder of this chapter is associated with the derivation of a flow theory of plasticity adequate for the treatment of concrete in tension and with efforts to determine the shape of the tensile response curve (Fig. 2.2d) which will adequately predict wall segment behavior.

2.2 Fundamentals of Constitutive Theory

2.2.1 Introductory Remarks

The fundamental elements of a flow theory of plasticity are:

(a) the definition of a yield function in terms of current values of hardening parameters.

(b) the definition of a flow rule.

(c) the definition of a hardening rule.

The authors have previously published the derivation of a two-parameter theory for reinforced concrete which was developed under the sponsorship of this project [14, 15]. The derivation included herein is that for a three-parameter hardening theory.

The theory is purely a two-dimensional phenomenological theory. As such it does not maintain volume relationships and, when used with softening behavior, may violate thermodynamic principles. These facts do not perturb the investigators since they are primarily interested in the ability of the theory to simulate the observed macroscopic behavior of segments of structures. If the postulated relationships are capable of simulating adequately such behavior, this, in the opinion of the investigators, is sufficient justification for their use. On the other hand such an approach has the inherent disadvantage that, because of theoretical restrictions, it may not be sufficiently adaptable to obtain satisfactory correlation with test results. The only way of verifying the adequacy of such a theory is, therefore, to compare its predictions with test results. Since the theory is intended for use in an axisymmetric thin shell program, a two-dimensional principal stress-principal strain characterization is adequate.

2.2.2 Elements of Yield Function and Hardening Rule

It is a common practice to characterize biaxial 'failure' conditions of concrete by a plot in two-dimensional principal stress space [19] as shown symbolically by the outer curve in Fig. 2.3. The equation of this failure curve may be expressed as

$$F\ (\sigma_1,\ \sigma_2,\ \sigma_c^u,\ \sigma_t^u) = 0 \qquad (2.2.1)$$

where σ_c^u and σ_t^u are the maximum uniaxial compressive and tensile strengths (i.e. 'failure' strengths), respectively.

A failure curve is similar to a yield curve in the theory of plasticity and, if it is assumed that inelastic (i.e. plastic) behavior is initiated at some fraction of the uniaxial strengths, the failure function may be used to define an initial yield function in the form [7]

$$F\ (\sigma_1,\ \sigma_2,\ \sigma_c^\circ,\ \sigma_t^\circ) = 0 \qquad (2.2.2)$$

where σ_c° and σ_t° are the uniaxial stresses at which plastic strain is initiated in compression and tension, respectively. With this assumption the shape of the initial yield function is determined, as illustrated in Fig. 2.3, once a failure function is specified.

It is quite apparent that since concrete has a significantly different strength in tension than in compression, at least two strength parameters (σ_c and σ_t) are required to define the current yield curve (unless one assumes the parameters to be related).

In accordance with a plasticity theory it is assumed that total strains may be decomposed into elastic and plastic components. Thus, we may write

$$\{\varepsilon\} = \{\varepsilon^E\} + \{\varepsilon^P\} \tag{2.2.3}$$

where $\{\varepsilon^E\}$ represents the vector of principal components of elastic strain which are uniquely related to the stress state, while $\{\varepsilon^P\}$ represents the vector of accumulated principal components of plastic strain.

Epstein [14] introduced the assumption that plastic strains in compression have no influence on the tensile strength and vice versa. While this is not strictly true, it permits the formulation of a phenomenological model. It is further assumed herein that inelastic tensile strains in one principal direction have no influence on the tensile strength in the orthogonal direction. To describe this latter characterization it is necessary to introduce a minimum of three strength parameters, namely, σ_c, σ_{t1}, and σ_{t2}, which represent the current yield levels in biaxial stress space at any time, as illustrated by the dashed curve in Fig. 2.3.

Assume, therefore, that failure, initial yield, or subsequent yield conditions may be represented by the equation,

$$F(\sigma_1, \sigma_2, \sigma_c, \sigma_{t1}, \sigma_{t2}) = 0 \tag{2.2.4}$$

for the appropriate values of the parameters σ_c, σ_{t1} and σ_{t2}. Let the

strength parameters σ_c, σ_{t1} and σ_{t2} be related to the uniaxial stress-strain relationships, illustrated in Fig. 2.4, through equivalent plastic compressive and tensile strains. Define the total equivalent plastic strain $\bar{\varepsilon}^P$, in the normal manner, as

$$\bar{\varepsilon}^P = \int_0^t \langle \dot{\varepsilon}^P \rangle \{\dot{\varepsilon}^P\} \sqrt{d\,\tau} \tag{2.2.5}$$

where $\{\varepsilon^P\}$ is the (2 x 1) vector of principal plastic strains, τ is a time-like parameter, and $\cdot$ indicates differentiation with respect to τ. Assume the total equivalent plastic strain may now be decomposed into portions related to tensile and compressive strains. Thus, the equivalent compressive plastic strain rate $\dot{\lambda}$, and the equivalent tensile plastic strain rates $\dot{\mu}_1$ and $\dot{\mu}_2$ are introduced through the definition of

$$\dot{\lambda} = \alpha\, \dot{\bar{\varepsilon}}^P \tag{2.2.6a}$$

$$\dot{\mu}_1 = \beta_1\, \dot{\bar{\varepsilon}}^P \tag{2.2.6b}$$

$$\dot{\mu}_2 = \beta_2\, \dot{\bar{\varepsilon}}^P \tag{2.2.6c}$$

$$\alpha + \beta_1 + \beta_2 = 1 \tag{2.2.6d}$$

where α, β_1 and β_2 serve to decompose the total equivalent plastic strain rate into components related to compressive and tensile effects.

The parameters α, β_1 and β_2 which affect the decomposition are assumed to depend on the location of the stress point on the current yield curve. Thus, in the compression-compression (CC) zone ($\sigma_1 < 0$, $\sigma_2 < 0$)

$$\alpha = 1 \qquad \beta_1 = \beta_2 = 0; \tag{2.2.7a}$$

in the tension - tension (TT) zone ($\sigma_1 > 0$, $\sigma_2 > 0$)

$$\alpha = 0 \qquad \beta_1 + \beta_2 = 1; \tag{2.2.7b}$$

in the compression - tension (CT) zone ($\sigma_1 < 0$, $\sigma_2 > 0$)

$$\alpha + \beta_2 = 1 \qquad \beta_1 = 0; \tag{2.2.7c}$$

while in the tension-compression (TC) zone ($\sigma_1 > 0$, $\sigma_2 < 0$)

$$\alpha + \beta_1 = 1 \qquad \beta_2 = 0. \tag{2.2.7d}$$

In general, all the decomposition parameters are functions of σ_1, σ_2, σ_c, σ_{t1} and σ_{t2}. Their functional form varies from zone to zone, is somewhat arbitrary, and will be specified in Sect. 2.4. The precise form is not of concern at this point.

Defining now the components of equivalent plastic strains as the accumulation of their increments

$$\lambda = \int_0^t \dot{\lambda} \, d\tau \tag{2.2.8a}$$

$$\mu_1 = \int_0^t \dot{\mu}_1 \, d\tau \tag{2.2.8b}$$

$$\mu_2 = \int_0^t \dot{\mu}_2 \, d\tau \tag{2.2.8c}$$

the hardening rule may be stated as

$$\sigma_c = \sigma_c^o + g(\lambda) \tag{2.2.9a}$$

$$\sigma_{t1} = \sigma_{t1}^o + h(\mu_1) \tag{2.2.9b}$$

$$\sigma_{t2} = \sigma_{t2}^o + h(\mu_2) \tag{2.2.9c}$$

where $g(\lambda)$ and $h(\mu)$ are 'hardening functions' derived from the uniaxial compressive and tensile stress-strain curves, respectively.

In the following it is sometimes convenient to refer to increments in quantities rather than their rate of change. The authors will, rather arbitrarily, switch between the rate notation of this Section and the increment notation, as in Sect. 2.3.2, whenever either notation appears to have an advantage.

2.2.3 Equations of Flow Theory

The flow theory developed herein is based on the usual assumption for a work hardening material, i.e. - that plastic strains are normal to the current yield curve. Thus, we may write

$$\{\dot{\varepsilon}^P\} = \dot{\theta} \{\frac{\partial F}{\partial \sigma}\} \tag{2.2.10}$$

where $\dot{\theta}$ is a scalar multiplier. Substituting Eq. 2.2.10 into Eq. 2.2.5 allows the evaluation of $\dot{\theta}$, in terms of $\dot{\bar{\varepsilon}}^P$, as

$$\dot{\theta} = \dot{\bar{\varepsilon}}^P \Big/ \sqrt{\left\langle \frac{\partial F}{\partial \sigma} \right\rangle \left\{ \frac{\partial F}{\partial \sigma} \right\}} \tag{2.2.11}$$

For brevity, introduce the notation

$$\{B\} = \{\partial F/\partial \sigma\} \tag{2.2.12a}$$

and

$$B = \sqrt{\langle B \rangle \{B\}} \tag{2.2.12b}$$

so that Eq. 2.2.11 may be written as

$$\dot{\theta} = \dot{\bar{\varepsilon}}^P / B \tag{2.2.13}$$

Substituting Eq. 2.2.13 into Eq. 2.2.10 allows the flow rule to be expressed as

$$\{\dot{\varepsilon}^P\} = \{B\} \, \dot{\bar{\varepsilon}}^P / B \tag{2.2.14}$$

where it should be noted that $\{B\}/B$ defines a unit outward normal to the yield curve.

By virtue of Eq. 2.2.3 the stress rate may be written as

$$\{\dot{\sigma}\} = [D] \{\dot{\varepsilon} - \dot{\varepsilon}^P\} \tag{2.2.15}$$

where $\{\dot{\sigma}\}$ is the vector of principal stress rates and $[D]$ is the linear elastic constitutive relation.

For any iterative incremental finite element analysis it is desirable to express the plastic strain rate as

$$\{\dot{\varepsilon}^P\} = [C]\ \{\dot{\varepsilon}\} \tag{2.2.16}$$

so that Eq. 2.2.15 may be written as

$$\{\dot{\sigma}\} = [D_{EP}]\ \{\dot{\varepsilon}\} \tag{2.2.17a}$$

where the elastic-plastic constitutive matrix $[D_{EP}]$ is expressed as

$$[D_{EP}] = [D]\ [I - C] \tag{2.2.17b}$$

as can be deduced by a direct substitution of Eq. 2.2.16 into Eq. 2.2.15. Thus the primary problem in establishing the stress rate equations (Eqs. 2.2.17) is the determination of the [C] matrix. The subsequent derivation of this matrix follows the metal plasticity procedures of Marcal [22] and Bushnell [11].

For any plastic strain increment the stress point should remain on the updated yield curve. Thus, during 'loading' (i.e. - deformations involving plastic strains),

$$\dot{F} = 0 \tag{2.2.18}$$

Using Eq. 2.2.4

$$\dot{F} = \left\langle \frac{\partial F}{\partial \sigma} \right\rangle \{\dot{\sigma}\} + \frac{\partial F}{\partial \sigma_c}\dot{\sigma}_c + \frac{\partial F}{\partial \sigma_{t1}}\dot{\sigma}_{t1} + \frac{\partial F}{\partial \sigma_{t2}}\dot{\sigma}_{t2} \tag{2.2.19}$$

Evaluating $\{\dot{\sigma}\}$ from Eq. 2.2.15, $\{\dot{\varepsilon}^P\}$ from Eq. 2.2.14, $\dot{\sigma}_c$, $\dot{\sigma}_{t1}$, $\dot{\sigma}_{t2}$

from Eqs. 2.2.9, and $\dot{\lambda}$, $\dot{\mu}_1$, $\dot{\mu}_2$ from Eqs. 2.2.6, and using the definitions of Eqs. 2.2.12, Eq. 2.2.19 becomes

$$\langle B \rangle \left\{ [D] \{\dot{\varepsilon}\} - [D] \{B\} \dot{\bar{\varepsilon}}^P / B \right\} + \frac{\partial F}{\partial \sigma_c} g'(\lambda) \alpha \dot{\bar{\varepsilon}}^P \qquad (2.2.20)$$

$$+ \frac{\partial F}{\partial \sigma_{t1}} h'(\mu_1) \beta_1 \dot{\bar{\varepsilon}}^P + \frac{\partial F}{\partial \sigma_{t2}} h'(\mu_2) \beta_2 \dot{\bar{\varepsilon}}^P = 0$$

where g' and h' are total derivatives of the hardening functions of Eqs. 2.2.9. Solving for $\dot{\bar{\varepsilon}}^P$ yields

$$\dot{\bar{\varepsilon}}^P = \frac{\langle B \rangle [D]}{\frac{\langle B \rangle [D] \{B\}}{B} - \alpha g'(\lambda) \frac{\partial F}{\partial \sigma_c} - \beta_1 h'(\mu_1) \frac{\partial F}{\partial \sigma_{t1}} - \beta_2 h'(\mu_2) \frac{\partial F}{\partial \sigma_{t2}}} \{\dot{\varepsilon}\} \qquad (2.2.21)$$

Substituting Eq. 2.2.21 into Eq. 2.2.14 yields

$$\{\dot{\varepsilon}^P\} = \frac{\{B\} \langle B \rangle [D]}{\langle B \rangle [D] \{B\} - B\left(\alpha g'(\lambda) \frac{\partial F}{\partial \sigma_c} + \beta_1 h'(\mu_1) \frac{\partial F}{\partial \sigma_{t1}} + \beta_2 h'(\mu_2) \frac{\partial F}{\partial \sigma_{t2}}\right)} \{\dot{\varepsilon}\} \qquad (2.2.23)$$

which defines the matrix [C] of Eq. 2.2.16, and hence the $[D_{EP}]$ matrix of Eqs. 2.2.17, in terms of properties of the yield function and the hardening rules.

The equations of the constitutive theory have now been determined. However a number of aspects of the technique of implementing the theory for problem solution remain to be considered. Some of these are

discussed in the following section. However, it is recommended that the reader who is not interested in the details of computer implementation of the theory go directly to Sect. 2.4.

2.3 Techniques of Implementation*

2.3.1 Determination of Hardening Parameters

In the material representations used herein the uniaxial stress-strain curves, which give rise to the hardening functions $g(\lambda)$ and $h(\mu)$ of Eqs. 2.2.9, were approximated by linear segments.

Consider now, for example, the approximation of the uniaxial compressive curve illustrated in Fig. 2.5a. It is assumed that this curve is generated by a stress history in biaxial stress space as shown by the arrowed line in Fig. 2.5b, for which, from Eq. 2.2.7a, $\alpha = 1$, and Eq. 2.2.6a becomes

$$\dot{\lambda} = \dot{\varepsilon}^P_u \tag{2.3.1}$$

where the subscript u indicates uniaxial response.

From Eq. 2.2.14 the ratio of components of plastic strain is

$$\dot{\varepsilon}^P_{u2} = \frac{B2}{B1}\,\dot{\varepsilon}^P_{u1} \tag{2.3.2}$$

Differentiating Eq. 2.2.5 and evaluating $\dot{\varepsilon}^P_u$ by using the components of Eq. 2.3.2, yields

$$\dot{\lambda} = \dot{\varepsilon}^P_u = \sqrt{(\dot{\varepsilon}^P_{u1})^2 + (\dot{\varepsilon}^P_{u2})^2} = B\,|\dot{\varepsilon}^P_{u1}/B1| \tag{2.3.3}$$

---

* It is recommended that Sect. 2.3 be read only by those concerned with the details of computer implementation of the theory.

If the ratio of B1 to B2 remains constant for the stress path of Fig. 2.5b (which is the case for all F used herein), Eq. 2.3.3 can be integrated to yield

$$\lambda = B|\varepsilon^P_{ul}/B1| \tag{2.3.4}$$

Thus, given any value of λ, the corresponding value of the equivalent uniaxial plastic strain ε^P_{ul} can be determined and vice versa.

Given the value of the equivalent uniaxial plastic strain, ε^P_{ul}, the current strength parameter σ_c may be determined from the uniaxial stress strain curve as

$$\sigma_c = \sigma_i + \frac{(\sigma_{i+1} - \sigma_i)}{(\varepsilon^P_{i+1} - \varepsilon^P_i)} (\varepsilon^P_{ul} - \varepsilon^P_i) \tag{2.3.5}$$

where the notation is defined in Fig. 2.5a. Thus the hardening function itself does not have to be explicitly determined.

For the matrix [C] of Eq. 2.2.16, the derivatives of the hardening functions are required as indicated by Eq. 2.2.23. Now

$$\frac{d\,\sigma}{d\,\varepsilon^P_{ul}} = \frac{d\,\sigma}{d\,\varepsilon} \frac{d\,\varepsilon}{d\,\varepsilon^P_{ul}} = E_T \frac{d\,\varepsilon}{d\,\varepsilon^P_{ul}} \tag{2.3.6a}$$

where the tangent stiffness, E_T, is indicated in Fig. 2.5a. But, from the 'detail' in Fig. 2.5a,

$$\Delta\sigma = E_T \Delta\varepsilon = E \Delta\varepsilon^E = E(\Delta\varepsilon - \Delta\varepsilon^P_{ul}) \tag{2.3.6b}$$

or

$$\frac{\Delta \varepsilon}{\Delta \varepsilon^P_{ul}} = \frac{E}{E - E_T} \tag{2.3.6c}$$

Substituting Eq. 2.3.6c into Eq. 2.3.6a yields

$$\frac{d \sigma}{d \varepsilon^P_{ul}} = \frac{E_T E}{E-E_T} \tag{2.3.6d}$$

Now from Eq. 2.2.9a

$$g' = \frac{d \sigma}{d \lambda} = \frac{d \sigma}{d \varepsilon^P_{ul}} \frac{d \varepsilon^P_{ul}}{d \lambda} \tag{2.3.6e}$$

which, from Eqs. 2.3.6d and 2.3.4 yields

$$g' = \frac{E_T E}{E - E_T} \cdot |Bl/B| \tag{2.3.7}$$

Thus, given any accumulated λ, this is uniquely related to ε^P_{ul} by Eq. 2.3.4, the value σ_c may be found from the uniaxial curve by Eq. 2.3.5 and the value of g' from Eq. 2.3.7. The treatment of tensile hardening functions is identical to that described above for compressive hardening. Note that the technique is also applicable to strain softening.

2.3.2 The Subincrement Technique

BOSOR5 uses a subincrement technique to determine the stress increment associated with any strain increment which involves plastic

strains [11]. The procedure is illustrated schematically in Fig. 2.6 and may be described as follows.

Assume, for example, that the stress point prior to a strain increment is denoted symbolically by X1 while the stress point after the strain increment, evaluated by assuming linear elastic response, is denoted by X2, where X indicates the example designation. This second point may be referred to as a 'fictitious elastic point'. Fig. 2.6a illustrates five examples designated as A, B, C, D, and E. It should be noted that for points on the yield curve, $F = 0$; for points inside the yield curve, $F < 0$; and, for points outside the yield curve, $F > 0$; where F denotes the value of the yield function specified by the left hand side of Eq. 2.2.4.

For cases A and B, of Fig. 2.6, stress points A2 and B2 fall within the current yield curve indicating elastic response. Therefore

$$\{\Delta\sigma\} = [D]\ \{\Delta\varepsilon\} \tag{2.3.8a}$$

and

$$\{\sigma\}_2 = \{\sigma\}_1 + \{\Delta\sigma\} \tag{2.3.8b}$$

The matrix [D] is the elastic stiffness matrix, as in Eq. 2.2.15. The fact that the stresses $\{\sigma\}_2$ have been computed correctly is verified by evaluating

$$F_2 = F\ (<\sigma>_2,\ \sigma_c,\ \sigma_{t1},\ \sigma_{t2}) \tag{2.3.8c}$$

and noting that

$$F_2 < 0 \tag{2.3.9}$$

Consider now case C for which point C1 lies on the current yield curve. Upon evaluating F_2, using Eqs. 2.3.8,

$$F_2 > 0 \tag{2.3.10}$$

which is not permissible by the flow theory of Sect. 2.2.3. Since Eq. 2.3.10 indicates plastic 'loading', the matrix [C] of Eq. 2.2.16 may be evaluated at stress point C1 and the plastic components of the strain increment evaluated by Eq. 2.2.16. This effectively decomposes the strain increment into plastic components normal to the yield curve (i.e. - parallel to direction n of Fig. 2.6a) and a residual elastic strain increment which may be expressed as

$$\{\Delta\varepsilon^E\} = \{\Delta\varepsilon\} - \{\Delta\varepsilon^P\} \tag{2.3.11}$$

and which may be substituted, in place of $\{\Delta\varepsilon\}$, into Eq. 2.3.8a to evaluate $\{\Delta\sigma\}$. The 'correct' stress associated with the strain increment may now be evaluated, by employing this new estimate of $\{\Delta\sigma\}$, as

$$\{\sigma\}_3 = \{\sigma\}_1 + \{\Delta\sigma\} \tag{2.3.12}$$

and is indicated as point C3 on Fig. 2.6a. Alternatively, $\{\Delta\sigma\}$ for Eq. 2.3.12 can be evaluated directly from Eqs. 2.2.17. This 'correct' stress point C3 now differs, of course, from the fictitious elastic point C2.

The value of $\{\Delta\varepsilon^P\}$ obtained from Eq. 2.2.16 is now used to evaluated $\Delta\bar{\varepsilon}^P$ from the definition (Eq. 2.2.5) or, alternatively, $\Delta\bar{\varepsilon}^P$ may be evaluated directly from Eq. 2.2.21. Values of $\Delta\lambda$, $\Delta\mu_1$, and $\Delta\mu_2$ may then be determined from Eqs. 2.2.6 and new values of σ_c, σ_{t1}, and σ_{t2} are obtained from the incremental form of Eqs. 2.2.9, namely

$$\sigma_c\ (C3) = \sigma_c\ (C1) + g'\ \Delta\lambda \tag{2.3.13a}$$

$$\sigma_{t1}\ (C3) = \sigma_{t1}\ (C1) + h'\ \Delta\mu_1 \tag{2.3.13b}$$

$$\sigma_{t2}\ (C3) = \sigma_{t2}\ (C1) + h'\ \Delta\mu_2 \tag{2.3.13c}$$

Ignoring second order effects, evaluation of F at point C3 with the updated values of σ_c, σ_{t1} and σ_{t2} from Eqs. 2.3.13 should now result in

$$F_3 = 0 \tag{2.3.14}$$

That is, the current yield curve has been updated to pass through the new stress point, as indicated in Fig. 2.6a.

If the strain increment is large the linearization implied in the above procedure results in a drift of the stress point off the updated yield curve. To obtain a better approximation, the total strain increment may be divided into two equal subincrements as illustrated in Fig. 2.6b. Following the procedure of the previous paragraph point C3 may be located for one half the total strain increment. Using the values at point C3 the procedure may now be repeated for the remainder

of the strain increment to arrive at point C4 of Fig. 2.6b which, in general, will differ from point C3 of Fig. 2.6a. Bushnell implemented this subdivision of the total strain increment, calling it the "subincrement" procedure, by dividing the total strain increment into a rather arbitrary number of small subincrements [11]. However, this procedure does not guarantee that the final stress point would not change if a different number of subincrements were chosen. Therefore, the procedure initially implemented herein was to continue to double the number of subincrements, solving for a new final stress point each time, until the change in the final stress point between any two successive solutions was less than a specified small tolerance. This modification to the subincrement procedure has been described by Epstein and Murray [14]. This version of the procedure was eventually abandoned, however, because of numerical instabilities that arose when only a small number of subincrements were used. A more precise description of the final subincrement technique that was eventually adopted is discussed in Appendix B.

Consider now case D of Fig. 2.6a. Examining point D2, determined by Eqs. 2.3.8, yields the condition of Eq. 2.3.10 which implies that plastic strains must be considered. However, since $F_1 < 0$ Eqs. 2.3.8 should be applied to the initial portion of the strain increment to bring the stress point to the yield curve at point D3. Let μ be the fraction of the total strain increment required to arrive at point D3 on the yield line. The value of μ has been determined iteratively by solving the equation

$$F_3 = F(\langle\sigma\rangle_1 + \mu\langle\Delta\sigma\rangle, \sigma_c, \sigma_{t1}, \sigma_{t2}) = 0 \qquad (2.3.15)$$

using an interval halving technique to find the root of Eq. 2.3.15. (A complication associated with this procedure is mentioned briefly later in this Section). When the value of μ has been obtained which places the stress point on the yield curve the subincrement technique, as described in the last paragraph, is then applied to the strain increment $(1 - \mu)\{\Delta\varepsilon\}$ to determine an accurate solution for point D4 and the associated values of σ_c, σ_{t1} and σ_{t2}.

A variation of this procedure must be introduced if the elastic stress points are as indicated by points E1 and E2 of Fig. 2.6a. In this case since $F_1 = 0$ and $F_2 > 0$ the condition is transparently the same as case C discussed above. To detect such a condition when it occurs an additional check was used which evaluates the dot product of $\{\Delta\sigma\}$, evaluated by Eq. 2.3.8a, and the $\{B\}$ vector of Eq. 2.2.12a. Defining

$$DOT = \langle\Delta\sigma\rangle \{B\} \qquad (2.3.16)$$

a 'loading' condition requires that $DOT > 0$. If $DOT < 0$ and $F_2 > 0$ the μ factor discussed above is determined iteratively by working backward from point E2 and the subincrement technique is then applied from E3 to E4.

Since the direction of $\{B\}$ will change as the yield curve is updated from one subincrement to another, the sign of DOT is checked at the beginning of every subincrement. If, at any stage, DOT becomes negative, elastic response is used for that subincrement.

The subincrement procedure is further complicated by the fact that one of the breaks in the slope of the curve, as shown in Fig. 2.5a, may be contained between the equivalent uniaxial strains at the ends of any particular subincrement. In this case, the subincrement strain may be divided into two portions: that required to reach the break in the curve, and the remainder. For the former portion, the [C] and $[D_{EP}]$ matrices of Eqs. 2.2.16 and 2.2.17 may be evaluated at the initial point of the subincrement, while for the latter portion they may be evaluated immediately beyond the break. Since some plastic strain increments involve two hardening parameters, and a break in each curve may occur, the possibility of dividing the subincrement strains into more than two portions must also be included in the coding.

An additional problem that arises in the actual application of the method is that, for complex yield functions, false roots may appear on the stress plane at locations remote from the yield curve. Therefore the condition that $F_2 < 0$ does not guarantee that point 2 is within the yield line. The final strategy that was adopted for implementing the subincrement procedure is discussed in Appendix B.

2.3.3 Treatment of Corners

The yield function F used herein is expressed by different analytical forms in different regions of biaxial stress space. Specific forms will be discussed in Sect. 2.4. However, at the junction between two analytic forms, such as occurs at point C_o of Fig. 2.5b, there may be a discontinuity in the direction of the normal to the yield curve as the stress point progresses along the yield curve through the junction. Such

junction points are called 'corners' and present special problems. The general problem of a corner at an arbitrary point in stress space requires an assumption as to the translation of the corner during hardening. To avoid this, all corners considered herein will be located on the stress space coordinate axes, thereby simplifying the analysis. A description of the treatment of corners follows. A less detailed description has been given by Epstein and Murray in Ref. 14.

Consider the corner illustrated in Fig. 2.7a. Denote the yield function in the region $\sigma_2 > 0$ as F^+ and the yield function in the region $\sigma_2 < 0$ as F^-. Let n^+ and n^- be the associated normals at the corner C1. Similarly, two sets of quantities, denoted by + and - superscripts, will exist for all properties at point C1. The direction of plastic strains is, therefore, not uniquely defined at the corner. Assume the plastic strains occur in the direction of a unit vector $\{m\}$ which lies somewhere between the two limiting normals of $\{n\}^+$ and $\{n\}^-$. Assume α, β_1 and β_2 are continuous at any corner (Eqs. 2.2.7). Then, for the corner illustrated, $\alpha = 1$, $\beta_1 = 0$, $\beta_2 = 0$, and, from Eqs. 2.2.6,

$$\dot{\bar{\varepsilon}}^P = \dot{\lambda} \tag{2.3.17}$$

From Eqs. 2.2.14 and 2.2.15, for any orientation of $\{m\}$,

$$\{\dot{\sigma}\} = [D] \left\{ \{\dot{\varepsilon}\} - \dot{\lambda}\{m\} \right\} \tag{2.3.18}$$

where the unit vector {m} has now replaced the {n} vector which is expressed in Eq. 2.2.14 as {B}/B. Also, during the plastic strain increment Eq. 2.2.18 must be satisfied and Eq. 2.2.19 becomes

$$\langle B \rangle \{\dot{\sigma}\} + \frac{\partial F}{\partial \sigma_c} g' \dot{\lambda} = 0 \tag{2.3.19}$$

Eq. 2.3.19 can be satisfied for the vector <B>, and the $\partial F/\partial \sigma_c$, associated with either the F^+ or F^- functions.

Solving Eq. 2.3.19 for $\dot{\lambda}$ and substituting into Eq. 2.3.18 yields

$$\{\dot{\sigma}\} = [D] \{\dot{\varepsilon}\} + \frac{[D] \{m\} \langle B \rangle \{\dot{\sigma}\}}{\frac{\partial F}{\partial \sigma_c} g'} \tag{2.3.20}$$

or

$$\left[I - \frac{[D] \{m\} \langle B \rangle}{\frac{\partial F}{\partial \sigma_c} g'} \right] \{\dot{\sigma}\} = [D] \{\dot{\varepsilon}\} \tag{2.3.21}$$

Solving for $\{\dot{\sigma}\}$ yields

$$\{\dot{\sigma}\} = \left[I - \frac{[D] \{m\} \langle B \rangle}{\frac{\partial F}{\partial \sigma_c} g'} \right]^{-1} [D] \{\dot{\varepsilon}\} \tag{2.3.22}$$

Solution for the components of $\{\dot{\sigma}\}$ yields

$$\dot{\sigma}_1 = [-g' \, \partial F/\partial \sigma_c \, (D_{11} \dot{\varepsilon}_1 + D_{12} \dot{\varepsilon}_2) + \gamma B_2 (m_2 \dot{\varepsilon}_1 - m_1 \dot{\varepsilon}_2)]/A \tag{2.3.23a}$$

$$\dot{\sigma}_2 = [-g' \, \partial F/\partial \sigma_c \, (D_{21} \, \dot{\varepsilon}_1 + D_{22} \, \dot{\varepsilon}_2) + \gamma \, B_1 \, (-m_2 \, \dot{\varepsilon}_1 + m_1 \, \dot{\varepsilon}_2)]/A \qquad (2.3.23b)$$

where

$$A = -g' \, \frac{\partial F}{\partial \sigma_c} + B_1 \, (m_1 \, D_{11} + m_2 \, D_{12}) + B_2 \, (m_1 \, D_{21} + m_2 \, D_{22}) \qquad (2.3.23c)$$

and

$$\gamma = D_{11} \, D_{22} - D_{21} \, D_{12} = |D| \qquad (2.3.23d)$$

Eqs. 2.3.23 determine the components of $\{\dot{\sigma}\}$ for an arbitrary direction $\{m\}$ of plastic strain, and the function characteristics $\{B\}$ and $\partial F/\partial \sigma_c$ may be associated with either branch of the yield function. It is now possible to examine the limiting cases: (a) let $\{m\} = \{n\}^+$ and use the yield function characteristics associated with F^+; (b) let $\{m\} = \{n\}^-$ and use the yield function characteristics associated with F^-. Solving Eq. 2.3.23b for each of these cases yields four possible combinations of the signs of $\dot{\sigma}_2$. These combinations are shown in Fig. 2.6b. If the sign combinations are as in columns 1 and 2 the sign of $\dot{\sigma}_2$ immediately indicates which yield function should be applied. However, if the limiting conditions produce $\dot{\sigma}_2$'s of opposite sign then there must exist an $\{m\}$, between $\{n\}^+$ and $\{n\}^-$, such that $\dot{\sigma}_2 = 0$. That is, there must exist an $\{m\}$ such that the stress point will remain at the corner, which moves along the axis to point C2 of Fig. 2.7a. The components of $\{m\}$ for which this is true may be determined by solving for $\{m\}$ from Eq. 2.3.23b with $\dot{\sigma}_2 = 0$, and adding the additional condition

$$m_1^2 + m_2^2 = 1 \qquad (2.3.24)$$

to make the magnitude of the vector unity.

Thus, if the two limiting cases do not give a consistent indication of which way the stress point will move the direction of plastic strain at a corner is chosen such that the stress point stays at the corner and the corner translates along the axis. In this case it can be shown that it is immaterial which function characteristics are used.

If the corners of the yield function remain on the stress axes, the above logic can be applied to all corners with minor modifications.

2.4 Yield Function Forms and Comparison with Material Tests

The investigators have carried out a number of numerical experiments with various forms of failure functions in order to attempt to determine which forms give satisfactory correlation with test results.

Reliable testing for concrete response under multiaxial stress conditions is a very difficult task. One of the classic papers on biaxial testing is that of Kupfer, Hilsdorf and Rüsch [19] and these results (referred to hereafter as the KHR results) form the standard against which the current theory has been tested. The KHR failure envelope is similar to that shown in Fig. 2.3. No analytic form was given in Ref. 19 to approximate this envelope, although such forms have since been suggested (see, for example, [20]). It was pointed out in Sect. 2.3.2 that a failure envelope may be used to construct a yield surface by replacing the ultimate strength parameters with their corresponding initial yield values. To the authors' knowledge this approach was first used by Buyukozturk [7] and is the approach adopted herein.

Some of the functional forms used by the investigators in an attempt to simulate concrete response are illustrated in Fig. 2.8 and the analytical expressions associated with these forms are summarized in Tables 2.2, 2.3 and 2.4. The four forms are designated as Forms 1, 2, 3 and 4. A breakdown of the types of functions associated with the forms is given in Fig. 2.8 and it is of interest to trace their evolutionary development.

Form 1 is a two parameter form which was used to test the fundamental concept of decomposition of equivalent plastic strains into tensile and compressive portions. The feasibility of producing results

by incorporating this form into BOSOR5 was checked and it was demonstrated that meaningful problems could be solved in this fashion [14]. At this stage no attempt was made to check experimental observations.

Having demonstrated the feasibility of the approach an attempt was made to determine whether the functions could be adjusted to produce results reasonably consistent with observed material response. This resulted in the two-parameter Form 2. It was arrived at by trial through the following process.

The KHR failure envelope is shown in Fig. 2.9. The Form 2 curve of Table 2.2, with σ_c and σ_t corresponding to the KHR 'failure' values, is also shown in Fig. 2.9. It is now necessary to define the uniaxial compressive and tensile response. First yield from the uniaxial curves will define the σ_c and σ_t values which induce the initial yield curve shown on Fig. 2.9. The uniaxial compressive response from the KHR data is shown in Fig. 2.10 as curve A. For input of material properties this curve has been approximated by five linear segments as shown, the first break in the curve (and hence initial compressive yield) occurring at $0.3\ \sigma_c$. The uniaxial tensile response from the KHR data is shown as curve A of Fig. 2.11, and was approximated by two linear segments plus a decaying branch as shown in Fig. 2.12. The initial break in the curve (and hence initial tensile yield) occurs at $0.04\ f'_c$. The input of the three components, namely, the initial yield function, the uniaxial compressive curve, and the uniaxial tensile curve, serves to define the material properties from which the present theory attempts to predict the behavior for any stress path in biaxial stress space.

A comparison of predicted biaxial response for the Form 2 model with KHR measurements at various constant stress ratios is shown

in Figs. 2.10, 2.11 and 2.13. It should be noted that the theory predicts strains in both directions although only uniaxial strains are input. Comparison of the predicted strains with the KHR strains in the CC zone is shown in Fig. 2.10 for three different stress ratios. In this zone, it is apparent that the predicted response is somewhat stiffer than the KHR observations. The comparison in the TT zone, shown on Fig. 2.11, indicates good correlation between predicted and observed response for three different stress ratios. This, however, should be expected because the response is primarily elastic. It should be noted, however, that in order to obtain maximum strengths of the order of the KHR data, it was necessary to replace the TT circular yield line of Form 1 with the linear segments of Form 2 (compare Figs. 2.8a and 2.8b).

The most difficult zone to deal with, by the present theory, is the CT zone. Fig. 2.13 shows a comparison of predicted response with the KHR data for three different stress ratios in this zone. The maximum stresses predicted by the theory are somewhat lower than the KHR observations. In addition, although the compressive strains match reasonably well, the tensile strains are overestimated at higher stress levels. The linear CT segments of Form 1 (Fig. 2.8a) produced considerably lower peak stresses than those shown on Fig. 2.13, and the spline function was introduced into Form 2 in an attempt to overcome this problem.

A better perspective of the influence of the underestimation of peak strengths in the CT zone may be obtained by returning to Fig. 2.9. The peak strengths obtained from the predicted curves in Figs. 2.10, 2.11, and 2.13 (plus some intermediate runs) are shown here as the

triangular points. It can be seen that, in spite of the strain discrepancies, the maximum strengths compare reasonably with the failure envelope when viewed from this perspective. The above results were summarized in Ref. [15].

Since the two-parameter theory described above suffers from the obvious deficiency that tensile plastic strains in one direction reduce the tensile strength in the orthogonal direction, it was at this stage that the theory was extended to a three-parameter system. This allows the independent variation of the two tensile strengths as illustrated in Fig. 2.8c. Retaining the TT corner of Form 2, however, now requires an additional assumption relative to the translation of this corner during hardening, as discussed in Sect. 2.3.3. In order to avoid this problem the corner was eliminated in the three-parameter model, which gives rise to Form 3 of Fig. 2.8c and Table 2.3. This function was used for debugging during the implementation of three-parameter models into BOSOR5, and some results obtained from it are presented in Sect. 2.5.

Upon successfully implementing Form 3 an attempt was made to produce a three-parameter function with improved correlation to the KHR results. The shape in the TT region was 'squared-off' by using a modified hyperbolic function, the spline curves in the CT region were altered, and the ellipse in the CC region was replaced with a central ellipse with adjoining splines. The resulting function has been designated as Form 4 of Fig. 2.8 and Table 2.3.

A comparison of the Form 4 results with the KHR data is shown in Figs. 2.14 to 2.17. These comparisons follow the same pattern as

discussed above for Form 2. A comparison of Fig. 2.15 with Fig. 2.10 indicates that while Form 4 still underestimates compressive strains, it is not as stiff in the CC zone as Form 2. Comparison of Fig. 2.16 with Fig. 2.11 indicates the tensile response of Form 4 to be somewhat 'softer' than that of Form 2 at high strains, but this is to be expected because the square corner of Form 2 has been replaced by the modified hyperbola. Comparison of Fig. 2.17 with Fig. 2.13 indicates that the maximum tensile stress attained in the CT zone with the Form 4 function is somewhat greater than that attained with the Form 2 function. The maximum stress attained from a number of constant stress ratio runs are indicated by the triangular points in Fig. 2.14 where they are compared with the KHR failure envelope. Comparison of Fig. 2.14 with Fig. 2.9 indicates a substantial improvement in the CC region, while the Form 4 results are also somewhat better in the CT region for low compressive stresses.

In the following section, predictions of wall segment behavior, and comparisons with test observations, are carried out using both Form 3 and Form 4 failure functions.

2.5 BOSOR5 Implementation and Comparison with Segment Tests

2.5.1 Adaptation of BOSOR5

The incorporation of the previously described elastic-plastic-hardening - softening material characterization into the BOSOR5 code results in a program which has the capability of simulating the inelastic response of any segmented axisymmetric thin shell structure composed of reinforced or prestressed concrete. In principle, this adaptation is simple. In practice, it involved a considerable expenditure of effort.

The primary change was to insert subprograms, particular to the present material characterization, into the code's library of subprograms and to change the calling sequence to make use of these subprograms. In fact, it was necessary to adapt the investigators' version of BOSOR5 in the following ways:

(a) The UNIVAC source code was converted to one which would run on an IBM system. In particular, this involved a rewrite of the GASP subroutine.

(b) The appropriate material subroutines were inserted and the calling sequence altered. However, additional modifications were required because the material characterization used herein requires the storage, retention, and data transfer of more information than is required for the plastic material characterization originally contained in BOSOR5.

(c) The subincrement technique was modified, and convergence criteria altered, to suit the material characterization.

(d) The number of layers provided for in the shell wall was increased (from 6 to 15) with a consequent rearrangement of storage.

(e) The restart option, allowing the program to be stopped and restarted at any load level, which is essential for the solution of large inelastic problems, was debugged for the U. of A. system.

The subroutines required for the material characterization, and the test program to produce the results of Sect. 2.4, are contained in Appendix B.

2.5.2 Segment Test Modelling

Since the primary feature in the analysis of the inelastic reponse of a Gentilly-type containment building is the prediction of the behavior of concrete wall segments subjected to tensile membrane forces, a major testing program is being undertaken, in Phase II-76a of this project, to observe the response of such segments. This testing program will be the subject of future reports and it is not the purpose herein either to describe the program of tests or to present detailed analyses of observations. However, one of the purposes of the test series is to provide data which will serve to determine proper material characteristics for predictive techniques, such as the BOSOR5 capability which is the subject of this report. Two of the wall segment tests (designated Specimens 1 and 3) will be used herein to illustrate the capability of the present analytical technique.

Details of the laboratory specimens are shown in Figs. 2.19 to 2.21. The specimens are prestressed in two directions by tendons arranged as shown in the figures. Two layers of mild steel reinforcing bars are located near each face of the specimen.

The specimens have been modelled as shown in Fig. 2.22. Each

layer of reinforcing and prestressing is treated as a thin continuous two-dimensional layer with an area of steel per unit width equal to that provided by the bars or tendons and with uniaxial stiffness in the direction of the bars or tendons. This results in the thirteen layers which are identified in Fig. 2.22c. Since the BOSOR5 code uses the Love-Kirchhoff assumptions with respect to normals remaining straight and normal, a layer of zero stiffness (in a direction transverse to the uniaxial stiffness) does not disrupt the linear variation of normal strain.

BOSOR5 is limited to the analysis of axisymmetric shell structures. The wall segments are modelled, therefore, as short cylindrical shell segments of large radius. Internal pressure is applied to generate the 'circumferential' membrane force while a line load is applied to develop the 'longitudinal' membrane force. Five nodal points (plus 2 subsidiary points, one generated near each end of the segment by the program) were used along the height of the specimen model. The ends of the model were restrained against rotation but were permitted to displace in the radial direction, as indicated schematically in Fig. 2.22a.

The vertical direction of the laboratory specimen contains more prestressing tendons than the horizontal, because the capacity of the testing machine to apply load in this direction is greater than that of the hydraulic jacks used in the horizontal direction. On the other hand the vertical direction of the specimen simulates the horizontal direction of the structure. To avoid confusion the following terminology will be used. Direction 1 will refer to the vertical direction of the specimen which corresponds to the meridional direction of the BOSOR5

shell segment but the horizontal direction of a structure. The orthogonal direction will be referred to as direction 2. These directions are illustrated in Fig. 2.22b.

The prestressing effect was simulated by subjecting the prestressing layers to a temperature change. The surrounding concrete restrains the thermal contraction of the prestressing steel resulting in the development of tensile stresses in the steel and the associated compressive forces in the concrete and reinforcing layers. These initial stress conditions simulate the reference state stress conditions prior to the application of external load.

2.5.3 Material Properties

Five different material types are indicated on the analytical model of Fig. 2.22. Material types 2 and 3 both represent mild steel but have zero stiffness in direction 2 and direction 1, repsectively. The properties used for these two layers are plotted as the lower line on Fig. 2.23, which represents a material with E = 28.5 kips/in.^{2} and a yield point of 60 ksi. Materials 4 and 5 represent prestressing steel with cables running in direction 1 and direction 2, respectively. The properties of the prestressing steel, as provided by the supplier, were simulated as shown by the upper curve of Fig. 2.23. Material type 1 designates plain concrete.

The determination of material properties to simulate concrete behavior is somewhat more involved than that required for the steel. This is particularly so in view of the variability of the properties for different test specimens even from the same mix design. The chronology associated with the testing of the three wall segments completed at the

time of initial writing is shown in Table 2.5. It should be noted that all specimens were poured and grouted at the same time and that the control cylinder tests were carried out on the same day as the specimens were tested, except for Specimen 2.

The specimen strengths obtained from 6 x 12 standard cylinders (the Brazilian tensile test was used to obtain f'_t) are shown in Table 2.6a. The modulus of elasticity was not determined from the cylinder tests, but may be computed from the initial response of the segment tests. Assuming $\nu = 0.2$, the moduli in the two orthogonal directions, as computed from the equation

$$\sigma_1 = \frac{E}{1 - \nu^2} (\varepsilon_1 + \nu \varepsilon_2) \qquad (2.5.1)$$

are shown in Table 2.6b. For this purpose the strains ε_1 and ε_2 were obtained from 4 inch electrical resistance strain gauges applied to the surface of the specimens, while the stress was determined as the applied load divided by the transformed area of the cross-section. No data was available for Specimen 1.

It is now necessary to derive, from the measured properties and generally accepted relations for concrete, the parameters required for the material characterizations described in Sect. 2.4. It should be noted that the mix design was the same for all three specimens and hence the desired concrete properties were the same for all specimens. However, each specimen was poured from a different batch. Considering first the elastic stiffness, the average value from Table 2.6b is 3.67×10^6 psi. For isotropic response the value of E obtained from Eq. 2.5.1 should be the same in each direction. The significant

variation in the two orthogonal directions, as indicated in Table 2.6b, may arise from variability of the materials, the instrumentation, or the loading technique. The average compressive strength of all the cylinder tests in Table 2.6a is 4830 psi. The recommended relationship between strength and stiffness that is currently codified is, [26, pg. 313; 1; 2]

$$E = 57000 \sqrt{f'_c} \qquad (2.5.2)$$

Using the average of the cylinder strengths from Table 2.6a, the corresponding E value obtained from Eq. 2.5.2 is 3.96×10^6 psi. This is about 8% higher than the observed average of 3.67×10^6 psi. The average of the computed value and the observed value is 3.82×10^6 psi.

The precise value of E that is used in the material characterization is of significance only insofar as it influences elastic strains. An approximate value of 3.8×10^6 psi was used for the following analyses.

Since the specimens are being tested in tension rather than compression the value of maximum compressive strength f'_c is not of great significance in the specimens under consideration. The mix was designed for $f'_c = 4500$ psi. The average of the cylinder tests was 4830. A value of 4600 was selected for the compressive strength and an approximate uniaxial compression curve was determined, consistent with this value of f'_c and Hognestad's shape [17] up to the maximum compressive strength. This curve is derived in Table 2.7. It should again be noted that the form of the compression curve is not critical in the determination of the tensile response of the specimens. The adequacy of this form will

be subject to review once test results dependent on compressive behavior become available.

The modelling of tensile response is considerably more significant than f'_c for the prediction of the behavior of pressurized structures. Unfortunately tensile behavior is much more variable than compressive behavior. The objective of the testing program is to determine, on a semiempirical basis, what type of degrading tensile characteristics simulate the specimen response. The approach taken herein is to determine from Specimen 1 the nature of the degrading tensile curve, and to attempt to use this information for the prediction of the response of Specimen 3 which is subjected to a different ratio of applied loads. Since the tensile properties have been determined indirectly from specimen behavior they are discussed in the following section.

2.5.4 Segment Test Predictions and Observations

A photograph of Specimen 2 is shown in Fig. 2.24. This illustration is typical of the specimens tested to date in that it indicates a well developed crack pattern relatively uniformly distributed across the specimen. The current material characterization attempts to spread the effect of this cracking behavior uniformly throughout the specimen by representing the effects of cracks through a degrading stiffness of the material. Observation of the specimens indicates that it is erroneous to think of crack initiation as a condition where a single crack, or a set of cracks, penetrates through the specimen. Cracking starts in localized areas and generally penetrates to a rein-

forcing bar or prestressing duct, but does not penetrate through the specimen until considerably later in the test.

Furthermore, it has been reported in the literature that observable microcracks develop in direct tension tests at stresses around 200 psi which may be approximately 50% of the maximum tensile strength of concrete [16], and that the complete uniaxial stress-strain relationship is highly nonlinear with a degrading curve remarkably similar to that observed in compression [16]. Considerable extensibility is observed beyond the peak tensile stress with 'failure' occurring in direct tension tests at 25 to 40 percent of the maximum stress and at average strains as high as 0.002 [16]. The highly nonlinear behavior in direct tension indicates that microcracking may occur very early in the stress-strain history of the specimen and that the stress level at which cracking is detected may depend to a large extent on the sophistication of the detection techniques employed.

In developing a tensile stress-strain curve to simulate segment test results the primary problem is, then, to determine a suitable shape by which average gross strains may be related to average stresses. This problem is complicated at the present time by the fact that the precise level of prestress in the test specimens after grouting of the cables is unknown to the investigators. (The prestress can be determined up to this point by instrumentation of the anchorages. Subsequent tests will have strain gauges on the prestressing wires to estimate the prestress loss more accurately). Table 2.5 indicates that the specimens were grouted for approximately one-half of their life prior to testing.

The tendons in direction 1 were initially stressed to a force of $64.1^{k} \pm 2^{k}$ (153 ksi) per tendon, while those in direction 2 were initially stressed to a nominal force of $48.5^{k} \pm 2^{k}$ (135 ksi) per tendon. The resulting initial concrete stresses are 740 psi and 420 psi, respectively. The National Building Code of Canada [2] recommends an approximate prestress loss of 25 ksi due to creep, shrinkage and relaxation but excluding anchorage loss. Since the anchorage bearing stresses were high and the specimens were short, the prestress loss prior to testing was assumed to be 30 ksi in direction 1 but only 20 ksi in direction 2 because of the lower level of initial prestress in this direction.

A comparison of the test observations for Specimen 1 with a number of BOSOR5 predictions is shown in Fig. 2.25. It is instructive to follow the technique of approximating the tensile properties by referring to these comparisons. The experimental points are indicated by the solid symbols.

The concrete tensile response was first simulated as elastic-perfectly plastic. It was found that a tensile strength of approximately .6 f'_t, where f'_t is the strength from the Brazilian tensile test, (Table 2.6a) produced a reasonable simulation of the initial break in the curve. The BOSOR5 prediction with elastic-perfectly plastic tensile response of concrete and $f''_t = .60\ f'_t$ is shown in Fig. 2.25 by the open circles and dashed line. The corresponding uniaxial tensile material simulation is shown as the dashed line for Specimen 1 in Table 2.8, sketch b. Table 2.8 also lists possible factors that could account for a 40% reduction in effective tensile strength between the wall segment specimen and the Brazilian tensile test.

It should be noted on Fig. 2.25 that the elastic-perfectly

plastic prediction produces a stiffness after 'cracking' which is essentially equal to the stiffness of the steel only, while the test observations indicate the wall segment response is somewhat softer. Degrading the stiffness of the concrete may now be used to simulate this softening.

The characteristics of plain concrete in tension have been referred to briefly earlier in this Section. Complete stress strain curves showing a degrading stiffness have been reported in Refs. 16 and 18. It is evident from the results of these investigations that the rate of degradation is dependent on the concrete mix and strength, and probably on the rigidity of the testing machine. Ref. 16 indicates that the peak tensile strength may occur at strains between 0.00015 and 0.0008 and that the modulus of elasticity drops rapidly on the falling branch of the stress-strain curve, reaching an average value of 0.25×10^6 psi at a strain of about 0.0006. Nevertheless, the specimens could attain a strain well above 0.001 before failure occurs and the corresponding stress varies between 25 to 40% of the maximum tensile strength.

It is unreasonable to expect that the average response of concrete in a reinforced concrete section will correspond directly with that observed for plain concrete. The reinforcement probably serves to initiate cracks somewhat earlier and also to distribute them more uniformly and thus retain a greater effect from the concrete at higher strains. The arguments advanced in Sect. 2.1 would become effective after microcracks had propogated into cracks crossing the reinforcing steel. On the other hand, if the yielding of the reinforcement is to be properly simulated it is desirable to retain only a small residual stress in the concrete at the yield strain of the reinforcing, which is

0.0021 for the steel properties of Fig. 2.23.

An approximate tensile curve exhibiting the main features of the characteristics discussed above is displayed in Table 2.8b, where it has been assumed that:

(a) $f_t'' = 0.60\ f_t'$

(b) Initial nonlinearity occurs at $0.45\ f_t''$

(c) Maximum tensile stress occurs at a strain of 0.00012

(d) The maximum tensile stress is approximately maintained over a considerable range of strain, dropping to $0.95\ f_t''$ at a strain of 0.0003.

(e) The tensile stress reduces to 60 psi, (approximately 20% of f_t'') at the yield strain of the reinforcing.

(f) A small tensile stress (20 psi) is retained indefinitely by the concrete. (This is necessary for the material model developed herein to function).

At the yield strain of the reinforcing steel this concrete model will result in an underestimation of the maximum stress in the steel by approximately 5 ksi or 8.5% of its yield value, for the specimens under consideration.

The BOSOR5 specimen results for the tensile properties of concrete summarized above, and in the sketch of Table 2.8b, are plotted in Fig. 2.25 as the open squares for the Form 3 yield function of Sect. 2.4. It should be noted that the model simulates the gross strains very effectively in the direction of maximum strains but yields somewhat stiffer results in the orthogonal direction.

BOSOR5 results for a Form 4 type of yield function of Sect. 2.4,

with the same uniaxial properties as discussed above, are shown by the x's and +'s on Fig. 2.25. The result is somewhat stiffer than the Form 3 result, but substantially the same.

Specimen 1 was used to aid in deriving an approximate uniaxial tensile response for use in the current constitutive theory. If this tensile response has validity it should be possible to use similar uniaxial properties without modification of the technique of their determination in predicting the response of other segment tests. Specimen 3 has been used for this purpose. The single tensile specimen associated with this test indicates a value of f'_t of 426 as shown in Table 2.6a. The uniaxial tensile properties, determined as described above, are shown in the sketch of Table 2.8c. The test response of this specimen, which has a load ratio of 1:1 rather than 2:1, is shown in Fig. 2.26 by the solid symbols. The 1:1 load ratio was maintained only up to a load of 375 kips, beyond which the direction 2 load was held constant at 375 kips and the direction 1 load was increased until the termination of the test. The results of a Form 3 BOSOR5 analysis with the uniaxial tensile properties of Table 2.8c are shown on Fig. 2.26 by square symbols. This model represents the specimen behavior in the direction of maximum strains (direction 2) in an effective manner but underestimates the stiffness in the orthogonal direction. The results from a Form 4 BOSOR5 analysis are again shown by the x's and +'s. These results correlate somewhat better with the test observations than those of the Form 3 analysis.

The agreement between the experimental and theoretical load-strain curves for the degrading yield curve formulations is considered to be acceptable for the two specimens examined and tends to establish

the validity of the approach as an effective technique for practical prediction of the behavior of prestressed concrete structures. Application to a complete structure is discussed in Chapters 3 and 4.

3. PRELIMINARY ANALYSIS OF TEST STRUCTURE

3.1 Rationale for Analysis of Test Structure

Chapter 2 considered the problem of developing a material characterization and an analytical capability for predicting the behavior of axisymmetric containment structures. This capability was compared to the results from a very limited number (two) of laboratory tests of wall segments subjected to biaxial tension and it was demonstrated that, given the proper material parameters, a reasonable prediction of response could be obtained. Theoretically, if one can predict the behavior of structural segments, then the prediction of the behavior of a complete structure, which is simply an assemblage of segments, follows directly.

However, there are many aspects of the prediction of the response of a complete structure which are more complex than those involved in the prediction of behavior of wall segments. Some outstanding questions are:

(a) Can the analytical technique be successfully applied to large scale structural systems?

(b) Will the material characterization be adequate to predict behavior in a structure where significant moments exist in addition to tensile membrane forces?

(c) Will an axisymmetric model be adequate to predict the behavior of the structure when the symmetry of the structure is disrupted by anchorage buttresses in the cylinder wall?

(d) Will the behavior in the region of junctions between structural components (base connection and ring beam areas) be adequately simulated by thin shell theory?

(e) Will 'failure' be triggered by behavior in the region of penetrations, by transverse shearing effects, by bond failure, or by some other factor associated with detailing or construction practice?

This Chapter addresses itself to the first of these questions (question a). That is, the objective is to demonstrate the capability of the technique developed in Chapter 2 to analyze a complete Gentilly-type structure. However, the structure analyzed is not the prototype structure, but the test structure presently under construction and to which reference has been made in Sect. 1.2. A satisfactory comparison of predicted behavior with test observations of this structure would provide affirmative answers to questions a, b and c, above, (and possibly d). Since this is a preliminary analysis, prior to completion of construction, the material properties are subject to correction before actual comparison with test observations can be made. Nevertheless, a technique of modelling the structure can be explored at this time, and the capability of analyzing such a structure can be demonstrated.

3.2 Description of Test Structure

It is not the intent of this report to give a detailed description of the test structure. This information will be contained in reports associated with the experimental phase of the project (Phase II-76b). However, it is necessary to consider the geometry of the test structure and the arrangement of reinforcing and prestressing in order to discuss the modelling technique.

The principal dimensions of the structure are shown in Fig. 3.1. The structure consists of four principal components, namely, the base (3' - 6" thick), the cylindrical wall (5" thick with internal radius of 4' - 10"), the ring beam (10" thick by 1' - 4 1/2"), and the spherical dome (4" thick with internal radius of 9' - 8"). The dome is thickened at the springing line and has a smooth transition into the ring beam. Four buttresses of thickness equal to that of the ring beam are placed 90° apart around the cylinder wall to anchor the circumferential post-tensioning strands. The post-tensioning strands are indicated in Fig. 3.1.

The reinforcing is shown in Figs. 3.2, 3.3 and 3.4. The post-tensioning strands for the dome are shown in the upper quadrant of Fig. 3.4. All strands are on great circles and hence the spacing of the strand varies with the location on the midsurface of the dome. One of the problems in modelling the structure is to determine a radial and circumferential prestressing net which is equivalent to this (nominally) orthogonal net. This will be discussed in detail in Sect. 3.3.2.

The structure was designed from linear elastic analyses. Axisymmetric finite element analyses (using SAP IV [6]) and FLEXSHELL

analyses [25], were carried out. The proportioning of the component thicknesses and the level of prestress were chosen to yield a sequence of cracking in the test structure similar to that occurring in the Gentilly-2 containment structure. However, the internal pressures required to produce cracking are considerably higher in the test structure than those required in Gentilly-2.

In addition, the cylinder wall has been designed to have a strength comparable to (but slightly smaller than) the dome as distinct from the Gentilly-2 in which the strength of the dome is about half that of the wall. This is to ensure that useful information is obtained for as many components of the test structure as possible. The sequence of cracking, and the pressures at which cracks are expected, as predicted by elastic analyses during the design phase, are shown in Fig. 3.5.

3.3 Modelling the Test Structure for BOSOR5 (First Model)

3.3.1 The Geometry of the First Model

The BOSOR5 model of the test structure, as used in the first analysis herein, is shown in Fig. 3.6. Elastic analyses indicate that the 3' - 6" base component of Fig. 3.1 can be regarded as providing complete base fixity at the bottom of the cylinder wall. Hence the base has been replaced by a fixed boundary condition for the BOSOR5 model. The remainder of the structure was divided into 7 components, as indicated in Figs. 3.1 and 3.6 namely: (1) a thin cylindrical component to simulate the hinge (i.e. - shear key), (2) a heavily reinforced cylindrical component at the base of the wall (see Fig. 3.3), (3) the remainder of the cylinder wall, (4) the ring beam, (5) the tapered dome component at the springing line, (6) the central dome component and (7) the crown of the dome component. Post-tensioning strand and reinforcing bars were modelled as thin continuous layers in the same manner as the wall segments of Chapter 2 (Fig. 2.22). The number of layers in each structural component is summarized in Fig. 3.6. The number of BOSOR5 mesh points employed are also summarized in Fig. 3.6.

Schematic representations of the layering of the various components are shown in Fig. 3.7. The thicknesses of the layers in the components are summarized in Table 3.1. While Table 3.1 contains sufficient data for most purposes it should be noted that component 5 varies in thickness in a nonlinear manner along its length and a complete description of this component would require the specification of the component thickness and the layer thicknesses at a number of intermediate points.

It should be noted that the structural components are connected with kinematically rigid links where they are eccentrically joined (Fig. 3.6). These links are of essentially the same type as used in the BOSOR4 analyses of Refs. 12 and 13, and as in the FLEXSHELL analyses of Ref. 25. In order not to underestimate the prestressing effect, and thereby produce premature 'cracking', the area of overlap between the dome cross-section and the ring beam cross-section (see Fig. 3.6) was compensated for by a reduction in the height of the ring beam.

3.3.2 Reinforcing, Post-Tensioning, Materials, and Loading for the First Model

As with the segment tests of Chapter 2, the thicknesses of the steel layers were computed to provide the same area per foot as the reinforcing bars or wire, and the post-tensioning strand. Table 3.1 indicates that the thickness of the steel layers may vary from one end of a component to the other. For component 2 this variation in layers 4, 6, 8 and 12 is a result of the change in location of the inclined bars, shown in Fig. 3.3, which have been proportioned to the layers on either side. For component 4, the change in thickness of layer 10 results because the horizontal post-tensioning strands are not centered at midheight of the ring beam (one cannot discontinue a layer within a segment). The variation of thickness of layers 2 and 9 between components 5, 6 and 7 results because of changes in the spacing of the reinforcing shown in the lower quadrant of Fig. 3.4. However, the area was not varied within the components. The variation of thickness of the post-tensioning layers in the dome components (5, 6, and 7) are more complex and the reasons for this will now be discussed.

To simulate the effect of the 'orthogonal' net of post-tensioning strands in the dome with an axisymmetric model it is necessary to convert the orthogonal net to effective areas of strand in the radial and circumferential directions. It is also necessary to compute the effective 'axisymmetric' post-tensioning compressive membrane forces in the dome. These computations must be approximate since the orthogonal net is not axisymmetric. The following technique has been used. (Note that this type of technique can be adapted to the 'equilateral' pre-stressing net used on the Gentilly-2 containment structure).

Consider the orthogonal net of post-tensioning strand to be extended to cover a complete sphere as indicated in Fig. 3.8a. Since all strands are on great circles, each of the orthogonal layers must be associated with two poles which will be designated as P and P'. Let us refer to the layers of strand as the P_1 layer and the P_2 layer depending upon the pair of poles at which the strands of the layer intersect. Progressing along the great circles P_2' - M - P_2 and P_1' - M - P_1, the layers are orthogonal to each other. However, progressing along the quadrant of a great circle M-N-T, it is apparent from Fig. 3.8b that the angle of intersection of the layers varies from 90° to 0°. The net is, therefore, neither axisymmetric nor orthogonal and, furthermore, does not give a uniform prestressing effect for constant forces in the strand as is demonstrated by the following analysis.

The dome of the test structure may be visualized as the segment to the left of plane 1-1 of Fig. 3.8b. Plane 1-1 intersects the sphere in a circle which becomes the springing line of the dome, and the plan view of the dome is contained within the inner circle of Fig. 3.8a.

The problem of determining the angle which a strand passing through the springing line at N makes with the line MN, bisecting the angles of intersection between the two nets, is one of spherical trigonometry, and the angle MNS will define the geometry of the net at the springing line. The equations for a spherical triangle are shown in Fig. 3.8c, and the solution for the angle MNS is summarized in Fig. 3.8d (angle M N S = 48.83°).

It is also apparent that as one moves along a great circle the spacing between the strands changes. Assume that the spacing at the crown in the orthogonal net is s. The spacing of the P_1 strands as one moves along arc M V P_2 of Fig. 3.8a is maintained at s. However the distance between the P_1 strands as one moves along arc M S Q reduces. The distance between the strands is directly proportional to the sine of the angle measured from P_1 in the plane M Q P_1. The result is that the spacing Q J at the springing line is s.sin 61° = 0.8746 s. (All computations in this section assume an angle at the springing line of 29° measured from M. Since the final result of the computations is to produce an approximation, precision with respect to this variable is not required).

The geometry of the net at four points of the dome of Fig. 3.8a is shown in Fig. 3.9a. Point M is at the crown, points Q, N, V are at the springing line of the dome. The spacing computed above is applicable at points Q and V, as shown in Fig. 3.9a. A similar computation using the angle N O S of Fig. 3.8d (20.05°) is applicable at point N, resulting in a distance between the strands of s.sin 69.95 = 0.9394 s. The angle of intersection of the strands at point N has been determined in Fig. 3.8d.

Neglecting friction losses the inward force per unit length of strand is uniform for all strands since all strands are subjected to the same tension and have the same curvature. The inward force on the area enclosed by a cell of the mesh is, therefore, proportional to the perimeter of the cell, and the equivalent normal pressure is proportional to the ratio of the perimeter of the cell to the surface area within the cell. If the normal pressure exerted by the prestressing strand at the crown (point M) is denoted by p_o, the effective pressures exerted at points Q, N and V along the springing line are shown in Fig. 3.9a in the quarter-circle table. Although there is a variation in pressure when one travels along the springing line it is apparent that the pressure is reasonably constant. For analyses it is considered sufficiently accurate to assume a constant effective prestress pressure of 1.07 p_o at the springing line which decreases linearly to a value of p_o (less frictional losses) at the crown. This pressure distribution is, therefore, non-uniform but axisymmetric.

Turning now to the equivalence of strand areas between orthogonal and axisymmetric nets, the ultimate strength of the net is inversely proportional to the distance between the strands. The ratio of effective strand areas may be considered equivalent to the ratio of ultimate strengths. Defining the area of strand at the crown as A_o, the ratio of effective areas in the radial and circumferential directions (A_ϕ and A_θ, respectively) are shown in Fig. 3.9a in the quarter-circle table at the three locations along the springing line of the quadrant. It should be noted that there is an increase of effective meridional strand area of 14% from the crown to the springing line on the great circles through the crown parallel to the net directions. However, if

ultimate strengths are evaluated at point N, as indicated in Fig. 3.9b, there is a decrease of effective meridional strand area equal to 7.7%. A similar variation occurs in the effective circumferential strand areas, the variation in this direction being 20.6%. However, the point of greatest circumferential effective area is the point of minimum meridional effective area and vice-versa.

It is apparent from the above analysis that the orthogonal net is inhomogeneous and anisotropic in both strength and stiffness. Similar effects would be present in an 'equilateral' net, such as used on the Gentilly-2 structure, although the variations may be expected to be less severe. The investigators have not had the opportunity to study this type of net to the present time.

The analysis summarized in Fig. 3.9a indicates that, ignoring the strength contribution of the mild steel, 'failure' in the circumferential direction would probably initiate on a great circle through the crown parallel to one of the sets of strand, while 'failure' in the meridional direction would probably initiate at some location close to the springing line on a great circle passing through the crown at 45° to the directions of the net. Since the structure is to be analyzed as axisymmetric, the properties associated with the dome can be assumed as shown in the rectangular table of Fig. 3.9a and consists of the 'weakest' effective values in each direction. A linear variation with the angle ϕ, as measured from the central axis of symmetry, between the limits indicated in the table, can be used for the prestressing areas, and this approach forms the basis of the properties of the cross sections of

Table 3.1.* The value of A_o is computed in Table 3.2a.

The loss of prestress due to friction in the cables is also computed in Table 3.2a, and is approximately 12% at the crown. Applying this loss to the pressures in the table of Fig. 3.9a, the effective normal prestress pressure would vary from 0.88 p_o to 1.07 p_o from the crown to the springing line. The value of p_o is computed in Table 3.2a.

A linear elastic analysis of the test structure when subjected to the prestressing pressure described in the above paragraph was carried out to determine the membrane forces arising in the dome. Attempts to reproduce this distribution of membrane forces with thermal changes in the prestressing layers were unsuccessful because the membrane forces at any location are not directly related to the strand forces at that location (i.e. - the structure is statically indeterminate). The effect of prestressing was therefore simulated with external pressure for the entire model.

Since it is incorrect to vary the external pressure to account for friction, without adding corresponding tangential surface tractions, and since the initial BOSOR5 program could not process pressure loads with different time variations in the normal and tangential directions, frictional losses in the dome were neglected in the first analysis of the test structure. Therefore, an external pressure to simulate dome prestress varying linearly from p_o at the crown to 1.07 p_o at the springing line would be the most effective estimate for the model. Over each

---

* A discrepancy between the computations of this section and the initial modelling procedure resulted in A_ϕ varying (erroneously) in the model from 1.12 A_o at the springing line to A_o at the crown.

component a uniform pressure was used which produces the same membrane force at the end of the segment as the linear variation. This simulation is shown in Fig. 3.10.*

When the prestressing forces are simulated with external pressure the stress level in the strand is grossly underestimated. This is in contrast to the thermal simulation of the wall segments where the proper strand stress is maintained at all load levels. In order to properly simulate the yielding behavior of the strand an artificial origin was introduced into the stress-strain curve of the strand at a stress level equal to the effective prestress plus the negative of the stress computed in the externally loaded prestressed reference state. This adjustment to the properties of the strand allows a proper simulation of its nonlinear stiffness at any load level. The properties of the prestressing strand, together with the initial stress levels which properly simulate the reserve strength of the strand in various components of the structure, are shown in Fig. 3.11.

The level of prestress in the cylinder wall is computed in Table 3.3. Prestress losses for $\theta = \pi/4$ are those at the mid-line between buttresses which represents the section subjected to the minimum prestressing effect.

The properties of the reinforcing bars and wire are shown in Fig. 3.12, while the concrete properties for the tensile strength of concrete are those of Table 2.8b. A total of 9 material types were, therefore, used for the model as shown in Table 3.4.

---

* A discrepancy between this discussion and the preliminary modelling procedure resulted in a prestress pressure varying (erroneously) on the model from 1.26 p_o at the springing line to p_o at the crown.

Gravity loads were approximated as shown in Fig. 3.13 and the variation due to hydrostatic pressure was approximated as shown in Fig. 3.14. The internal pressure load referred to in the following analysis is, therefore, the pressure at the crown.

3.4 Results from First Model

3.4.1 Description of Runs

The results obtained from the first full analytical run, presented in this Section, were obtained during the month of March, 1978. The accumulated run time (including wastage) was 87.9 CPU minutes on the AMDAHL 470 V/6 (equivalent to an IBM 370) with an accumulated high speed storage VMI of 12439 page-minutes. Roughly one half of this time was productive in the sense that suitable convergence was obtained to permit a subsequent load increment.

Since nonlinear runs are extremely sensitive, each load increment is run independently and an examination of the results must be carried out prior to the next load increment. In this way the behavior of the structure may be continuously monitored in order to make a proper judgement about the nature of the following load increment. A full 'run' may, therefore, take several weeks. A summary of the load levels at which results were output is contained in Table 3.5.

The run was terminated after 26 load increments at an internal pressure of 108.75 psi. The reason for termination was failure to converge in the hinge area. An examination of the strains in this region indicates that compressive strain in the region had reached -0.042. Concrete is usually considered to fail by crushing at a strain of -0.003. Since the predicted strain is an order of magnitude greater than this limit there is little doubt that a crushing failure would have occurred in the hinge region at a significantly lower pressure. (A strain of 0.003 was reached at a pressure of 89 psi). However, the loading was continued beyong this failure level in an attempt to identify

the final failure mode. A more complete discussion will be undertaken after a presentation of the results.

3.4.2 Presentation of Results (First Model)

3.4.2.1 Cracking in First Model

The initial distress shown by the structure is tensile cracking. Some indication of the extent of cracking at different load levels is presented in Figs. 3.15 to 3.18. Fig. 3.15 shows the penetration of cracking at a pressurization of 65 psi. Although there are horizontal cracks at a number of points, produced by combined membrane action and flexure, it is apparent that these cracks are confined by compression blocks and the significant cracks, from a possible leakage point of view, are the vertical cracks in the wall which are through-cracks covering approximately 3/4 of the length of the cylinder. Figs. 3.16, 3.17, and 3.18 indicate the progressive spread of the cracked regions throughout the structure as the load is increased to the terminal pressurization.

3.4.2.2 Deflections in First Model

Fig. 3.19 shows deflection plots referenced to the basic structural configuration for two pressurizations. (One should be careful not to interpret this plot literally since deflections are to a different scale than the reference structure). The nature of the deformations is clearly evident.

Pressure-deflection plots at a point approximately 1/3 of the distance up the cylinder wall (Sect. 3-4 on Fig. 3.19) and at the crown

of the dome are shown in Fig. 3.20. It is apparent that cracking begins to influence horizontal deflections in the cylinder at pressures above 40 psi and vertical deflections in the dome at pressures above 60 psi. However, after extensive cracking the points continue to displace with relatively constant stiffness.

3.4.2.3 Stress Resultants in First Model

The distribution of stress resultants at selected internal pressures is shown in Figs. 3.21 to 3.23. Nondimensionalized pressure variation of stress resultants at selected locations is shown in Figs. 3.24 and 3.25. It can be seen from Fig. 3.24 that the increase in N_1 membrane forces is essentially linear with load. This is, however, not the case for the N_2 stress resultants, nor for the moment stress resultants or curvatures as may be seen from Fig. 3.24 and 3.25. It is apparent that there is significant redistribution and reduction of moment once through-cracking has occurred.

3.4.2.4 Steel Strains in First Model

The strains in the reinforcing steel are shown in Figs. 3.26 to 3.29, inclusive, for pressurization of 65 and 108.75 psi. Yield strains consistent with the properties of Fig. 3.12 are indicated. The non-linearity of steel strain with pressurization is apparent. The effect of the meridional moment concentrations in Fig. 3.23, on the steel strains shown in Figs. 3.26 and 3.27 is also apparent. However, the maximum strain produced is of the order of 1.2% at 108.75 psi and a significant reserve of ductility remains throughout.

3.4.2.5 Prestressing Strand Stress in First Model

The stress in the prestressing strand is shown in Figs. 3.30 and 3.31 for pressure of 0, 84.5 and 108.75 psi. First yield consistent with Fig. 3.11 is also shown. These stress distributions are extremely important since the tendons become the primary load carrying elements in the structure near ultimate load. First tendon failure signifies the pressure at which the structure will explode [24].

The circumferential tendon stresses are relatively uniform, as would be expected (Fig. 3.31). However, the meridional tendon stresses (Fig. 3.30) exhibit high concentrations of stress because of the moment effects of Fig. 3.23. The ultimate strength of the tendons is 270 ksi.

3.5 Discussion of Results from First Model

The results from the first model make it possible to trace a continuous relationship between load and cracking conditions, deflections, steel stresses, concrete stresses, and tendon stresses. A perusal of these results indicates that the first model predicts the following limit states:

1. First cracks are horizontal cracks occurring on the inside of the hinge at a pressure of 42 psi. (Cracking is predicted on the outside of the hinge prior to the application of internal pressure).
2. First cracking of the main structure consists of horizontal cracks on the interior of the ring beam at the junction with the dome at a pressure of 45 psi.
3. The first significant through-cracks are vertical cracks in the cylinder wall at a pressure of 58 psi.
4. First yield of meridional steel occurs at the junction between the dome and the ring beam at a pressure of 87.5 psi.
5. First yield of circumferential steel occurs at the crown of the dome at a pressure of 105 psi. Meridional steel at the crown yields also at this pressure.
6. First yield of the meridional prestressing strand occurs at the junction between the dome and the ring beam at a pressure of 98.5 psi.
7. First yield of the circumferential prestressing strand occurs over a signifcant portion of the cylinder wall at a pressure of 91 psi.

8. First failure consists of concrete crushing in the hinge which occurs at a pressure of 89 psi as measured by compressive strains of 0.003.

Since the final collapse will be triggered by failure of the prestressing tendons, and the loading had to be terminated prior to attaining this state, the ultimate load has been determined by extrapolation of tendon stresses. The variation of prestressing stresses at selected points in the structure is plotted in Figs. 3.32 and 3.33. These extrapolations indicate explosive failure at an internal pressurization of 123 psi due to tendon failure in the ring beam at the junction with the dome.

The fact that the model predicts collapse due to a stress concentration effect at Sect. 4-6 (Fig. 3.30) is, however, somewhat disturbing since this point is directly influenced by the modelling technique. An examination of the variation of stress in the meridional tendons on Fig. 3.30 indicates three points of high stress concentration once the structure becomes nonlinear:

(a) The point at which the rigid link between the ring beam and the dome attaches to the ring beam.

(b) The point of abrupt change in cross-section between the cylinder wall and ring-beam.

(c) The point at which there is an abrupt change in reinforcing between the lower portion of the cylinder wall and the central portion of the cylinder wall.

All of these concentrations are somewhat artificial. Therefore, a new modelling technique was evolved to mitigate these effects. The model is discussed in Chapter 4.

4. ANALYSIS OF SECOND MODEL OF TEST STRUCTURE

4.1 Changes in Modelling Technique

The primary deficiency of the modelling technique presented in Chapter 3 appears to be the cusp-like concentrations of stress in the prestressing strand at points of geometric discontinuity, section property discontinuity and rigid link connections. The high gradients in stress would probably lead to bond failure which would mitigate the concentration in the immediate vicinity of the peak stress.

To minimize any artificial stress concentrations introduced by the modelling technique the following improvements were made to the model:

1. All rigid links were eliminated. This was accomplished, in the area of the junction between the dome and ring beam, by defining a continuously curved reference surface, and handling the changes in geometry by variations of thickness and locations of the layers. At the junction between the ring beam and the wall, a tapered transition zone was introduced to allow a smooth variation in the location of the compression block.
2. Instead of abruptly cutting off steel layers, these layers were tapered over a transition length to one-quarter of their areas. The argument for this is to allow a development length in which bond stress transfer has an opportunity to develop the full effective area of the bar. This mitigates the effect of the abrupt transition which occurs, for instance, at the junction between segments 2 and 3 in Fig. 3.30.

3. The simulation of prestress anchorage forces was altered in such a way that the forces were distributed to three sections in the immediate vicinity of the anchorage. The argument for this is that plane sections do not remain plane at the point of application of concentrated loads. The effect of this is to 'smear out' the transfer of load from the point of concentration over a finite length.

In addition to these changes in modelling technique a number of changes to the properties of the structure were made, which reflect alterations in the actual test structure caused by material supply problems and examination of the results of the preliminary analysis. These were:

1. The wire reinforcing originally purchased for the structure proved unsatisfactory from a materials point of view. This was replaced with rolled bar reinforcing imported from Europe. The yield stress of the new material is 50.9 ksi rather than the 75 ksi used in the first model.
2. An additional circumferential prestressing tendon was placed in the cylinder wall, with a consequent increase in prestressing force in this direction, in order to delay the vertical cracking somewhat.

A modification was made to the BOSOR5 program which permitted independent time variation of tangential surface tractions and normal pressures. Therefore, frictional losses in the dome prestressing strand could properly be taken into account.

To prevent convergence problems in the hinge area an elastic

perfectly-plastic concrete compression curve was used for the hinge segment, only, and a small amount of circumferential steel was provided in this area.

4.2 Geometry, Reinforcing, Prestressing, Materials and Loading for the Second Model

The geometry of the second model is shown in Fig. 4.1 where the component segments are also identified. While the principal dimensions are identical to those of the first model, the changes in modelling technique of the ring beam, and the ring beam to dome and ring beam to cylinder wall connections, is clearly apparent.

The layering of the segments is similar to that of the first model but differs considerably in detail.* The ring beam area is the most difficult portion to model and a detail of the area is shown in Fig. 4.2. Layering of components is described in Table 4.1.

The material properties of the rebars are shown in Fig. 4.3, those of the prestressing strand in Fig. 4.4 and those of the concrete in Table 2.8b. The fact that the prestressing is again simulated as an external load necessitates an adjustment in the effective yield stress, which varies from section to section in the structure as discussed in Sect. 3.3.2, and accounts for the different reference points indicated on Fig. 4.4. The identification of material types, as indicated for the segment layers of Table 4.1, is given in Table 4.2. The pressure simulation of the prestressing is shown in Fig. 4.5**; the gravity load simulation in Fig. 4.6; the hydrostatic pressure approximation is essentially that of Fig. 3.14; and the prestressing anchorage and ring

---

* The area of meridional prestressing in the dome is subject to the same discrepancy as covered by the footnotes in Sect. 3.3.2.

** The magnitude of normal pressure to simulate dome prestressing is subject to the same discrepancy as covered in the footnotes of Sect. 3.2.2.

beam forces are shown in Fig. 4.7 where they are identified as to source and by the fictitious ring numbers used in the BOSOR5 model to apply concentrated loads.

4.3 Results from Second Model

4.3.1 Description of Runs

The results for the second full analysis of the test structure, presented in this Section, were obtained over the period May 15 to June 18, 1978. Approximately 12 working days of this period were used to investigate the effect on initial cracking patterns of various geometric configurations connecting the ring-beam to dome. The accumulated run time (including wastage) for the second analysis was 120 minutes on the AMDAHL 470 V/6 with 22150 page-minutes high speed storage VMI. Approximately 76% of this time was productive. A total of 27 load increments were completed as summarized in Table 4.3. The run was terminated at an internal pressure of 120.5 psi because of instabilities arising in the cylinder wall due to the yielding of circumferential reinforcing. The (negative) degrading stiffness of the concrete could not then be overcome by the stiffness of the (partially yielded) prestressing strands only. However, this terminal loading does not represent the ultimate capacity of the structure as will become apparent in the subsequent discussion.

4.3.2 Presentation of Results (Second Model)

4.3.2.1 Cracking in Second Model

An indication of the distribution and progression of cracking as predicted by the analysis is shown in Figs. 4.8 to 4.12. Initial horizontal cracking of the structure begins at an internal pressure of

30 psi in the ring beam junction area (Fig. 4.8). However, these cracks are localized. Significant through-cracking first occurs as vertical cracking in the cylinder wall (see Fig. 4.9). Cracking continues to spread throughout the structure as indicated in Figs. 4.10 to 4.12.

4.3.2.2 Deflections in Second Model

The deflections of the second model are plotted in Fig. 4.13 for an internal pressure of 74 psi and the terminal pressure. The reader is again cautioned not to interpret the plot of deflection as the actual shape of the deformed structure.

4.3.2.3 Stress Resultants in Second Model

The stress resultants in the second model are shown in Figs. 4.14 to 4.16 for pressures of 0, 74 and 120.5 psi. The variation of stress resultants is somewhat smoother than those from the first model except for the perturbation of N_1 at the junction between segments 4 and 5. A plot of the pressure variation of nondimensionalized stress resultants and curvatures at selected locations is shown in Fig. 4.17 and 4.18. It is again apparent that, except for N_1, the assumption of linear variation of variables with pressure is not justified.

4.3.2.4 Steel Strains in Second Model

The steel strains in the second model are shown in Figs. 4.19 to 4.22, inclusive, for pressures of 74 and 120.5 psi. The maximum steel strain indicated is 1.2% in the meridional steel at the junction of the dome to the ring beam.

4.3.2.5 Prestressing Strand Stress in Second Model

The stress in the prestressing strand is shown in Figs. 4.23 and 4.24 for a number of internal pressures. Stresses at which breaks in the stress strain curves of Fig. 4.4 occur are indicated by the vertical lines on these figures. The highest stresses occur in the circumferential strand in the cylinder wall.

Since failure of the prestressing strand would trigger explosive collapse, the strand is the critical factor in the ultimate strength of the structure. Some indication of the pressure at which the ultimate strength of the strand may be reached can be obtained by extrapolating the strand stress to its ultimate strength on a pressure-strand stress plot. Pressure-strand stress plots are presented in Figs. 4.25 and 4.26 for selected locations. From the extrapolation of the circumferential strand stresses, shown on Fig. 4.25, the critical section is Section 3-4 where failure is indicated at a pressure of 132 psi. The extrapolations of Fig. 4.26 indicate failure in the meridional strand at the junction of the wall with the ring beam at a pressure of 140 psi.

4.4 Discussion of Results from Second Model

The results from the second model give an indication of the relationship between internal pressure and cracking, deflections, and stresses. A set of limit states may be identified as follows:

1. Disregarding the hinge, first cracks are horizontal cracks occurring on the interior of the ring beam, in the region where the dome prestressing strands are anchored, at a pressure of 30 psi.
2. First cracking in other regions of the structure consists of horizontal cracks on the inside of the wall at the junction with the ring beam, and on the inside of the dome at the region near the junction with the ring beam, at a pressure of 61 psi.
3. The first significant through cracks are vertical cracks in the cylinder wall at a pressure of 62 psi.
4. First yield of meridional steel occurs at the junction between the dome and the ring beam at a pressure of 95 psi.
5. First yielding of circumferential steel occurs at the crown of the dome at a pressure of 109 psi. Meridional steel at the crown also yields at this pressure.
6. First yielding of the meridional prestressing strand occurs at the junction between the dome and the ring beam at a pressure of 106 psi.
7. First yielding of the circumferential prestressing strand occurs at the crown of the dome at a pressure of 110 psi.
8. Extrapolation indicates that explosive failure would occur at a pressure of 132 psi.

Since the material properties in the hinge area were altered to prevent degradation of the stress in the concrete, crushing failure in the hinge, and the resulting numerical instability that arose in the first model, did not occur. However, a compressive strain of 0.016 was indicated in the hinge at the terminal pressure. A compressive strain of 0.003, normally considered to be a limiting compressive strain, occurs at a pressure of 95 psi which can be considered to be the pressure at which crushing failure would occur.

4.5 Effect of Modelling

A summary of the limit states predicted by the two modelling techniques is shown in Table 4.4. There are enough differences between the real test structures associated with the two models to make direct comparison difficult. However, stress concentration effects in the meridional direction have been considerably reduced in the second model and the authors believe that the modelling technique used for the second model is a significant improvement over that used for the first model.

Numerical instabilities necessitated termination of each analysis prior to reaching the ultimate strain in the prestressing strand. It is believed that sufficient experience has been gained so that careful modelling will allow future runs to attain the ultimate strain in the strands without encountering numerical instabilities. The instability in the second model was caused by the combination of material properties associated with the circumferential direction in the cylinder wall. This can be prevented by employing a less severe degradation of concrete properties.

To demonstrate that this instability can be eliminated segment tests were run at the critical section (point 3-4) of the second model. The pressure-strain plot for this point, as extracted from the BOSOR5 analysis of the test structure, is shown in Fig. 4.27, where it is compared to the 'steel-only' response [24]. A simulation of the response at this point, obtained from a proportional loading of a wall segment specimen (as described in Chapter 3), is also shown. The segment adequately simulates the response of the structure at this point and is subject to numerical instabilities at approximately the same pressure as the total structure. Thus the fact that this type of segment was

responsible for failure of convergence is established.

The degrading part of the concrete stress-strain curve was then altered as shown on Fig. 4.28. The alteration reduces the negative stiffness in the region of the yield strain of the rebars (ε = 0.0015 to ε = 0.0028). A reanalysis of the segment then produces the result shown in Fig. 4.29. Numerical instabilities are eliminated and the segment behaves well to a strain of 0.019 at which point the run was discontinued. This alteration of the tensile properties of concrete would allow the structural analysis to be continued to higher pressures. A complete reanalysis was not undertaken because of the costs involved.

5. CLOSURE

This report has attempted to develop an elastic-plastic constitutive model for concrete which, when used with the concept of a degrading tensile stress-strain curve, is capable of simulating the gross stress-strain response of 'thin-shell' prestressed concrete structures loaded primarily in tension. Such a theory has been developed and, while only limited success has been achieved in simulating strains from pure concrete biaxial tests, it has proved adequate for simulation of experimental results from tests of large scale prestressed concrete wall segments. The model includes the effect of cracking in tension and nonlinear response in compression and these properties can be adjusted for various concretes by the input of uniaxial tension and compression response. While the uniaxial compression response may be obtained from a standard test, that for tension must be deduced indirectly from observations of the response of reinforced or prestressed specimens. Preliminary recommendations to determine the appropriate tensile characteristics from standard test results have been made.

The constitutive relationship developed herein has been incorporated into a modified version of the BOSOR5 computer code and this code then becomes capable of simulating the inelastic response of large scale axisymmetric segmented thin shell structures constructed of reinforced or prestressed concrete. The capability of the program to analyze such structures has been demonstrated by analyzing the University of Alberta test structure associated with this research project.

An analysis with the BOSOR5 code predicts the distribution of strains, stress resultants and deflections throughout the structure. The stresses associated with each layer of reinforcing and prestressing

are determined. Onset and progression of concrete cracking (in a gross strain sense), and yielding and strain hardening of steel components are determined. Limit states associated with the response of the structure can thereby be determined.

The effects of the modelling technique with respect to geometry, layering, loading and materials simulation have been investigated and sufficient experience obtained to allow undesirable effects dependent upon these factors to be mitigated.

The report has, therefore, achieved its basic objectives of developing a technique, and demonstrating the feasibility, of analyzing for the inelastic response of Gentilly-type structures. An assessment of the reliability of the analytical capability developed herein will have to await the experimental results from the test structure currently under construction.

REFERENCES

1. "Building Code Requirements for Reinforced Concrete (ACI Standard 318-71)", American Concrete Institute, P.O. Box 4754, Redford Station, Detroit, Michigan, 48219.

2. "Canadian Structural Design Manual (1970). Supplement No. 4 to the National Building Code of Canada", Issued by the Associate Committee on the National Building Code, National Research Council of Canada, Ottawa.

3. "MARC-CDC: User Information Manual", Vols. 1 to 4, Control Data Corporation, CYBERNET Publications Department, HQW05F, P.O. Box O, Minneapolis, Minnesota 55440, 1972.

4. "Safety Report: Gentilly-2 600 MW Nuclear Power Station", Report to the Atomic Energy Control Board for Hydro-electrique de Québec, Atomic Energy of Canada Limited.

5. Bathe, K.J., Wilson, E.L. and Idling, R.H., "NONSAP - A Structural Analysis Program for Static and Dynamic Response of Nonlinear Systems", UC SESM Report No. 74-3, Structural Engineering Laboratory, University of California, Berkeley, California, February 1974.

6. Bathe, K.J., Wilson, E.L. and Peterson, F.E., "SAP IV - A Structural Analysis Program for Static and Dynamic Response of Linear Systems", Report No. EERC 73-11, Earthquake Engineering Research Center, University of California, Berkeley, California, 1974.

7. Buyukozturk, O., "Nonlinear Analysis of Reinforced Concrete Structures", Second National Symposium on Computerized Structural Analysis and Design, George Washington University, Washington, D.C., March 29 - 31, 1976.

8. Bushnell, D., "Finite-Difference Energy Models vs. Finite-Element Models" Two Variational Approaches in One Computer Program", Numerical and Computer Methods in Structural Mechanics, edited by S.J. Fenves, et. al., Academic Press, New York, 1973.

9. Bushnell, D., "Stress, Stability and Vibration of Complex Branched Shells of Revolution: User's Manual for BOSOR4", Lockheed Missile and Space Company, Inc., Sunnyvale, California.

10. Bushnell, D., "BOSOR5 - A Computer Program for Buckling of Elastic-Plastic Complex Shells of Revolution Including Large Deflections and Creep; Vol. 1: User's Manual, Input Data", Lockheed Missiles and Space Company, Inc., Sunnyvale, California, December 1974.

11. Bushnell, D., "BOSOR5 - A Computer Program for Buckling of Elastic-Plastic Complex Shells of Revolution Including Large Deflections and Creep; Vol. 3: Theory and Comparison with Tests", Lockheed Missiles and Space Company, Inc., Sunnyvale, California, December 1974.

12. Epstein, M. and Murray, D.W., "An Elastic Stress Analysis of a Gentilly Type Containment Structure: Volume 1", Structural Engineering Report No. 55, Department of Civil Engineering, University of Alberta, Edmonton, Alberta, T6G 2G7, April 1976.

13. Epstein, M. and Murray, D.W., "An Elastic Stress Analysis of a Gentilly Type Containment Structure: Volume 2 (Appendices B to F)", Structural Engineering Report No. 56, Department of Civil Engineering, University of Alberta, Edmonton, Alberta, T6G 2G7, April 1976.

14. Epstein, M. and Murray, D.W., "A Biaxial Law for Concrete Incorporated in the BOSOR5 Code", Computers and Structures, Vol. 9, No. 1, July 1978, pp. 57-63.

15. Epstein, M., Rijub-Agha, K. and Murray, D.W., "A Two-Parameter Concrete Constitutive Law for Axisymmetric Shell Analysis", Symposium on Applications of Computer Methods in Engineering, University of Southern California, Los Angeles, California, August 23 - 26, 1977.

16. Evans, R.H. and Marathe, M.S., "Microcracking and Stress-Strain Curves for Concrete in Tension", Materials and Structures, Vol. 1, No. 1, January - February 1968, pp. 61-64.

17. Hognestad, E., "A Study of Combined Bending and Axial Load In Reinforced Concrete Members", Bulletin Series No. 399, University of Illinois Experiment Station, Vol. 49, No. 22, November 1951.

18. Hughes, B.P. and Chapman, G.P., "The Complete Stress-Strain Curve for Concrete in Direct Tension", Bulletin RILEM No. 30, March 1966, pp. 95-97.

19. Kupfer, H., Hilsdorf, H.K. and Rüsch, H., "Behavior of Concrete Under Biaxial Stresses", Journal of the American Concrete Institute, Vol. 66, No. 8, August 1969, pp. 656-666.

20. Kupfer, H.B. and Gerstle, K.H., "Behavior of Concrete Under Biaxial Stresses", Journal of the Engineering Mechanics Division, ASCE, Vol. , No. EM4, August 1973, pp. 853-866.

21. Libby, J.R., "Modern Prestressed Concrete", Van Nostrand Reinhold Company, New York, 1971.

TABLES

Table 2.1 - Approximate Segment Analysis

(a) Properties of Segment

Gross area of concrete = A_c = 331 in.^{2}
Area of reinforcement = A_s = 2.20 in.^{2}
Area of prestress steel = A_f = 1.68 in.^{2}
Net area of concrete = A'_c = 327 in.^{2}

Yield stress of reinforcing steel = σ_{ys} = 60 ksi
Yield stress of prestressing steel = σ_{yf} = 264 ksi
Tensile strength of concrete = f'_t = 0.45 ksi
Initial stress in prestressing = σ_{fo} = 153 ksi

Modulus of elasticity of steel = E_s = 29.4 x 10^3 ksi
Modulus of elasticity of concrete = E_c = 3.8 x 10^3 ksi
Modulus ratio = E_s/E_c = 29.4/3.8 = 7.74

Transformed area with reinforcement = 327 + 2.20 x 7.74 = 344 in.^{2}
Transformed area with all steel = 327 + 3.88 x 7.74 = 357 in.^{2}

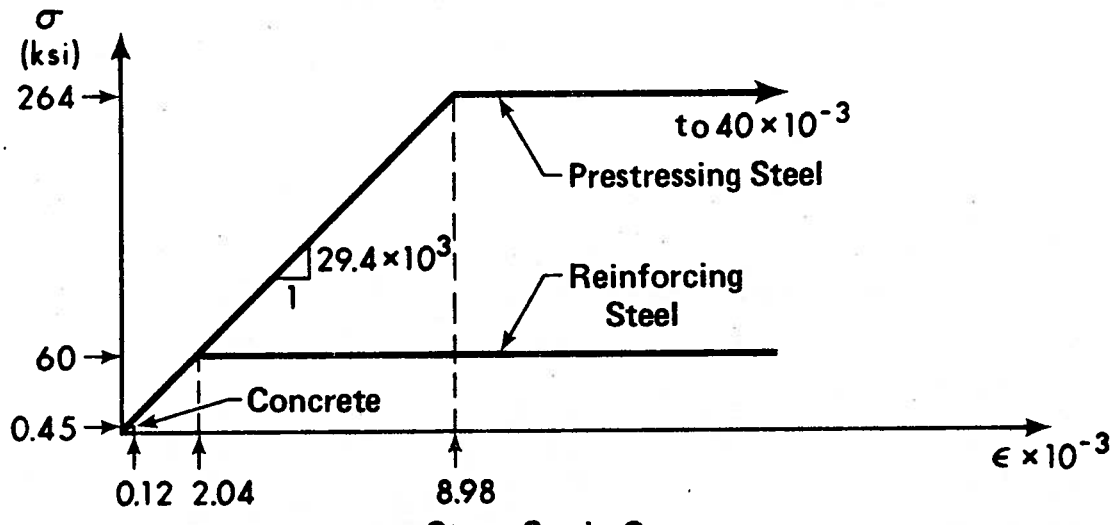

Stress-Strain Curves

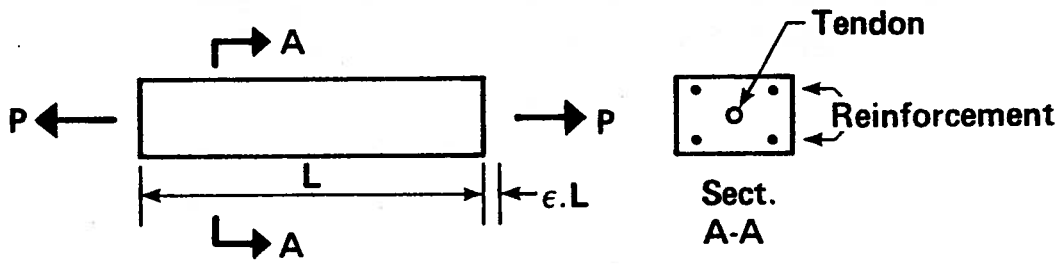

Segment

TABLE 2.1 - Approximate Segment Analysis (Continued)

(b) Limit Loads and Strains

Initial State (after all losses)

Effective Initial prestress force = 153 x 1.68 = 257 k

Effective Initial concrete stress = 257/344 = 0.747 ksi

Effective Initial steel stress = 0.747 x 7.74 = 5.78 ksi

Initial strain = $0.747/3.8 \times 10^3 = 0.0001966$

Cracking state:

1. Cracking strain in concrete = $0.45/3.8 \times 10^3 = 0.00011842$

   Change in strain to cracking = 0.00011842 + 0.0001966 = 0.000315

   Cracking load = $0.000315 \times 3.8 \times 10^3 \times 357 = 427$ k.

   Point (a) on load-strain curve = (0.000315, 427) ←

   (Check cracking load = 357 (0.747 + 0.45) = 427 k.)

2. After cracking assume all load carried by steel.

   Change in steel stress = (427 - (257 - 2.2 x 5.78))/3.88 = 47.1 ksi

   Strain after cracking = $47.1/29.4 \times 10^3 = 0.00160$

   Point (b) on load-strain curve = (0.00160, 427) ←

Reinforcing yield:

Load at yield = 60 x 2.20 + (60 + 153 + 5.78) x 1.68 = 500^k

Strain at yield = $65.78/29.4 \times 10^3 = 0.00224$

Point (c) on load-strain curve = (0.00224, 500) ←

(Check strain at point (b) = $0.00224 - (500 - 427)/29.4 \times 10^3/3.88$ = 0.00160)

Tendon yield:

Load at yield = 60 x 2.20 + 1.68 x 264 = 576^k

Strain at yield = $(264 - 153)/29.4 \times 10^3 = 0.00378$

Point (d) on load-strain curve = (0.00378, 576) ←

FORM	ZONE	FUNCTION	RANGE OF		DECOMP. OF $\dot{\bar{\varepsilon}}^p$	
			σ_1/σ_c	σ_2/σ_c	α	β
1	CC	$[\sigma_1^2 + \sigma_2^2 - \sigma_1 \sigma_2]^{1/2} - \sigma_c$	< 0	< 0	1	0
	CT	$\sigma_2 - \sigma_1 - \alpha \sigma_c - (1 - \alpha)\sigma_t$	< 0	< 0	$-\sigma_1/\sigma_c$	$1 - \alpha$
	TT	$[\sigma_1^2 + \sigma_2^2]^{1/2} - \sigma_t$	> 0	> 0	0	1
2	CC	$[\sigma_1^2 + \sigma_2^2 - 1.26\ \sigma_1 \sigma_2]^{1/2} - \sigma_c$	< 0	< 0	1	0
	CT	$\sigma_2 - \sigma_t \cdot f_1\ (\sigma_1/\sigma_c)$	$[-1/2, 0]$	> 0	$-\sigma_1/\sigma_c$	$1 - \alpha$
		$\sigma_2 - \sigma_t \cdot f_2\ (\sigma_1/\sigma_c)$	$(-1, -1/2)$	> 0	$-\sigma_1/\sigma_c$	$1 - \alpha$
	TT	$\sigma_2 - \sigma_t$	$< \sigma_2/\sigma_c$	> 0	0	1

NOTES:

1. f functions are specified in Table 2.4.
2. Variables defined in Sects. 2.1 and 2.2.
3. Equations for TC zone similar to those for CT zone but with interchange of variables and limits.

TABLE 2.2 - Two Parameter Yield Functions

FORM	ZONE	FUNCTION	RANGE OF		DECOMPOSITION OF $\dot{\varepsilon}^p$		
			σ_1/σ_c	σ_2/σ_c	α	β_1	β_2
3	CC	$[\sigma_1^2 + \sigma_2^2 - 1.26\ \sigma_1\ \sigma_2]^{1/2} - \sigma_c$	< 0	< 0	1	0	0
	CT	$\sigma_2 - \sigma_{t2} \cdot f_1(\sigma_1/\sigma_c)$	$[-1/2, 0)$	> 0	$-\sigma_1/\sigma_2$	0	$1 - \alpha$
		$\sigma_2 - \sigma_{t2} \cdot f_2(\sigma_1/\sigma_c)$	$(-1, -1/2)$	> 0	$-\sigma_1/\sigma_c$	0	$1 - \alpha$
	TT	$[\sigma_1^2\ \sigma_{t2}^2 + \sigma_2^2\ \sigma_{t1}^2]^{1/4} - [\sigma_{t1}\ \sigma_{t2}]^{1/2}$	> 0	> 0	0	$(B_1/B)^2$	$(B_2/B)^2$
4	CC	$\sqrt{\sigma_1^2 + \sigma_2^2 - 1.23\ \sigma_1\ \sigma_2} - \sigma_c$	< -0.8	< -0.8	1	0	0
		$\sigma_c \cdot f_3(\sigma_2/\sigma_c) - \sigma_1$	< -0.8	> -0.8	1	0	0
	CT	$\sigma_{t2} \cdot f_4(\sigma_1/\sigma_c) + \sigma_2$	$[-1, -0.5]$	> 0	$-\sigma_1/\sigma_c$	0	$1 - \alpha$
		$\sigma_2 - \sigma_{t2} \cdot f_5(\sigma_1/\sigma_c)$	$(-0.5, 0]$	> 0	$-\sigma_1/\sigma_c$	0	$1 - \alpha$
	TT	$\sqrt{\sigma_{t1}\ \sigma_{t2}} \cdot f_6(\sigma_1/\sigma_{t1}, \sigma_2/\sigma_{t2})$	> 0	> 0	0	$(B_1/B)^2$	$(B_2/B)^2$

NOTES:

1. f functions are specified in Table 2.4.
2. Variables defined in Sects. 2.1 and 2.2.
3. Equations for TC zone similar to those for CT zone but with interchange of variables and limits.

TABLE 2.3 - Three Parameter Yield Functions

$$f_1 = (x) = 1.0 - 2.4356\ x^2 - 2.5808\ x^3$$

$$f_2\ (x) = 2.1452 + 6.8712\ x + 11.3068\ x^2 + 6.5808\ x^3$$

$$f_3\ (x) = -1 + 1.1\ x + 1.46150732\ x^2 + 0.631430697\ x^3$$

$$f_4\ (x) = -0.4 + 2.4\ x + 2.8\ x^2$$

$$f_5\ (x) = 1 - 0.4\ x^2$$

$$f_6\ (x_1, x_2) = 0.01 - \frac{(1 - 0.99\ x_1 + 0.0098\ x_1\ x_2)(1 - 0.99\ x_2 + 0.0098\ x_1\ x_2)}{(1 - 0.0001\ x_1\ x_2)^2}$$

TABLE 2.4 - f Functions of Tables 2.2 and 2.3

SPECIMEN	CONCRETE POUR	TENDON STRESSING	GROUTING	CYLINDER TESTS	SPECIMEN TESTING	LOAD RATIO*
1	May 30	June 29 (30 days)	July 5 (36 days)	Aug. 22 (84 days)	Aug. 22 (84 days)	2:1
3	May 30	July 4 (35 days)	July 5 (36 days)	Sept. 15 (108 days)	Sept. 6 (99 days)	1:1
2	May 30	June 29 (30 days)	July 5 (36 days)	Aug. 30 (92 days)	Aug. 30 (92 days)	2:1

* DIRN. 1/DIRN. 2

TABLE 2.5 - Chronology of Specimens

SPECIMEN	1	2	3
AGE @ TESTING	90 days	114 days	97 days
(a) Compression (f_c)	5093	4540	5694
		4670	
		4170	
Avg. f'_c	5093	4460	5694
Analysis	4600	4600	4600
(b) Tension (f'_t)	504	406	442
	477	424	411
		477	
Avg. f'_t	490	436	426
Analysis f'_t	490	-	426

(a) Concrete Strengths (psi)

SPECIMEN	2	3
AGE	104	98
STRESS RATIO	2:1	1:1
E_{c1}	3.95	3.55
E_{c2}	4.21	2.96

(b) Derived Concrete Moduli (x 10^6 psi)

TABLE 2.6 - Specimen Concrete Data

A. HOGNESTAD RELATIONS (17)

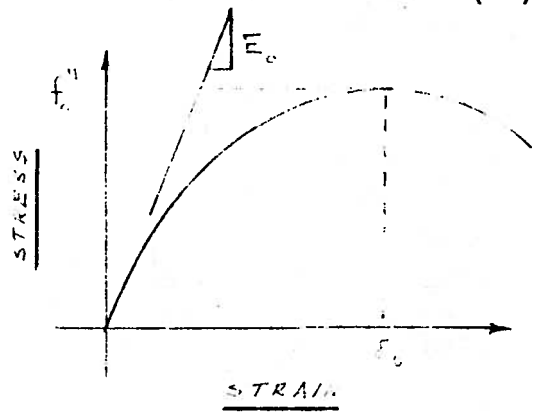

$$f_c'' = 0.92\, f_c' \qquad (1)$$

$$f = \left[2\,\frac{\varepsilon}{\varepsilon_o} - \left(\frac{\varepsilon}{\varepsilon_o}\right)^2\right] f_c'' \qquad (2)$$

$$\varepsilon_o = \frac{2\, f_c'}{E_o} \qquad (3)$$

B. ASSUMPTIONS FOR UNIAXIAL COMPRESSION CURVE

$f_c' = 4600$ psi $\qquad E_o = 3.8 \times 10^6$ psi

$f_c'' = 4230$ psi (Eq. A.1) $\qquad \varepsilon_o = \dfrac{2 \times 4600}{3.8 \times 10^6} = 0.0024$ (Eq. 3)

Consider a uniaxial curve defined by the five points a - e of C. Point c has been determined above as (0.0024, 4230). For Point a, assume initial yield at $0.45\, f_c'' = 1904$ psi. The corresponding strain is $\varepsilon_a = 1904/3.8 \times 10^6 = 0.501 \times 10^{-3}$. Place Point b on the Hognestad curve at $\varepsilon = 0.0015$. Solve Eq. A.2 for $f_b = 3637$ psi. Arbitrarily place points d and e as shown below.

C. APPROXIMATE UNIAXIAL COMPRESSION CURVE

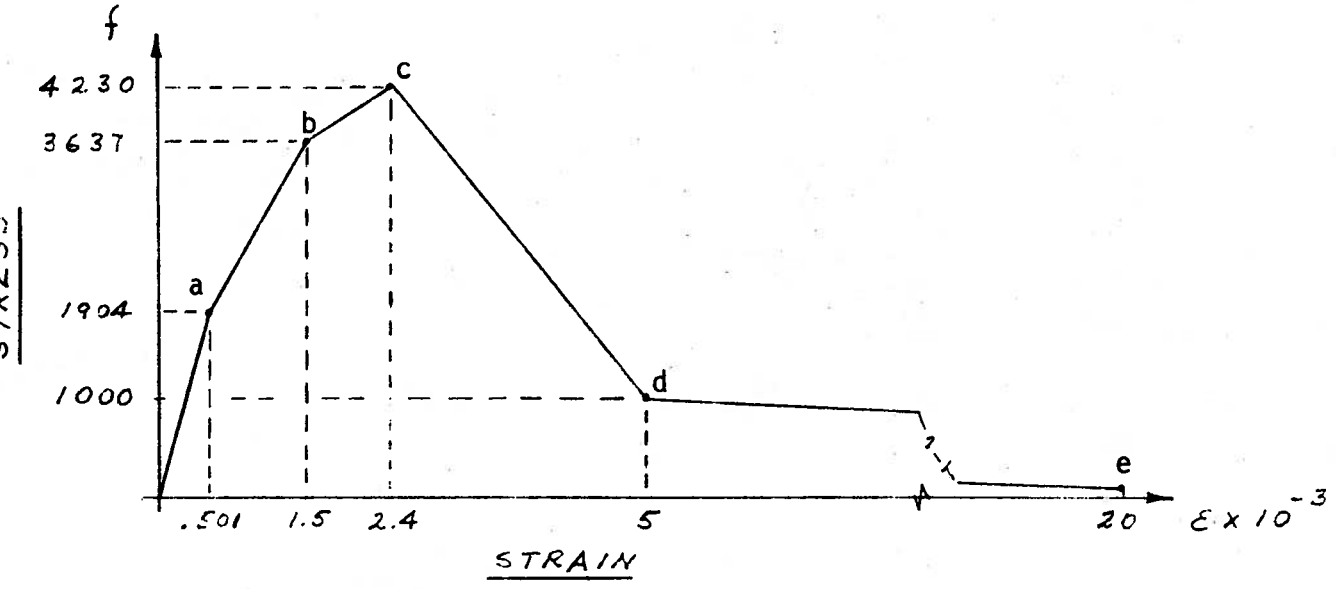

TABLE 2.7 - Approximate Uniaxial Compression Curve

(a) TENSILE RESPONSE ASSUMPTIONS

Brazilian test tensile strength = f_t' = 490 psi

x .90 reduction to direct tensile strength (26, pg. 483)

x .83 reduction for loading rate (23, pg. 759)

x .85 reduction for size effects (26, pg. 492)

= .63

Assume effective f_t'' = .60 x 490 = 294 psi

Assume strain at maximum strength = 1.2×10^{-4} (15)

Assume initial nonlinearity at .45 f_t'' = 132 psi

Assume initial softening to 0.95 f_t'' = 280 psi at ϵ = 0.0003.

(b) TENSILE RESPONSE: SPECIMEN 1

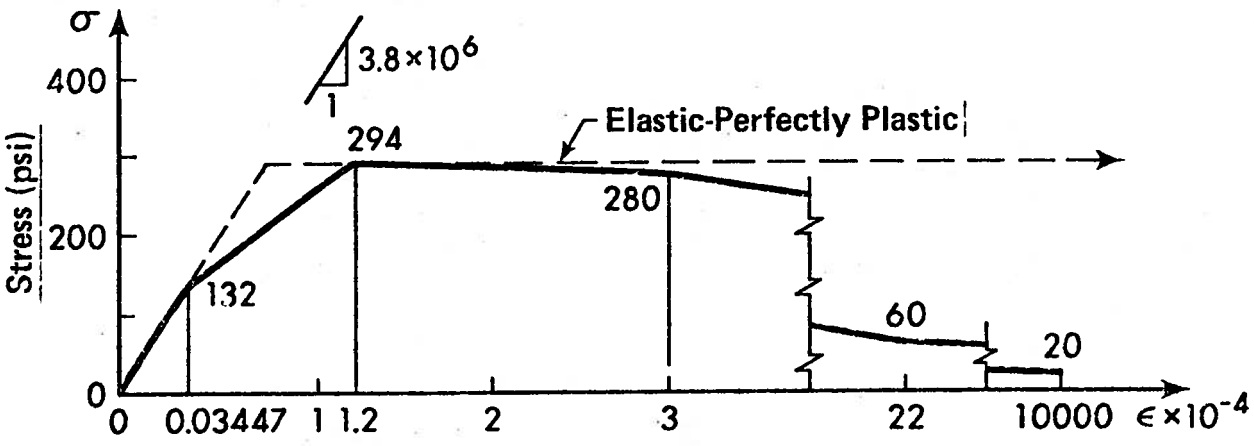

(b) Effective Tensile Stress-Strain Curve (f_t=490)

TABLE 2.8 - Estimation of Tensile Response

(c) TENSILE RESPONSE: SPECIMEN 3

Brazilian test = 424+

Assumed effective $f_t'' = 0.60 \times 424 = 254$ psi

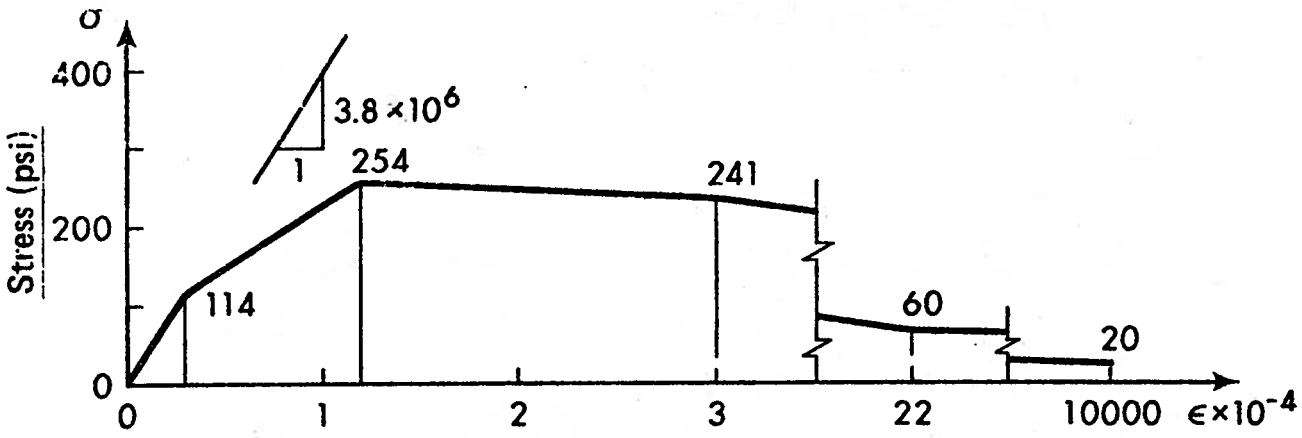

(c) Effective Tensile Stress-Strain Curve (f_t=424)

\+ The actual test value was 426 psi, but the above stresses were used for BOSOR5 analysis.

TABLE 2.8 - Estimation of Tensile Response
(continued)

COMPONENT	LAYER		1	2	3	4	5	6	7	8	9	10	11	12	13	14	15
	1	t ID d	1.16395 C 2.5	0.08205 VR	0.008 VS	0.08205 VR	1.16395 C										
	2	t_1 ID t_2* d	0.7923 C 5	0.0267 HW	0.01 VW	0.05 VR 0.0004	1.58725 C 1.58455	0.03875 VR 0.08205	0.08 VS	0.03875 VR 0.08205	0.7009 C 0.06576	0.0127 HS	0.86465 C 0.91425	0.05 VR 0.0004	0.01 VW	0.0267 HW	0.7923 C
	3	t ID d	0.7923 C 5	0.0267 HW	0.01 VW	1.6670 C	0.008 VS	0.73965 C	0.0127 HS	0.91465 C	0.01 VW	0.0267 HW	0.7923 C				
	4	t_1 ID t_2+ d	0.7923 C 10	0.0267 HW	0.010 VW	1.667 C	0.008 VS	1.667 C	0.01 VW	0.0267 HW	1.0285 C 1.0422	0.0276 HS 0.0002	3.695 C 3.7087	0.0412 HR	0.040 VR	0.96 C	
	5	t_1 ID t_2 d_1, d_2	0.7117 C 4	0.0133 VW 10.98	0.0133 HW	1.24975 C 4.48935	0.02392 VS 0.02466	0.7870 C 0.7866	0.0221 HS	0.44065 C 4.18065	0.0133 HW	0.0133 VW	0.7117 C				
	6	t ID t d	0.7086 C 4	0.0164 VW	0.0133 HW	1.2502 C 1.24975	0.02301 VS 0.02392	0.78745 C 0.7870	0.0221 HS	0.44065 C	0.0133 HW	0.0164 VW	0.7086 C				
	7	t ID t d	0.7110 C 4	0.0140 VW	0.0133 HW	1.25065 C 1.2502	0.0221 VS 0.02301	0.7879 C 0.78745	0.0221 HS	0.44065 C	0.0133 HW	0.0140 VW	0.7110 C				

Notes:
1. All dimensions in inches.
2. ID NOTATION: C = Concrete
   H = Horizontal (θ); S = Strand
   V = Vertical (ϕ); R = Reinforcing
   W = Wire
3. t_1 = thickness at top of component
   t_2 = thickness at bottom of comp.
   d_1 = thickness of section (top)
   d_2 = thickness of section (bottom)
4. When t_2 is not shown it is = t_1.
5. * Tapers to t_1 in 3 inches.
6. + Extends for 3.58 inches.

TABLE 3.1 - Details of Component Layers

(a) Determination of A_o and p_o:

1 - 0.62'' ϕ strand: $A = 0.232$ in.^{2}

10" spacing: $A_o = \frac{0.232 \text{ in.}^2}{10 \text{ in.}} \times 12 \frac{\text{in.}}{\text{ft.}} = 0.278$ in^2/ft

Strand stress @ 57% of $f_{pu} = 0.57 \times 270$ ksi $= 154$ ksi

Strand force/unit width $= 154 \times 0.278 = 42.8$ kips/ft

$p_o = 2 \times 42.8/R = 85.6/9.833 = 8.71$ k/ft$^2 \times 144 = 60.5$ psi

(b) Prestress losses

From § 18.6.2 of ACI Standard 318-71

$$P_s = P_x (1 + K x + \mu \alpha)$$

P_s = force at anchorage

P_x = force at distance x from anchorage

K = wobble coefficient = 0.008 } as estimated by

μ = curvature coefficient = 0.20 } local manufacturers

α = angle change in radians.

Solve for P_x,

$$P_x = \frac{P_s}{1 + \gamma x}, \quad \gamma = K + \frac{\mu}{R} = 0.0211$$

Anchorage angle to outside of ring beam $= \sin^{-1}(5.67/9.833)$

$= 0.6142$ rad (35.19)

Length to crown $= 0.6142 \times 9.833 = 6.039$ ft.

Non-dimensional form: $P_x/P_s = 1/(1 + 0.1274\ x/L)$

At crown $x/L = 1$, $P_x/P_s = 0.887$ (Loss = 11.3%)

TABLE 3.2 - Computations for Dome Prestressing
(First Model)

(a) Prestress loss in cylinder wall

R = 5.115 ft. $\quad \gamma = 0.0399$

For $\alpha = \pi/4 \quad P_x/P_s = 1/(1 + 0.0399 \times 5.115 \times \pi/4)$

$= 0.8619 \quad$ (Loss = 13.8%)

(b) Level of frictionless cylinder prestress:

Horizontal: 1 - 0.5'' ϕ strand/ft. @ 0.60 f_{pu}

$= 0.152$ in.^{2} x 0.60 x 270 ksi = 24.6 k/ft.

Vertical: 20 - 0.5'' ϕ strand @ 0.38 f_{pu}

$= 20 \times 0.152$ in.^{2} x 0.38 x $270/(2\pi \times 5.0417)$

= 9.85 k/ft.

(c) Effective prestressing pressure:

Mid-surface pressure to produce 24.6 k/ft.

$= \frac{24.6}{5.042} = 4.88$ psf

Reduced effective pressure = 0.862 x 4.88 = 4.206 psf

TABLE 3.3 - Computations for Cylinder Prestressing (First Model)

Layer / Segment	MATERIAL TYPES														
	1	2	3	4	5	6	7	8	9	10	11	12	13	14	15
1	1	2	3	2	1										
2	1	4	5	2	1	2	3	2	1	6	1	2	5	4	1
3	1	4	5	1	3	1	6	1	5	4	1				
4	1	4	5	1	3	1	5	4	1	7	1	4	2	1	
5	1	5	4	1	8	1	9	1	4	5	1				
6	1	5	4	1	8	1	9	1	4	5	1				
7	1	5	4	1	8	1	9	1	4	5	1				

TABLE 3.4 - Material Types for Component Layers
(First Model)

STEP	LOAD (psig)	LOAD INCREMENT	NO. OF TRIALS[1]
1	Gravity		2
2	Gravity & Prestress		3
3	Gravity & Prestress & wt. wt. of water		3
4	20.0	20.0	2
5	40.0	20.0	3
6	55.0	15.0	5
7	65.0	10.0	6
8	75.0	10.0	6
9	82.0	7.0	4
10	83.25	1.25	3
11	84.50	1.25	2
12	85.50	1.00	2
13	86.50	1.00	8
14	87.50	1.00	5
15	91.00	3.50	14
16	94.00	3.00	12
17	95.50	1.50	4
18	97.00	1.50	6
19	98.50	1.50	8
20	100.00	1.50	7
21	101.50	1.50	5
22	103.00	1.50	8
23	105.00	2.00	9
24	107.00	2.00	9
25	108.00	1.00	9
26	108.75	0.75	5

1 The number of trials refers to the number of sets of Newton-Raphson iterations required by BOSOR program to obtain convergence.

TABLE 3.5 - Summary of Productive Runs for First Model

Seg.	Pt	1	2	3	4	5	6	7	8	9	10	11
1 t = 2.5" ℓ = 0.75"	-	Mat 1 1.14395	Mat 2 .02	Mat 3 .08205	Mat 4 .008	Mat 3 .08205	Mat 2 .02	Mat 1 1.14395				
2 t = 5" ℓ = 30"	 1 5 7 12 14	Mat 5 .8383 .8383	Mat 2 .0367 .0367	Mat 3 .0001 .0071 .0170 .0170 .0170	Mat 3 .0117 .0433 .0500 .0125 .0001	Mat 5 1.5388 1.5260 1.5152 1.5914 1.6038	Mat 3 .0704 .0446 .0388 .0001 .0001	Mat 4 .008 .008	Mat 3 .0704 .0446 .0388 .0001 .0001	Mat 5 .6680 .6938 .6996 .7383 .7383	Mat 6 .0152 .0152	Mat 5 .8556 .8170 .8004 .8379 .8503
3 t = 5" ℓ = 90"	-	Mat 5 .0838	Mat 2 .0367	Mat 3 .0170	Mat 5 1.604	Mat 4 .008	Mat 5 .7384	Mat 6 .0152	Mat 5 .8504	Mat 3 .0170	Mat 2 .0367	Mat 5 .8383
4 Fig. 4.2 ℓ = 7.6155"	 1 3 5 6 7 10	Mat 5 .8383 .8383 .8383 .8383 .6667 .6673	Mat 2 .0367 .0367	Mat 3 .0170 .0304 .0396 .0445 .0466 .0460	Mat 5 1.6040 1.5906 1.5814 1.8065 2.1460 2.5260	Mat 4 .008 .008	Mat 5 1.6040 1.5837 1.5977 1.6049 1.6081 1.6209	Mat 3 .0153 .0373 .0233 .0161 .0129 .0001	Mat 2 .0367 .0367	Mat 5 .1690 1.0882 1.0882 1.0882 1.0413 1.0413	Mat 6 .0001 .0001 .0001 .0001 .0940 .0940	Mat 5 .1690 .6515 3.8375 3.8375 3.9522 3.9522
5 Fig. 4.2 ℓ = 3.1904"	 1 2 4 6 7	Mat 5 .7040 .7008 .7031 .7090 .71045	Mat 3 .0460 .0492 .0440 .0410 .03955	Mat 2 .0594 .0486 .0440 .0440 .0440	Mat 5 2.4666 2.5374 2.70205 3.4444 3.7525	Mat 4 .0080 .0080 .0079 .0072 .0070	Mat 5 6.22595 5.7479 3.95675 .88315 .2656	Mat 7 .0001 .0137 .0159 .0208 .0218	Mat 5 .46845 .93410 2.7805 6.46565 7.3133	Mat 2 .0515 .0623 .0669 .0668 .0448	Mat 10 .0449 .0461 .0452 .0393 .0343	Mat 11 .7051 .7039 .7148 .7807 .8597

(Continued ...)

TABLE 4.1 - Details of Component Layers (Second Model)

Seg.	Pt	1	2	3	4	5	6	7	8	9	10	11
6		Mat 5	Mat 3	Mat 2	Mat 5	Mat 7	Mat 5	Mat 4	Mat 5	Mat 6	Mat 5	Mat 2
Fig. 4.2	1	.71045	.03955	.0440	4.0251	.0218	.1056	.007	2.1585	.056	5.0092	.0558
ℓ = 3.164"	2	.7119	.0381	.0440	3.7341	.0227	.7458	.0068	2.2486	.056	5.2172	.0448
	4	.7193	.0307	.0355	3.3418	.0242	2.0895	.0060	2.4850	.056	1.3580	.0540
	5	.7300	.0200	.0128	3.0739	.0253	3.7954	.0052	.3473	.0001	.6072	.0128
	7	.7372	.0119	.0128	2.8652	.0258	3.5077	.0001	.2229	.0001	.2072	.0128
7		Mat 5	Mat 3	Mat 8	Mat 5	Mat 7	Mat 9	Mat 5	Mat 8	Mat 3	Mat 5	
ℓ = 15.47"	1	.7372	.0119	.0128	2.8652	.0258	.0232	3.6113	.0128	.0266	.7372	
	3		.0122		2.63495	.0257		3.00595		.0180		
	5		.0127		2.2845	.0256		2.4313		.0127		
	6		.0133		1.92395	.0255		1.89075		.0133		
	7		.0140		1.6733	.0254		1.5201		.0140		
	8		.0149		1.4525	.0252		1.3293		.0149		
	9	.7372	.0158	.0128	1.22165	.0251	.0232	1.19845	.0128	.0158	.7372	
8		Mat 5	Mat 3	Mat 8	Mat 5	Mat 7	Mat 9	Mat 5	Mat 8	Mat 3	Mat 5	
t = 4"	1	.7372	.0158	.0128	1.22165	.0251	.0232	1.19845	.0128	.0158	.7372	
ℓ = 22.13"	2		.0169		1.2206	.0250		1.1974		.0169		
	7	.7372	.0134	.0128	1.22455	.0241	.0232	1.20135	.0128	.0134	.7372	
9		Mat 5	Mat 3	Mat 8	Mat 5	Mat 7	Mat 9	Mat 5	Mat 8	Mat 3	Mat 5	
t = 4"	1	.7372	.0134	.0128	1.22455	.0241	.0232	1.20135	.0128	.0134	.7372	
ℓ = 22.13"	4		.0150		1.2232	.0236		1.2000		.0150		
	8	.7372	.0128	.0128	1.2256	.0232	.0232	1.2024	.0128	.0128	.7372	

(Continued ...)

TABLE 4.1 - Details of Component Layers (Second Model)

Additional Layers

Seg.	Pt	12	13	14	15
2	-	Mat 3	Mat 3	Mat 2	Mat 5
	1	.0117	.0001	.0367	.8383
	5	.0433	.0071		
	7	.0500	.0170		
	12	.0125	.0170		
	14	.0001	.0170	.0367	.8383
4	-	Mat 2	Mat 3	Mat 5	
	1	.0001	.0001	.500	
	3	.0075	.0080	.500	
	5	.0375	.0410	.8340	
	6	.0375	.0405	.8345	
	7	.0375	.0400	.6733	
	10	.0375	.0449	.6684	
6	-	Mat 3	Mat 5		
	1	.0368	.8232		
	2	.0343	.8597		
	4	.0417	.7343		
	5	.0340	.6450		
	7	.0266	.5734		

(Final ...)

TABLE 4.1 - Details of Component Layers
(Second Model)

Material Number	Description	Figure No.
1	Concrete: Elastic-Plastic: f'_t = 60 psi; f'_c = 3000 psi	
2	#3 Rebars: f_y = 50.9 ksi	Fig. 4.3b
3	6 mm. Meridional Rebars: f_y = 72.5 ksi	Fig. 4.3b
4	0.5" ϕ Meridional Strands; f_{pi} = 90 ksi	Fig. 4.4a
5	Concrete: Degrading: f'_t = 490 psi	Table 2.8b
6	0.5" ϕ Circumferential Strands; f_{pi} = 137.7 ksi	Fig. 4.4a
7	0.62" ϕ Meridional Strands: f_{pi} = 113.1 ksi	Fig. 4.4b
8	6 mm. Circumferential Rebars: f_y = 72.5 ksi	Fig. 4.3b
9	0.62" ϕ Circumferential Strands: f_{pi} = 113.1 ksi	Fig. 4.4b

TABLE 4.2 - Identification of Material Types
(Second Model)

STEP	LOAD (psig)	LOAD INCREMENT	NO. OF TRIALS
1	Gravity		3
2	Gravity & Prestress		4
3	30.0	30.0	4
4	50.0	20.0	7
5	55.0	5.0	5
6	60.0	5.0	3
7	67.0	7.0	10
8	74.0	7.0	7
9	79.5	5.5	9
10	84.5	5.0	12
11	87.25	2.75	8
12	90.00	2.75	7
13	92.50	2.50	6
14	95.00	2.50	5
15	98.50	3.50	5
16	102.00	3.50	5
17	105.50	3.50	4
18	109.00	3.50	6
19	111.50	2.50	4
20	114.00	2.50	5
21	116.00	2.00	5
22	117.00	1.00	6
23	118.50	1.50	11
24	119.00	0.50	9
25	119.50	0.50	10
26	120.00	0.50	10
27	120.50	0.50	7

TABLE 4.3 - Summary of Productive Runs for Second Model

	Limit State	Model 1	Model 2
1.	Hinge Cracking	42	-
2.	First Cracking	45	30
3.	Through Cracking	58	62
4.	First Meridional Rebar Yield	87.5	95
5.	First Circumferential Rebar Yield	105	109
6.	First Meridional Strand Yield	98.5	106
7.	First Circumferential Strand Yield	91	110
8.	First Concrete Crushing at the Hinge	89	95
9.	Extrapolated Ultimate Load	123	132

TABLE 4.4 - Comparison of Limit States

FIGURES

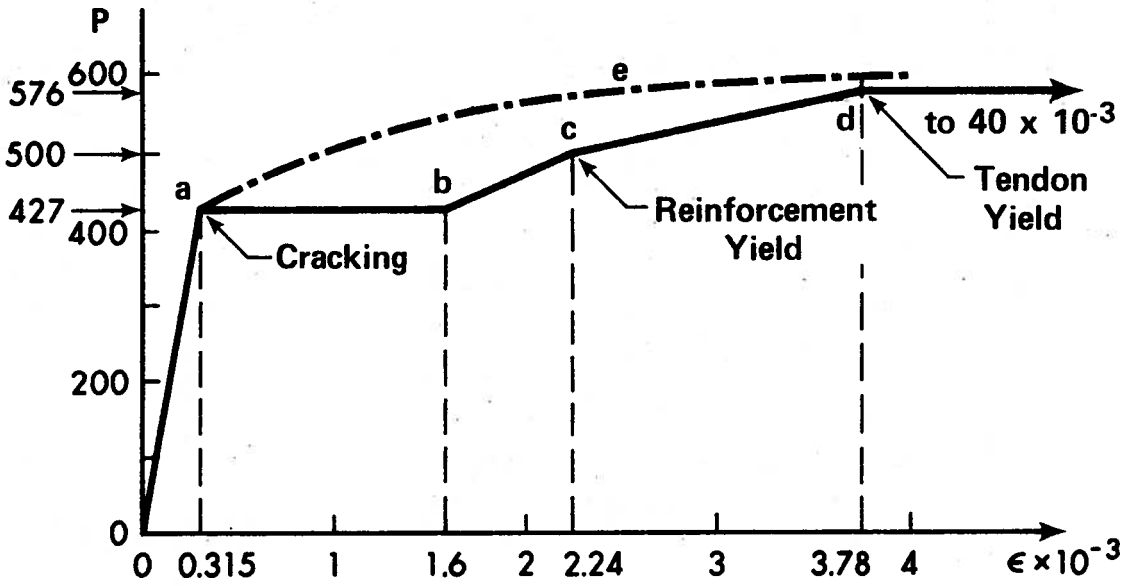

Figure 2.1 - Approximate Load-Strain Plot for Segment

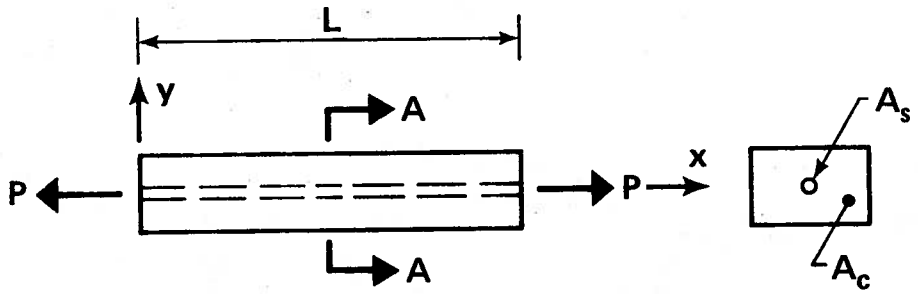

(a) Specimen

Sect. A-A

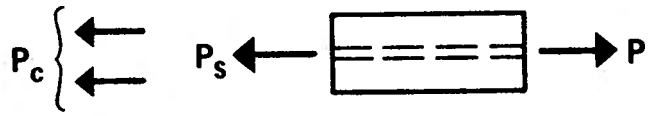

(b) Free Body Diagram

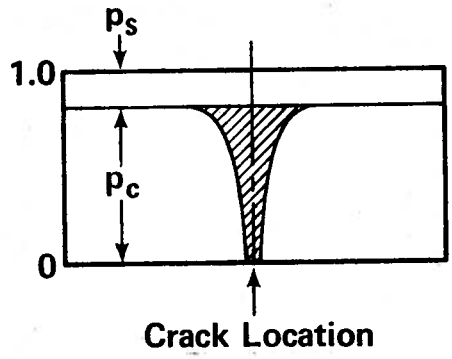

(c) Division of Load Between Steel and Concrete

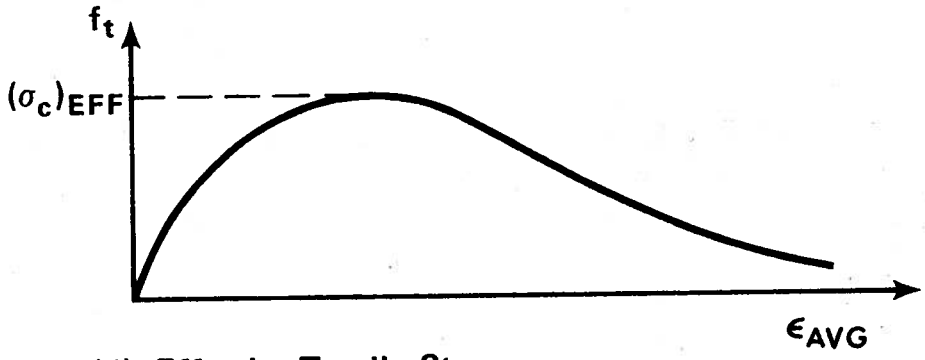

(d) Effective Tensile Stress - Strain Relationship for Concrete

Figure 2.2 - Simulation of Tensile Behavior for Concrete

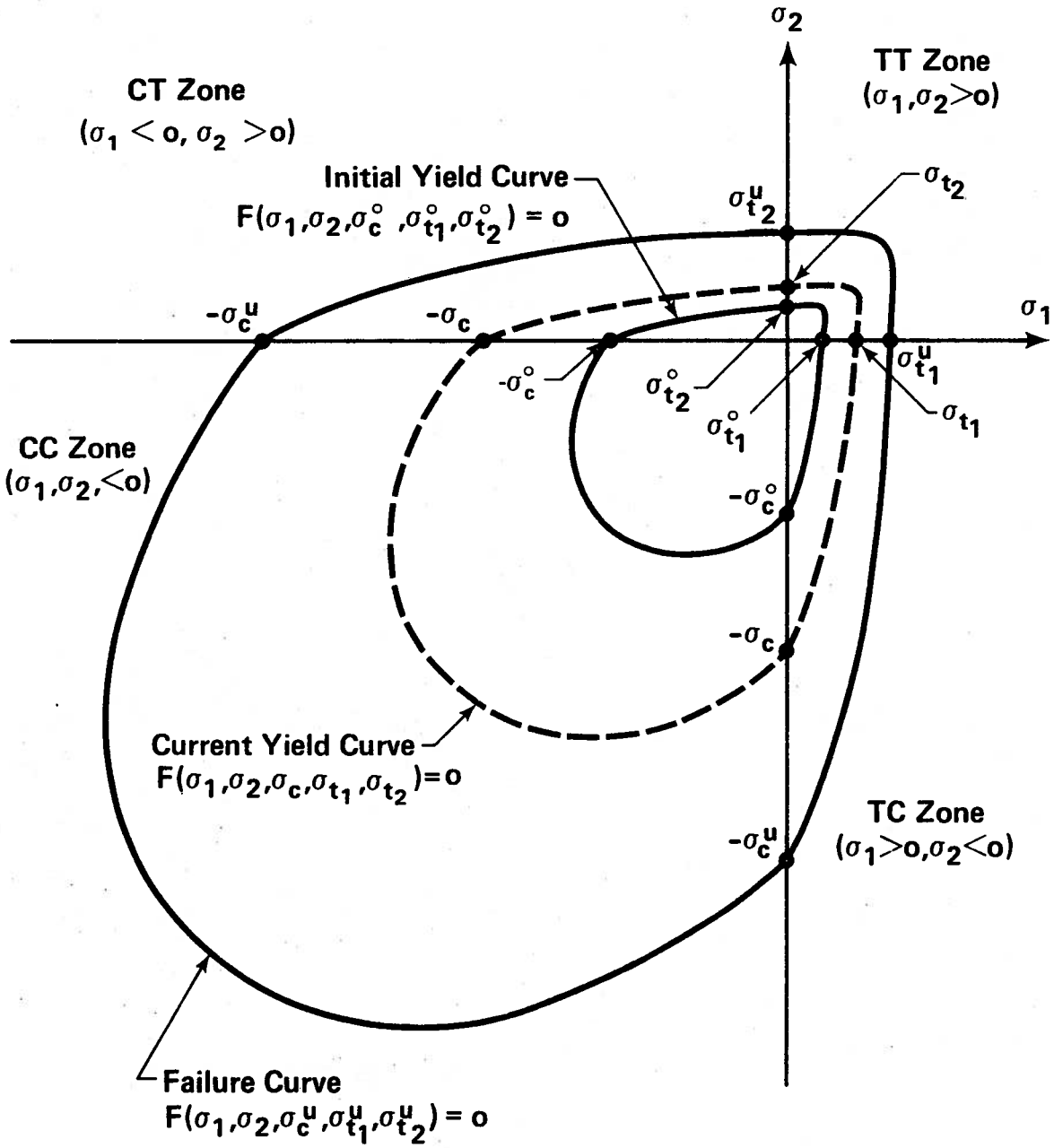

Figure 2.3 - Schematic of Failure, Initial Yield, and Current Yield Curves

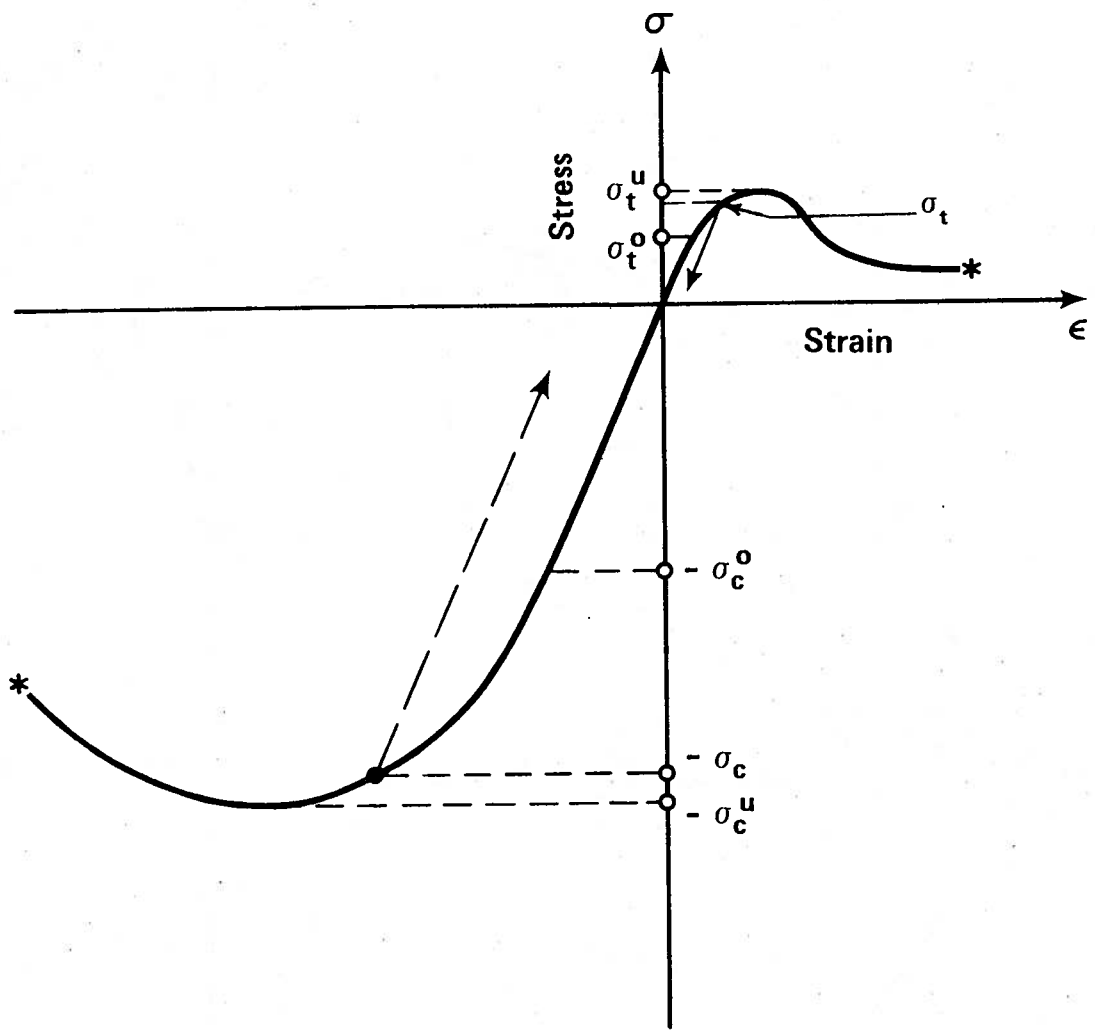

Figure 2.4 - Idealized Uniaxial Response of Concrete

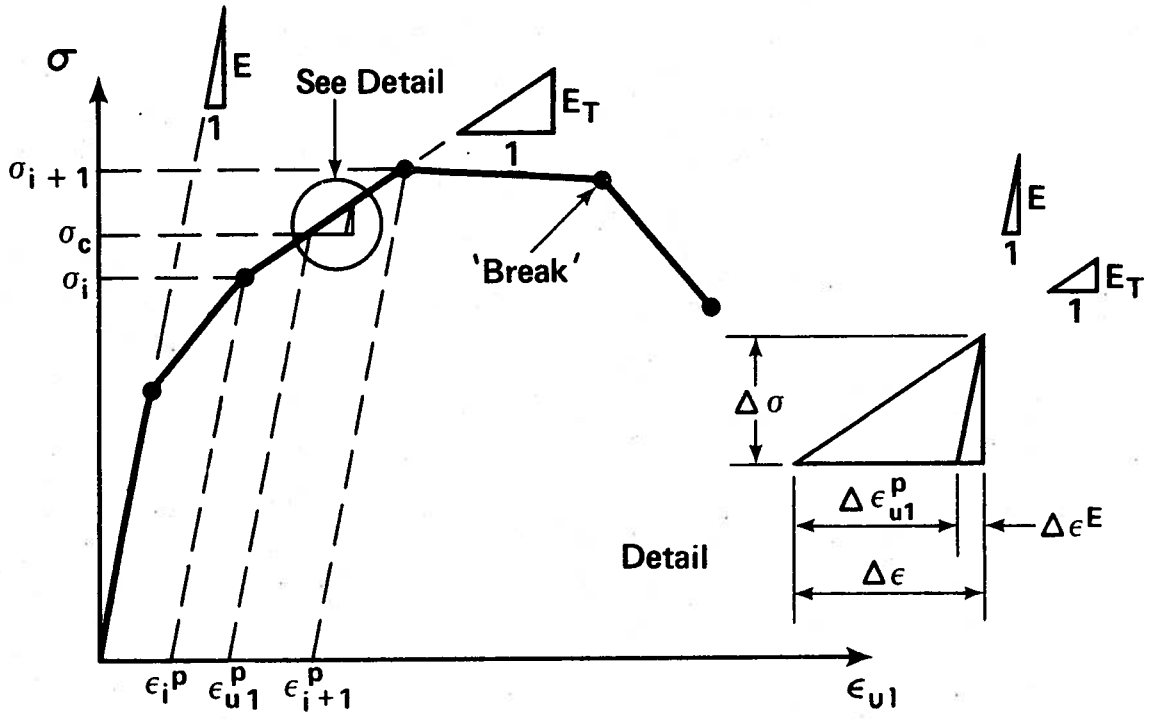

(a) Linearized Uniaxial Strain (Compressive)

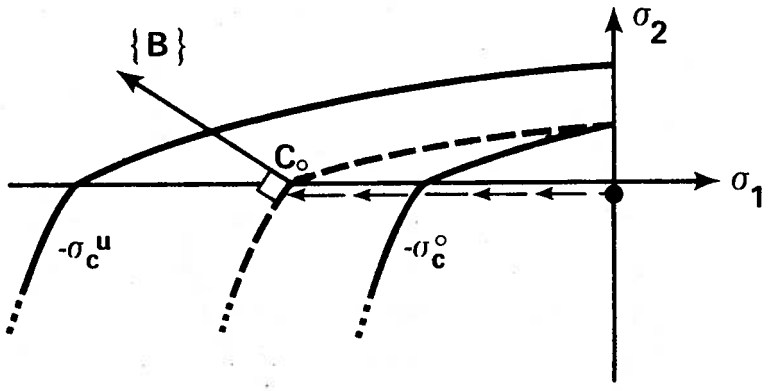

(b) Stress Path (Uniaxial Compression)

Figure 2.5 - Uniaxial Hardening

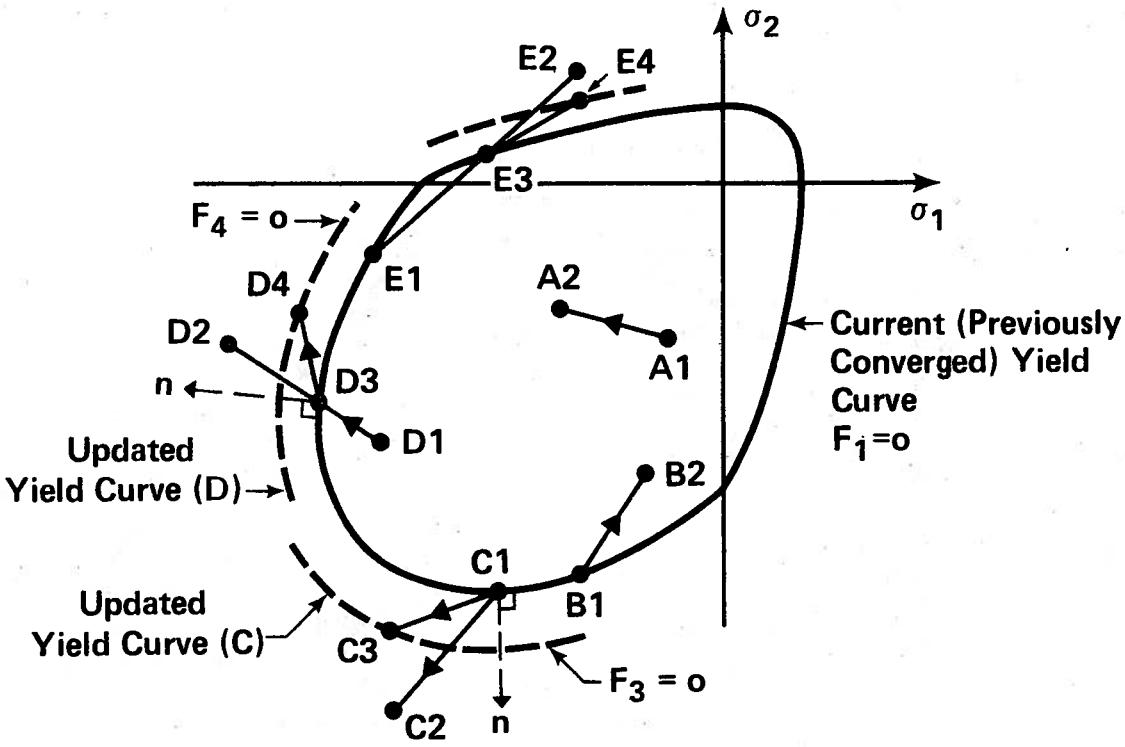

(a) Possible Stress Points

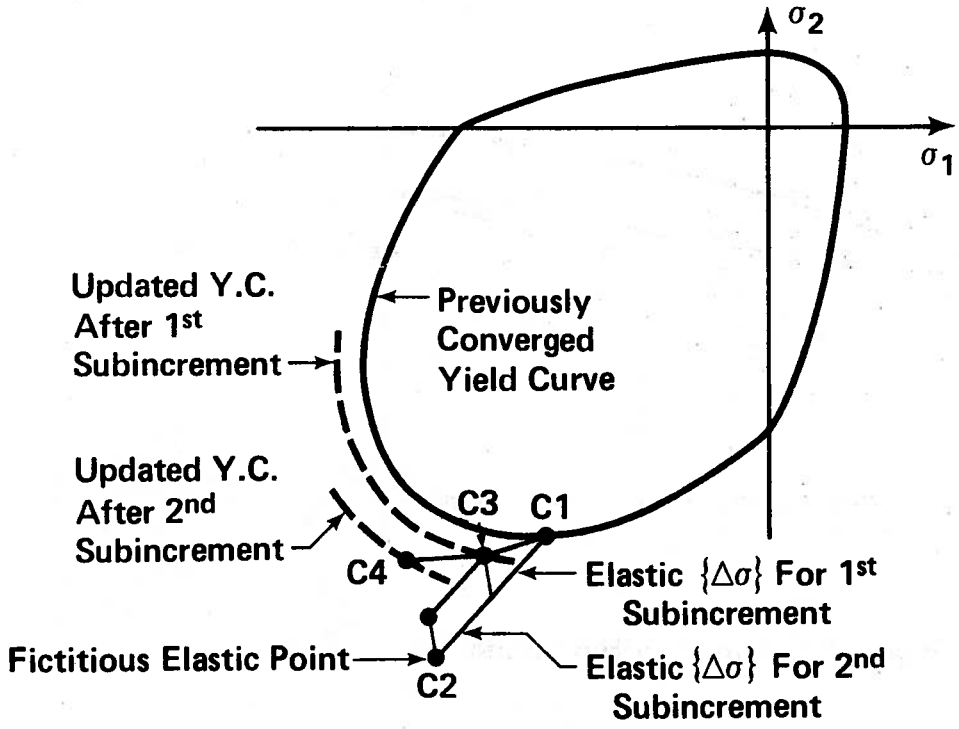

(b) Subincrement Technique (2 Subincrements)

Figure 2.6 - The Subincrement Technique

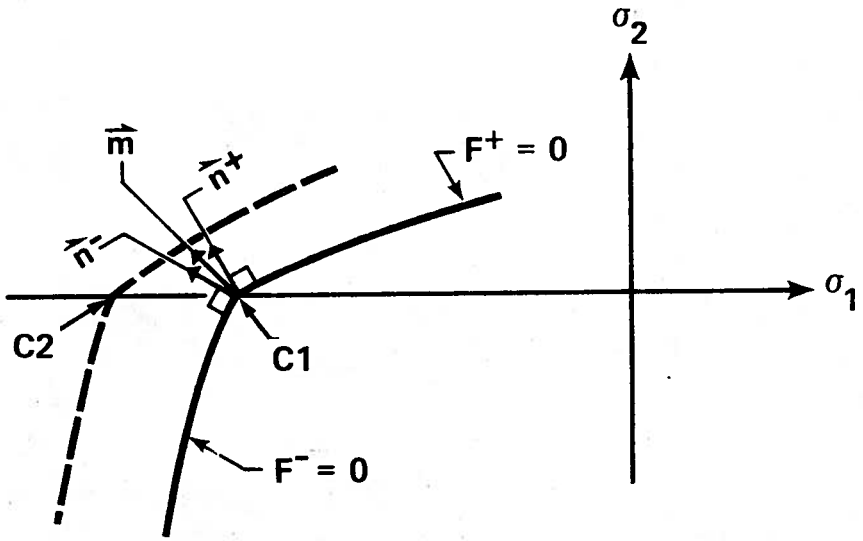

(a) Unit Vectors at Corner

Combination	1	2	3	4
Sign of $\dot{\sigma}_2$ with $\vec{m} = \vec{n}^+$	+	−	+	−
Sign of $\dot{\sigma}_2$ with $\vec{m} = \vec{n}^-$	+	−	−	+
Use $\vec{m} = \vec{n}^+$ and F^+	*			
Use $\vec{m} = \vec{n}^-$ and F^-		*		
Use $\vec{m}$ between $\vec{n}^+$ and $\vec{n}^-$			*	*

(Note: $\dot{\sigma}_2$ evaluated by Eq. 2.3.23 b)

(b) Decision Table for Corner

Figure 2.7 - Corner Criteria

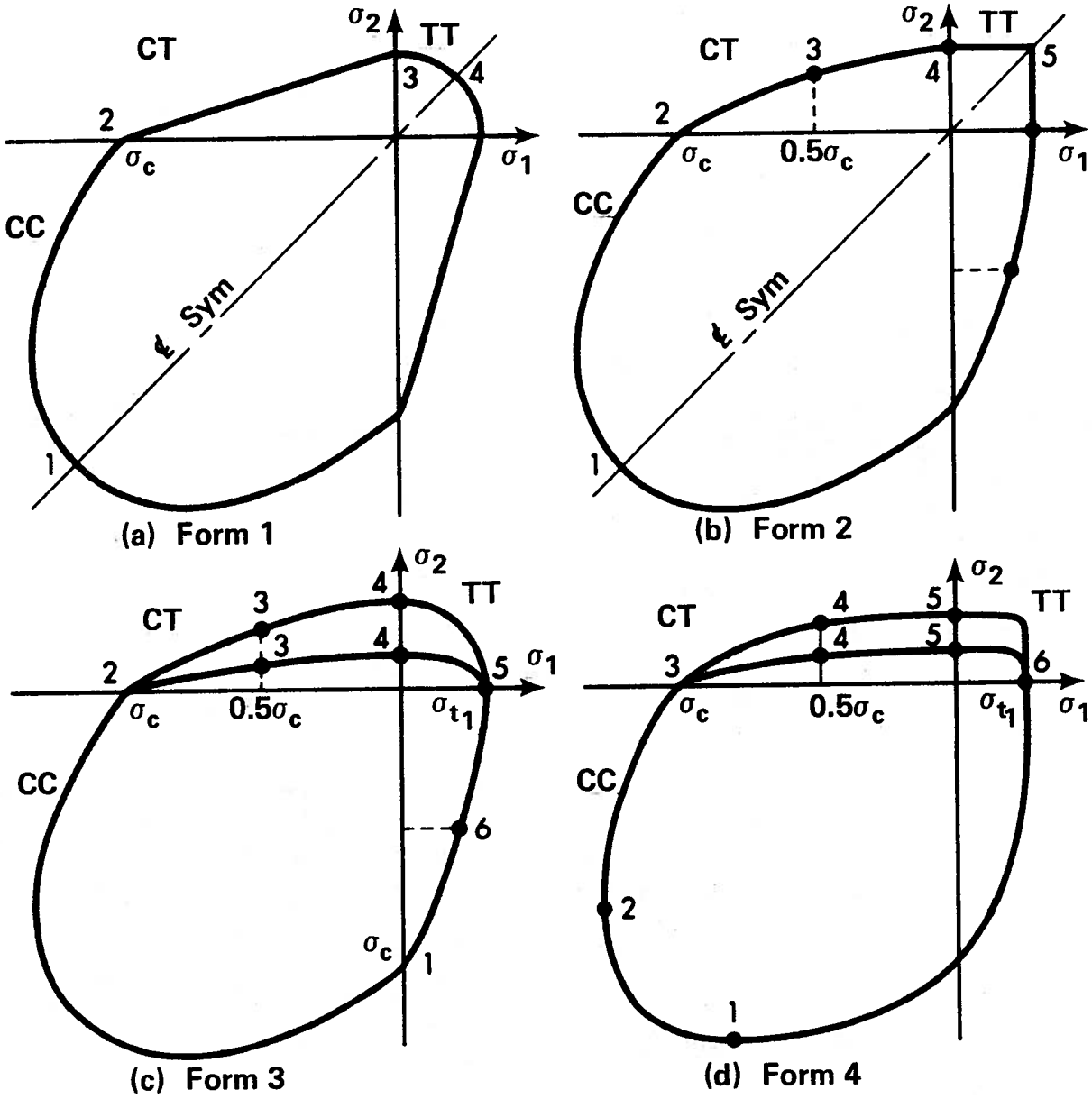

Notes: a) • = Point of Tangency
b) Yield Functions are not to Scale

Curve Segment	Form 1	Form 2	Form 3	Form 4
1-2	Mises ellipse	Elong ellipse	Elong ellipse	Elong ellipse
2-3	Straight line	Cubic spline	Cubic spline	Cubic spline
3-4	Circle	Cubic spline	Cubic spline	Quadratic spline
4-5		Straight line	Ellipse	Quadratic spline
5-6				Hyperbola

(e) Identification of Curve Segments

Figure 2.8 - Yield Functions

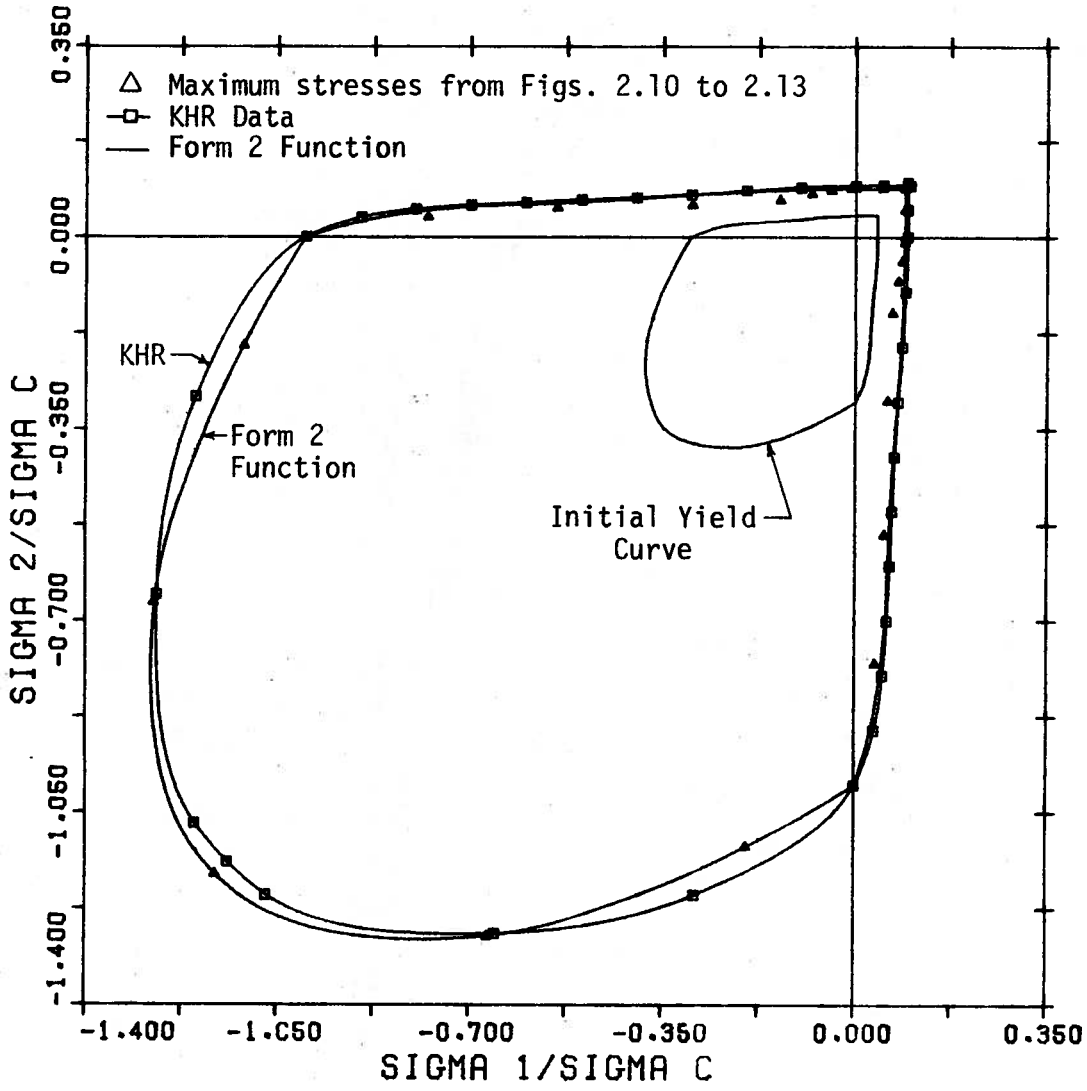

FIGURE 2.9 - Form 2 Function Failure Curve Comparisons

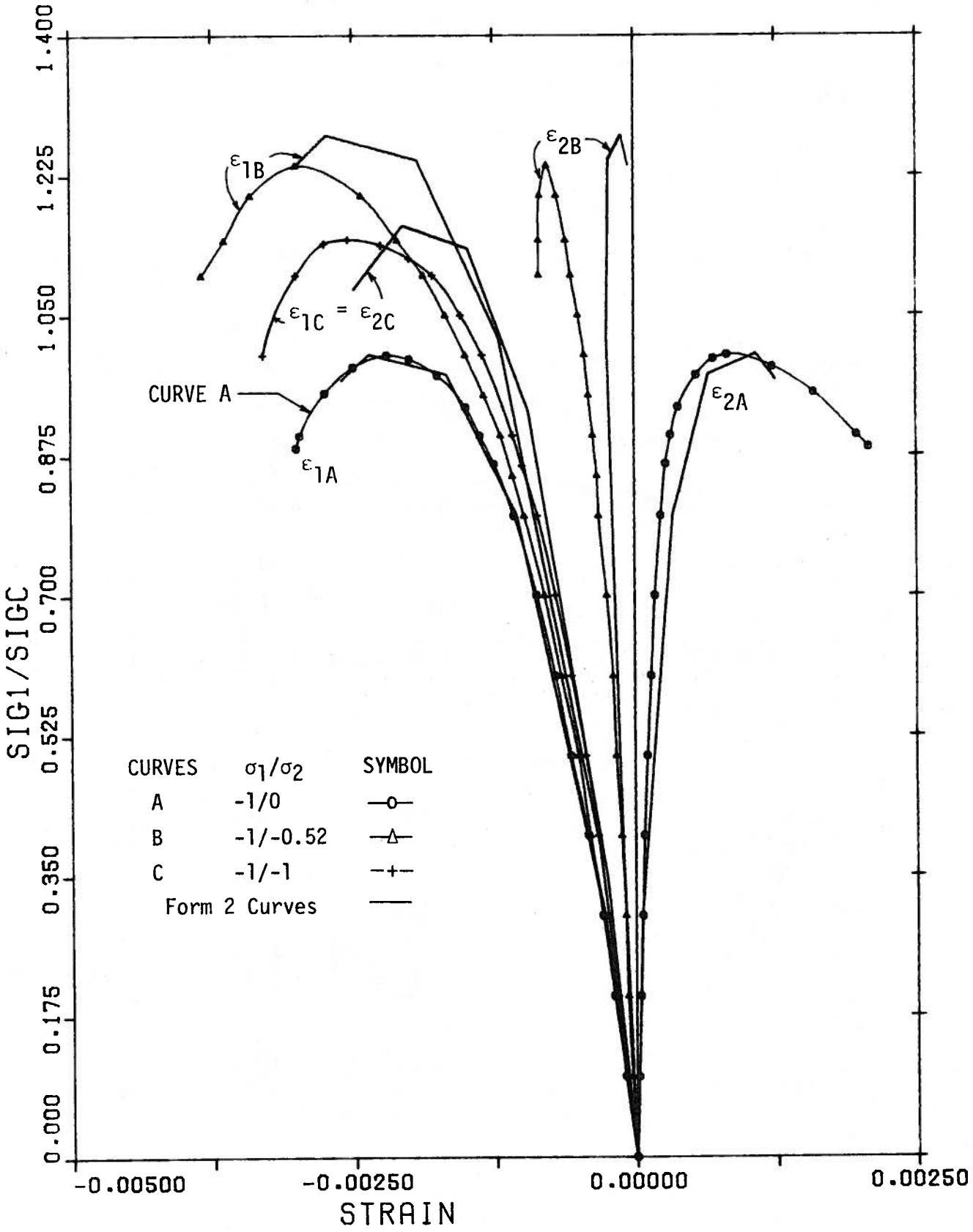

FIGURE 2.10 - Form 2 Function Compression - Compression Comparisons

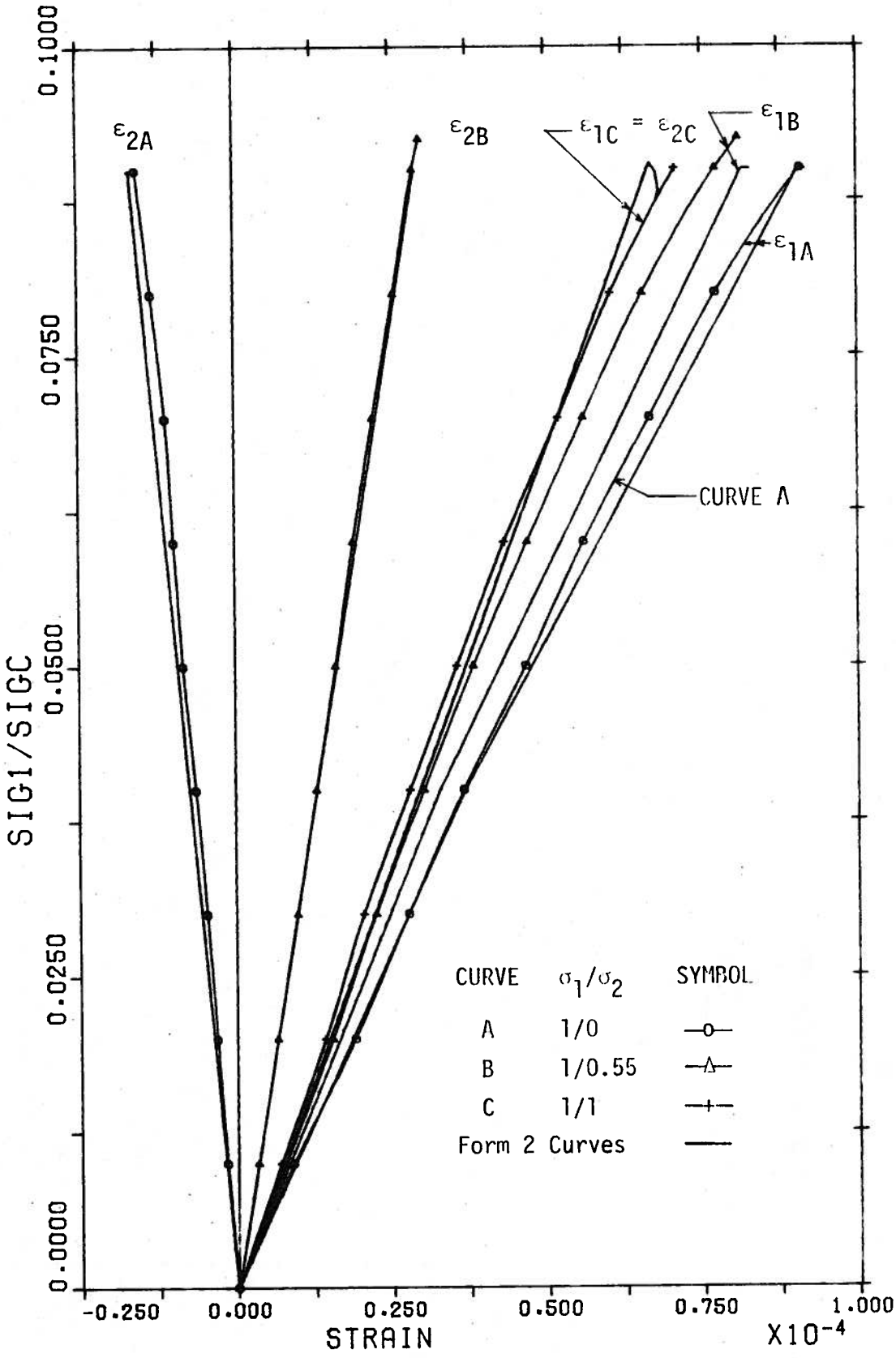

FIGURE 2.11 - Form 2 Function Tension - Tension Comparisons

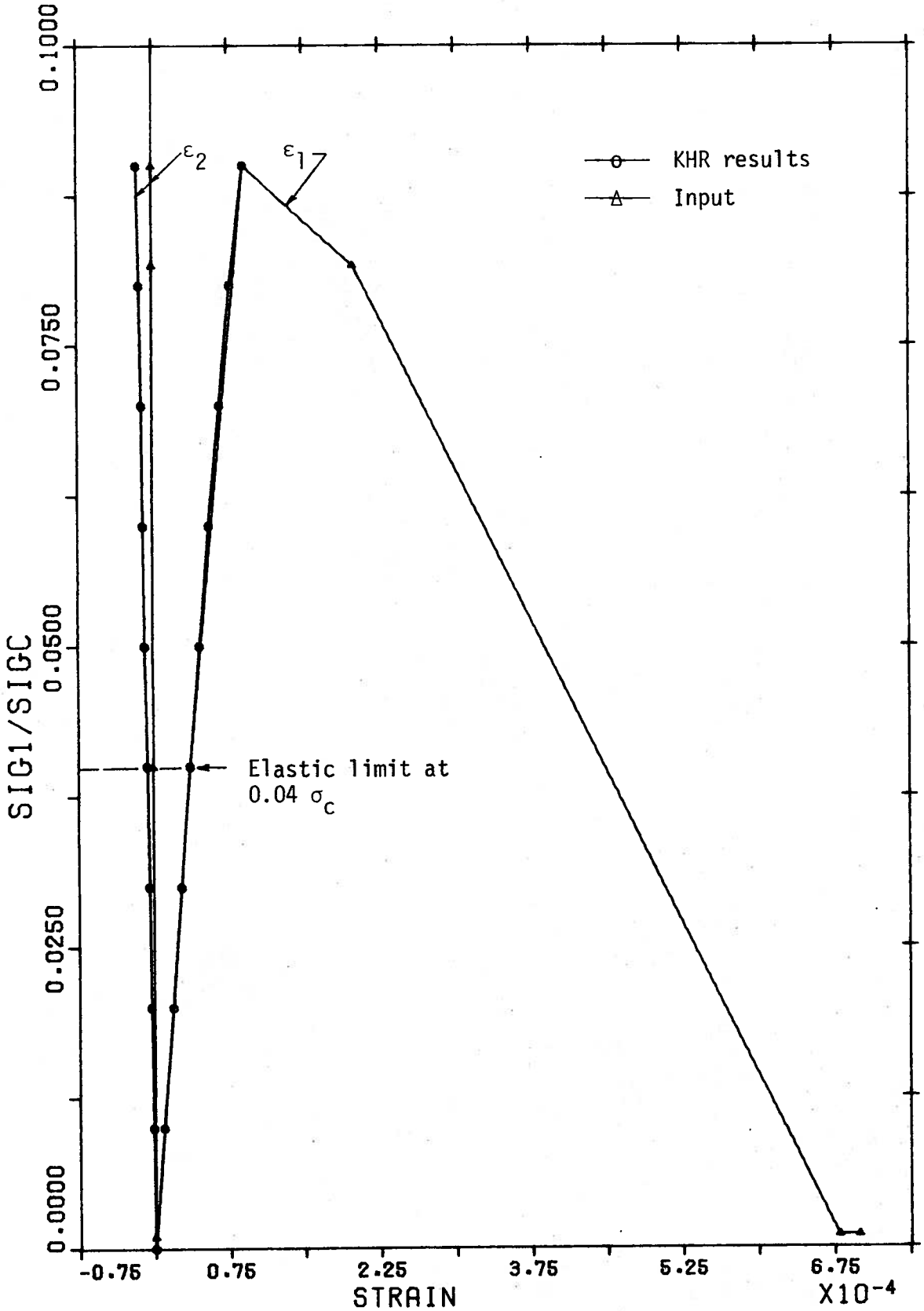

FIGURE 2.12 - Form 2 Function Degrading Tension Assumptions

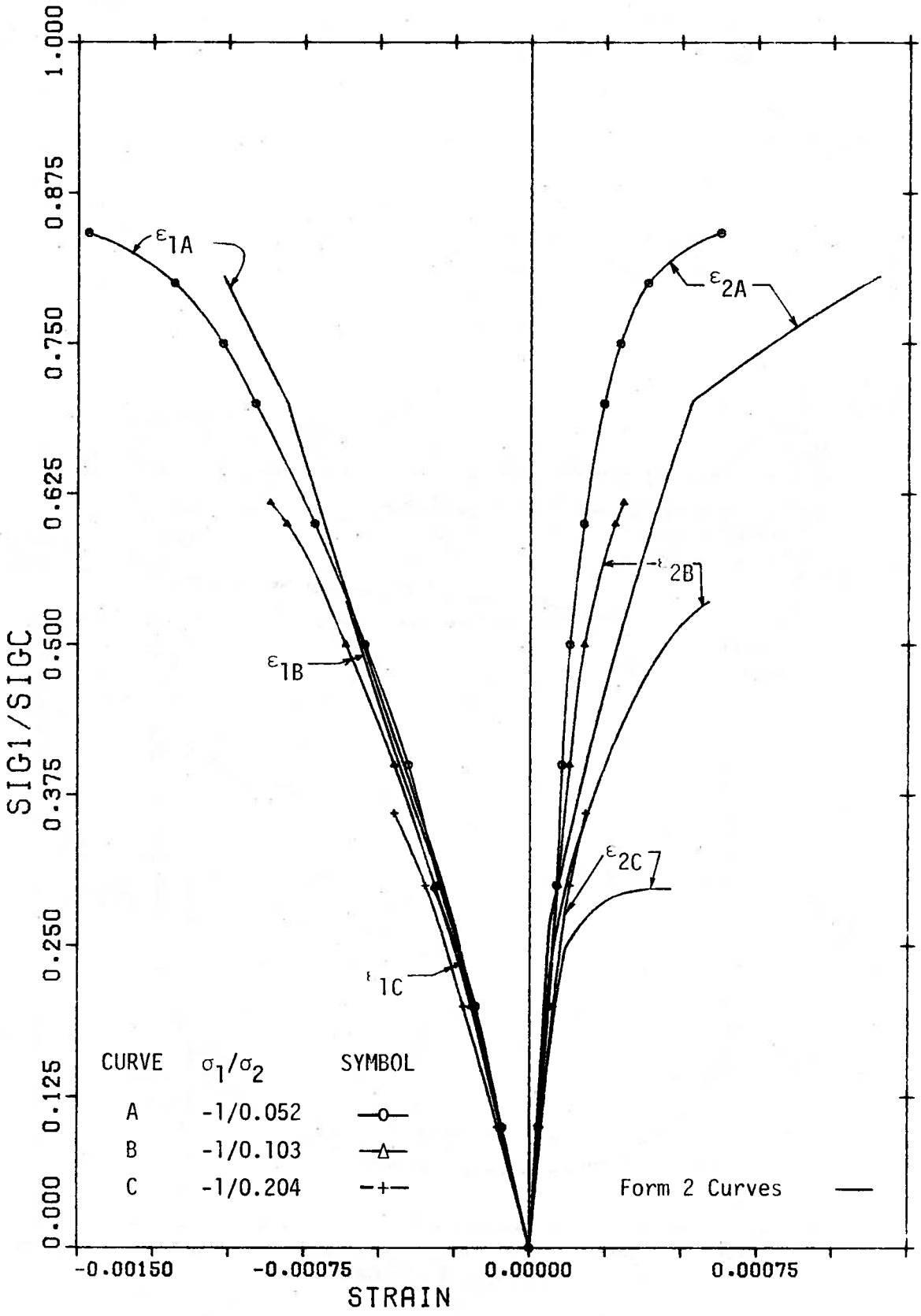

FIGURE 2.13 - Form 2 Function Tension - Compression Comparisons

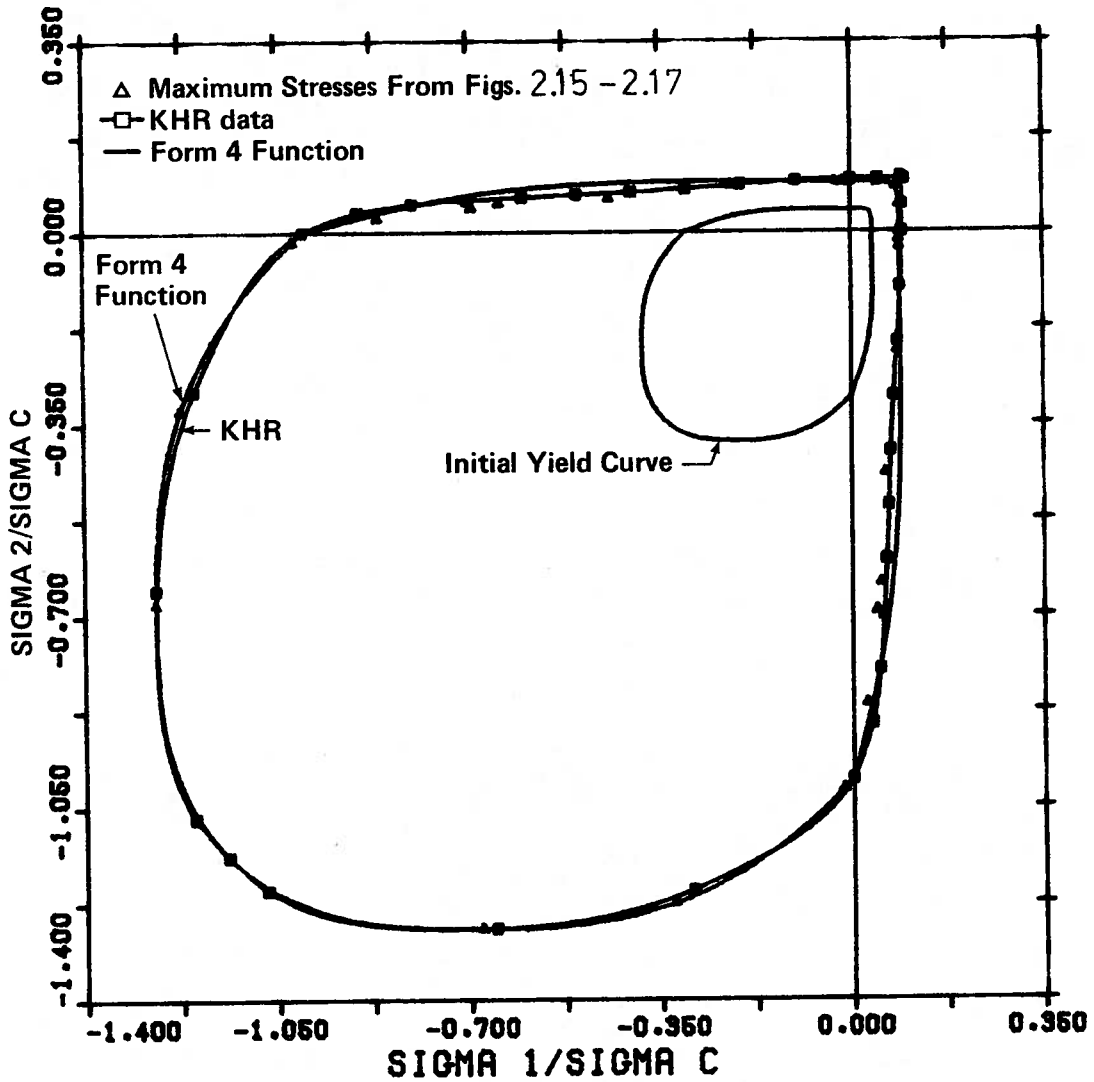

FIGURE 2.14 - Form 4 Function Failure Curve Comparisons

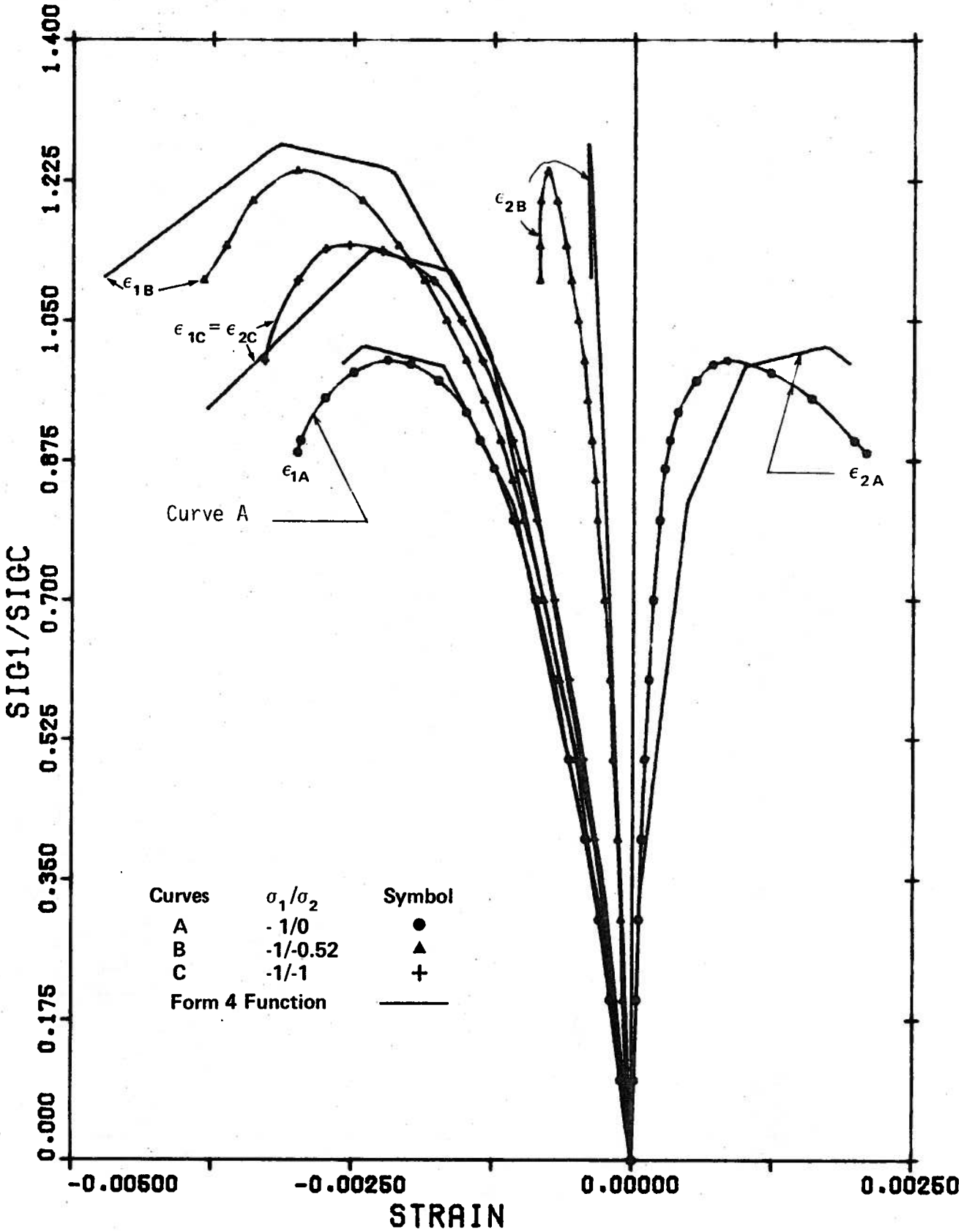

FIGURE 2.15 - Form 4 Function Compression - Compression Comparisons

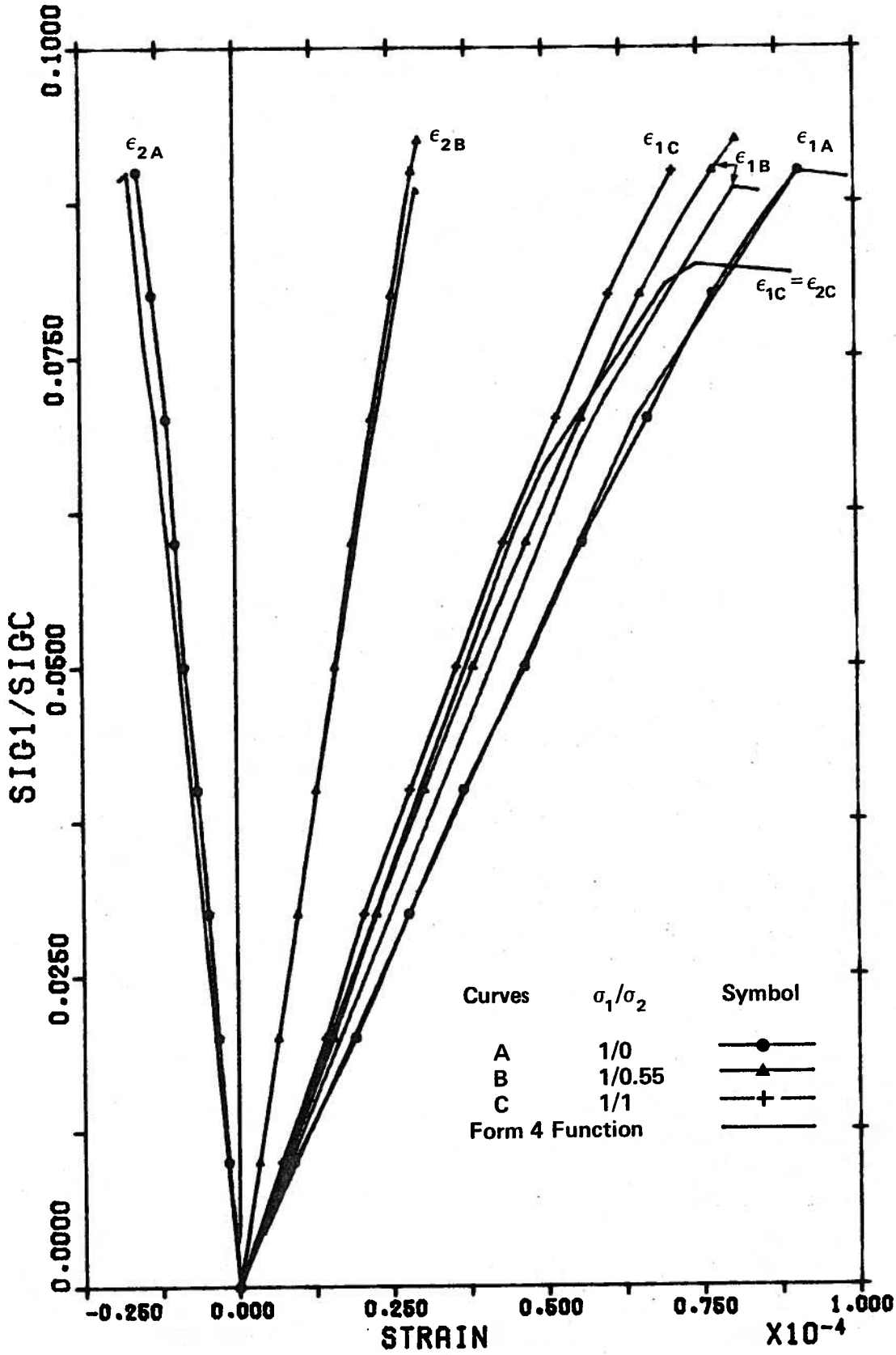

FIGURE 2.16 - Form 4 Function Tension - Tension Comparisons

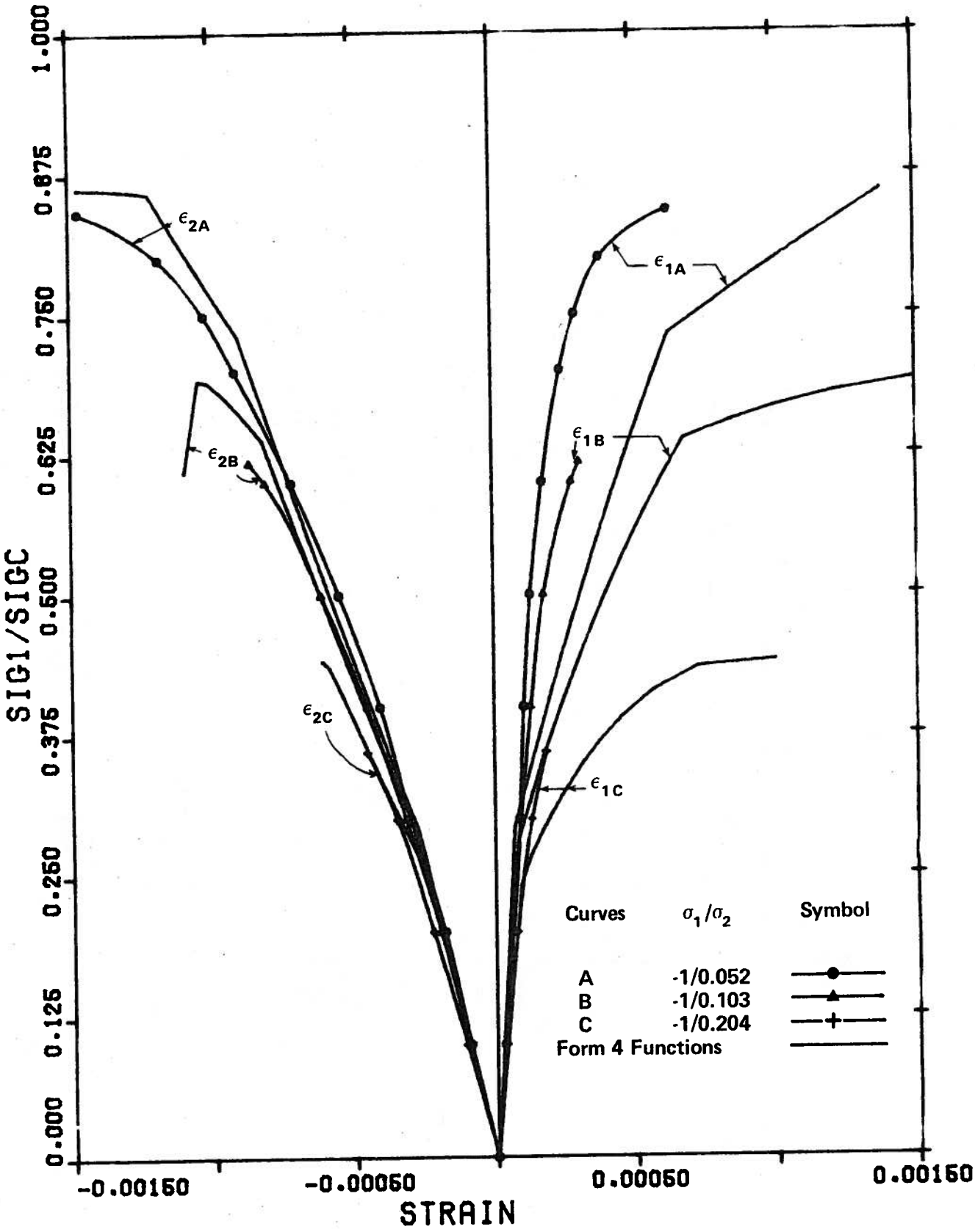

FIGURE 2.17 - Form 4 Function Tension - Compression Comparisons

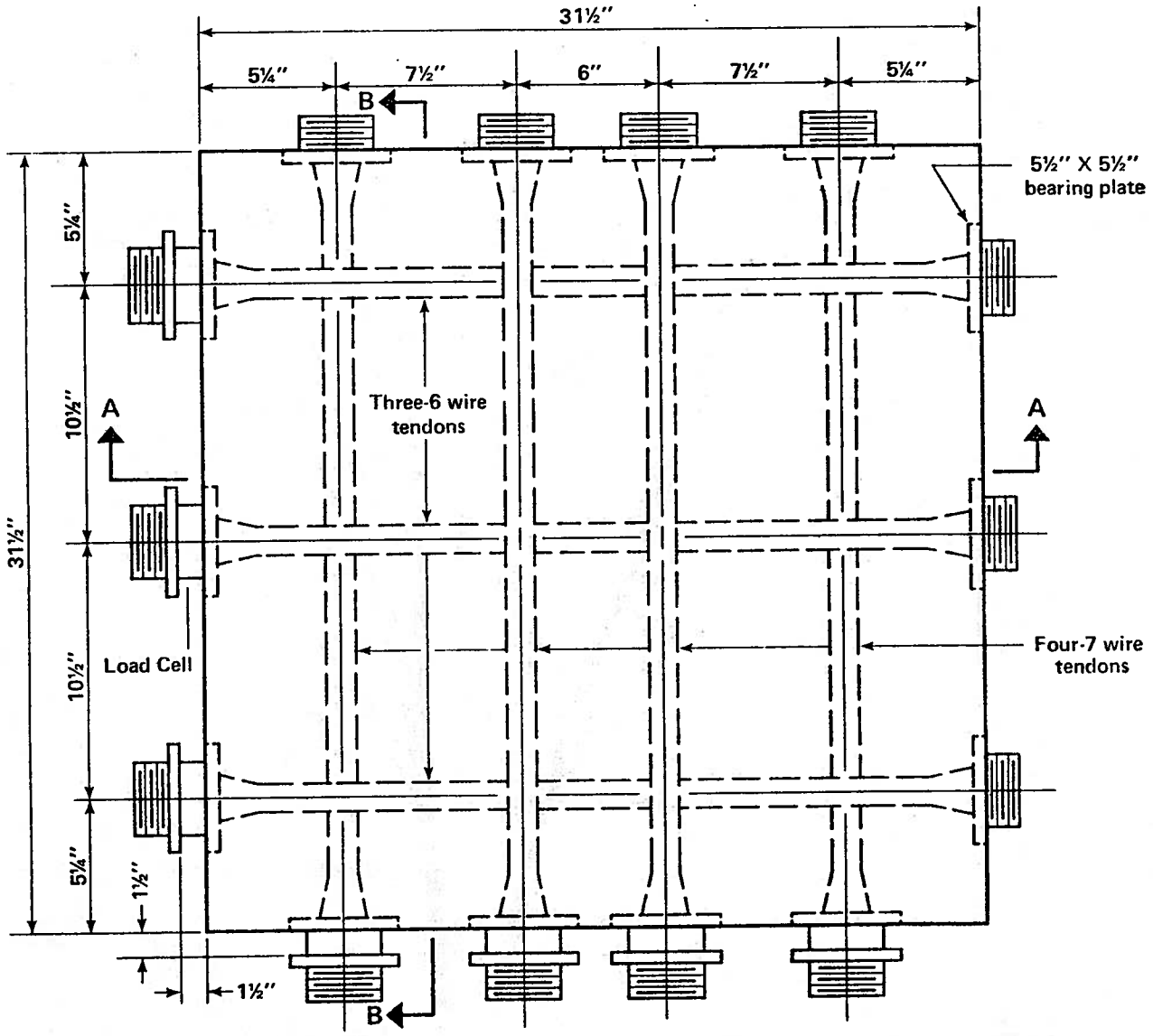

FIGURE 2.19 - Segment Test Specimen Dimensions

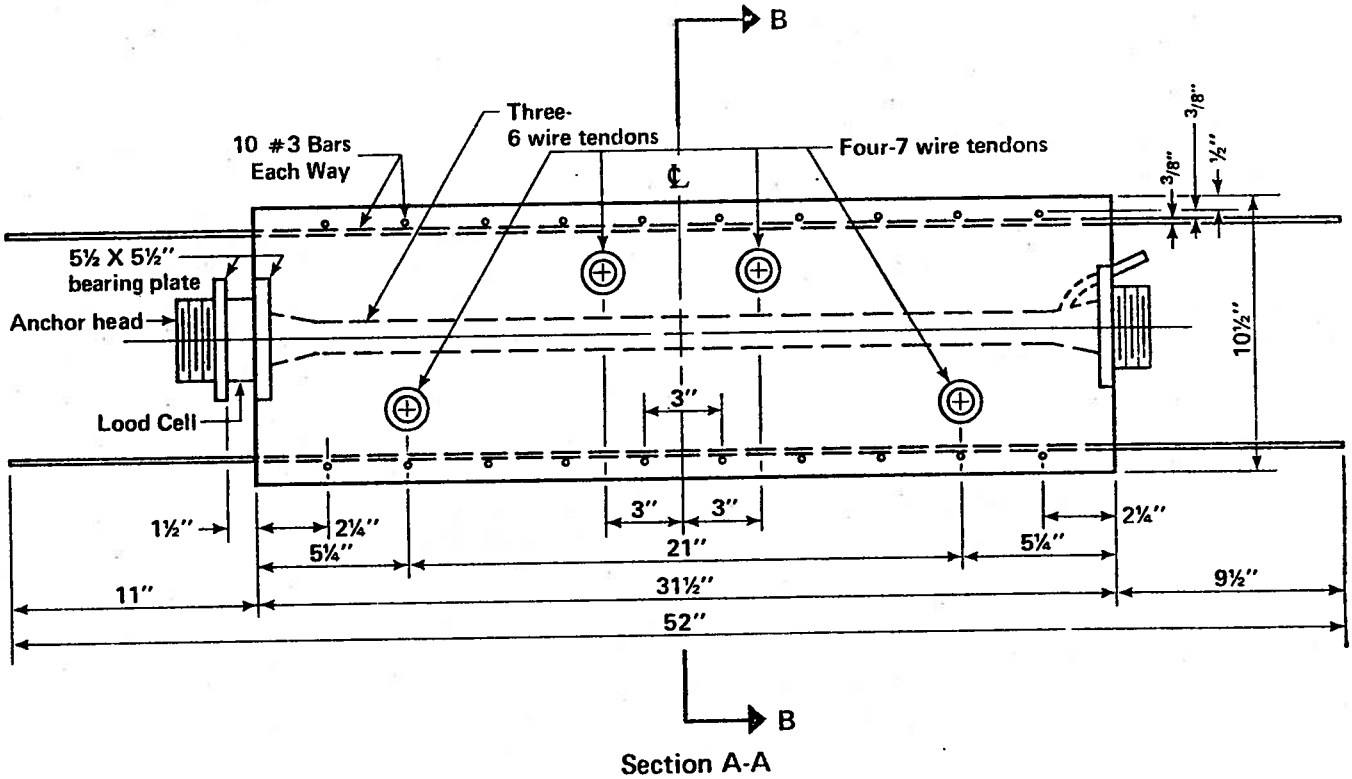

Section A-A

FIGURE 2.20 - Typical Section A-A through Segment Test Specimens

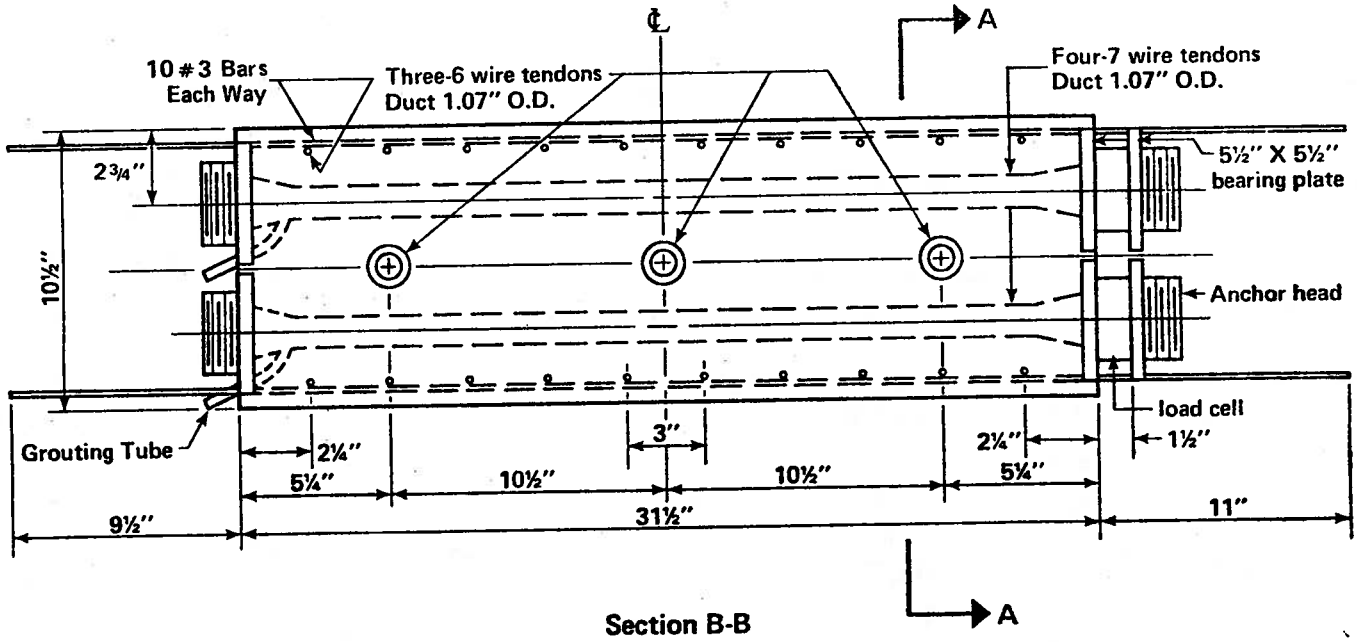

Section B-B

FIGURE 2.21 - Typical section B-B through Segment Test Specimens

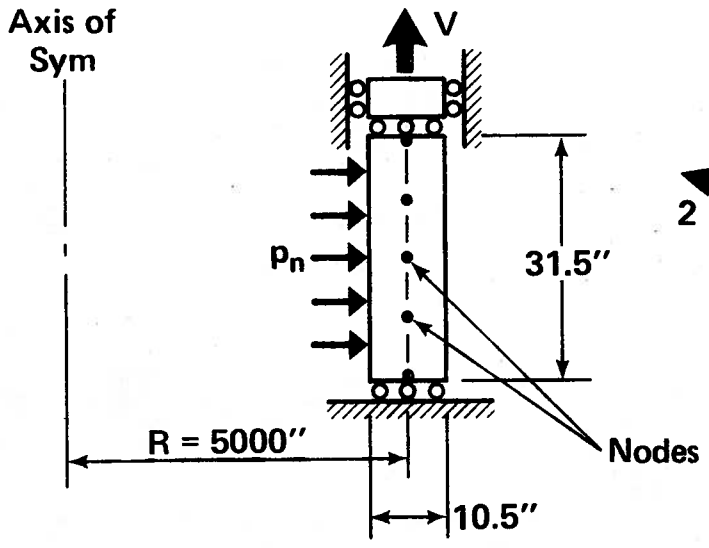

(a) Bosor5 Segment Model

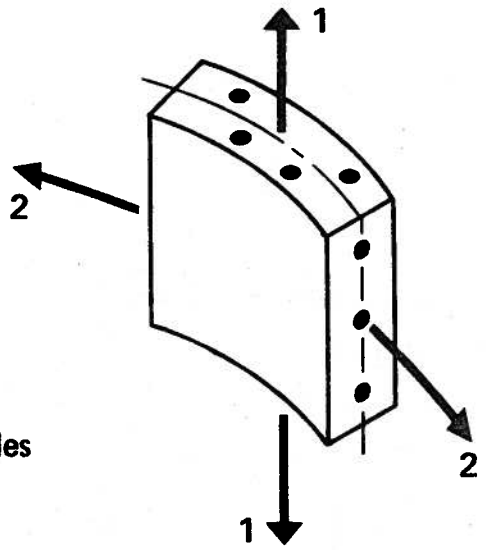

(b) Bosor5 Reference Directions

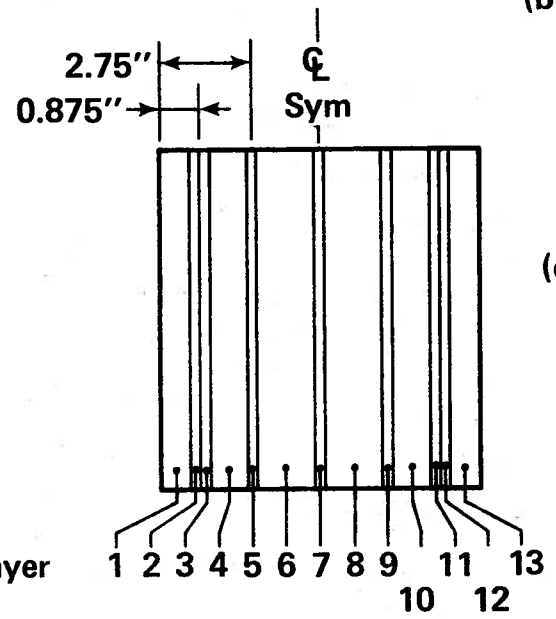

(c) Side Elevation of Wall Segment

Layers	Thickness	Material*
1,13	0.8401	1
4,10	1.8268	1
6,8	2.4696	1
2,12	0.0349	2
3,11	0.0349	3
5,9	0.0266	4
7	0.0342	5

*See Sect. 2.5.3.

(d) Details of Layers

Figure 2.22 - Bosor5 Segment Test Model

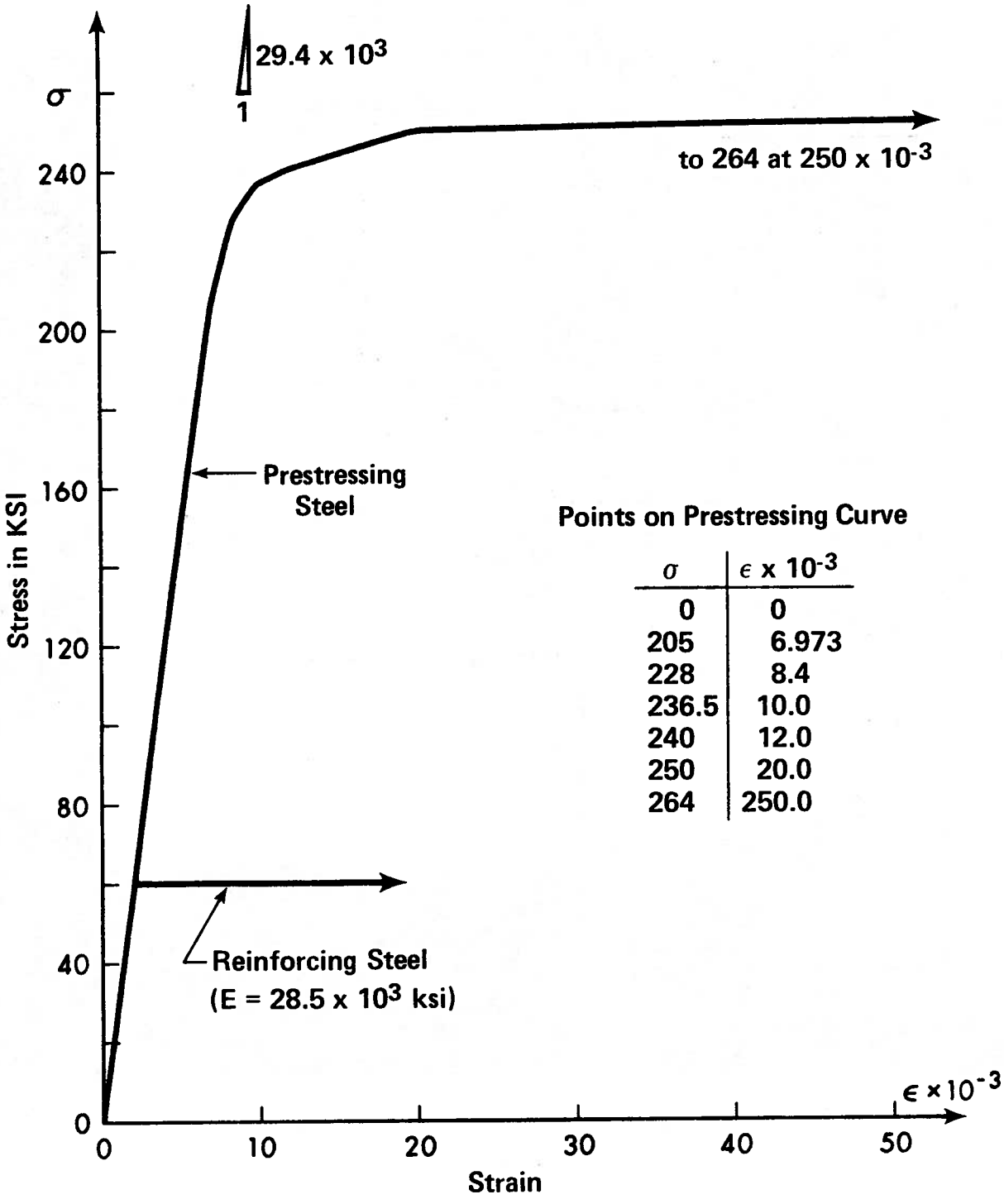

Figure 2.23 - Steel Properties for Segment Test Model

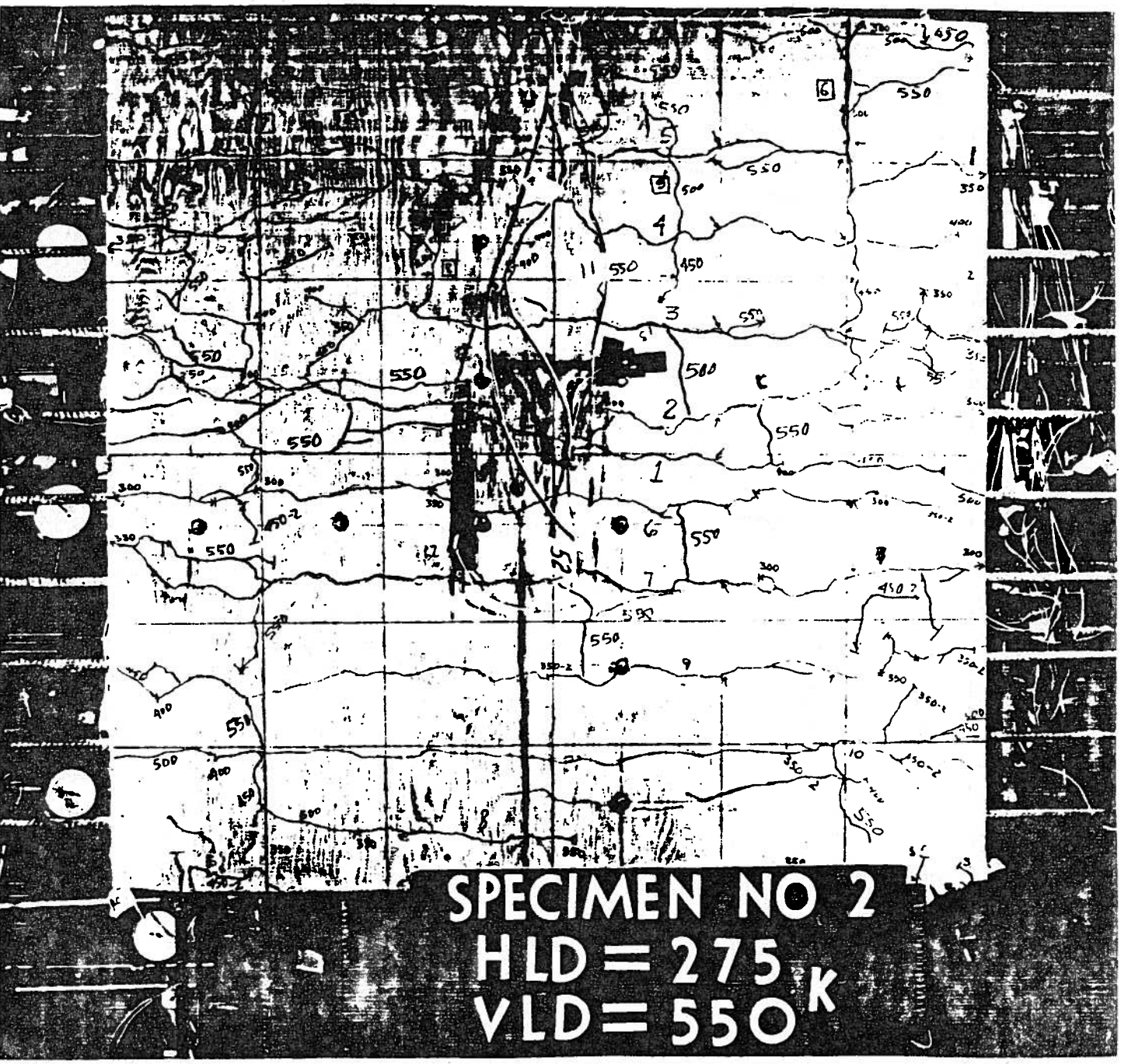

FIGURE 2.24 - SPECIMEN 2 AT END OF TEST

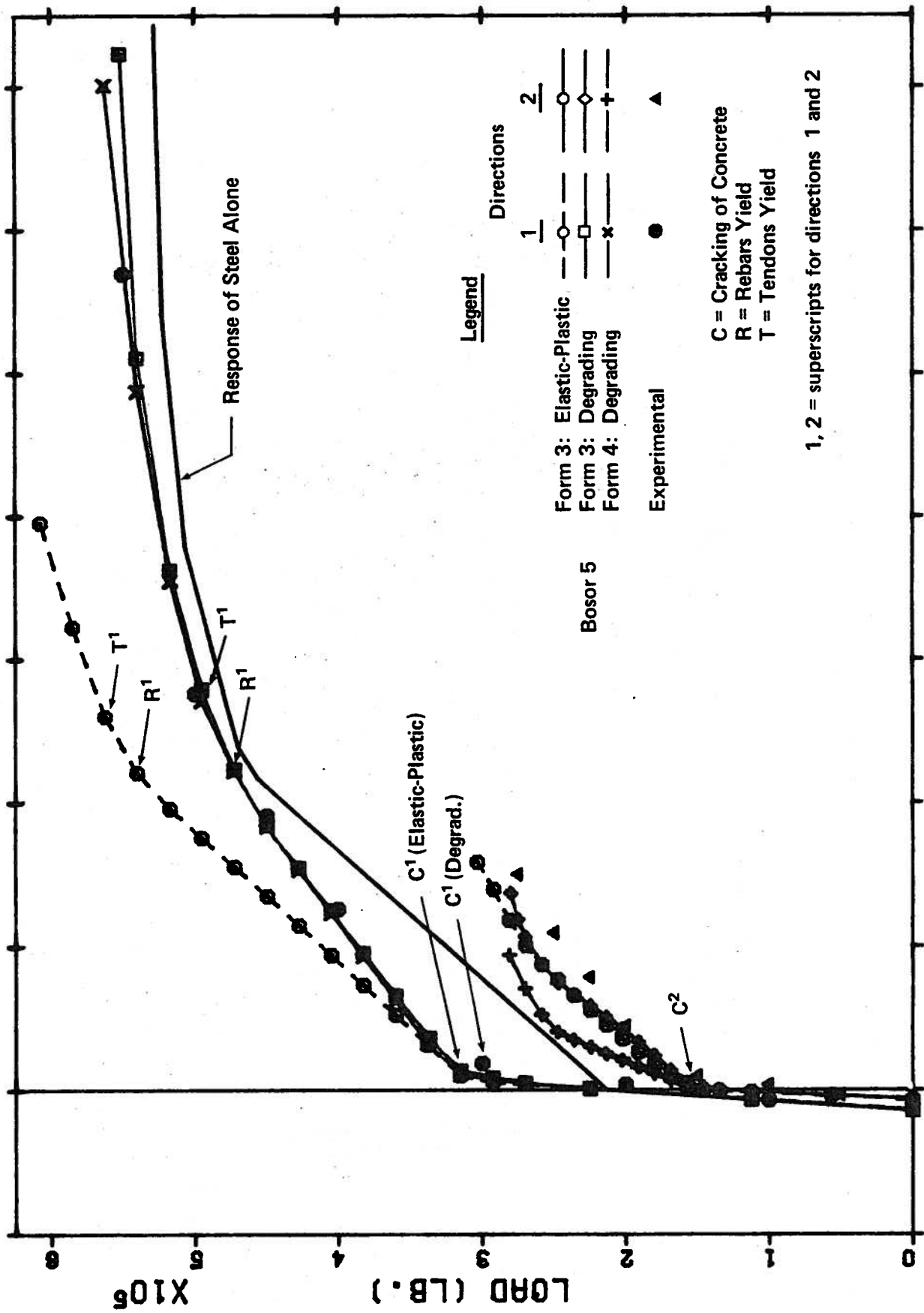

FIGURE 2.25 - Segment No. 1: Comparison of Results

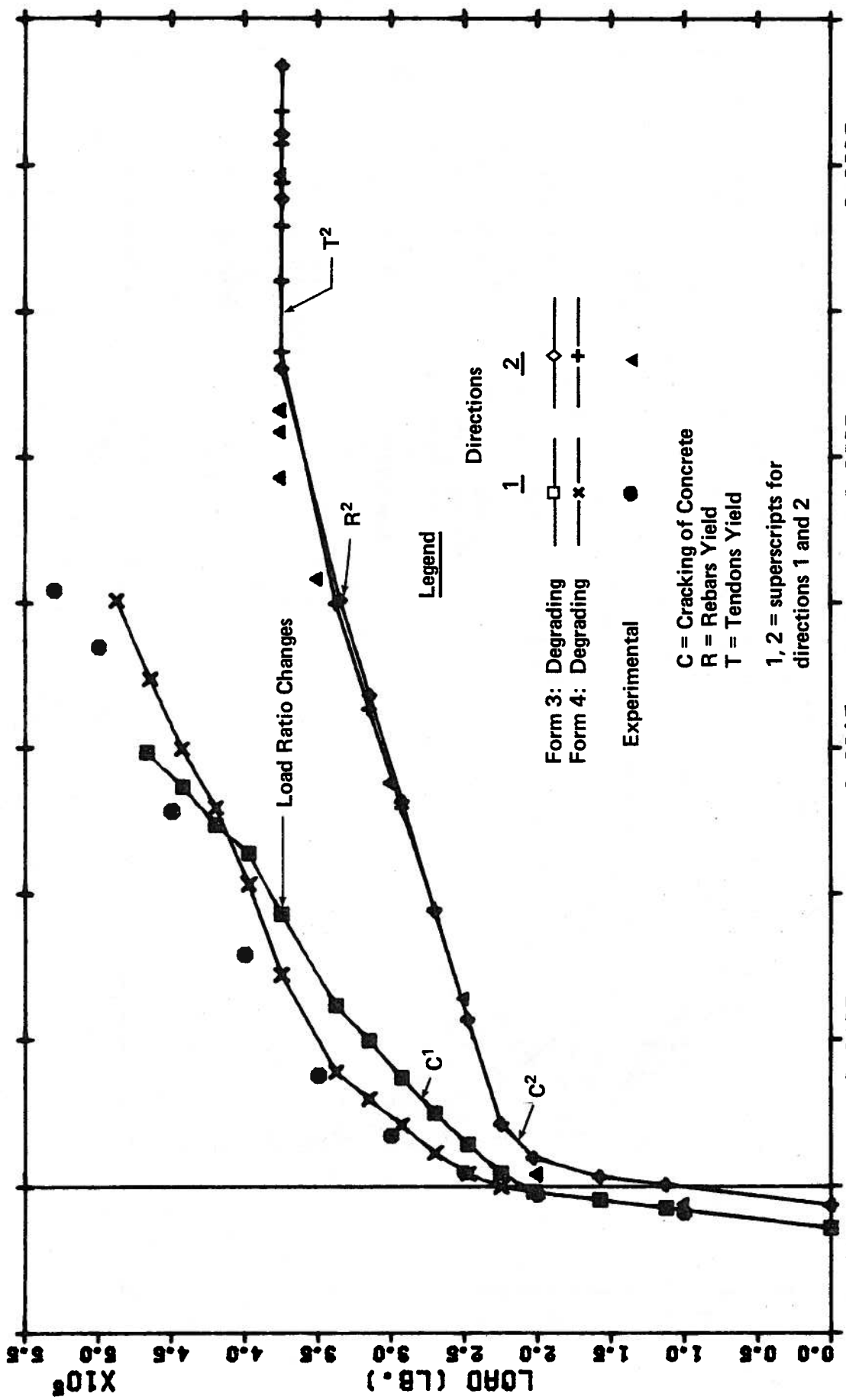

FIGURE 2.26 - Segment No. 3: Comparison of Results

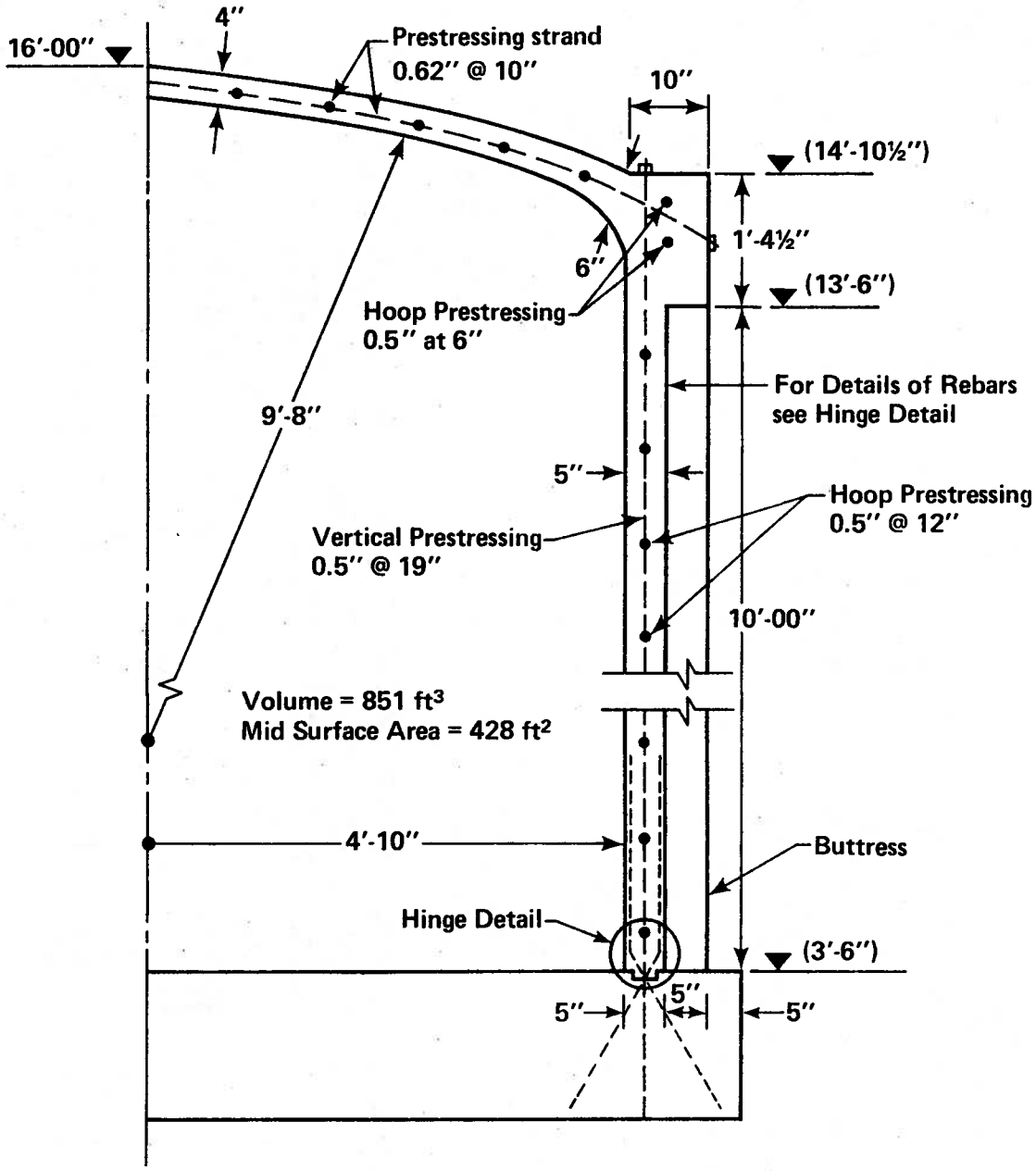

Figure 3.1 Vertical Section Through Test Structure

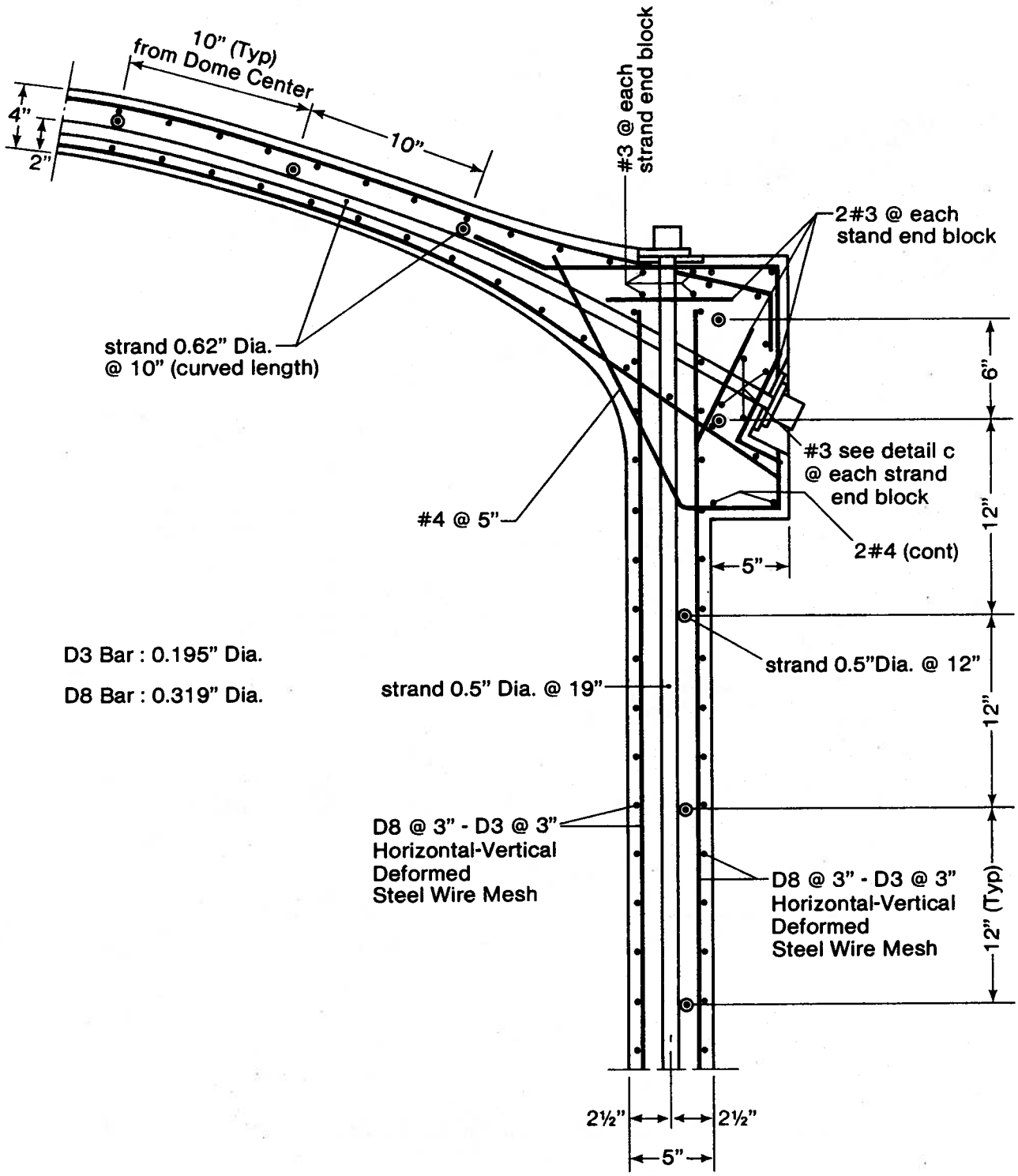

Figure 3.2 Ring Beam Detail of Test Structure

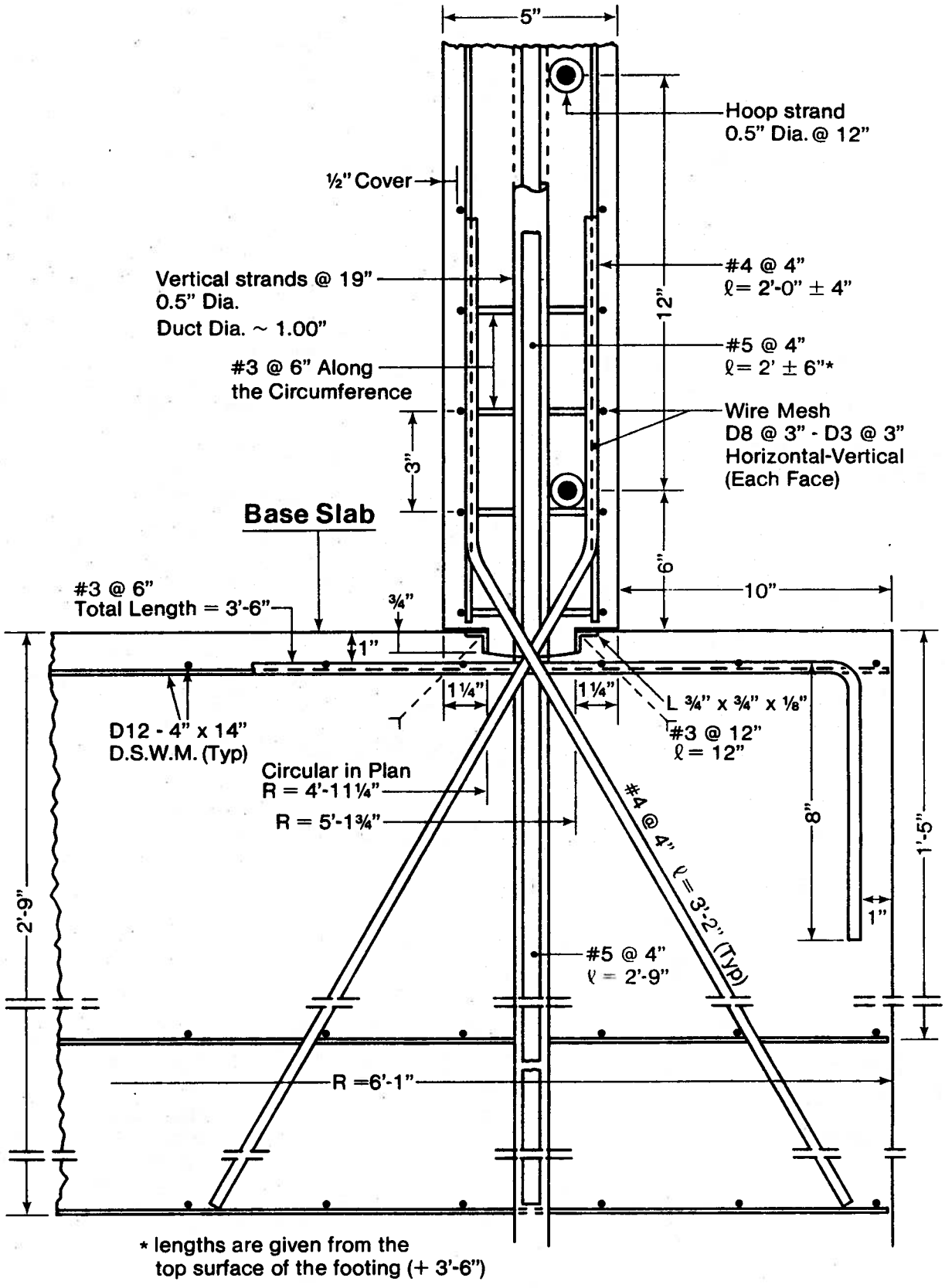

* lengths are given from the top surface of the footing (+ 3'-6")

Figure 3.3 Hinge Detail of Test Structure

Strand Type	Total Length	No. Required
st 1	11'-10"	2
st 2	11'-9"	4
st 3	11'-4"	4
st 4	10'-8"	4
st 5	9'-6"	4
st 6	7'-8"	4

Total = 22 0.62" Dia.

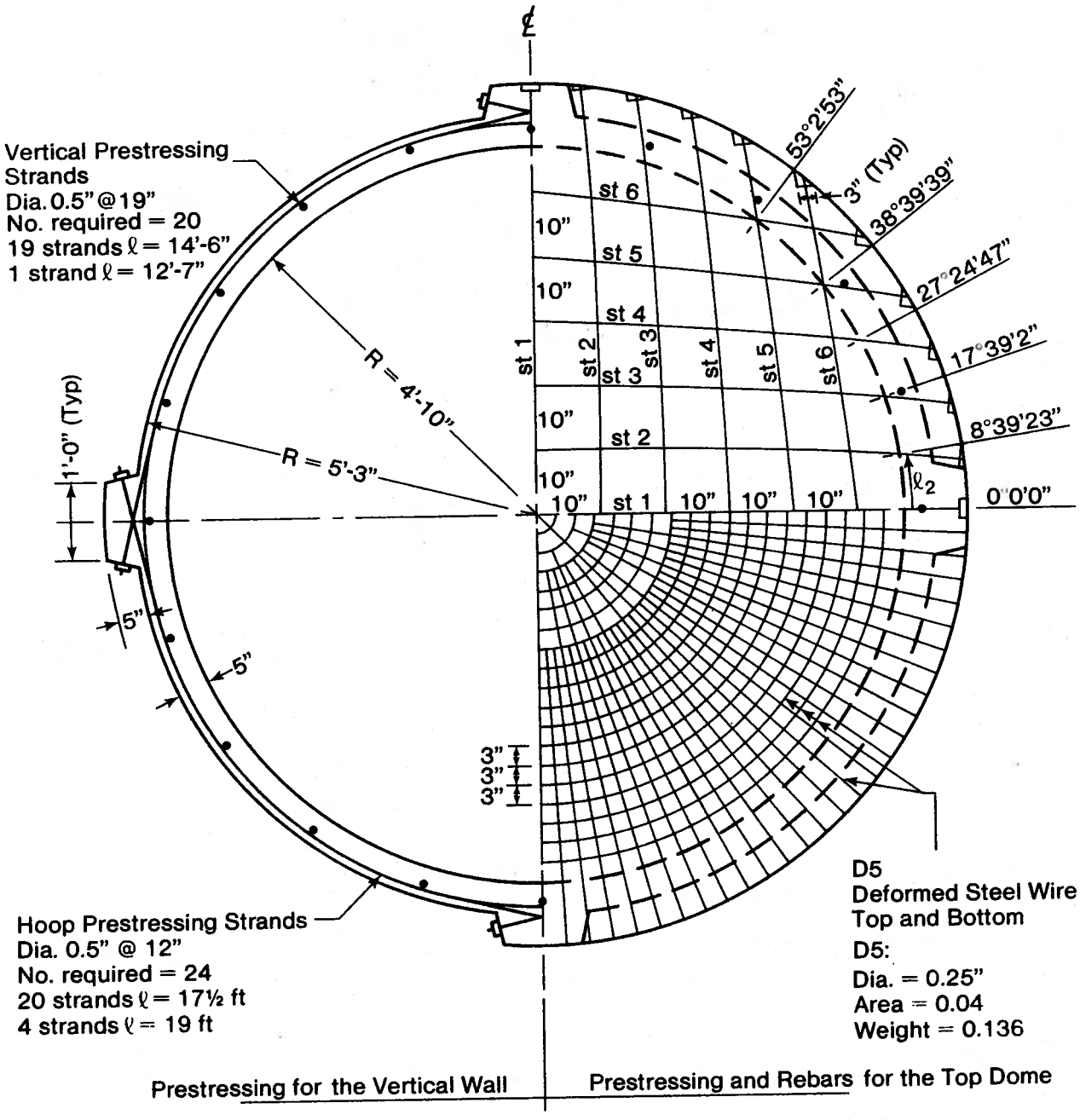

Figure 3.4 Dome Reinforcing of Test Structure

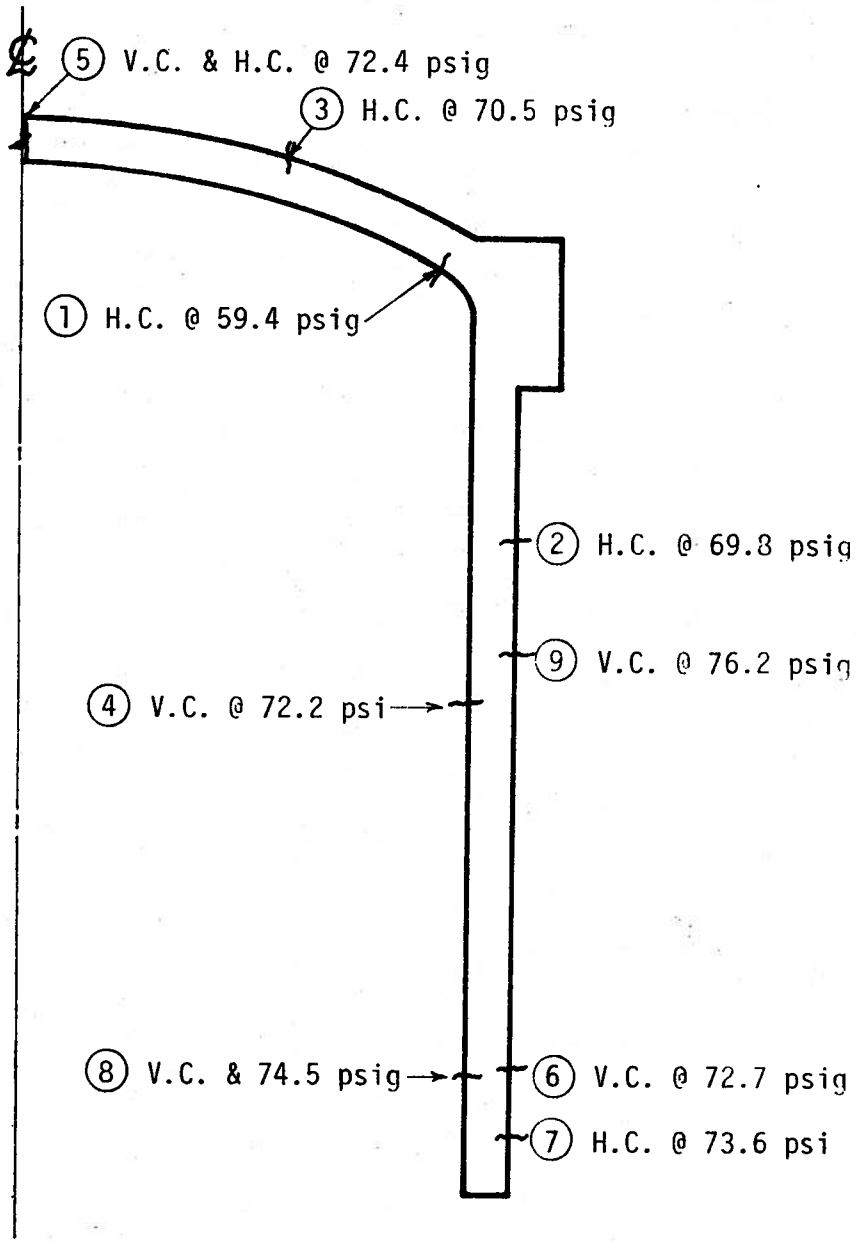

H.C. = Horizontal crack
V.C. = Vertical crack

FIGURE 3.5 - Predicted Cracking Sequence of Test Structure (Elastic Analysis)

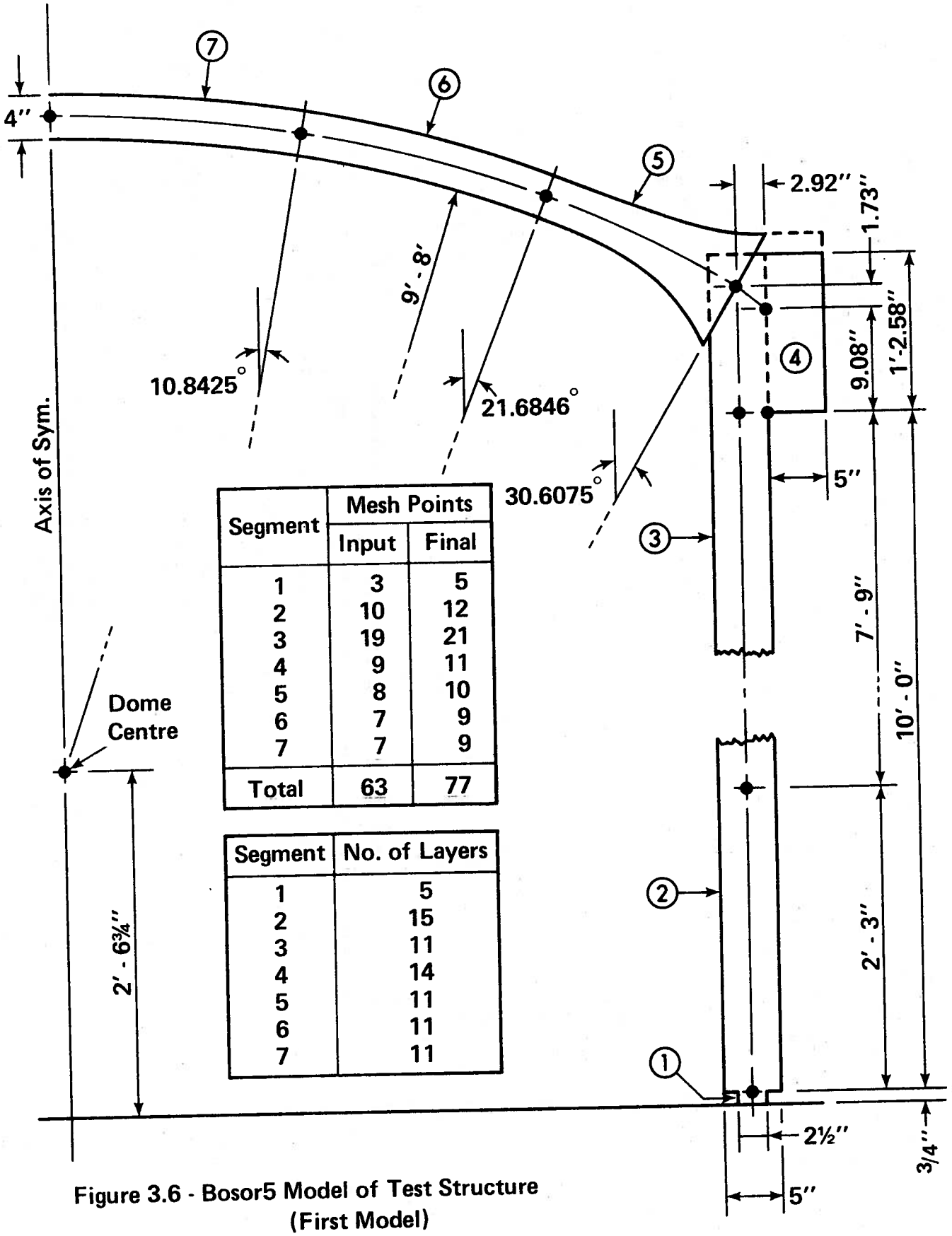

Segment	Mesh Points	
	Input	Final
1	3	5
2	10	12
3	19	21
4	9	11
5	8	10
6	7	9
7	7	9
Total	63	77

Segment	No. of Layers
1	5
2	15
3	11
4	14
5	11
6	11
7	11

Figure 3.6 - Bosor5 Model of Test Structure
(First Model)

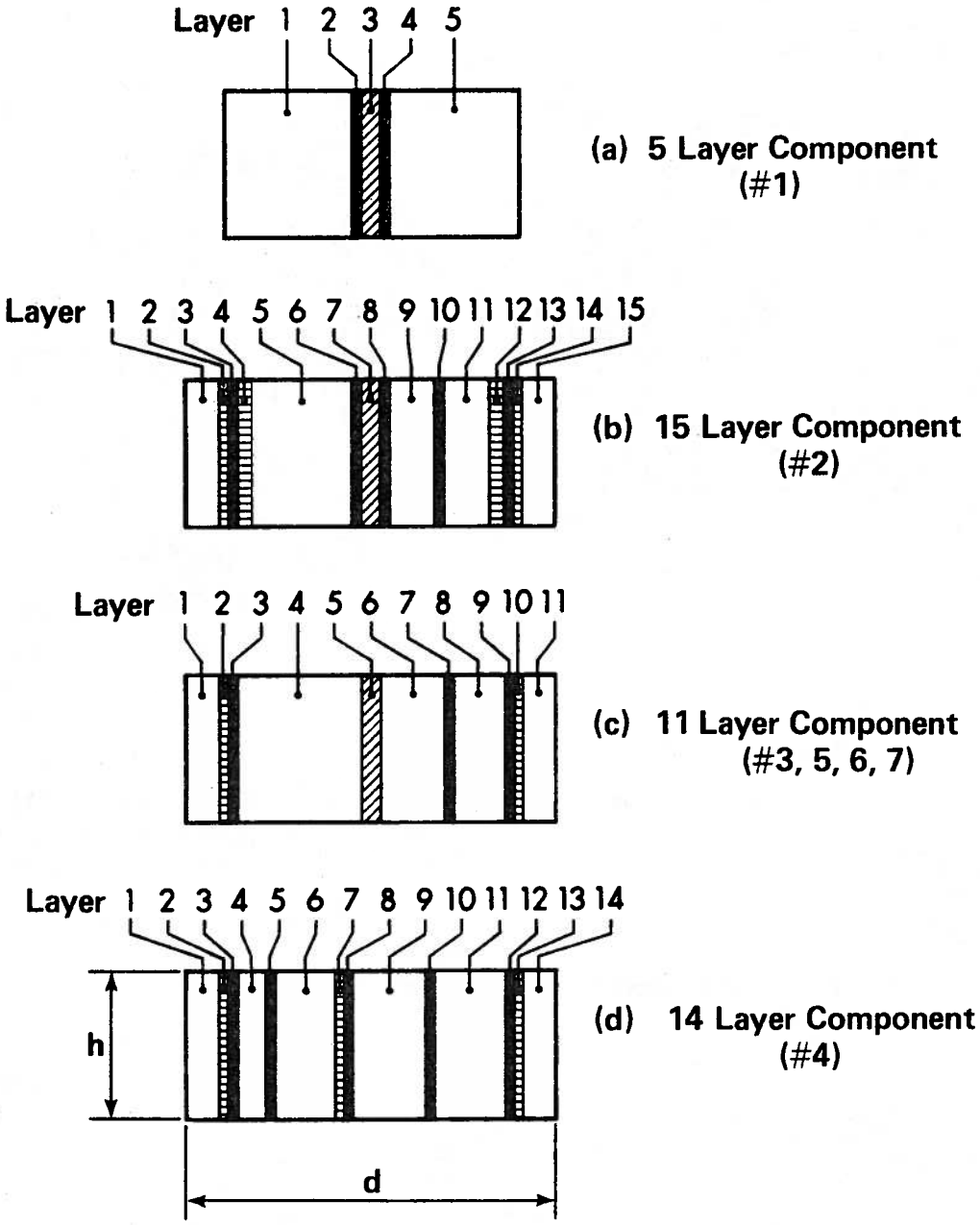

Figure 3.7 - Bosor5 Component Layers (First Model)

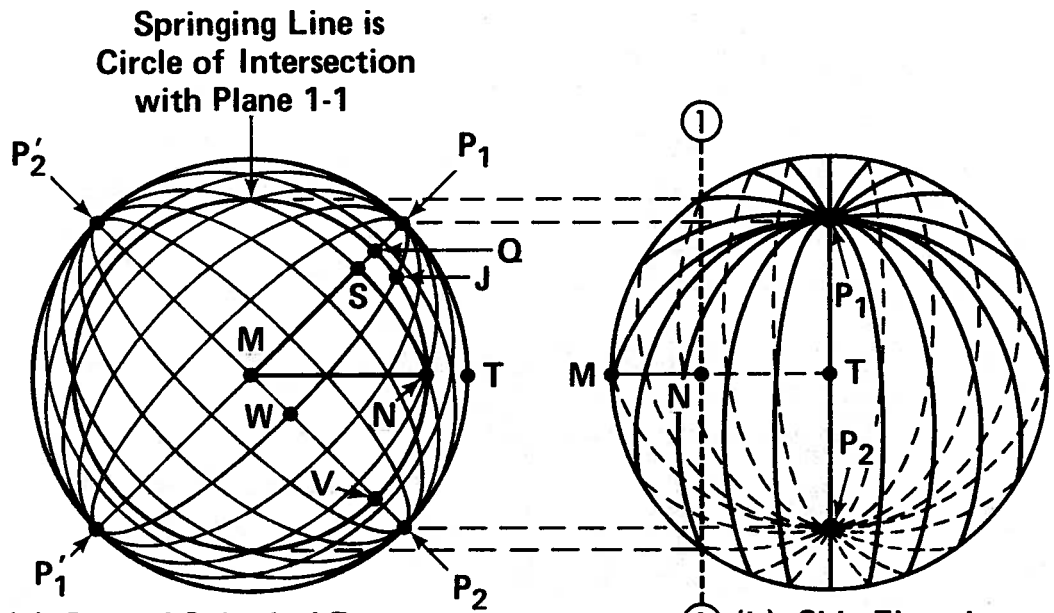

(a) Plan of Spherical Dome

(b) Side Elevation of Sphere

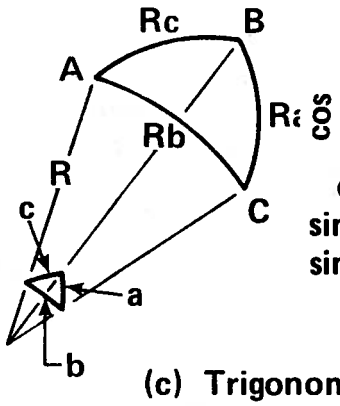

$$\cos a = \cos b \cos c + \sin b \sin c \cos A \quad (I)$$

$$\sin a \quad B = \cos b \sin c - \sin b \cos c \cos A \quad (II)$$

$$\sin a \sin B = \sin b \sin A \quad (III)$$

(c) Trigonometry of Spherical Triangle

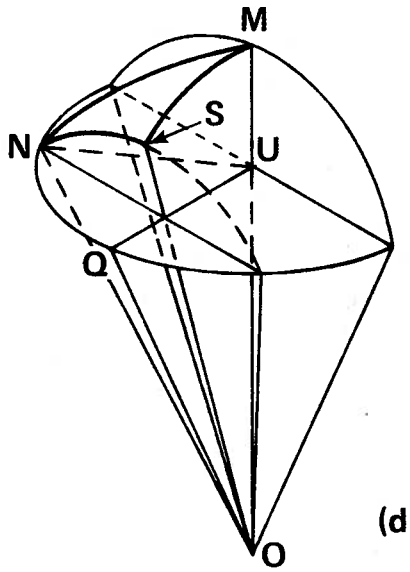

Data:

$\measuredangle MOQ = 29°$

$\measuredangle NUQ = 45°$

Solve by plane trigonometry to find:

$\measuredangle NOS = 20.05°$

Solve by spherical trigonometry to find:

$\measuredangle MNS = 48.83°$

(d) Solution for $\measuredangle MNS$

Figure 3.8 - Spherical Post-tensioning Layout

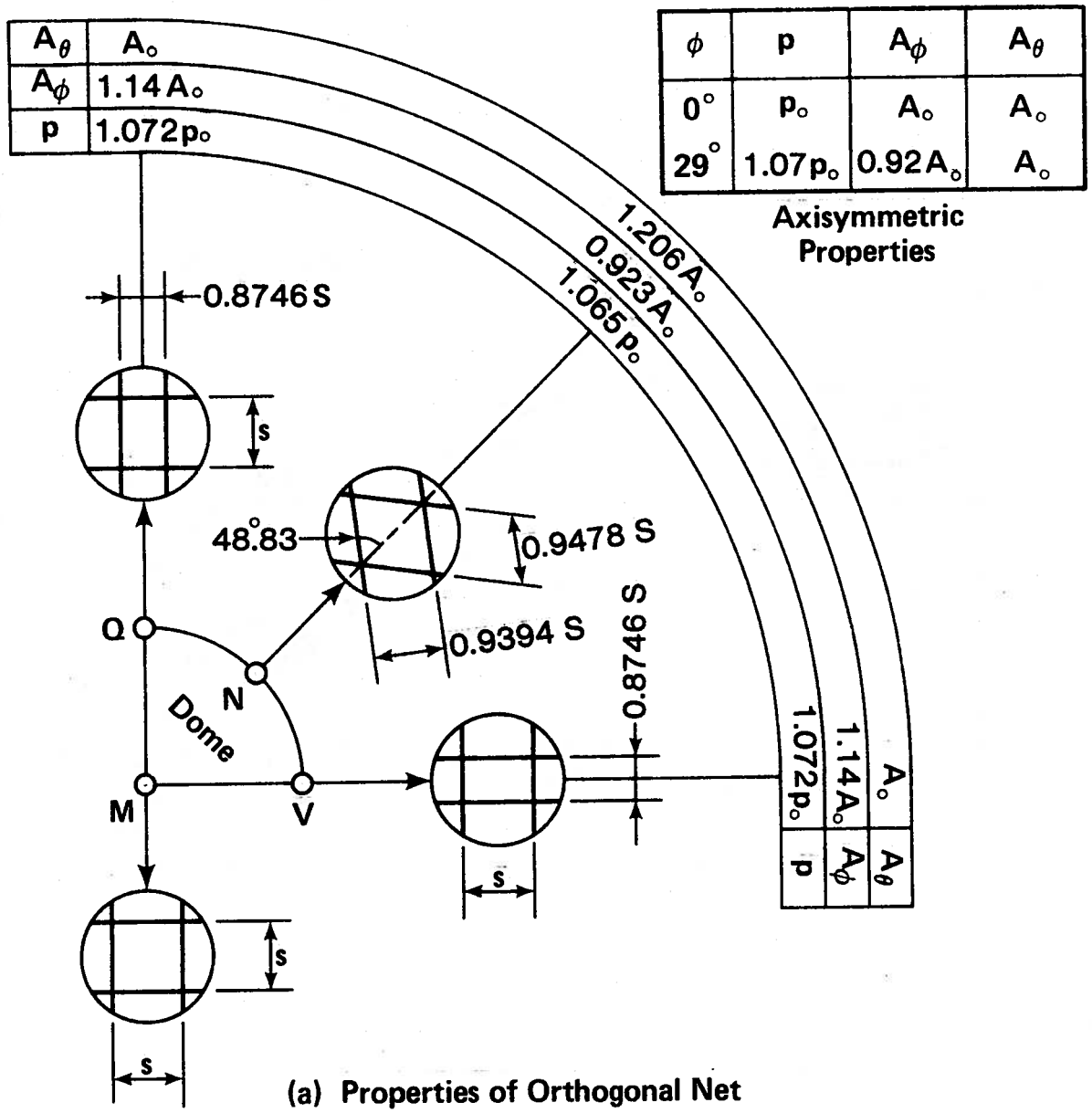

ϕ	p	A_ϕ	A_θ
0°	p_o	A_o	A_o
29°	1.07 p_o	0.92 A_o	A_o

Axisymmetric Properties

(a) Properties of Orthogonal Net

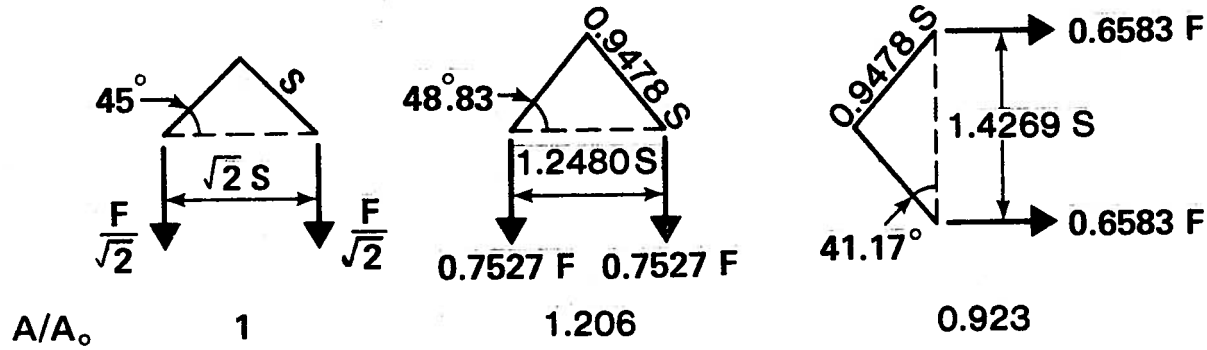

(b) Ultimate Strength Ratios

Figure 3.9 - Equivalent Prestressing Effects

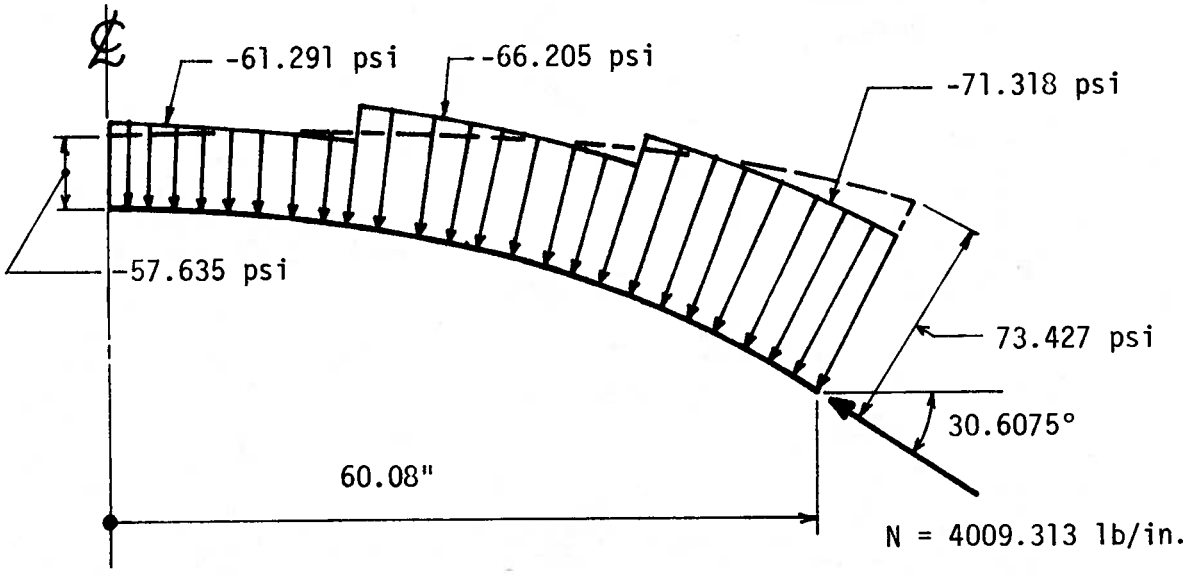

Figure 3.10 - Pressure Simulation of Dome Prestressing
(First Model)

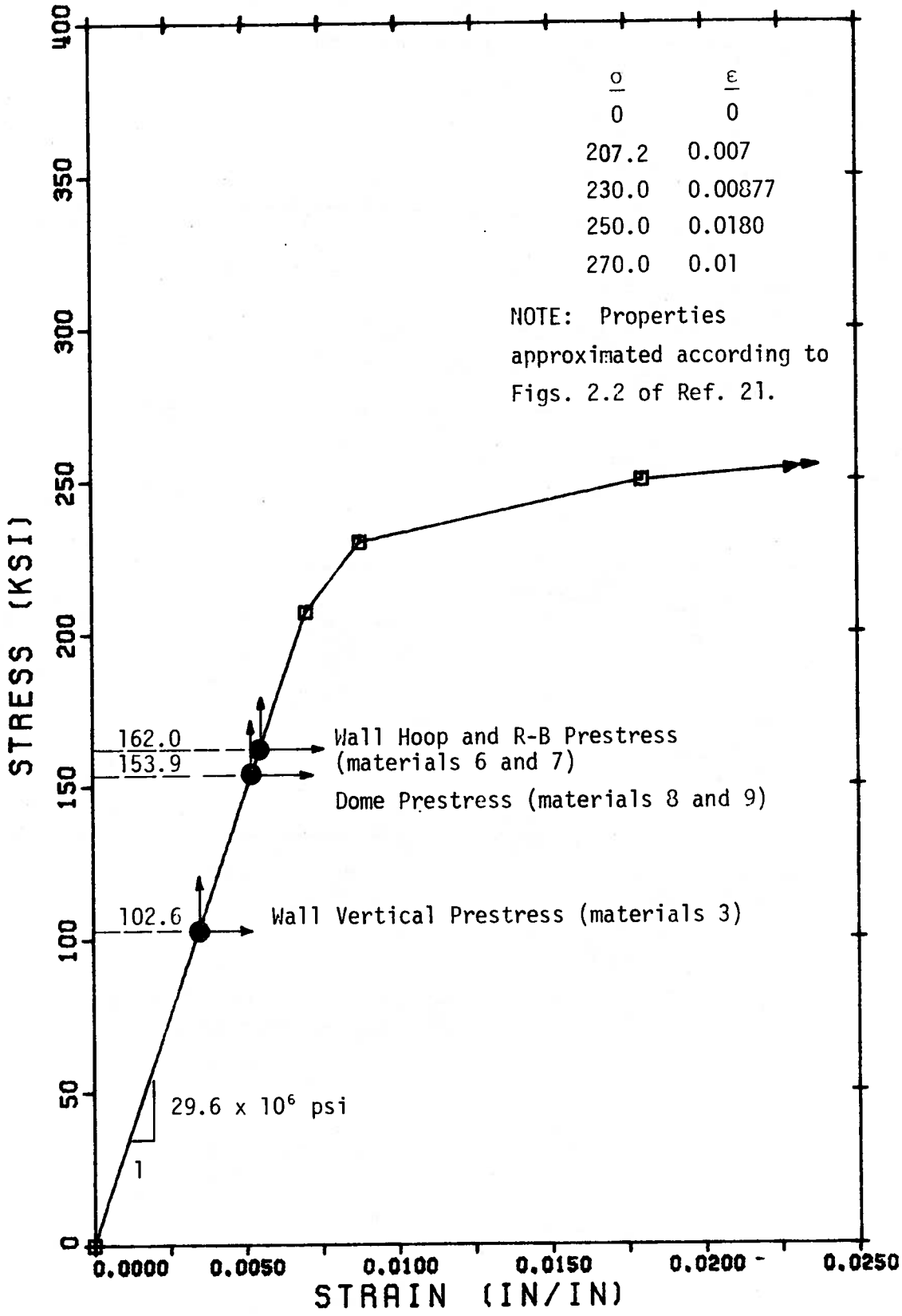

FIGURE 3.11 - Prestressing Strand Properties and Initial Stress Levels

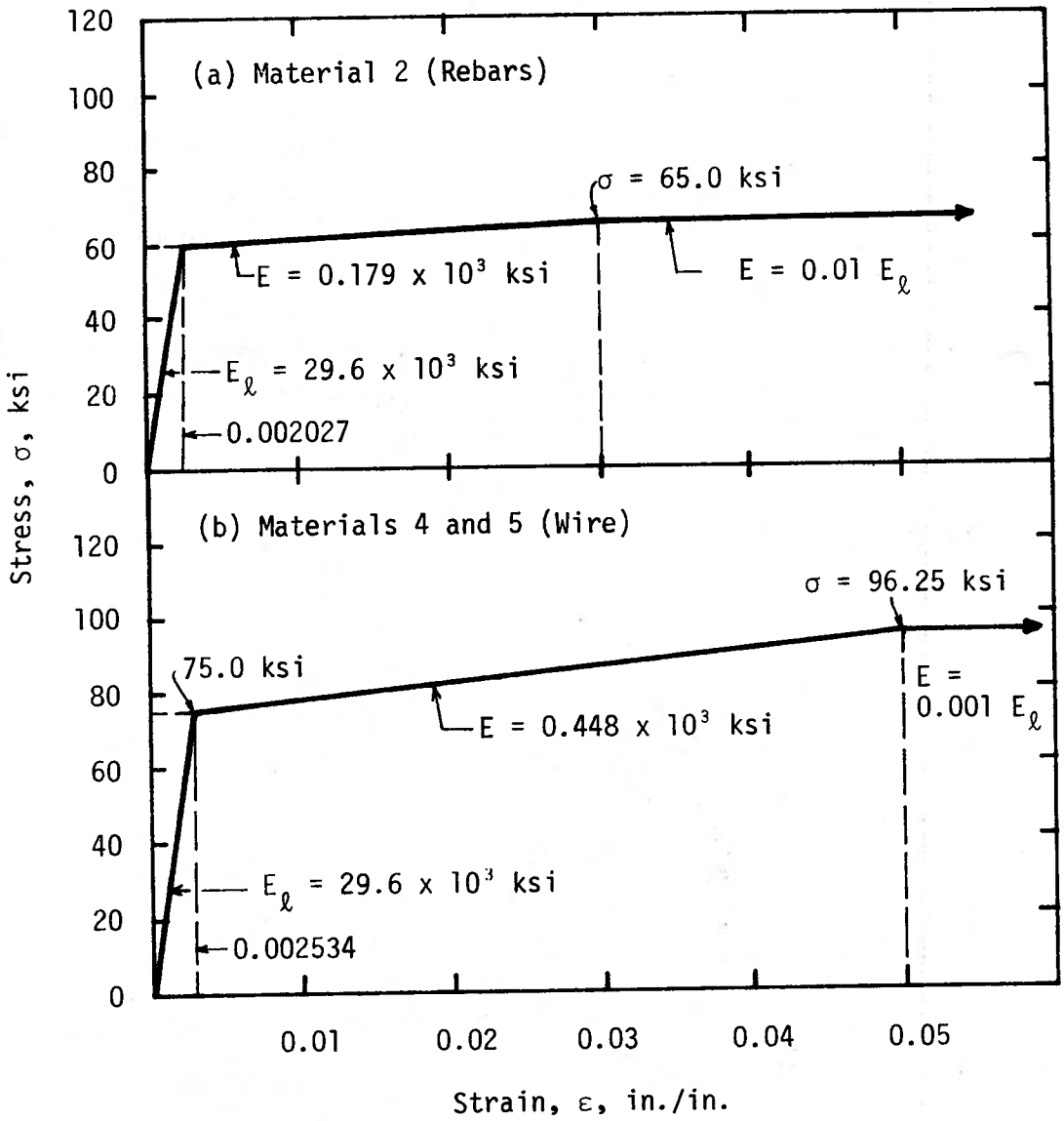

FIGURE 3.12 - Properties of Reinforcing Bars and Wires (First Model)

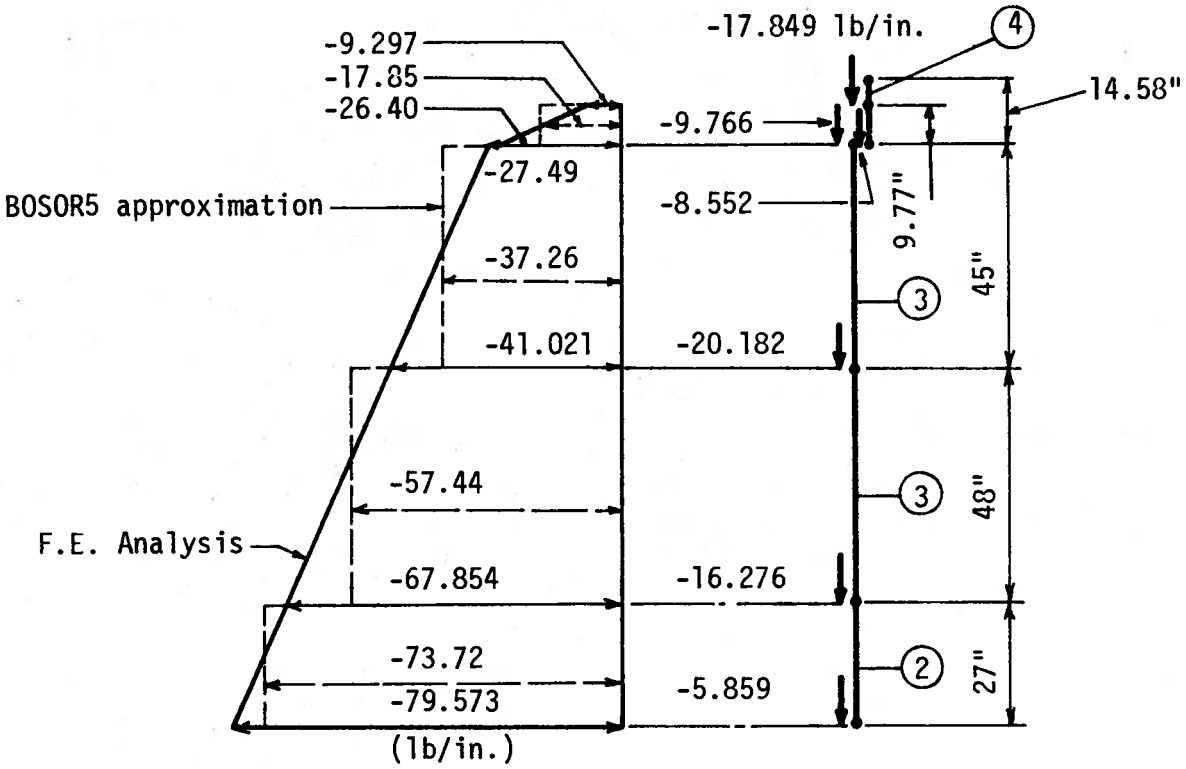

FIGURE 3.13 - Approximation of Gravity Loading (First Model)

Segment	p_h (psi)
7	0.03815
6	0.1892
5	0.4483
4	0.7675
3	2.6223
2	4.7925
1	0.0

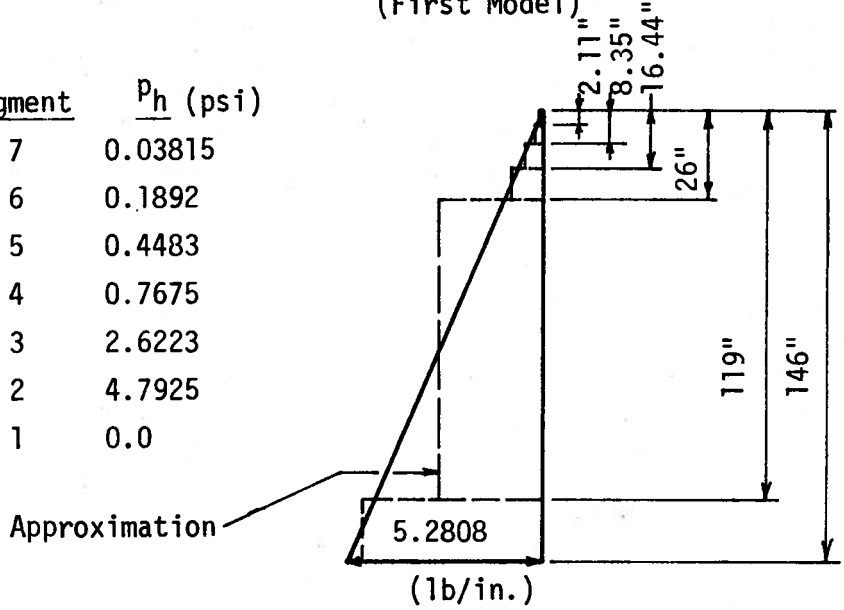

FIGURE 3.14 - Approximation of Hydrostatic Pressure Variation

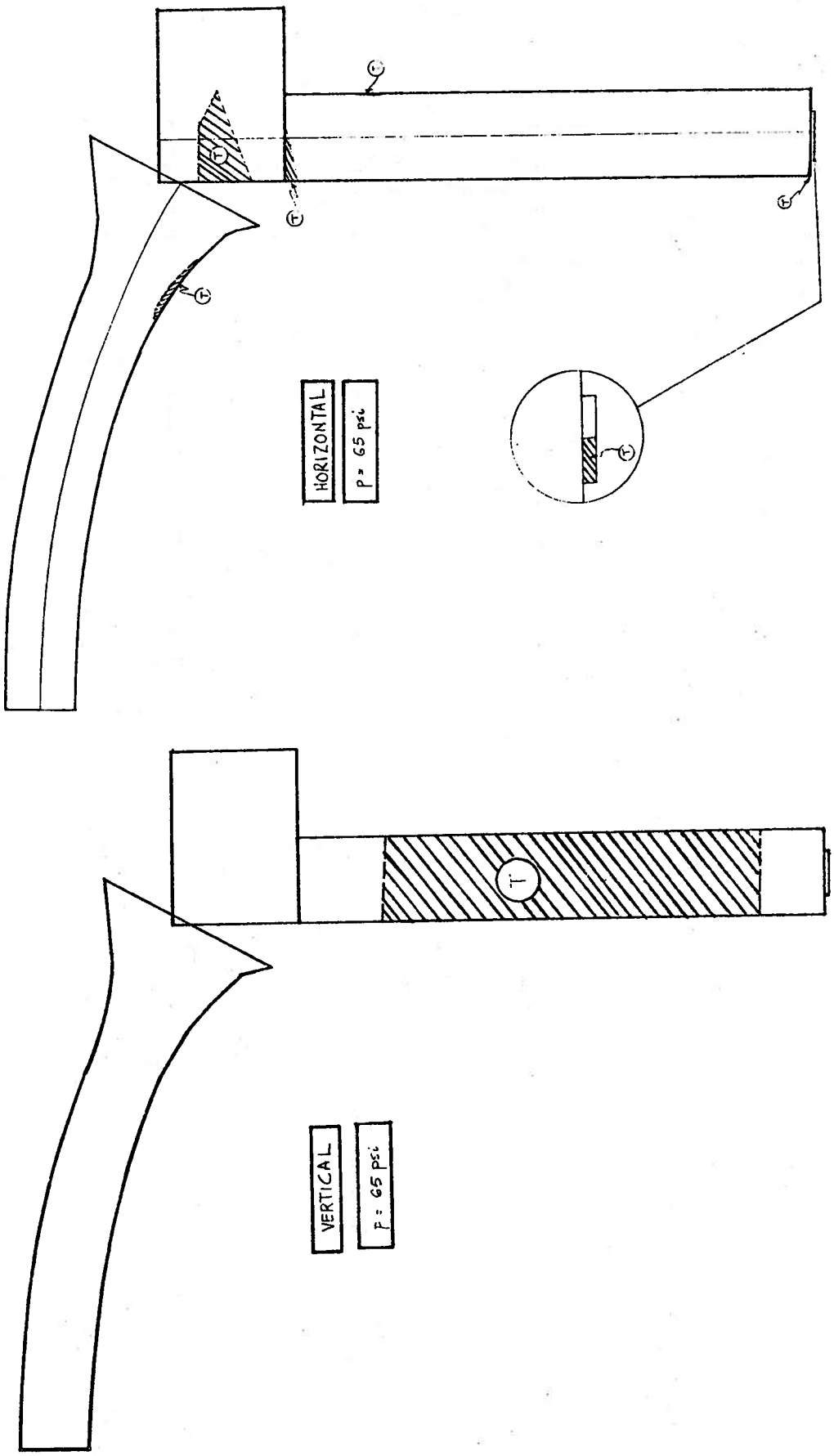

FIGURE 3.15 - Cracking in Structure at 65 psi
(First Model)

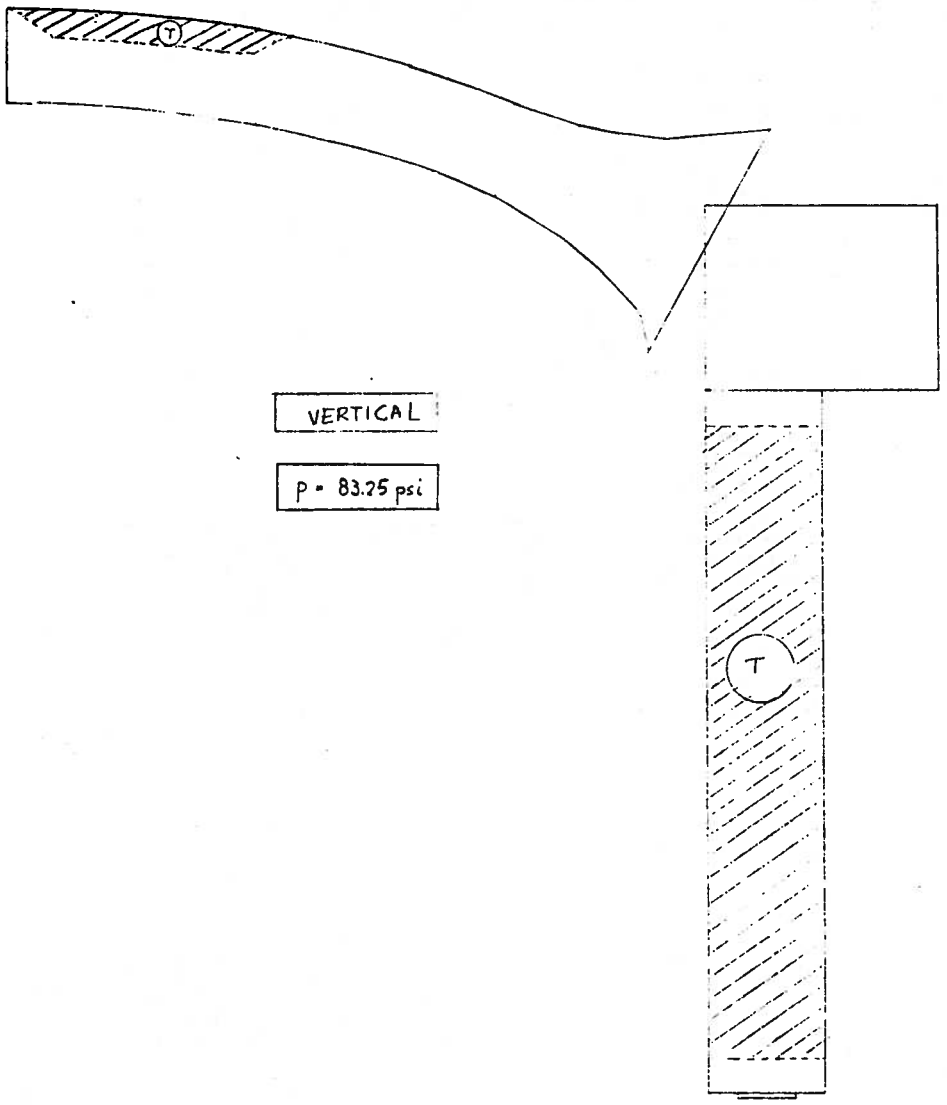

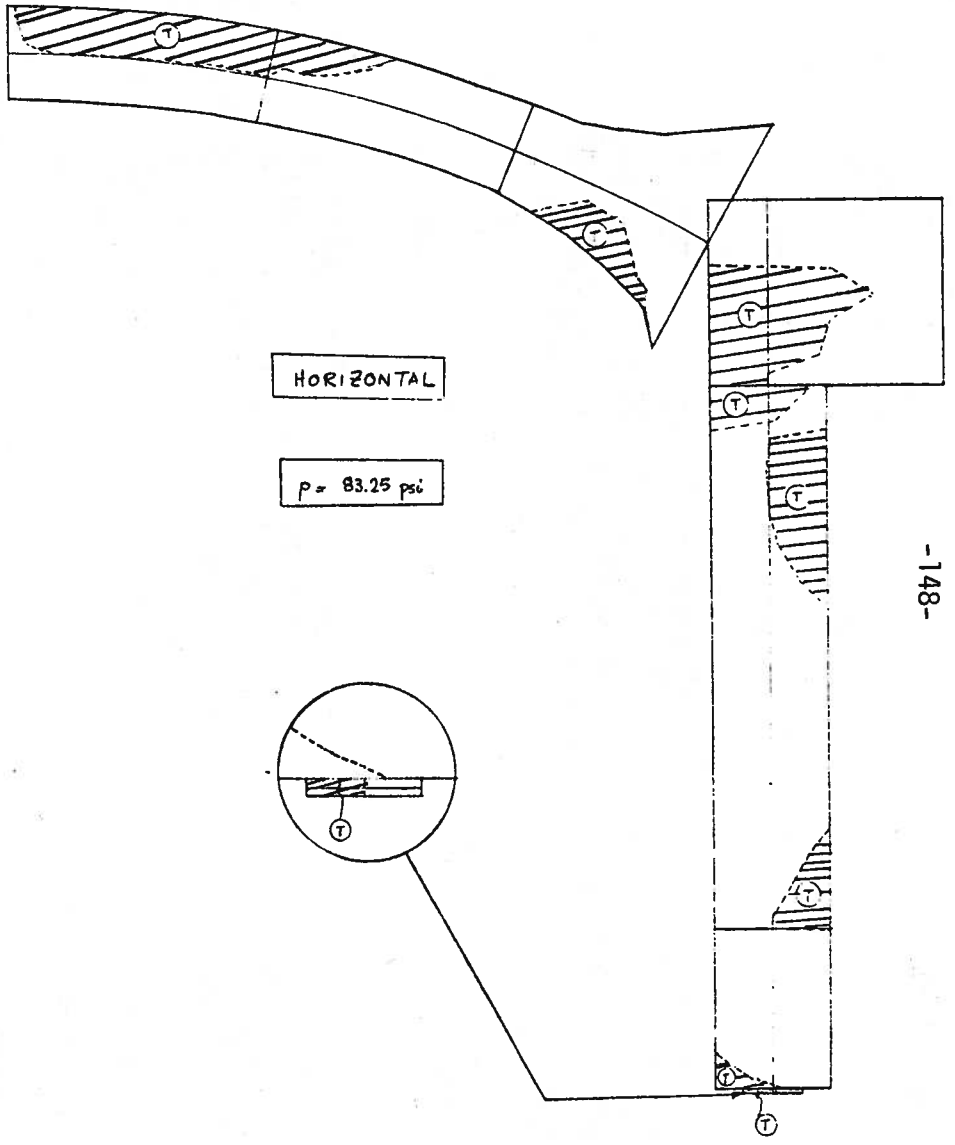

FIGURE 3.16 - Cracking in Structure at 83.25 psi
(First Model)

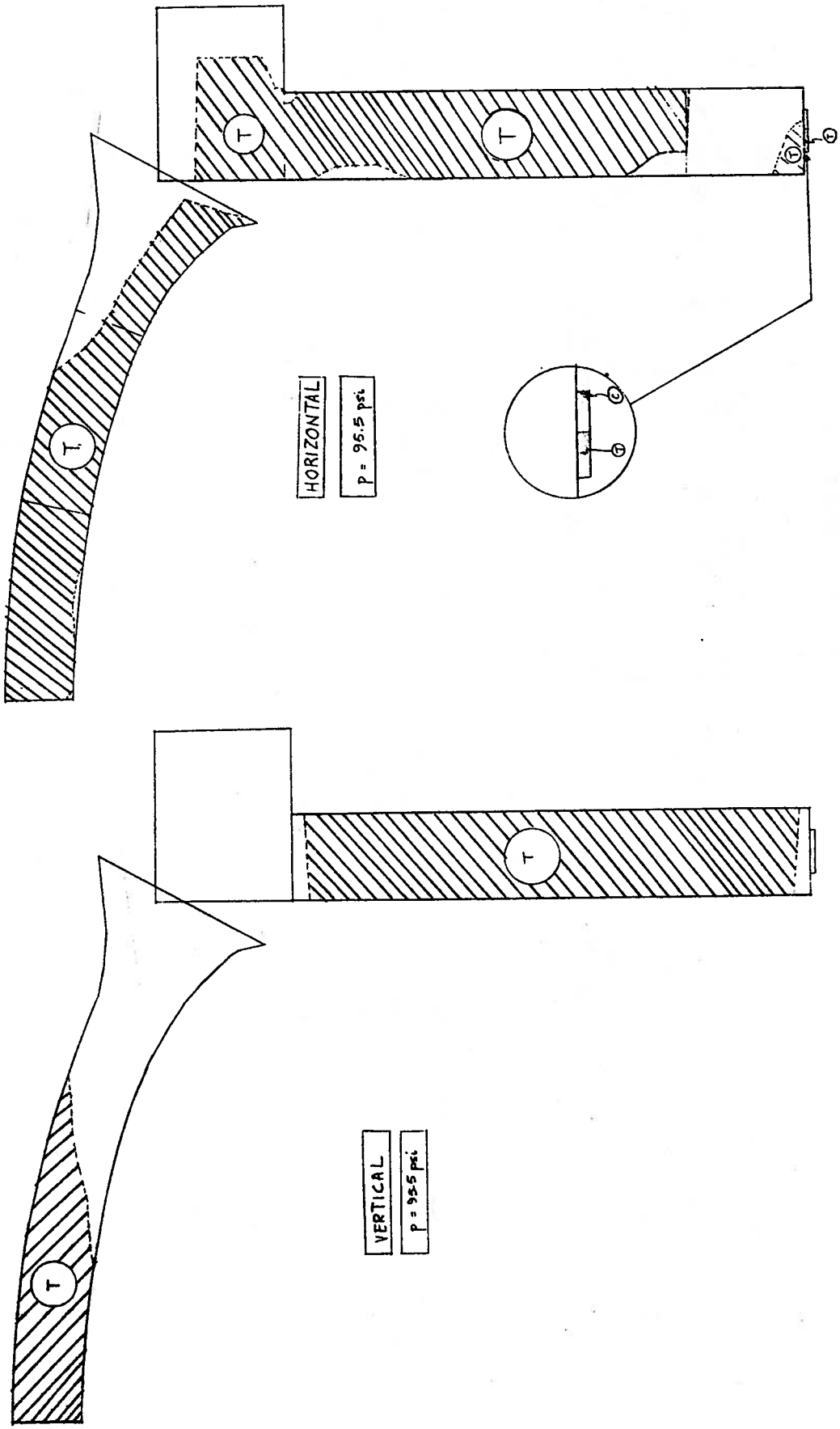

FIGURE 3.17 - Cracking in Structure at 95.5 psi
(First Model)

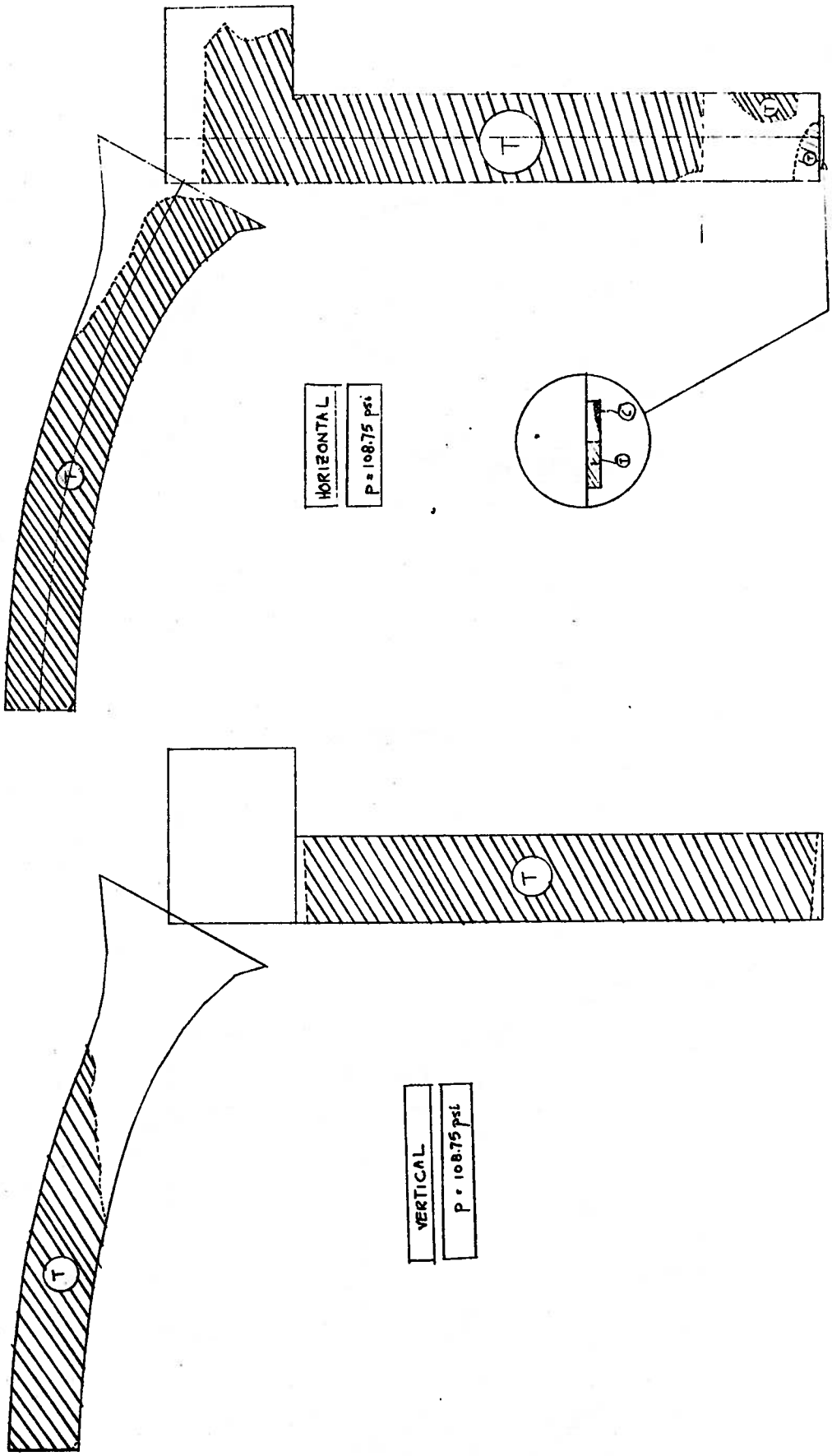

FIGURE 3.18 - Cracking in Structure at 108.75 psi
(First Model)

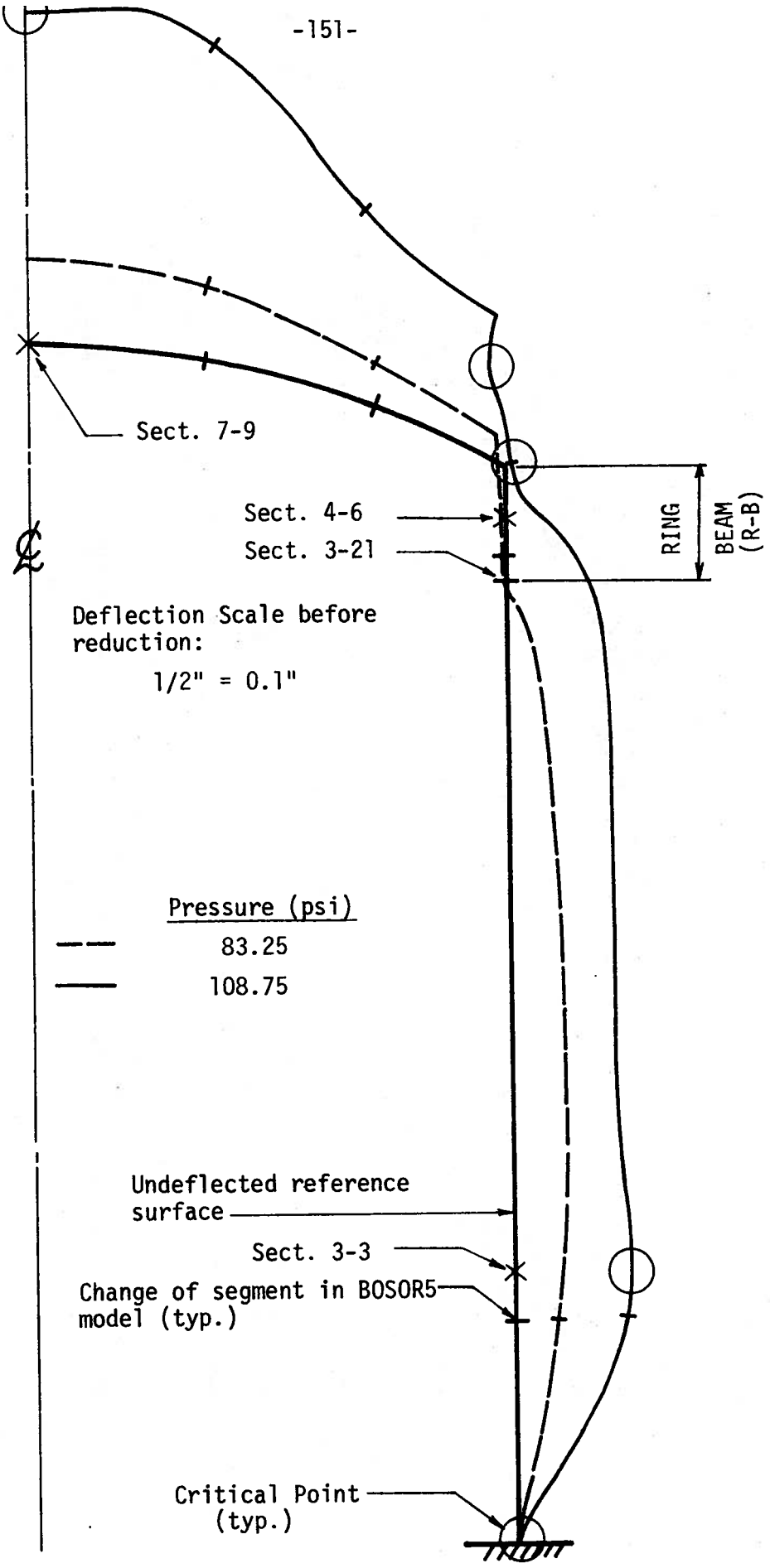

FIGURE 3.19 - Deflections at 83.25 psi and Terminal Pressure (108.75 psi)

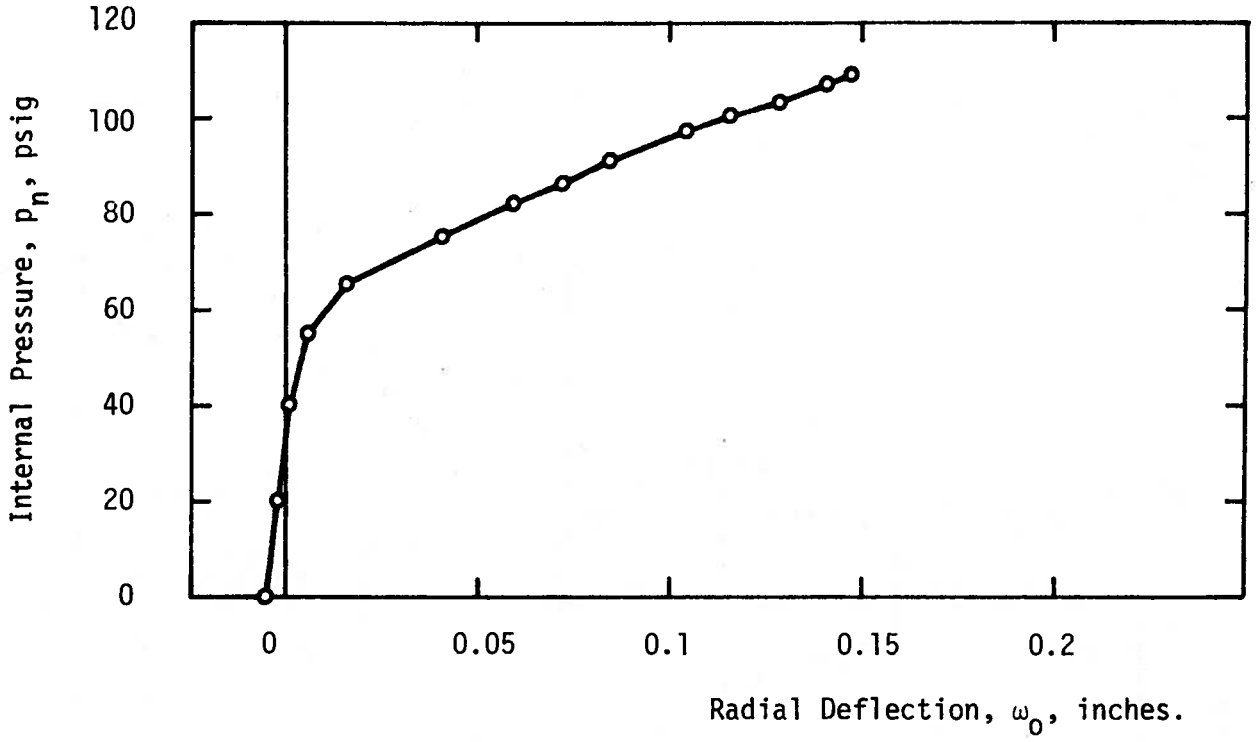

(a) Load-Deflection Curve at 34.5" from the Base.

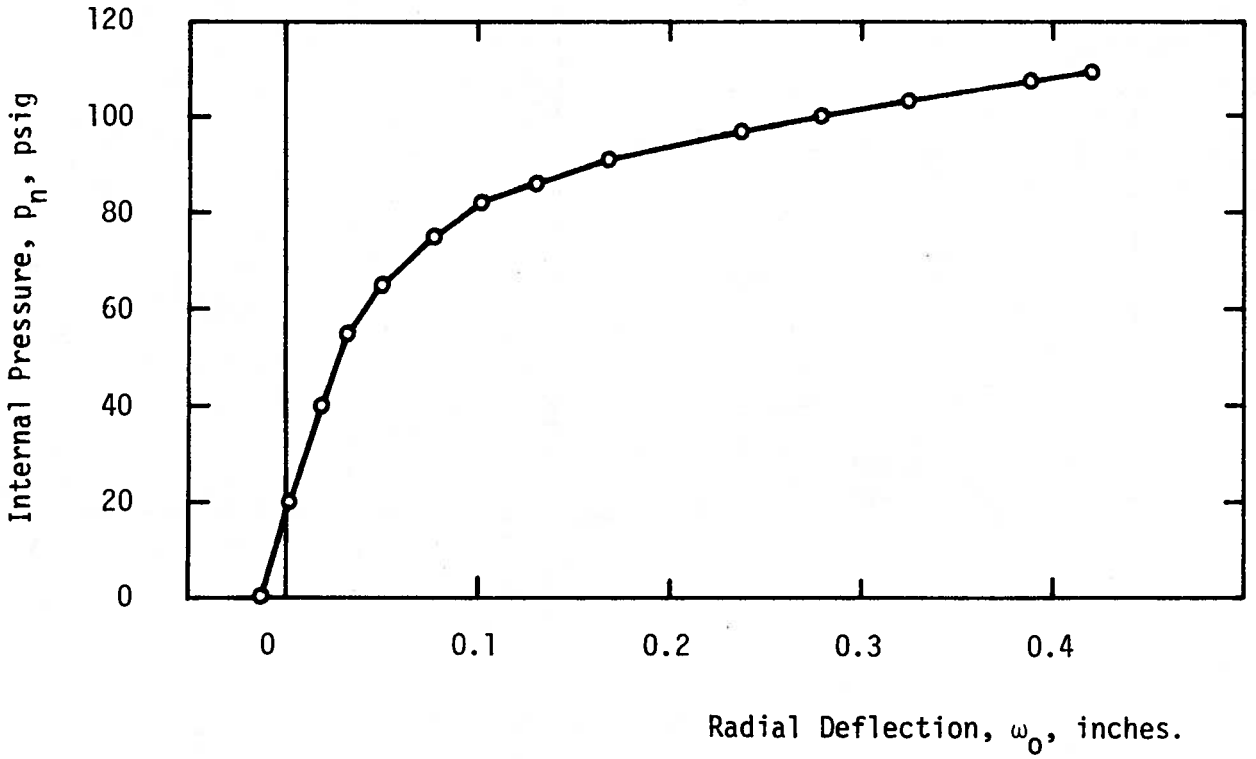

(b) Load-Deflection Curve at the Crown of the Dome.

FIGURE 3.20 - Pressure-Deflection Curves
(First Model)

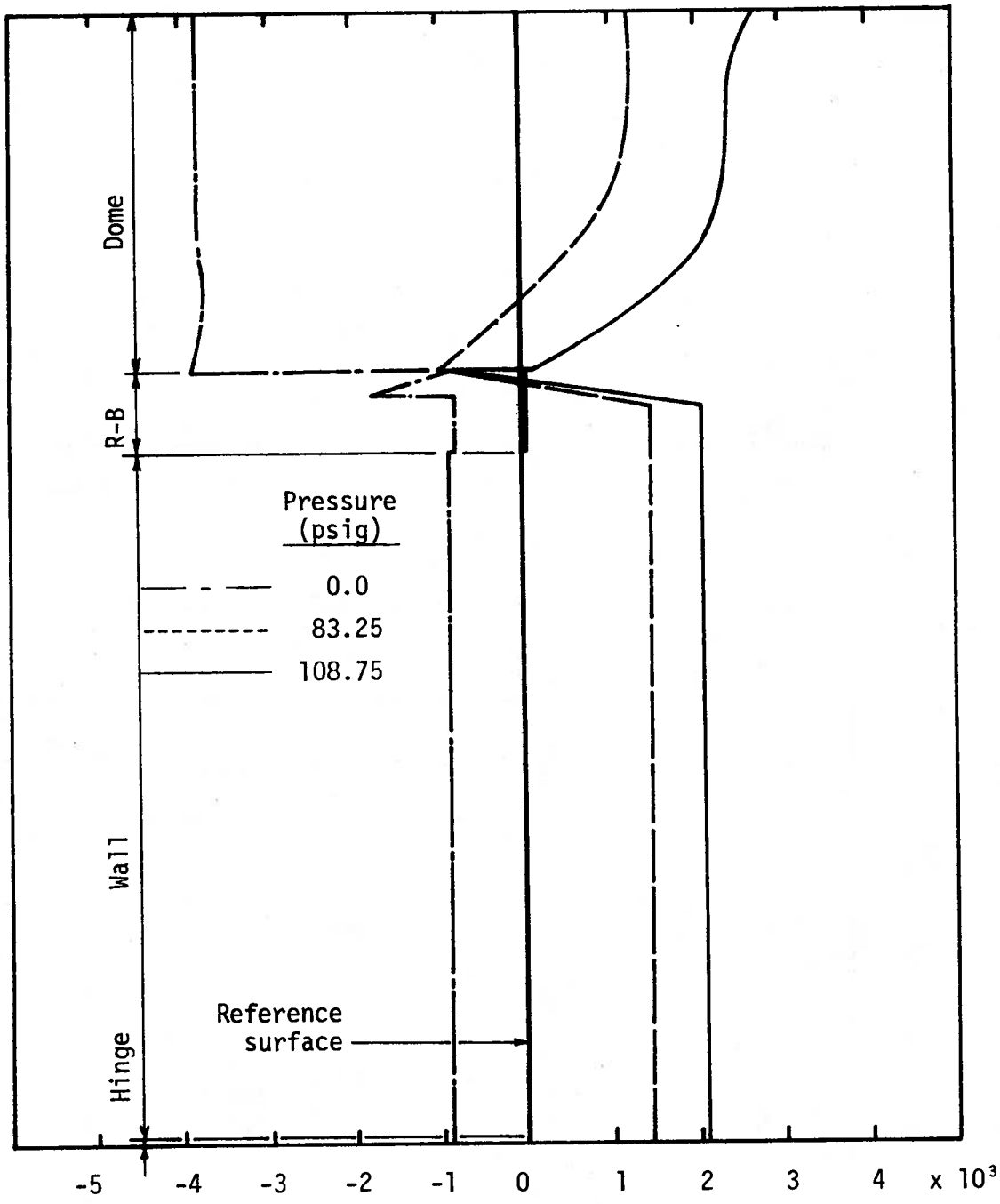

FIGURE 3.21 - Meridional Force N1 (First Model)

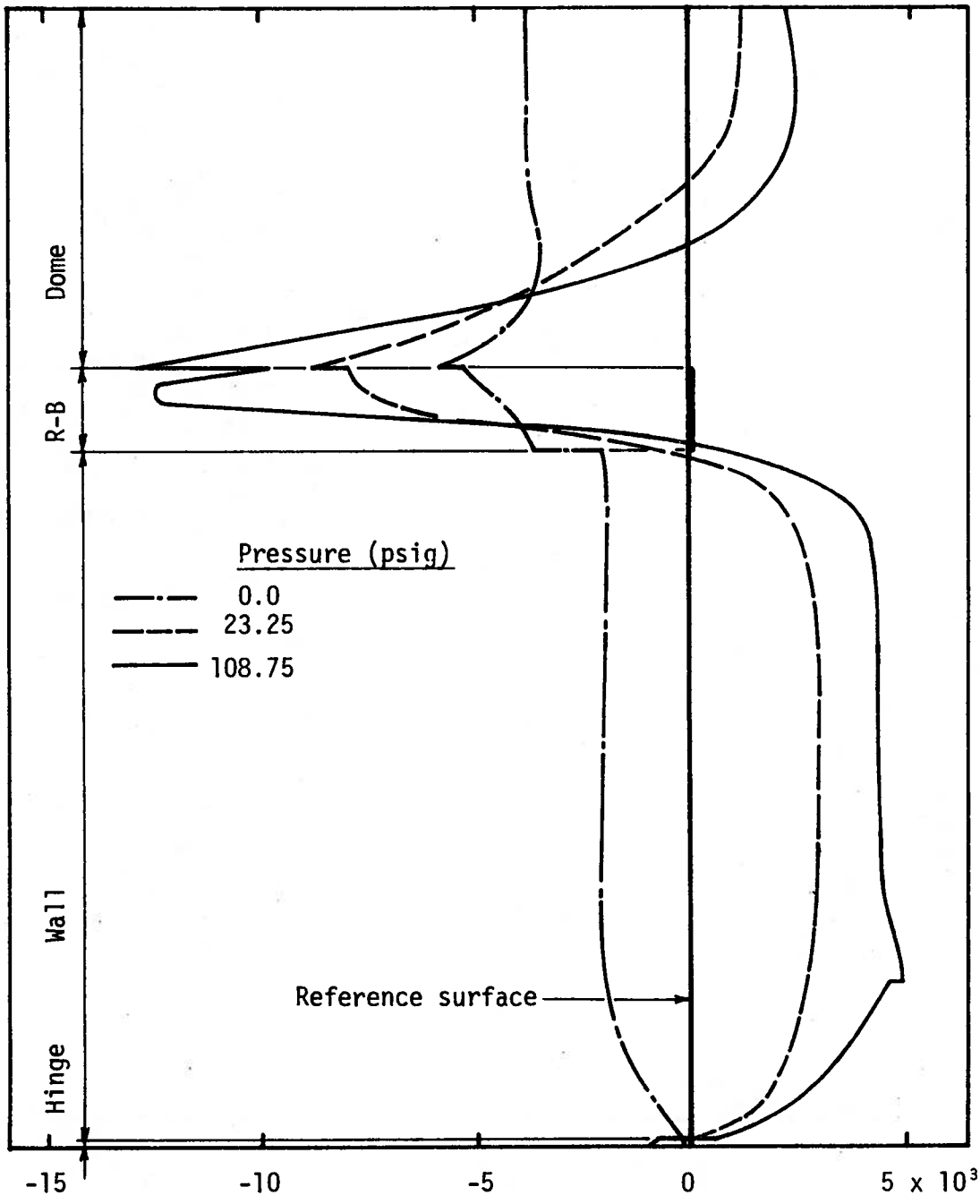

FIGURE 3.22 - Circumferential Force N2 (First Model)

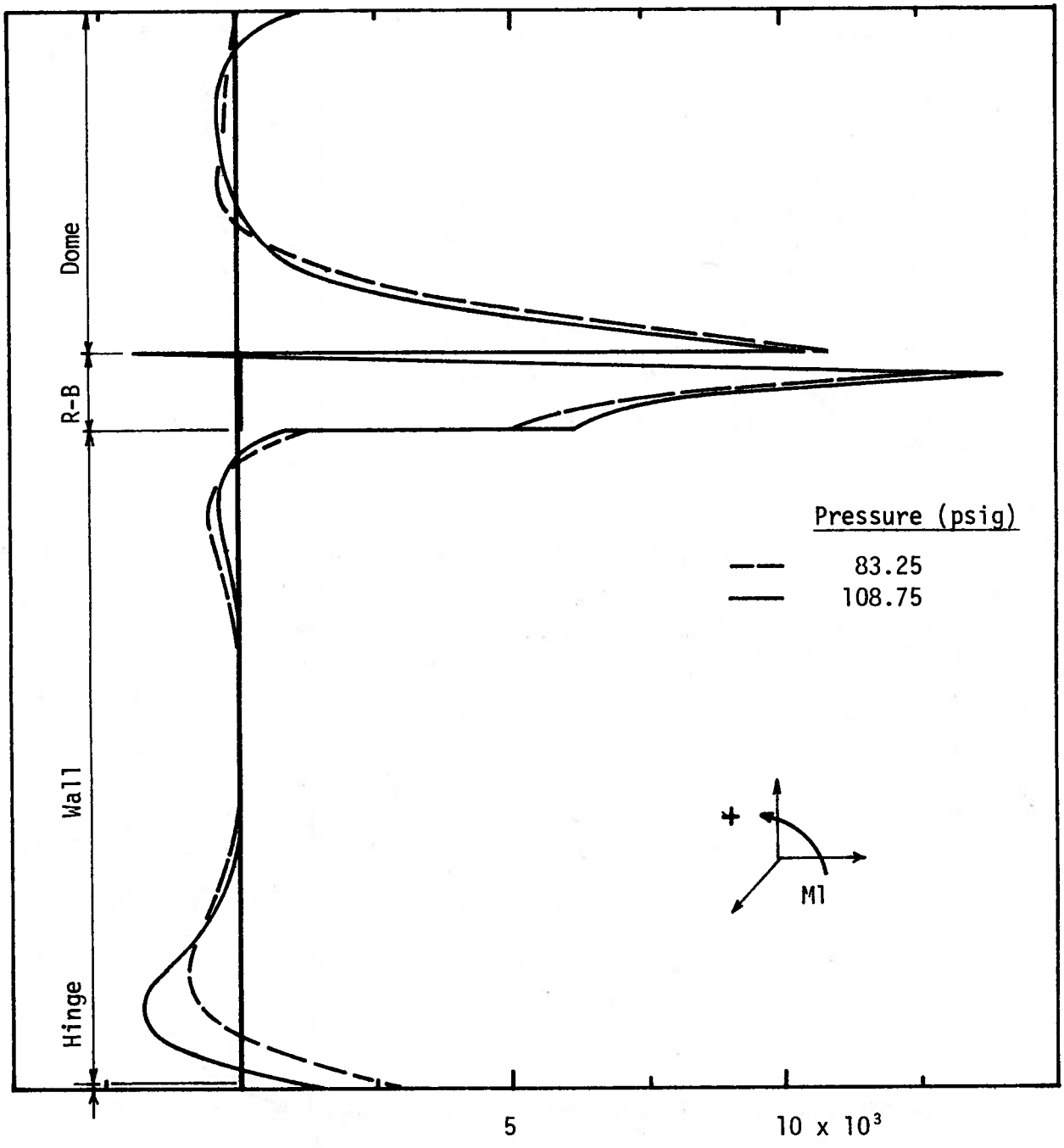

FIGURE 3.23 - Meridional Moment M1 (First Model)

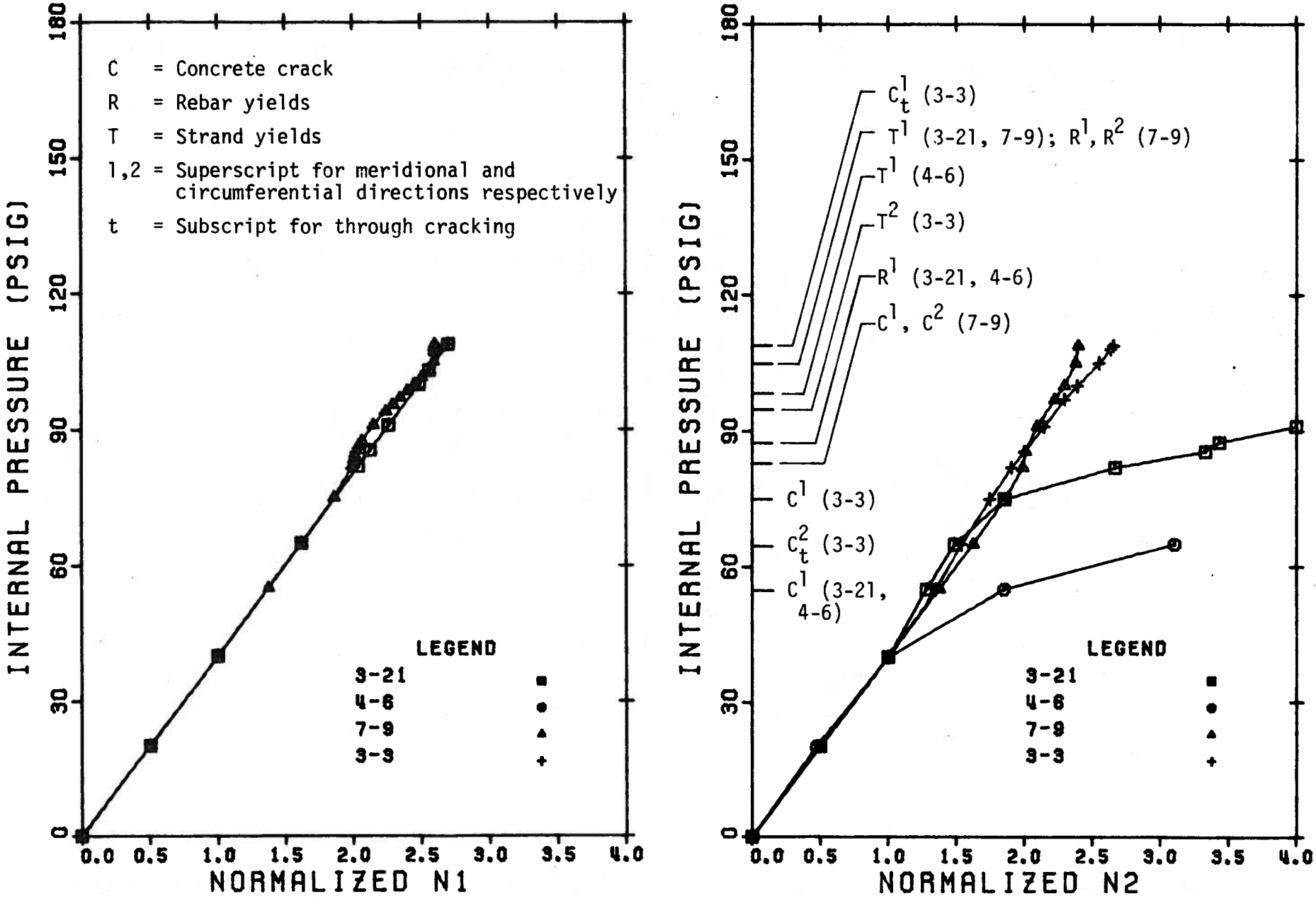

FIGURE 3.24 - Selected Nondimensionalized Pressure - Force Plots (First Model)

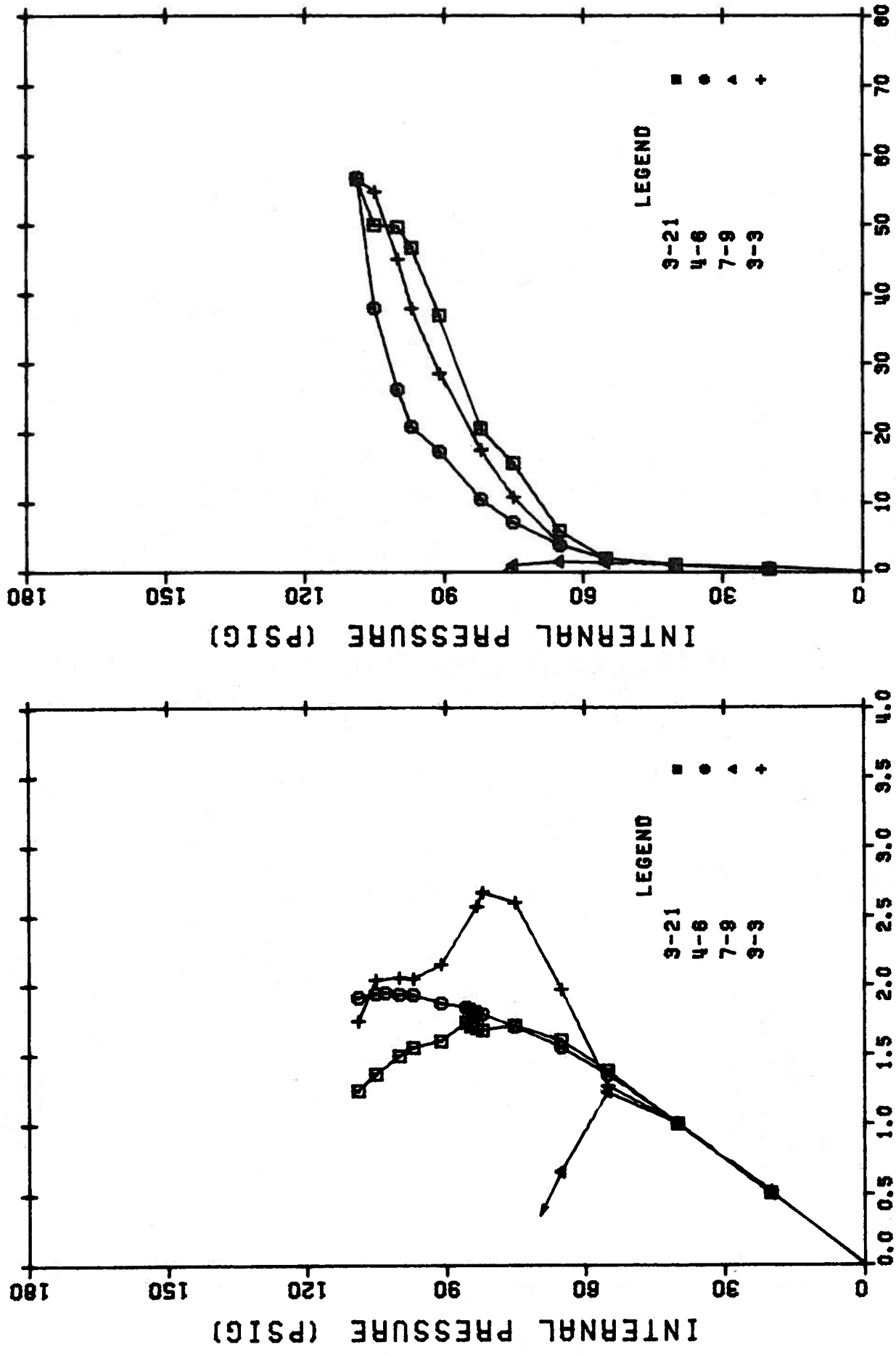

FIGURE 3.25 - Selected Nondimensionalized Pressure - Force Plots (First Model)

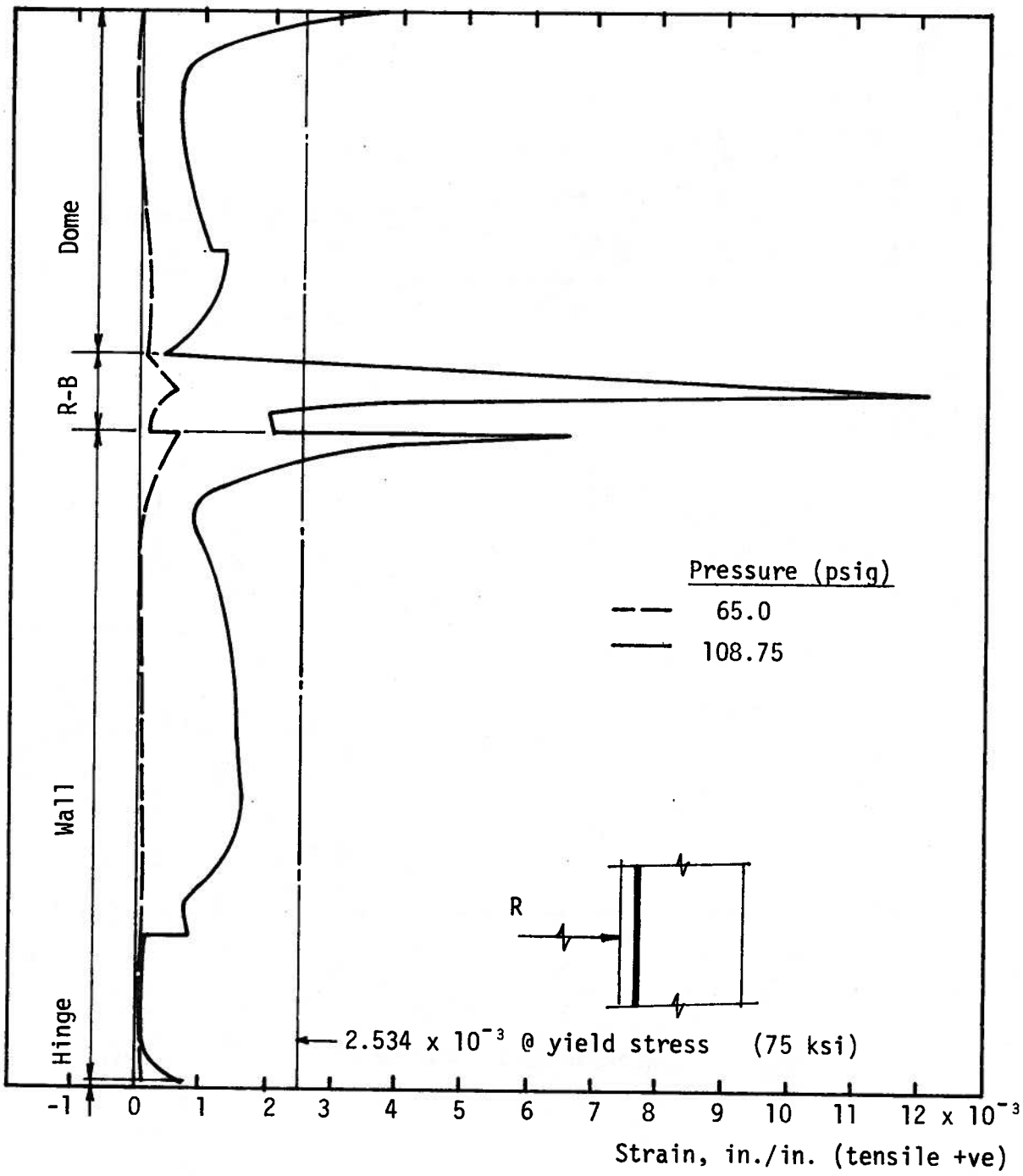

FIGURE 3.26 - Interior Meridional Steel Strain (First Model)

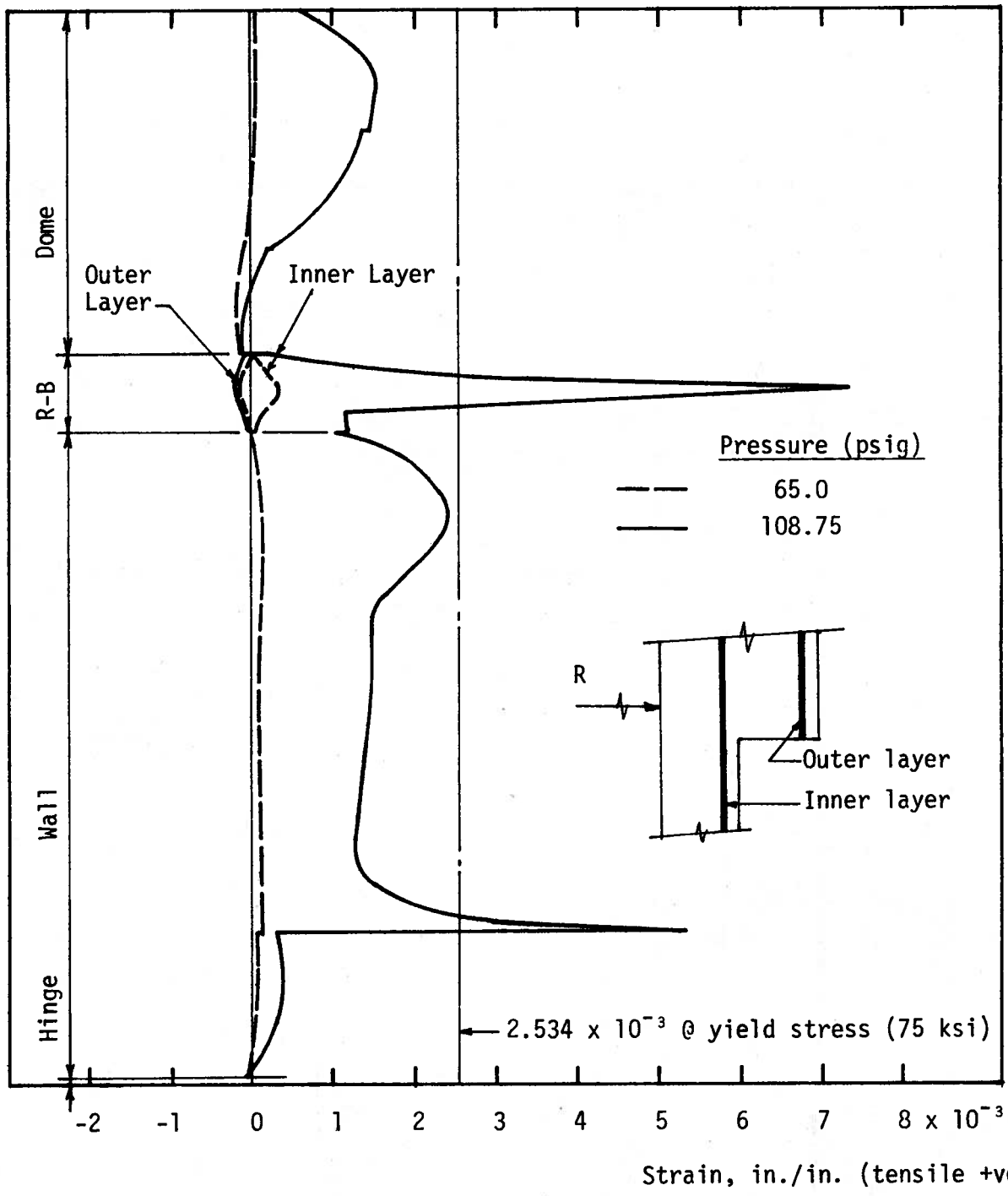

FIGURE 3.27 - Exterior Meridional Steel Strain (First Model)

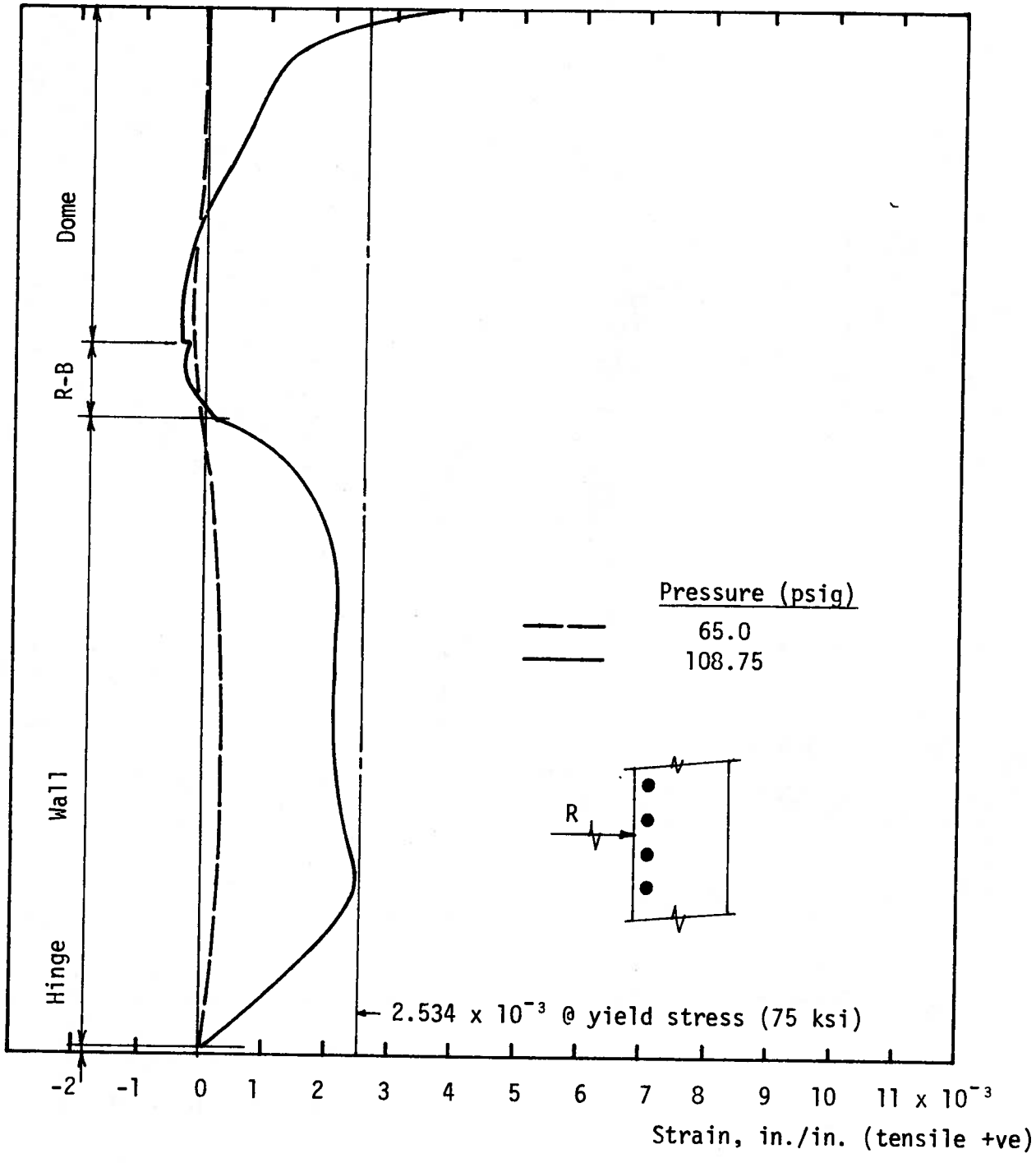

FIGURE 3.28 - Interior Circumferential Steel Strain (First Model)

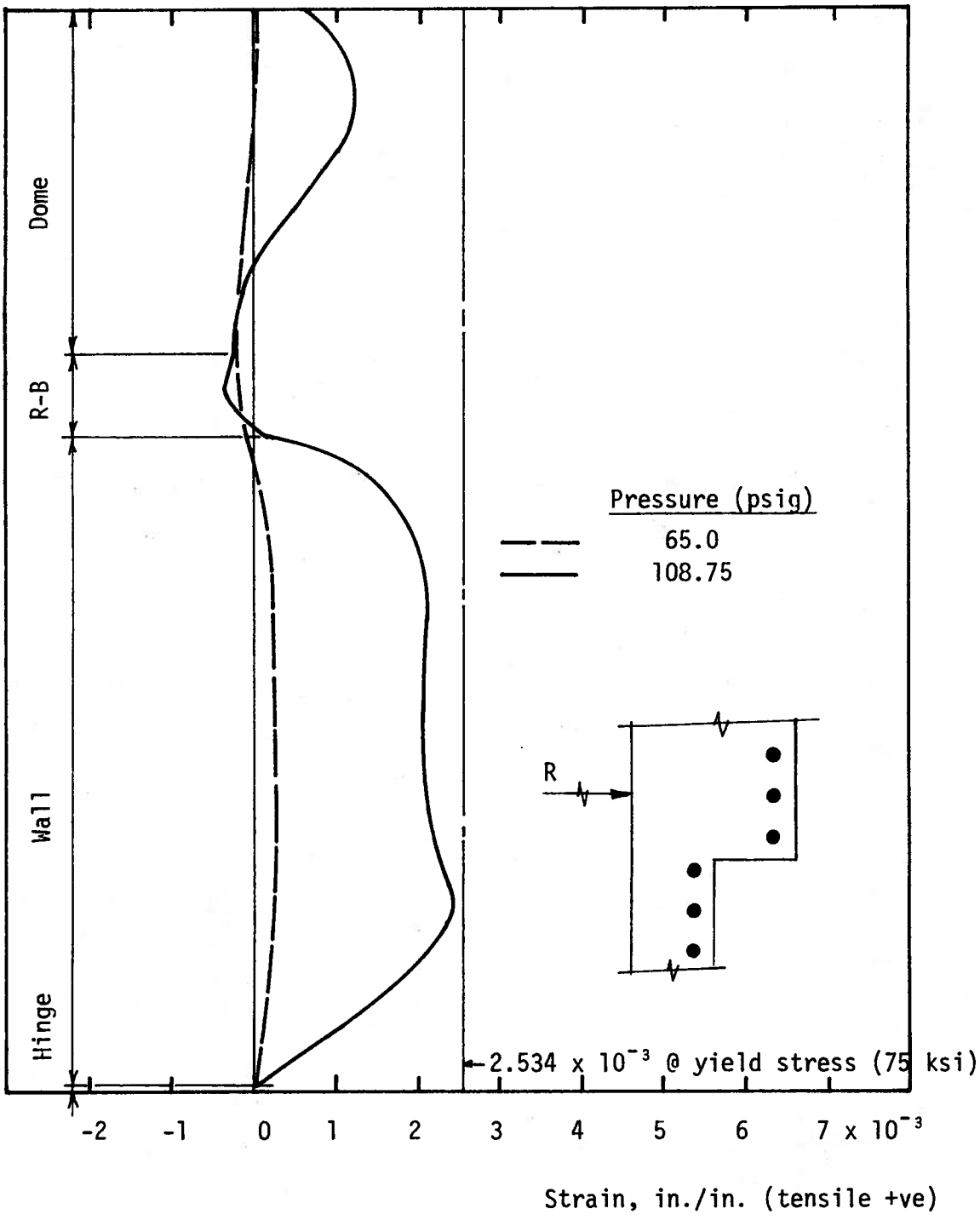

FIGURE 3.29 - Exterior Circumferential Steel Strain (First Model)

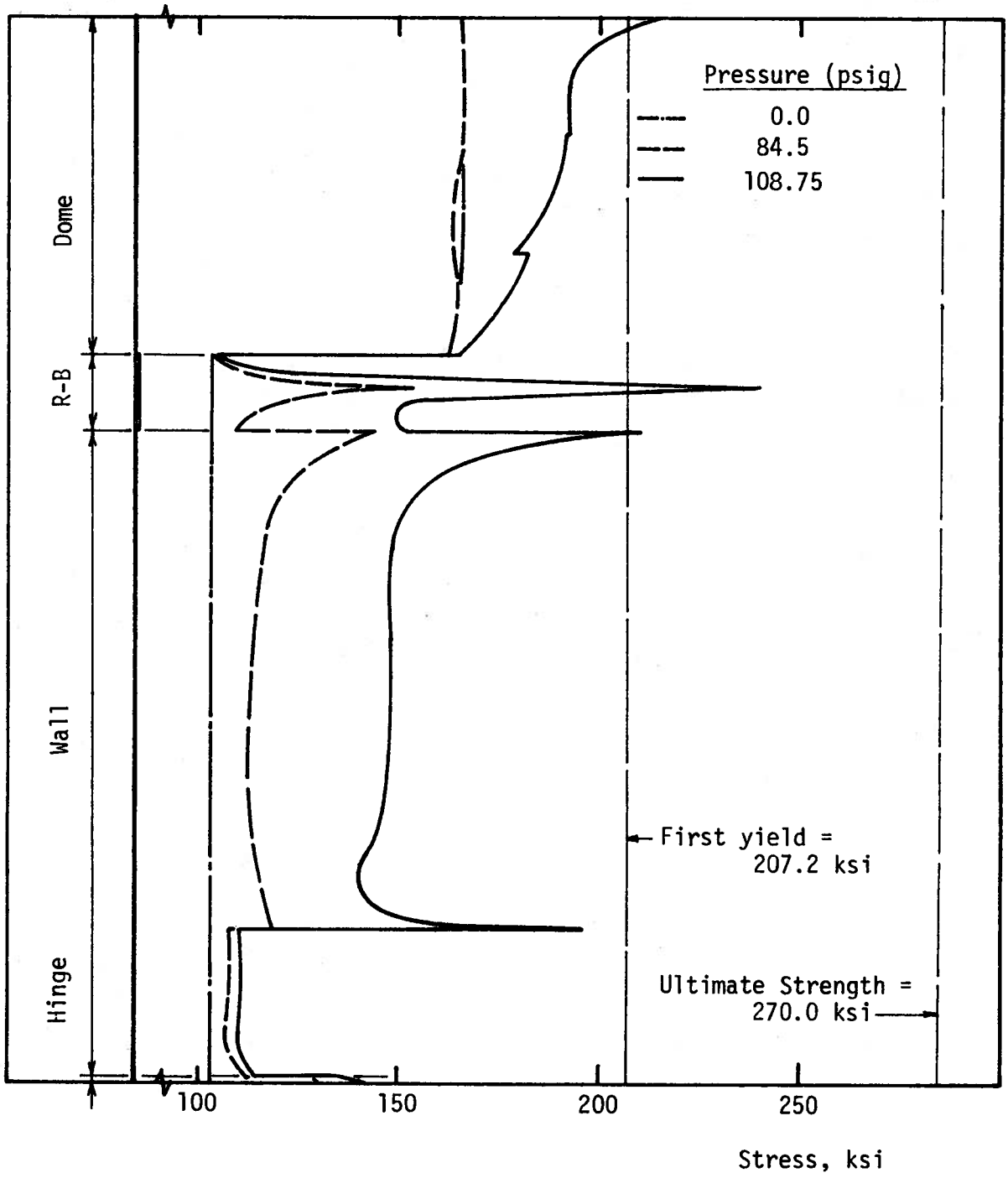

FIGURE 3.30 - Meridional Tendon Stresses (First Model)

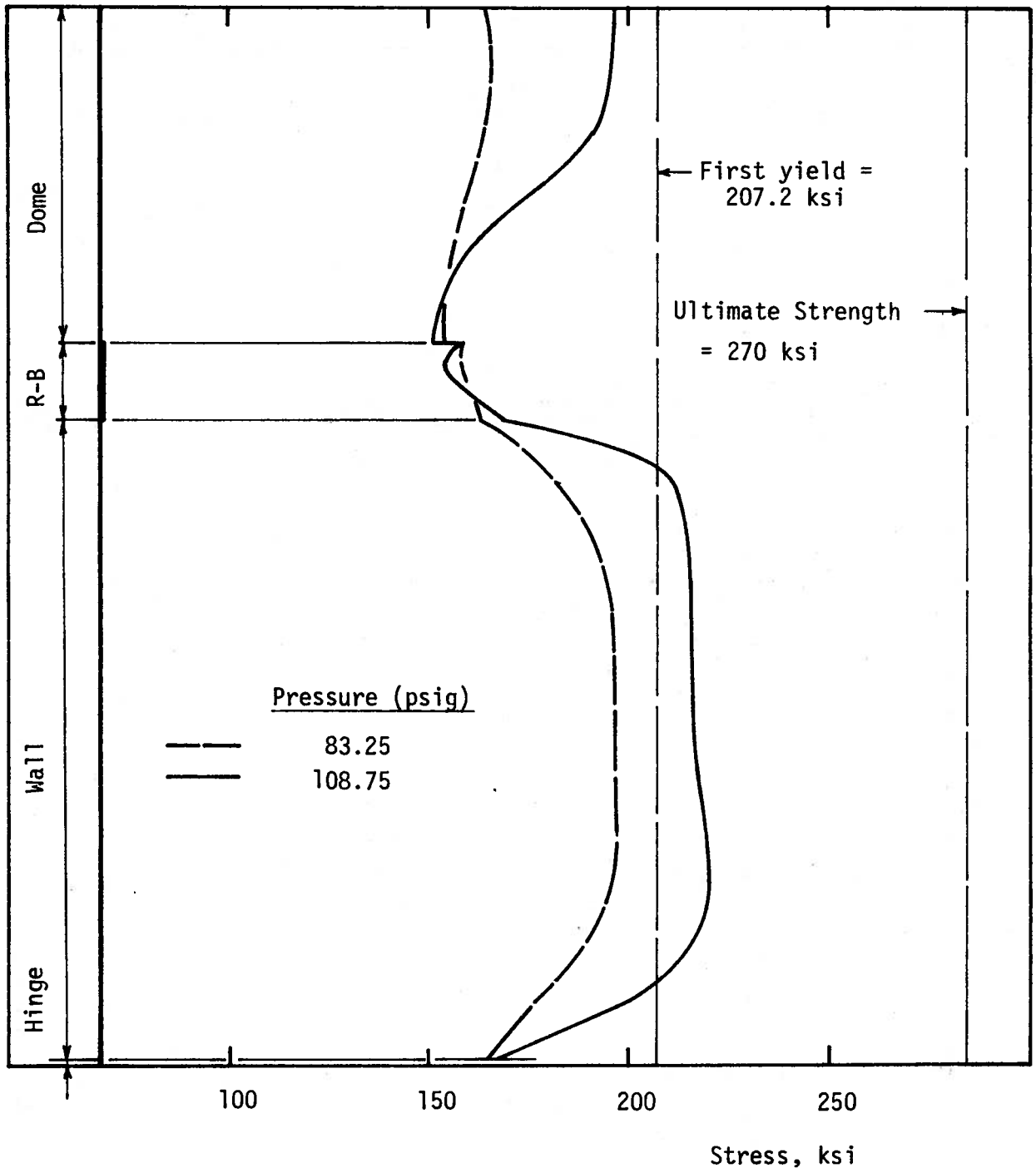

FIGURE 3.31 - Circumferential Tendon Stresses (First Model)

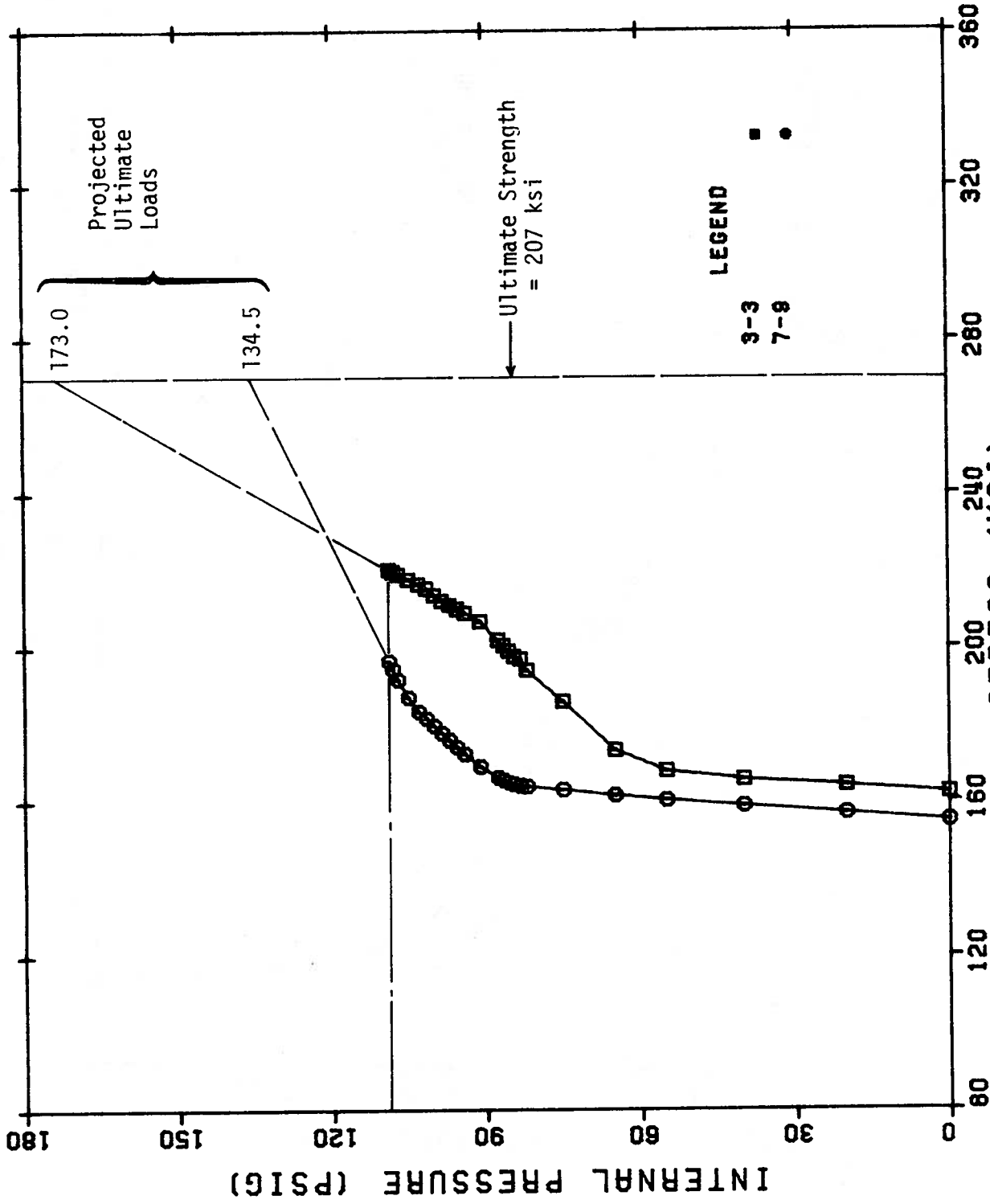

FIGURE 3.32 - Extrapolation of Circumferential Tendon Stresses

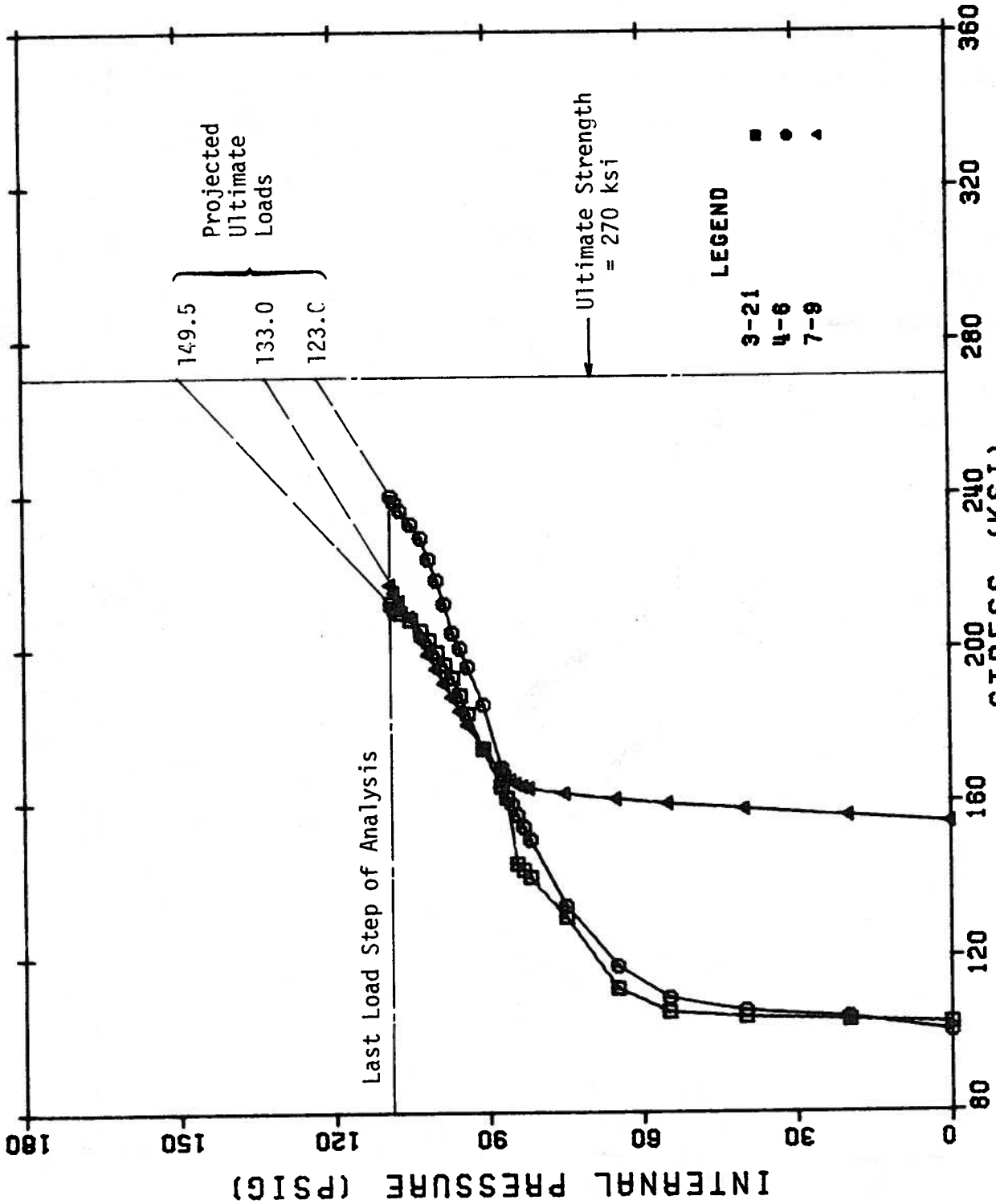

FIGURE 3.33 - Extrapolation of Meridional Tendon Stresses

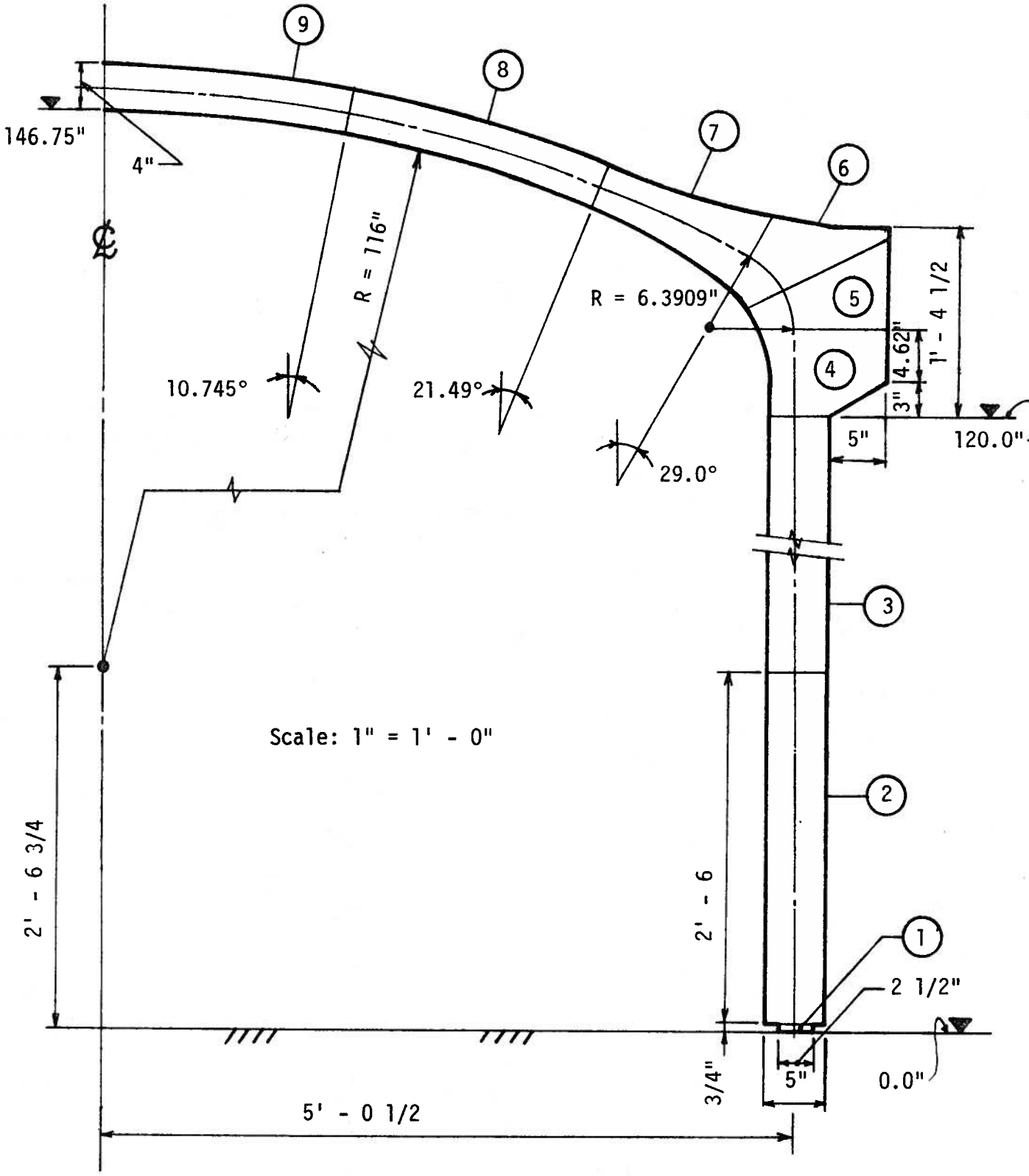

FIGURE 4.1 - Overall Geometry of Second Model

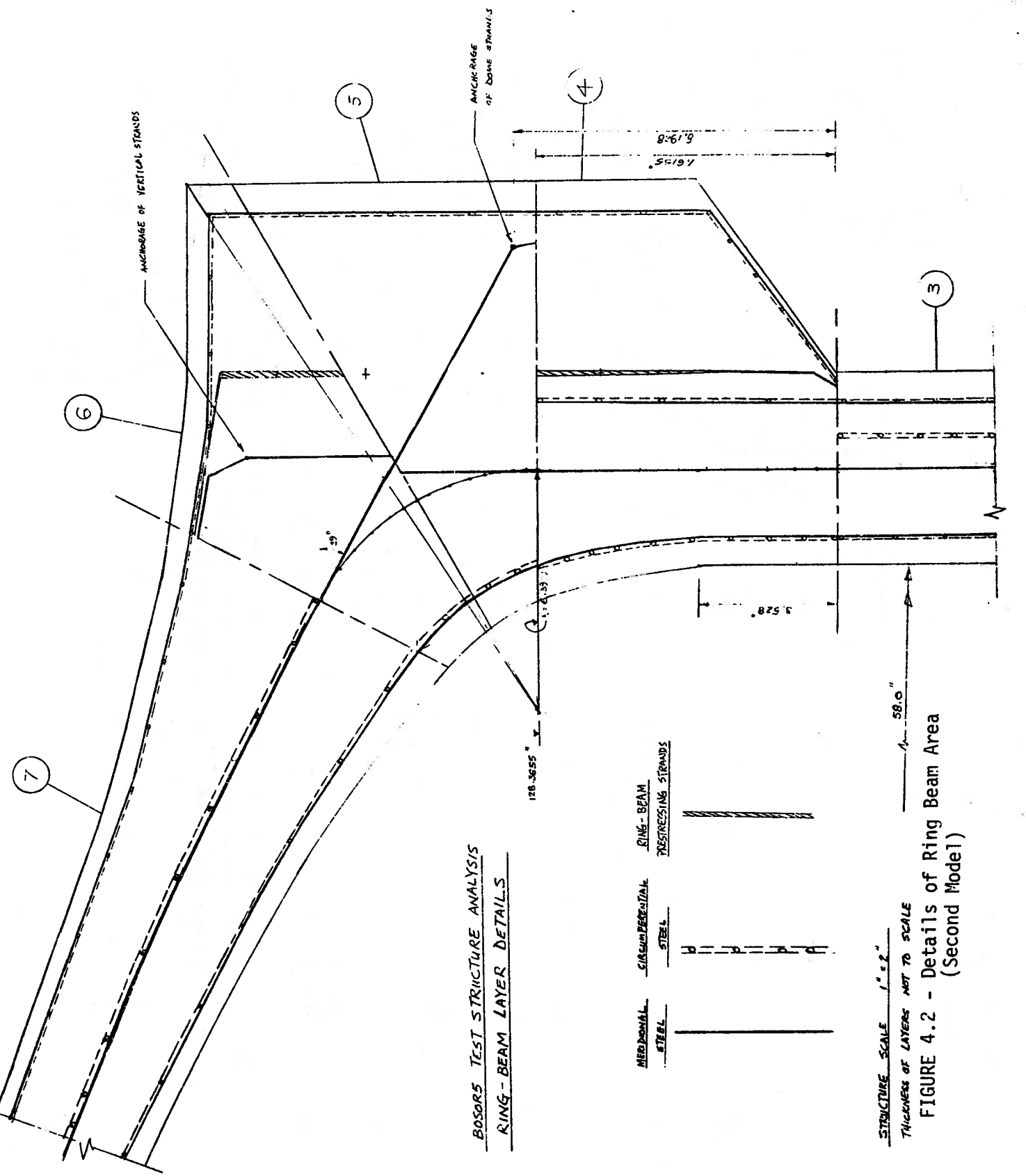

FIGURE 4.2 - Details of Ring Beam Area
(Second Model)

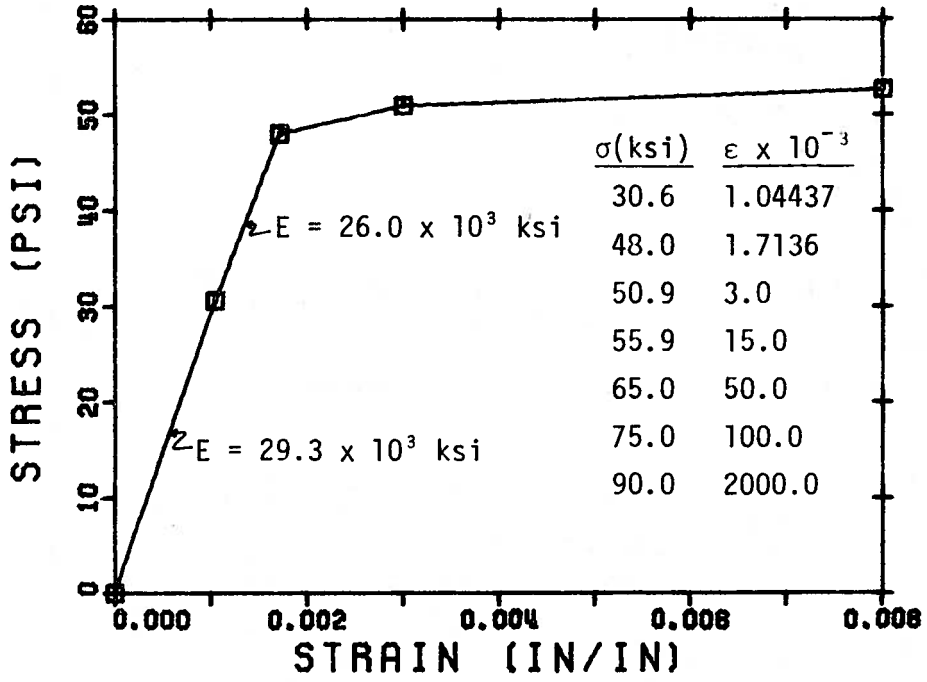

(a) Stress-Strain Curve for #3 Rebar (Mat. type 2)

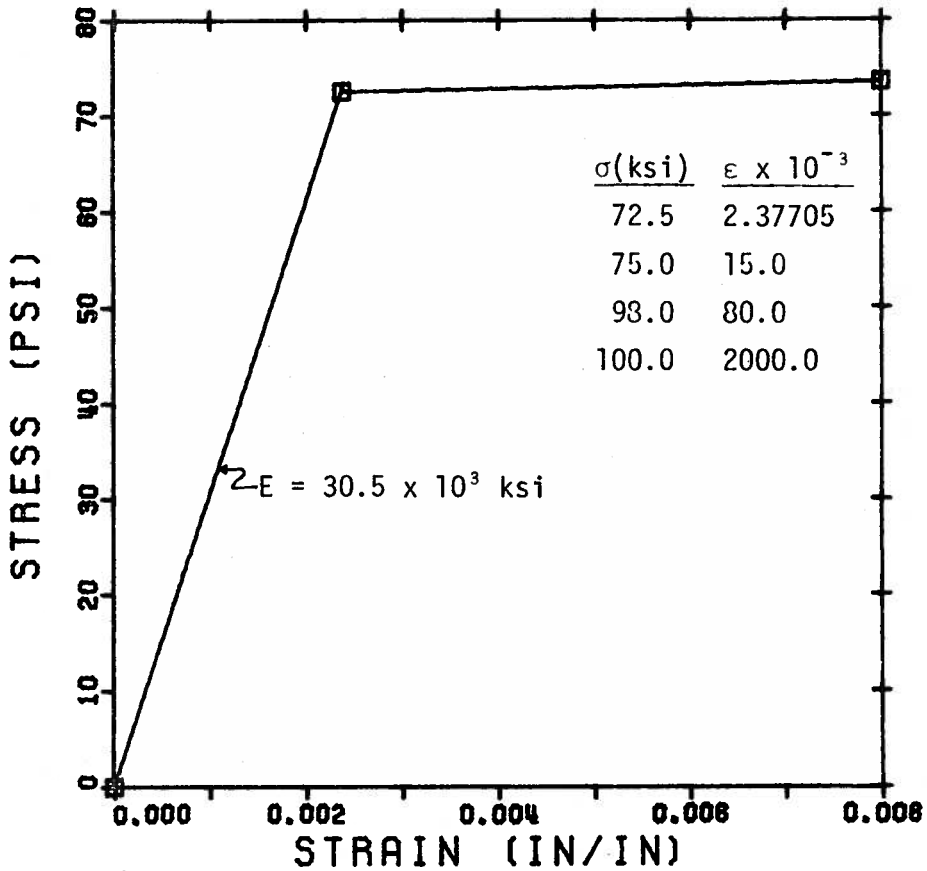

(b) Stress-Strain Curve for 6 mm ϕ bar (Mat. type 3 and 8)

FIGURE 4.3 - Material Properties of Reinforcing (Second Model)

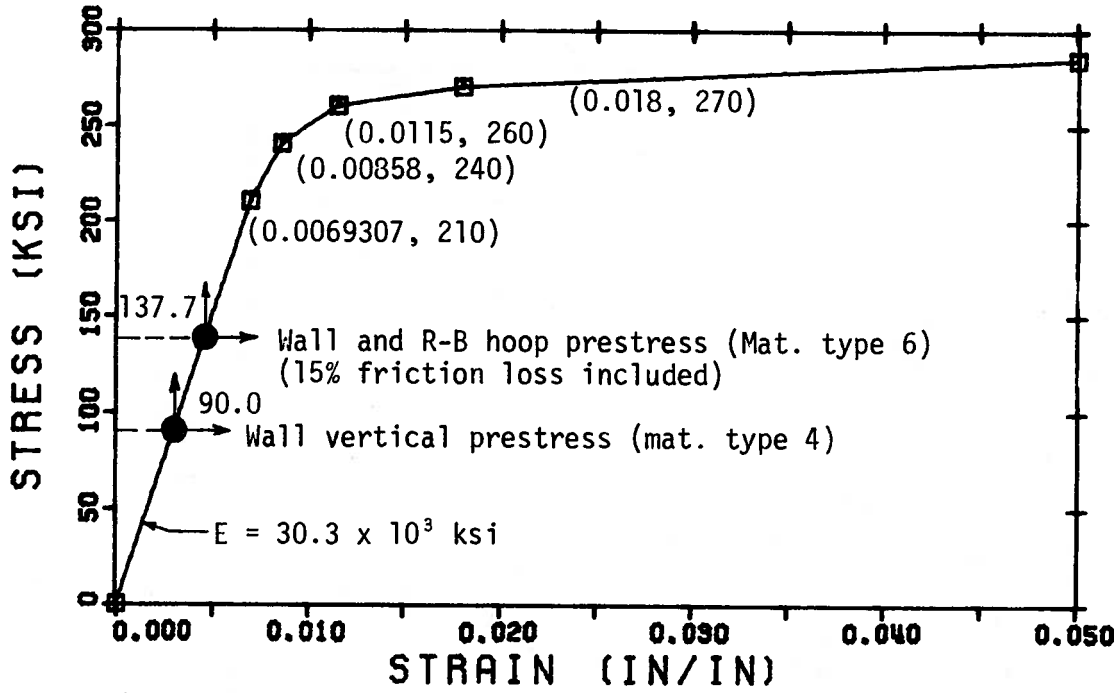

(a) Stress-Strain Curve for 0.5" ϕ Strand

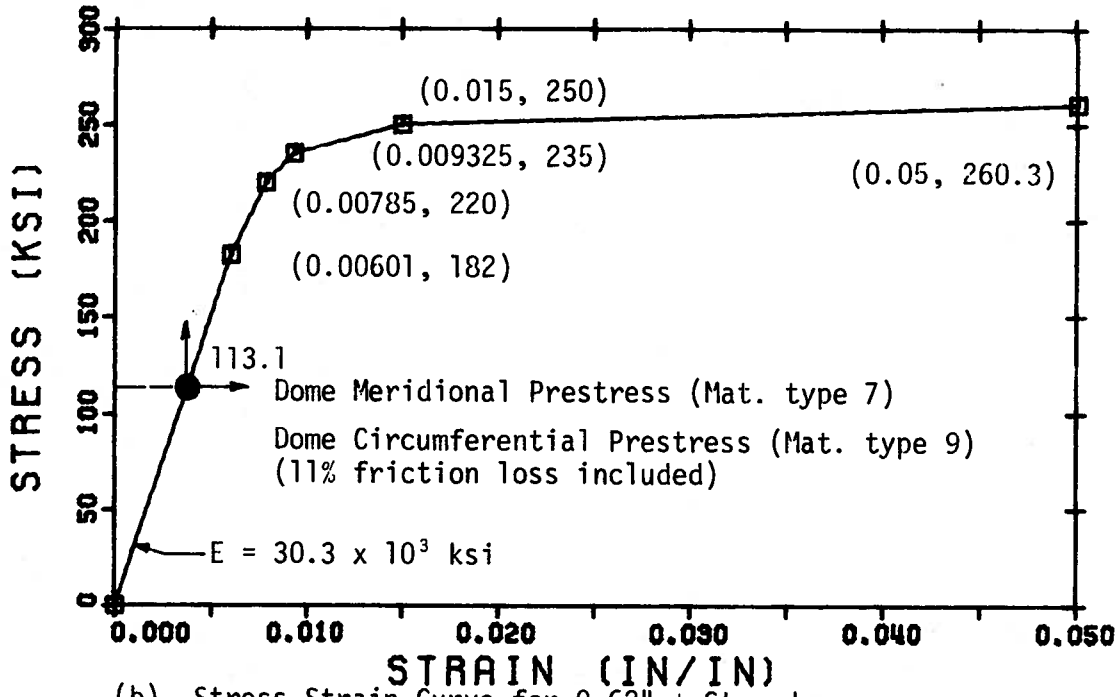

(b) Stress-Strain Curve for 0.62" ϕ Strand

FIGURE 4.4 - Prestressing Strand Properties and Initial Stress Levels (Second Model)

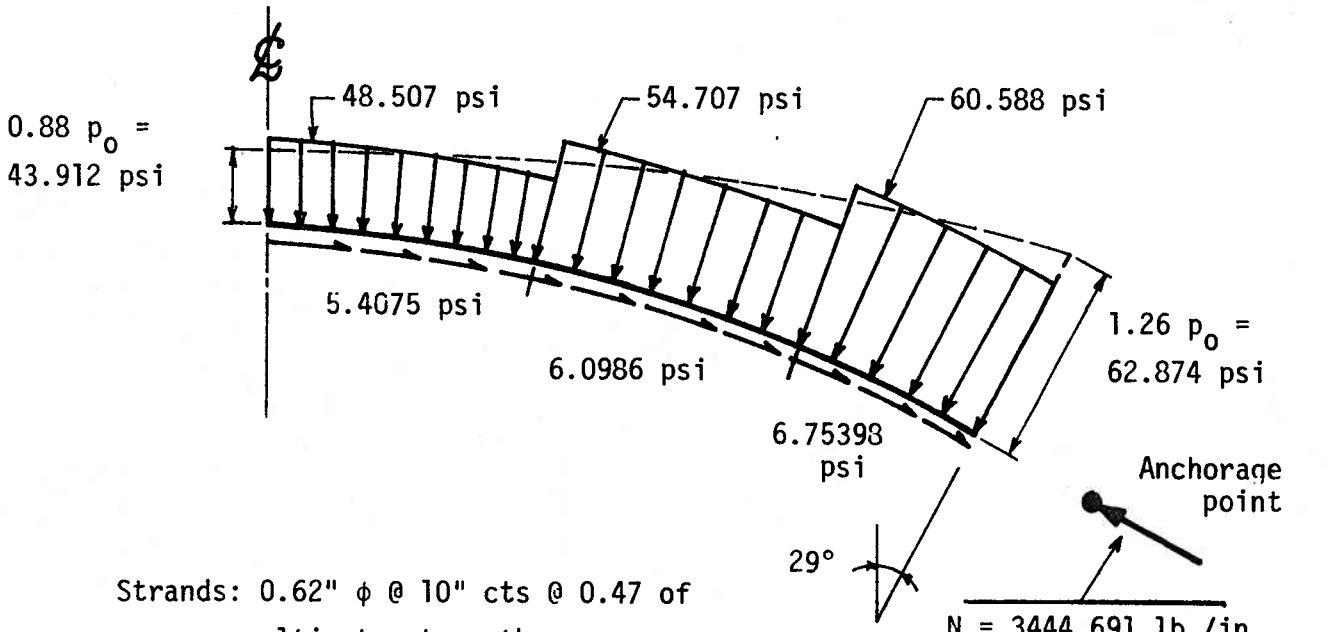

FIGURE 4.5 - Pressure Simulation of Dome Prestressing (Second Model)

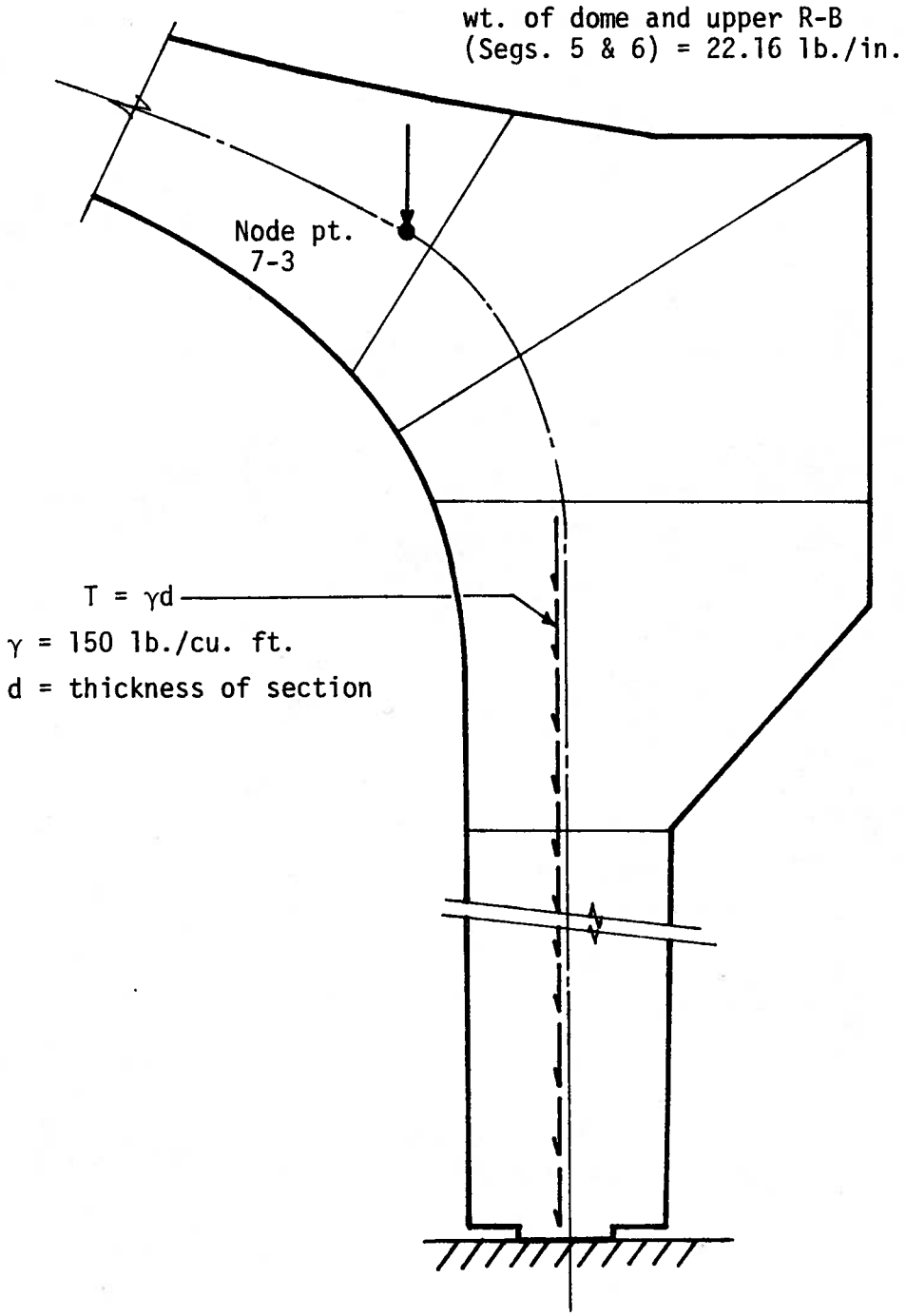

FIGURE 4.6 - Gravity Load Approximation (Second Model)

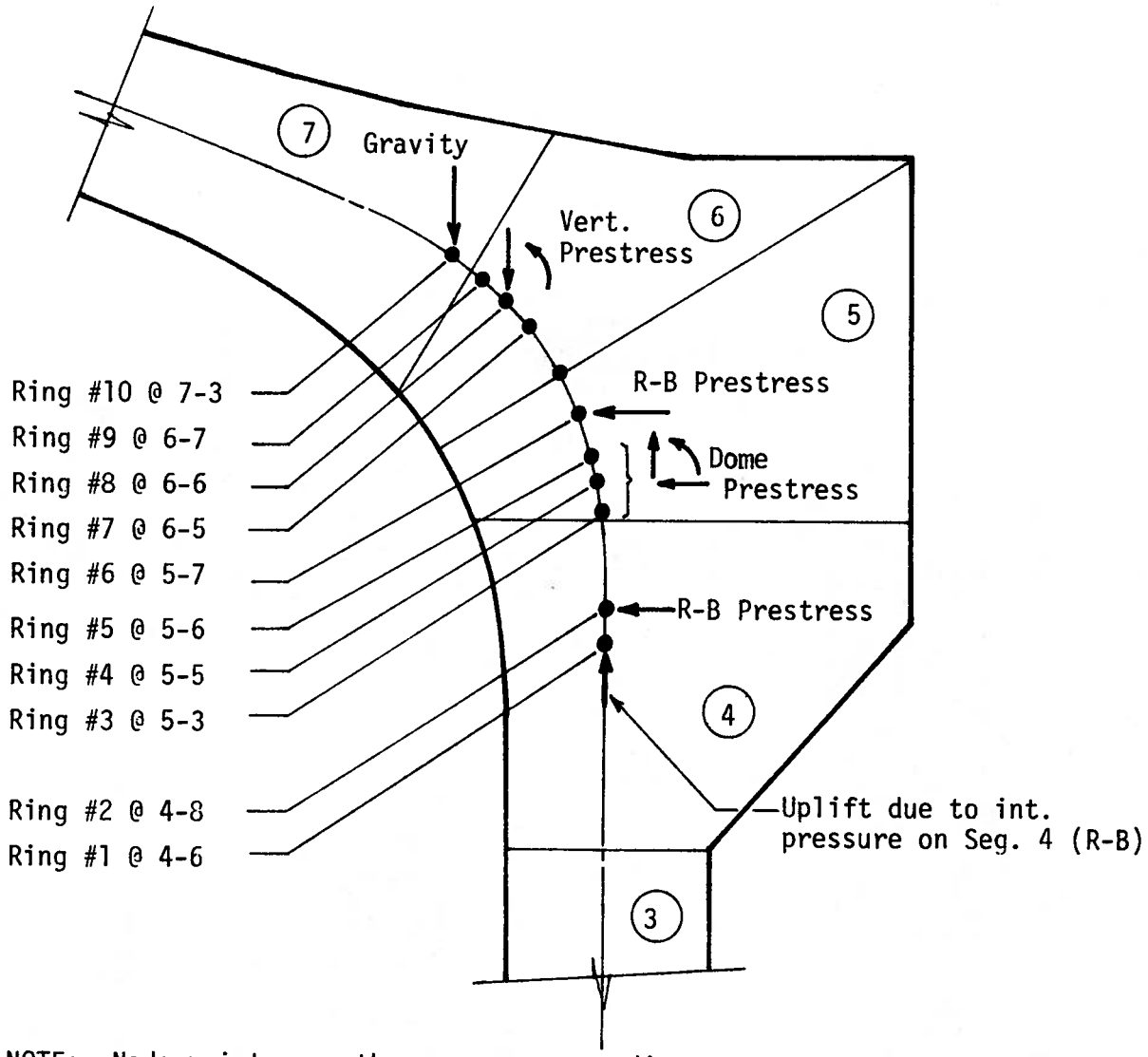

NOTE: Node points are the ones corresponding to the generated numbering, not the input numbering.

BOSOR Ring Number	Radial Force #/in. (Inward)	Vertical Force #/in. (Upward)	Moment "#/" ( )	Source
1	0	0.74274 p #/in.	0	Correction for internal pressure
2	345.957	0	0	Lower Ring Beam Tendon
3	949.750	526.455	3262.35	Anchorage of Dome Tendons
4	950.848	527.064	2670.37	Anchorage of Dome Tendons
5	953.813	528.707	1989.84	Anchorage of Dome Tendons
6	349.306	0	602.134	Upper Ring Beam Tendons
7	0	-246.263	-378.925	Anchorage of Wall Tendons
8	0	-249.193	-556.174	Anchorage of Wall Tendons
9	0	-251.400	-689.717	Anchorage of Wall Tendons
10	0	22.16	0	Dome and Upper Ring Beam Weight

FIGURE 4.7 - Prestressing Anchorage Forces (Second Model)

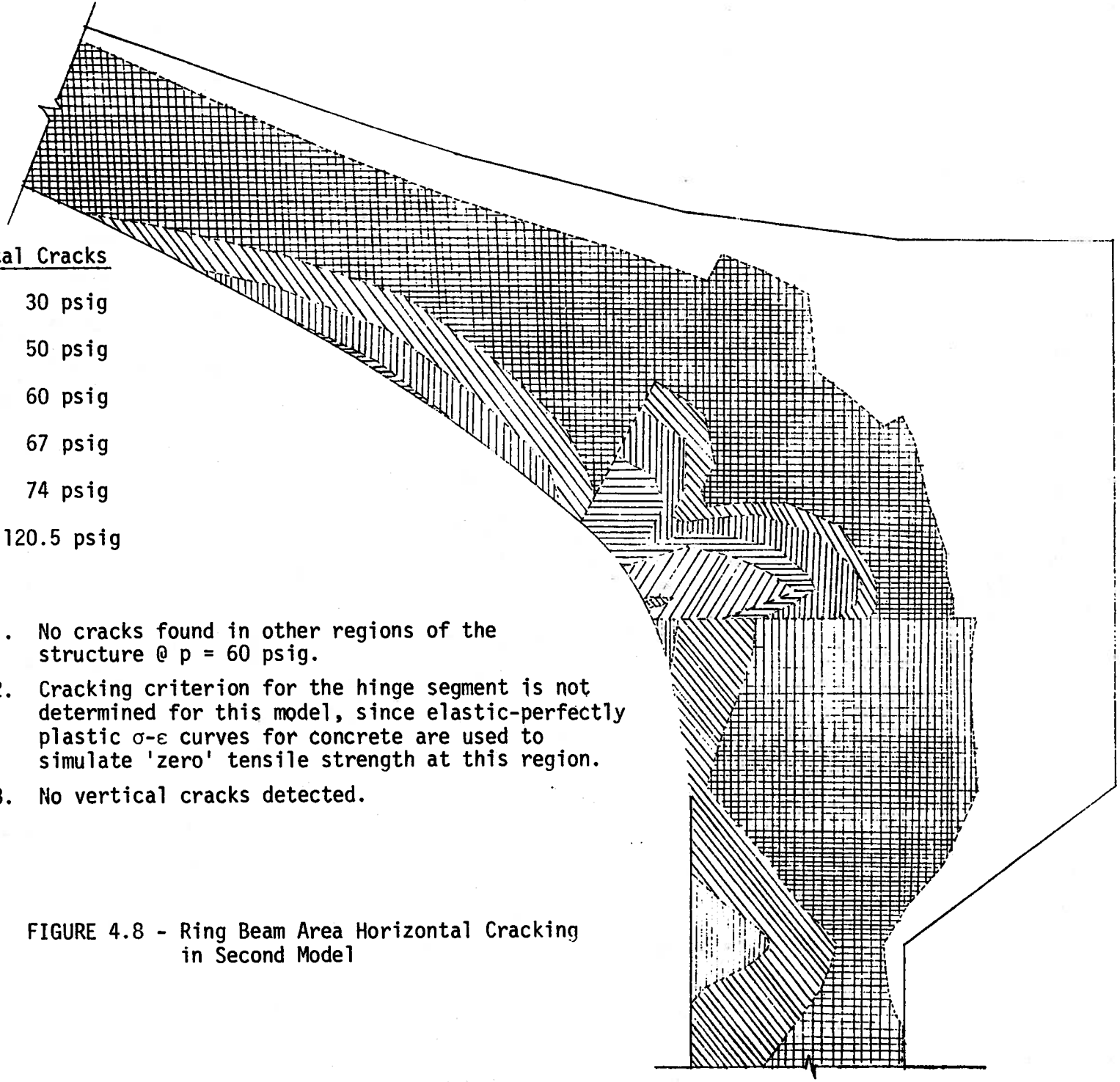

NOTE:
1. No cracks found in other regions of the structure @ p = 60 psig.
2. Cracking criterion for the hinge segment is not determined for this model, since elastic-perfectly plastic σ-ε curves for concrete are used to simulate 'zero' tensile strength at this region.
3. No vertical cracks detected.

FIGURE 4.8 - Ring Beam Area Horizontal Cracking in Second Model

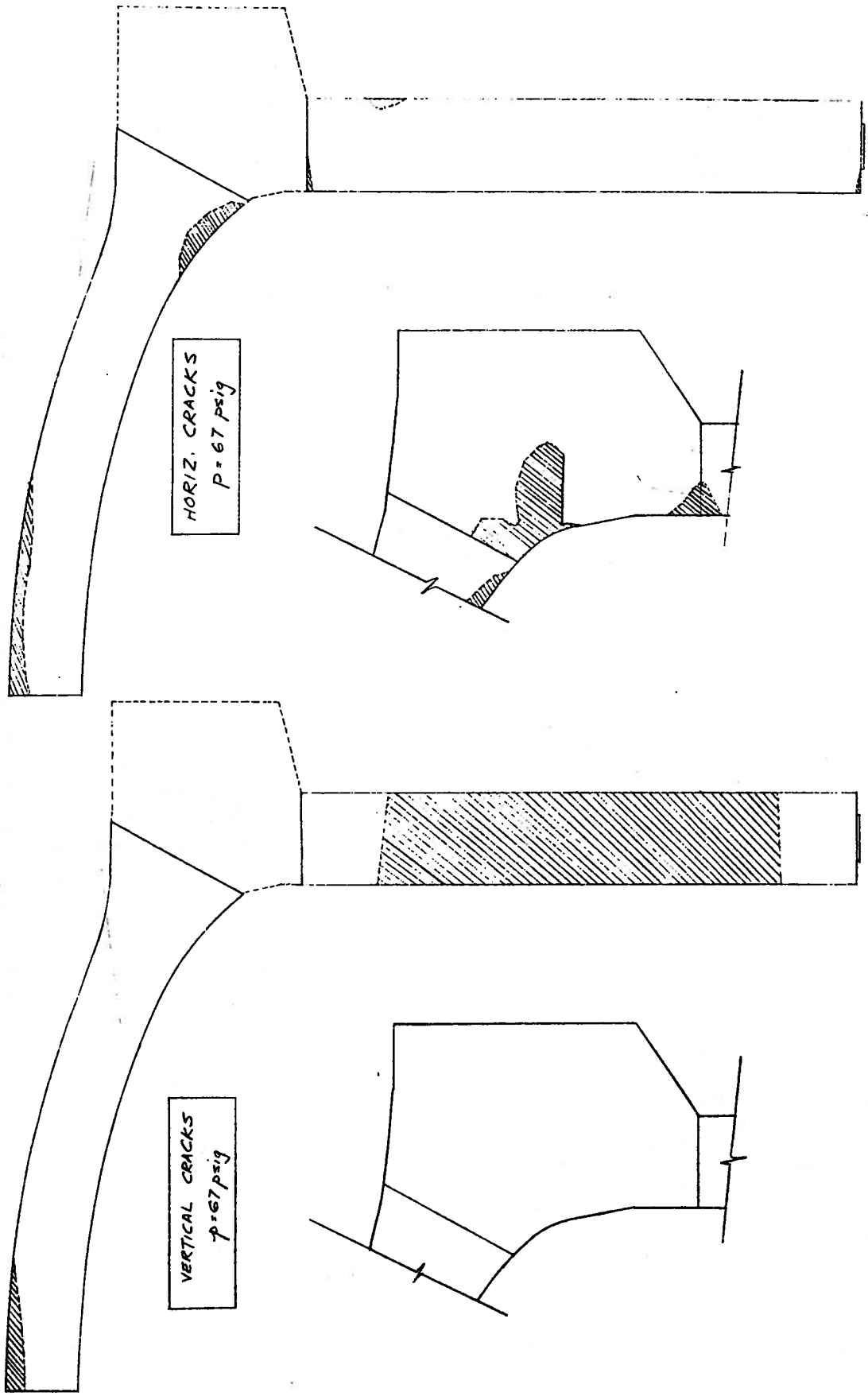

FIGURE 4.9 - Distribution of Cracking at 67 psi (Second Model)

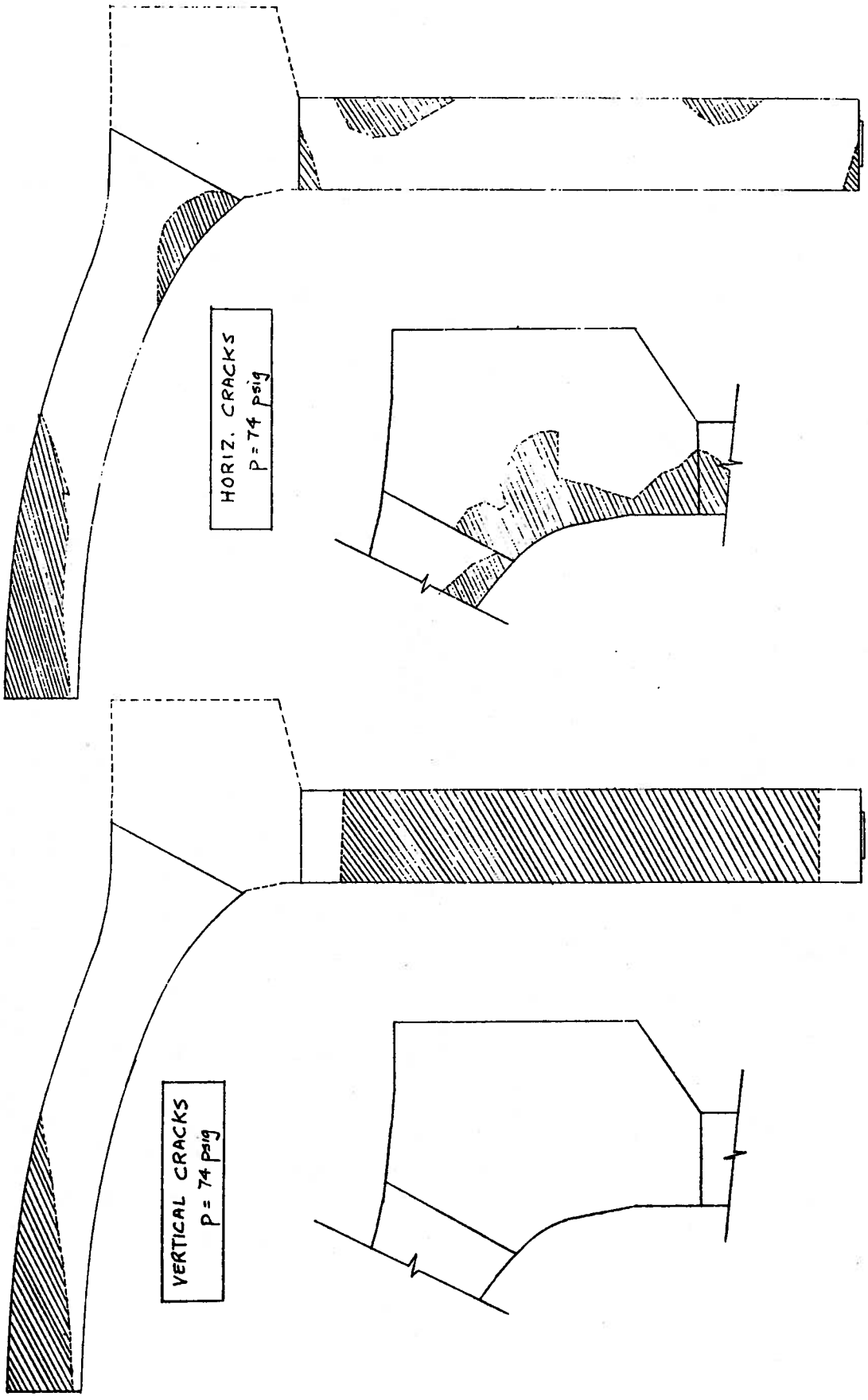

FIGURE 4.10 - Distribution of Cracking at 74 psi (Second Model)

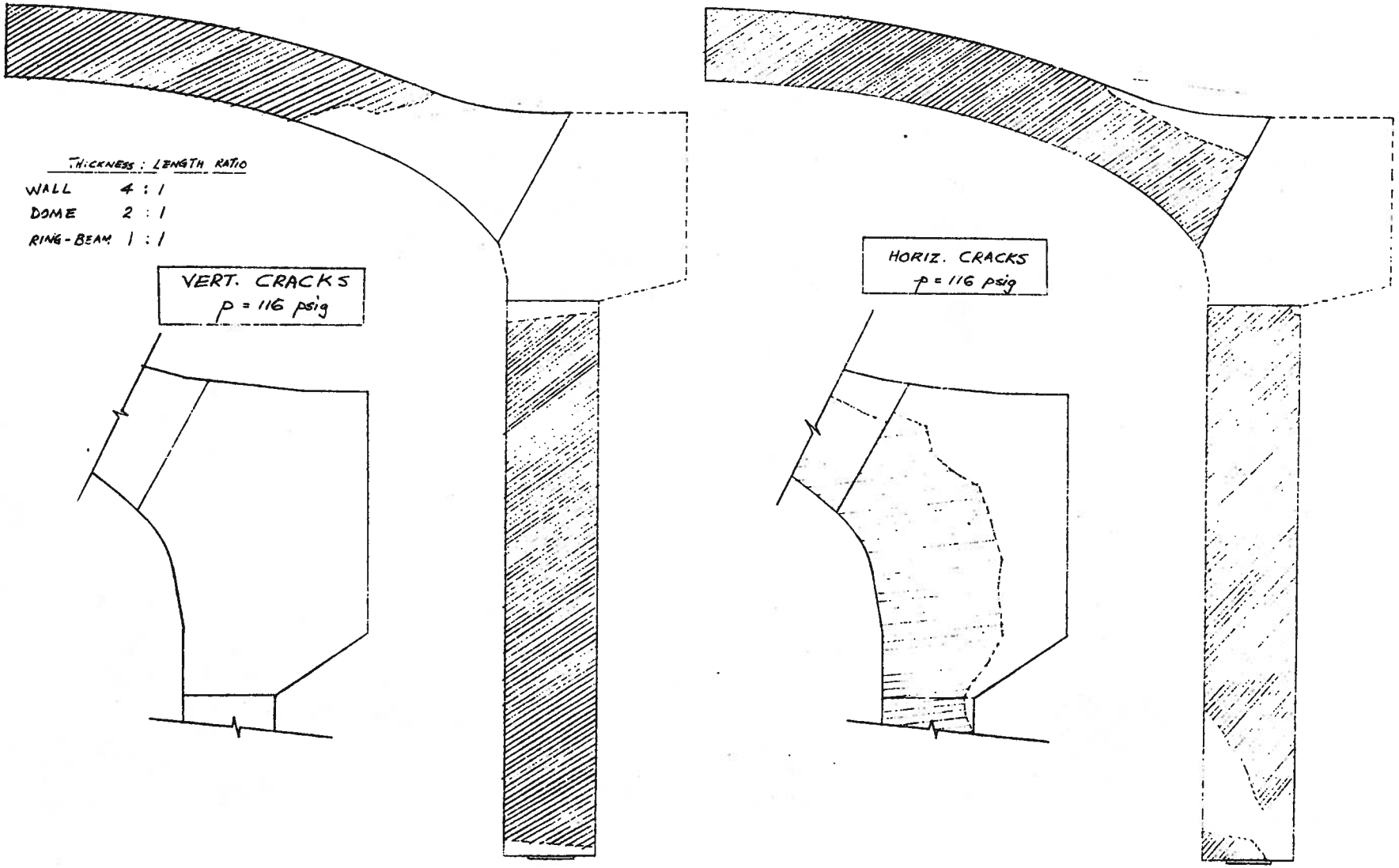

FIGURE 4.11 - Distribution of Cracking at 116 psi (Second Model)

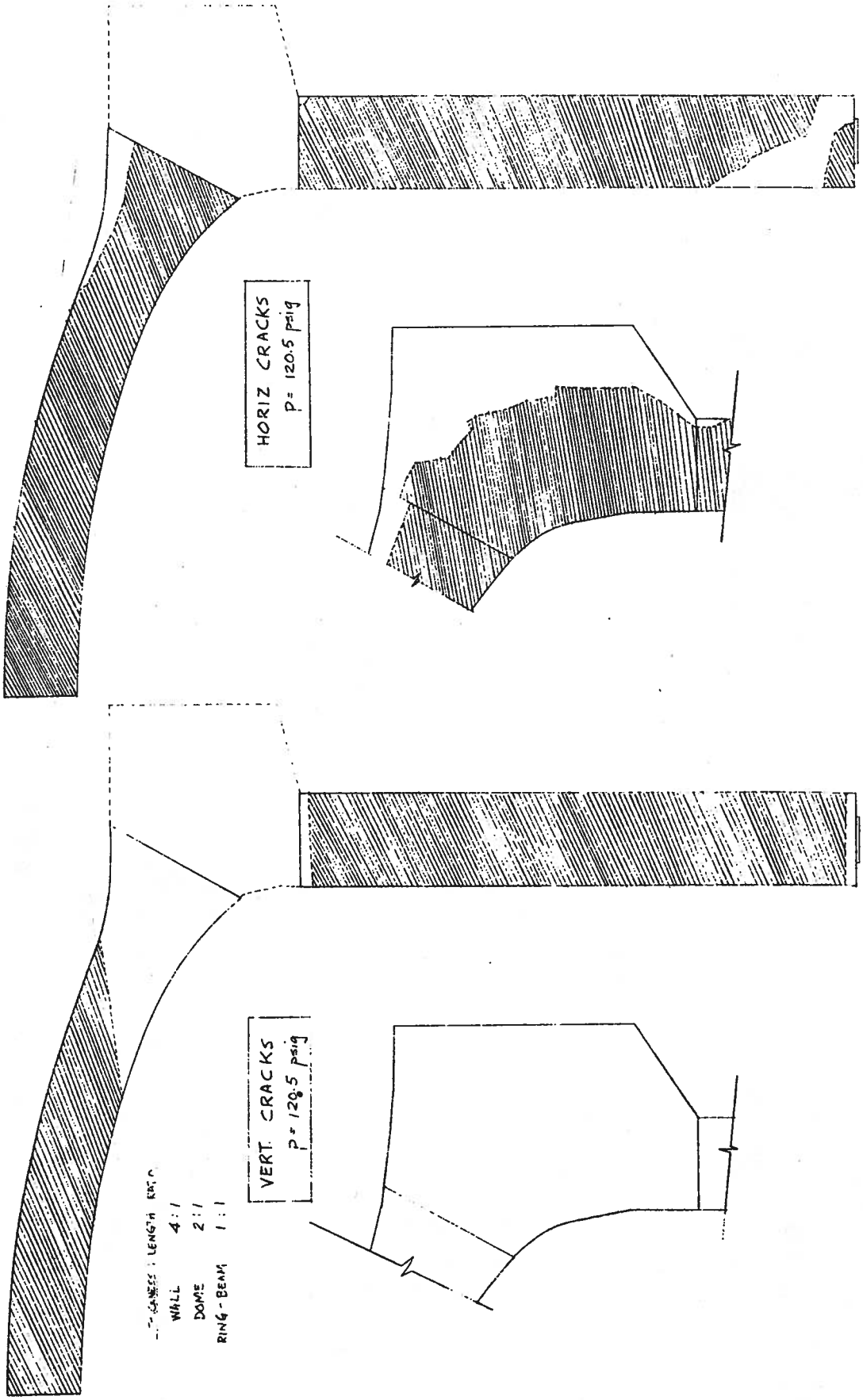

FIGURE 4.12 - Distribution of Cracking at 120.5 psi (Second Model)

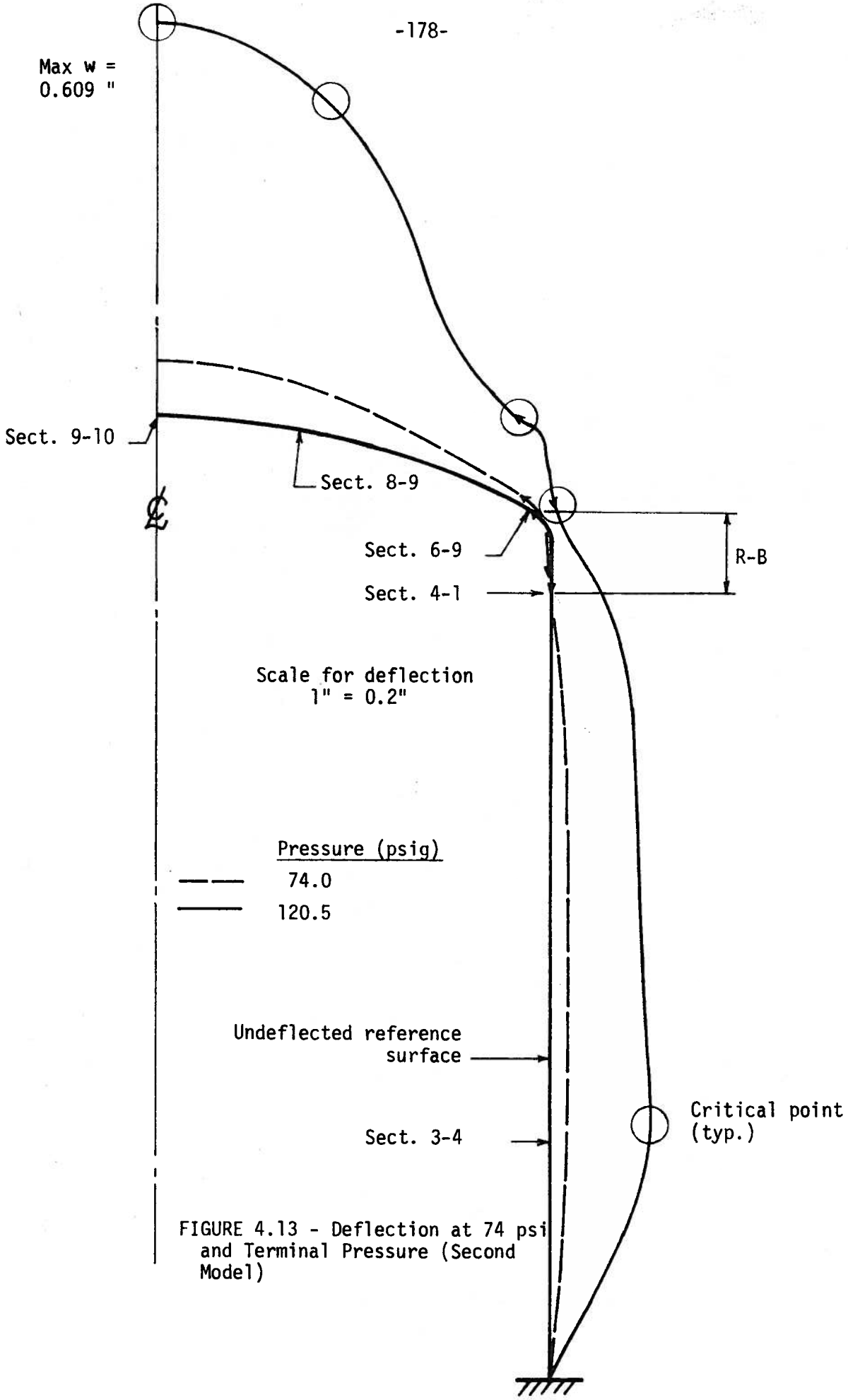

FIGURE 4.13 - Deflection at 74 psi and Terminal Pressure (Second Model)

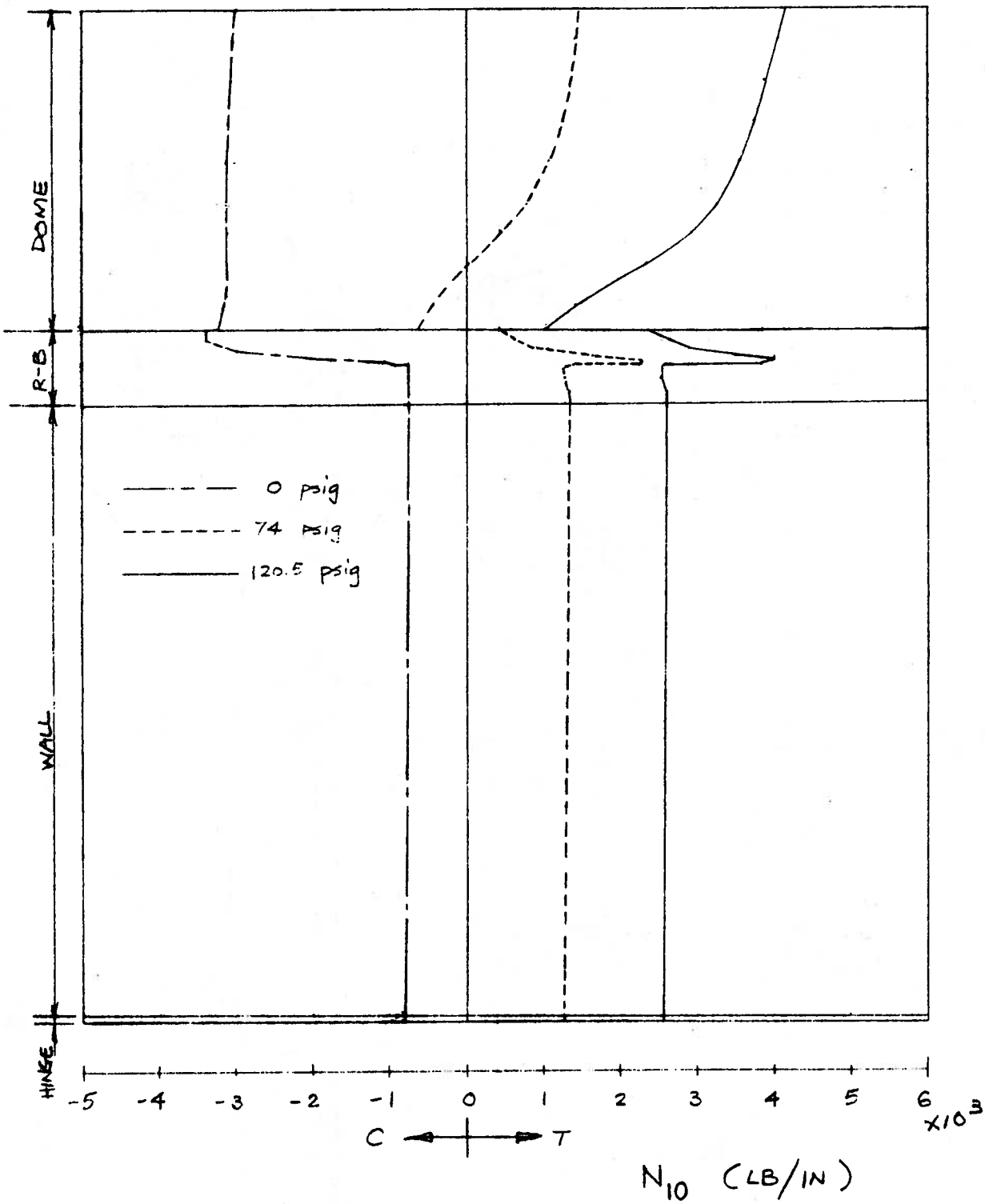

Figure 4.14 - Meridional Force N_{10} (Second Model)

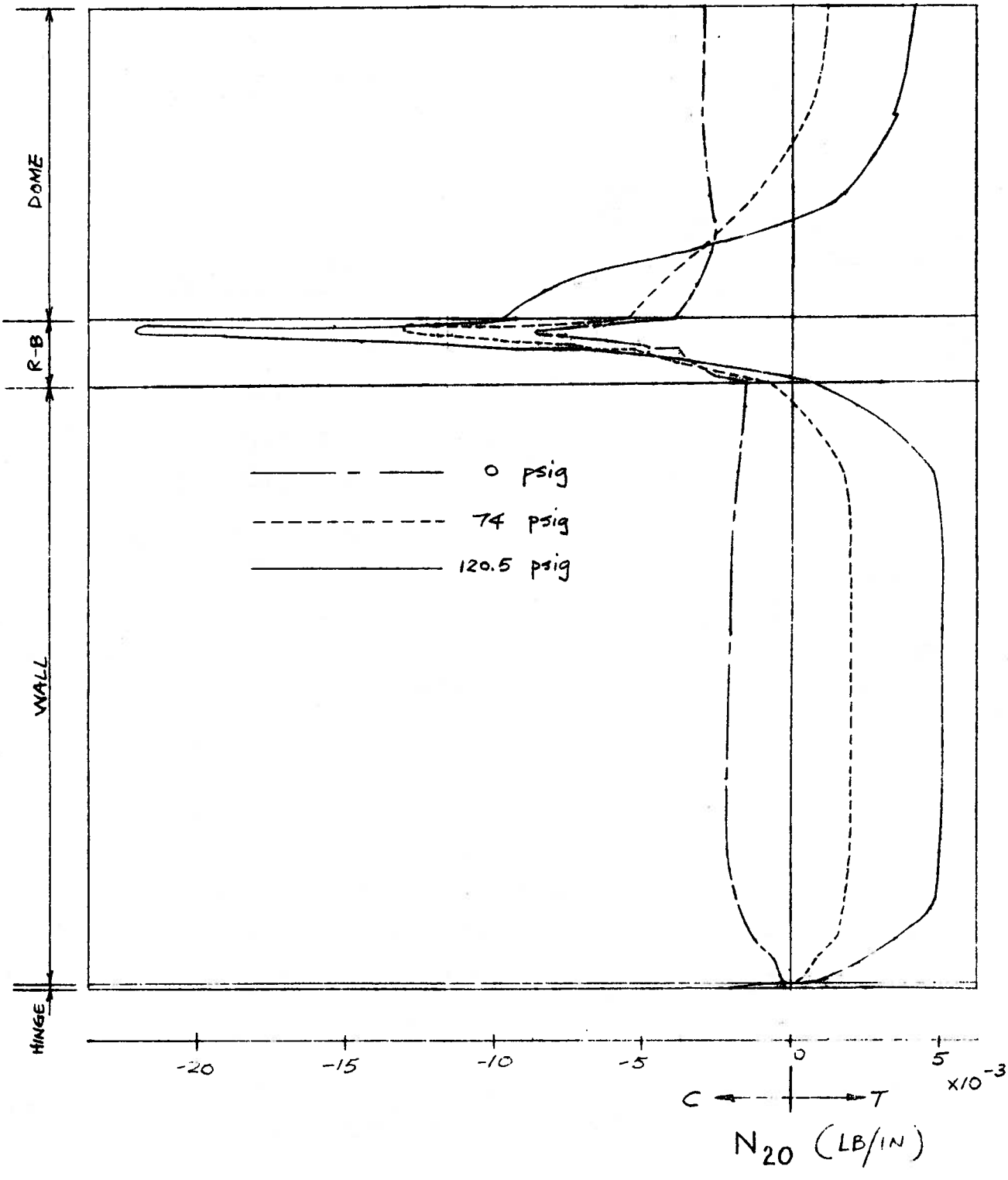

Figure 4.15 - Circumferential Force N_{20} (Second Model)

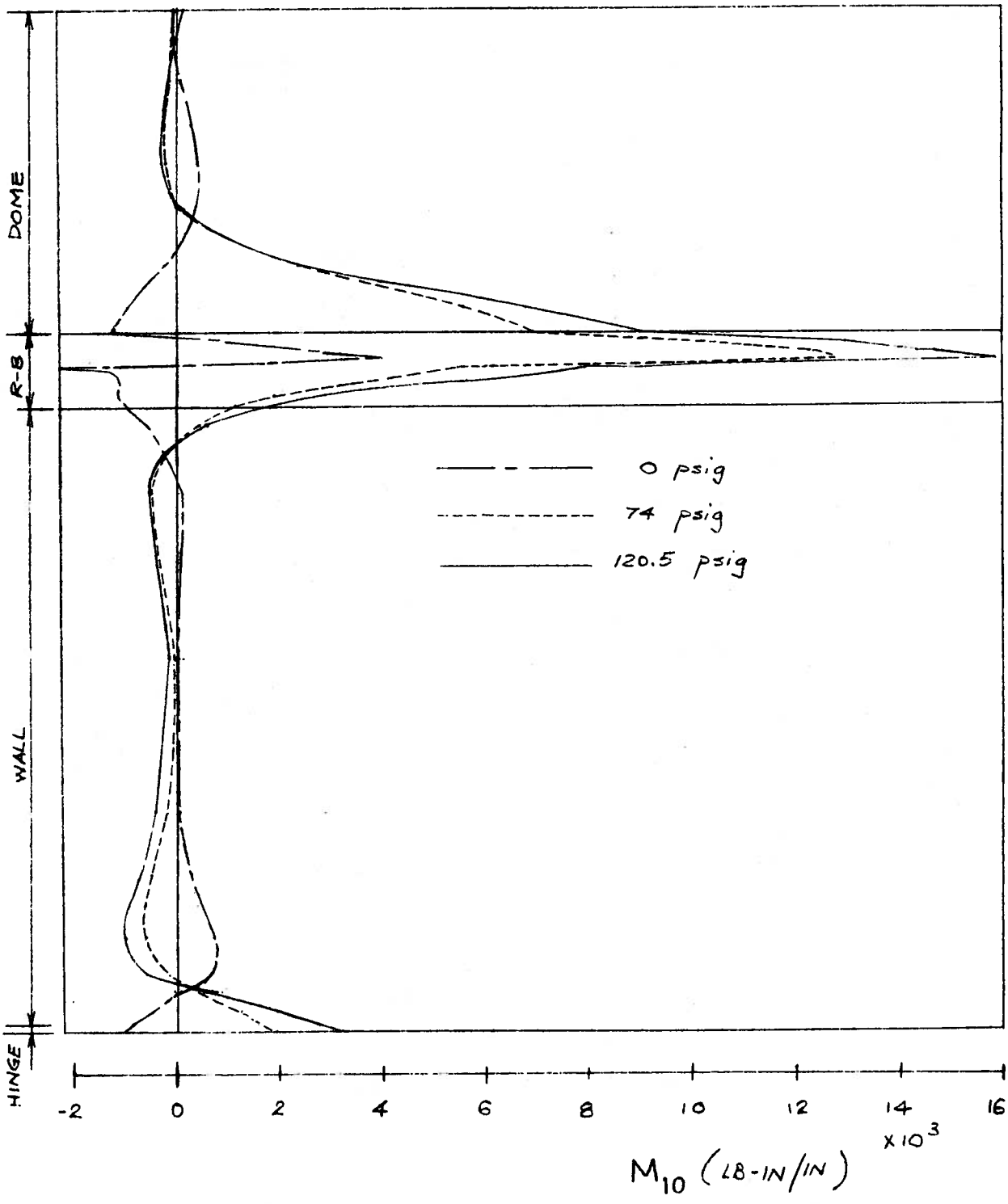

Figure 4.16- Meridional Moment M_{10} (Second Model)

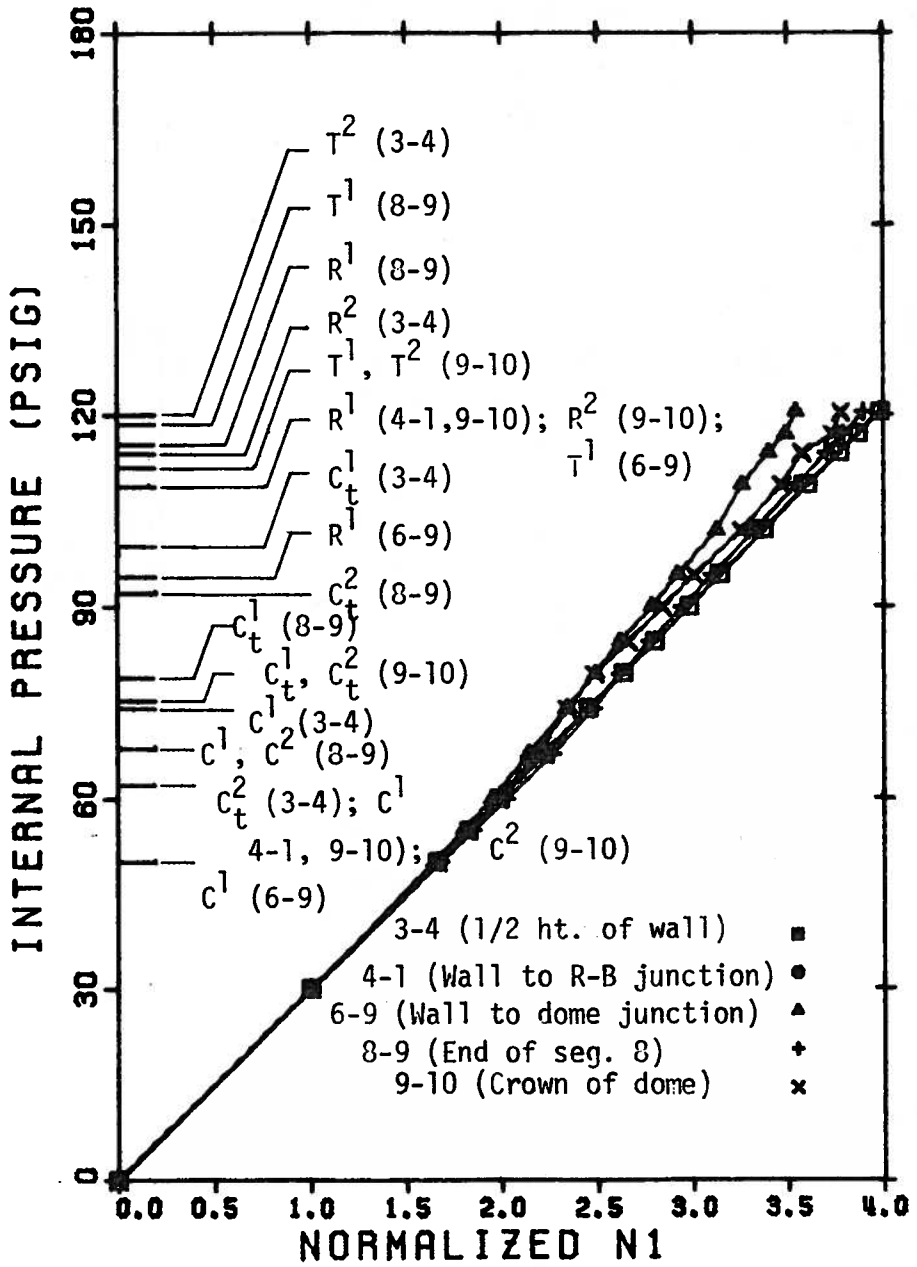

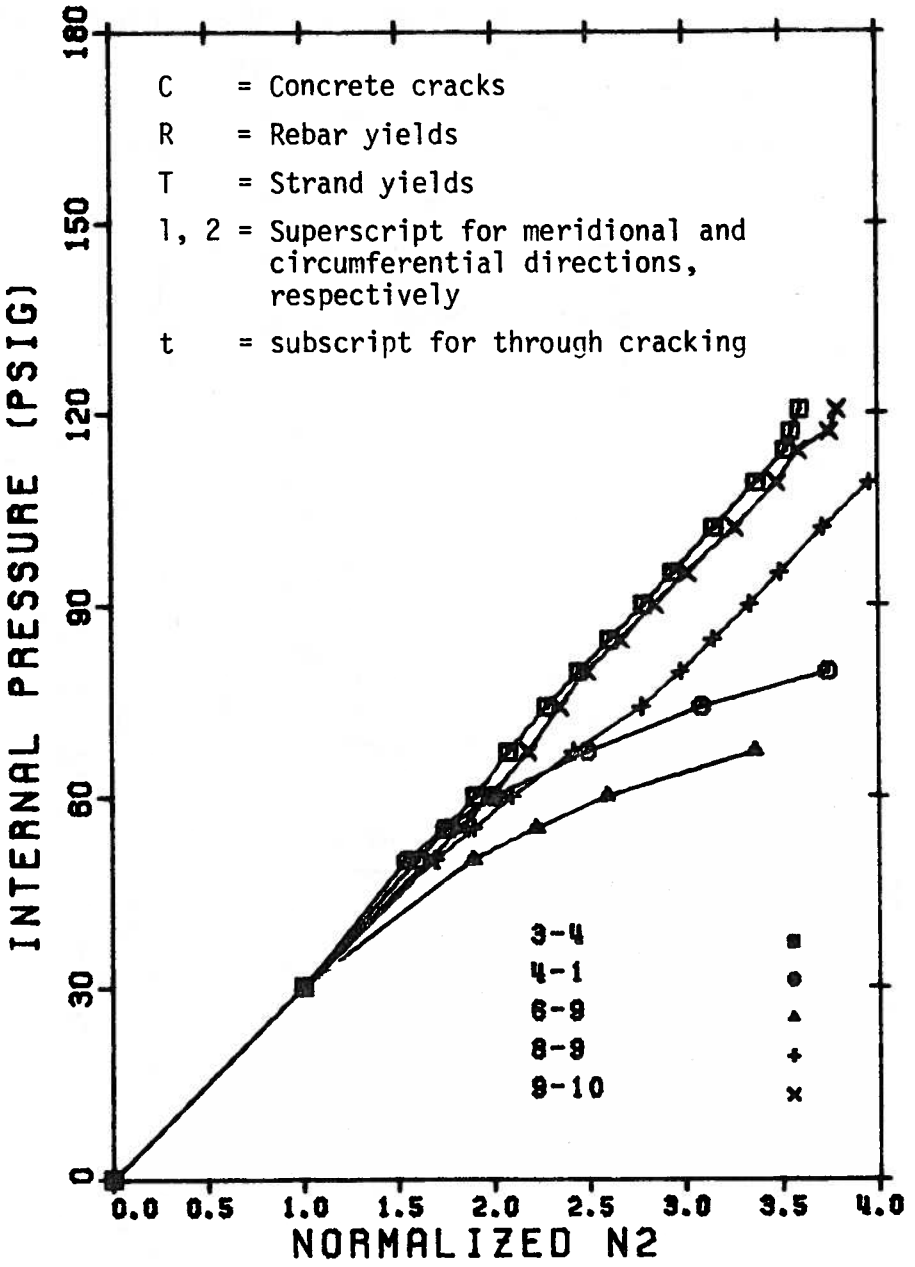

FIGURE 4.17 - Selected Nondimensionalized Pressure - Force Plots

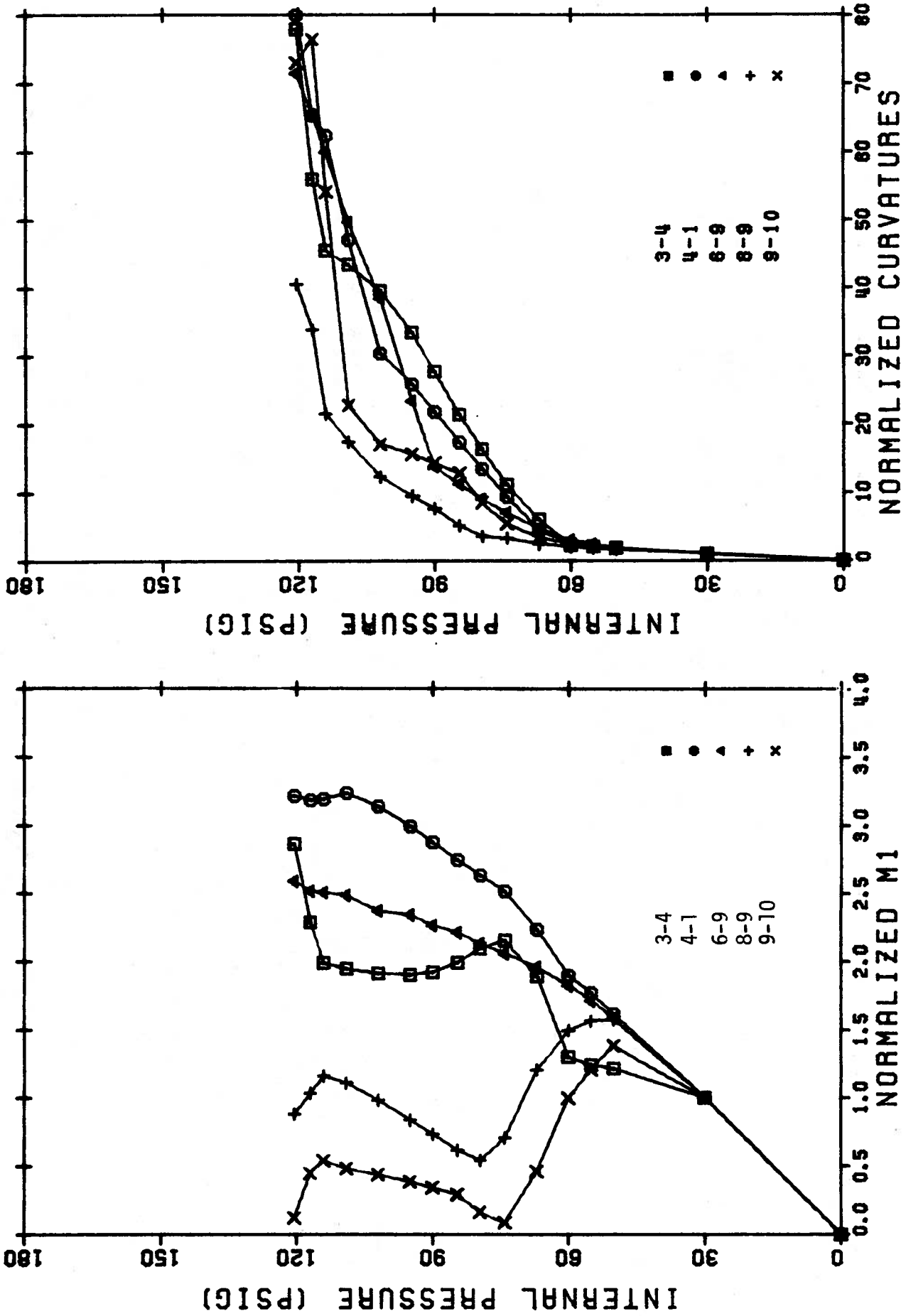

FIGURE 4.18 - Selected Nondimensionalized Pressure - Moment Plots

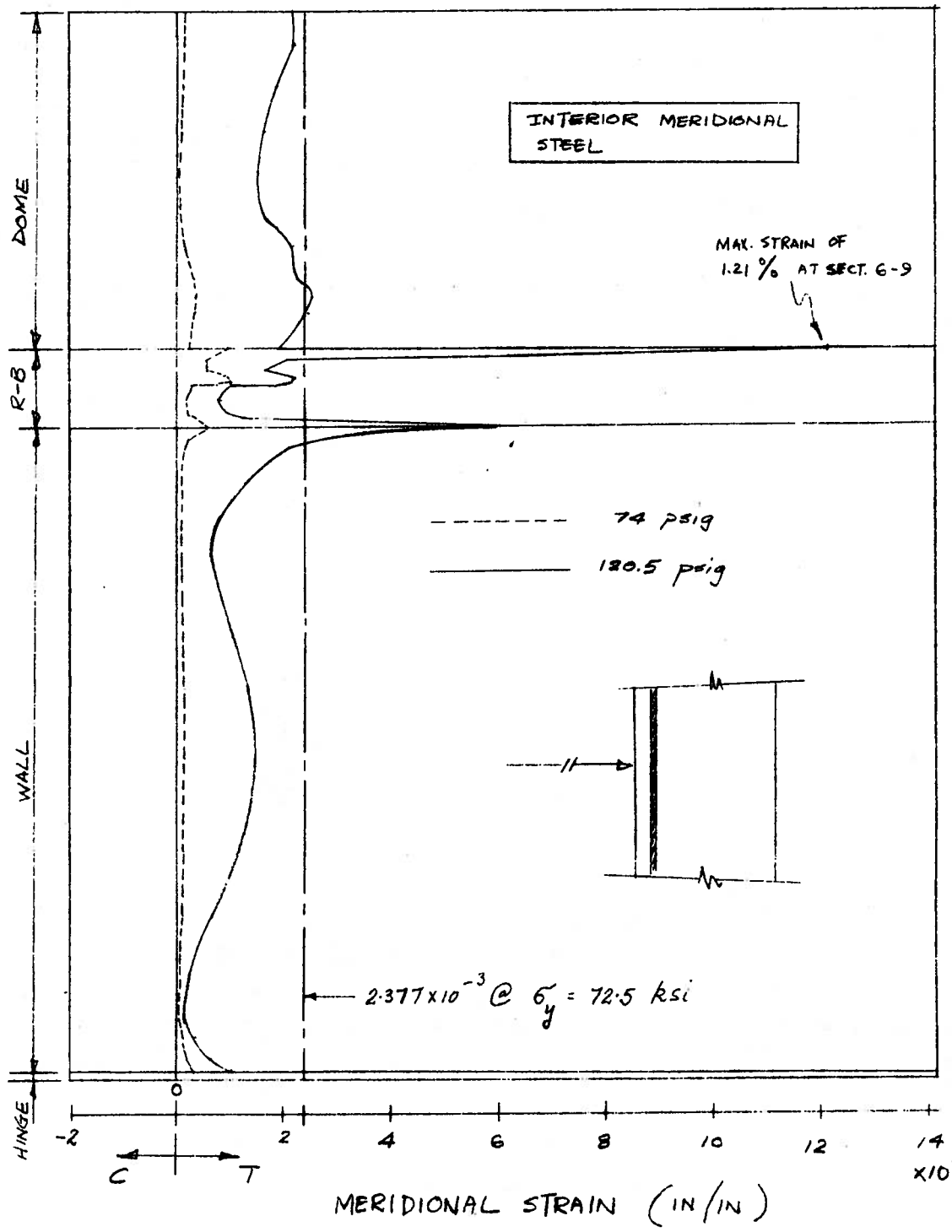

Figure 4.19- Interior Meridional Steel Strain (Second Model)

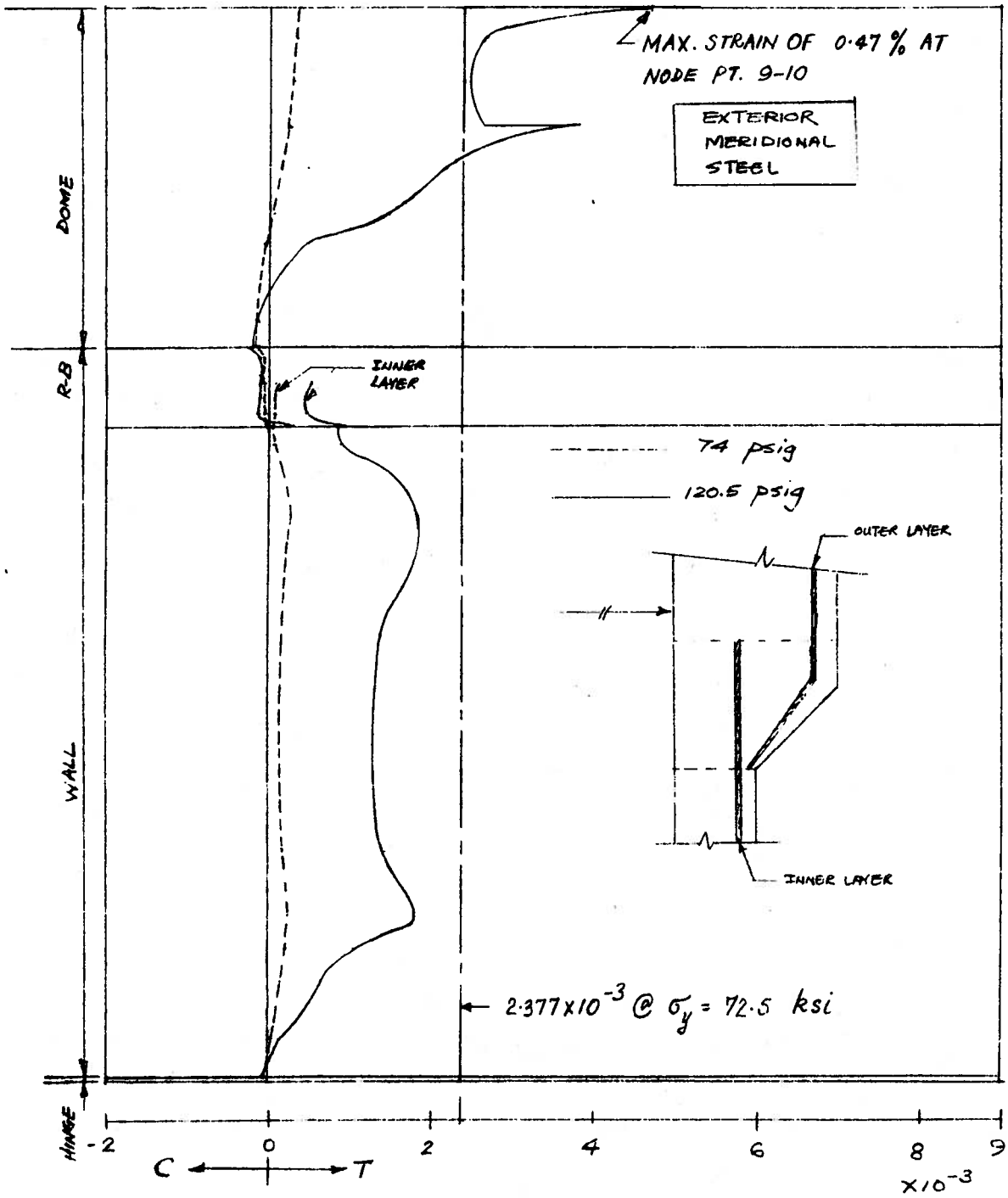

Figure 4.20 Exterior Meridional Steel Strain (Second Model)

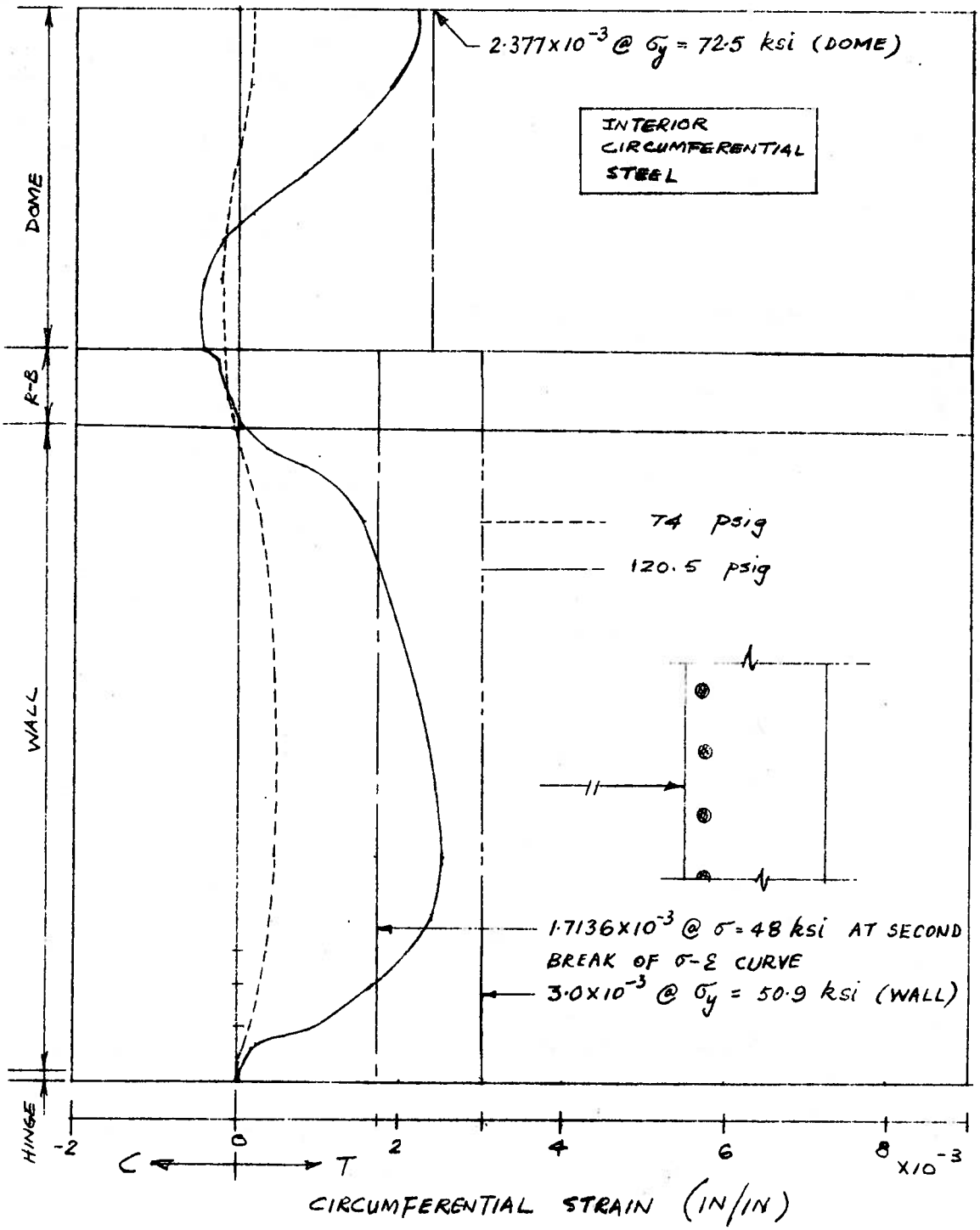

Figure 4.21 Interior Circumferential Steel Strain (Second Mode

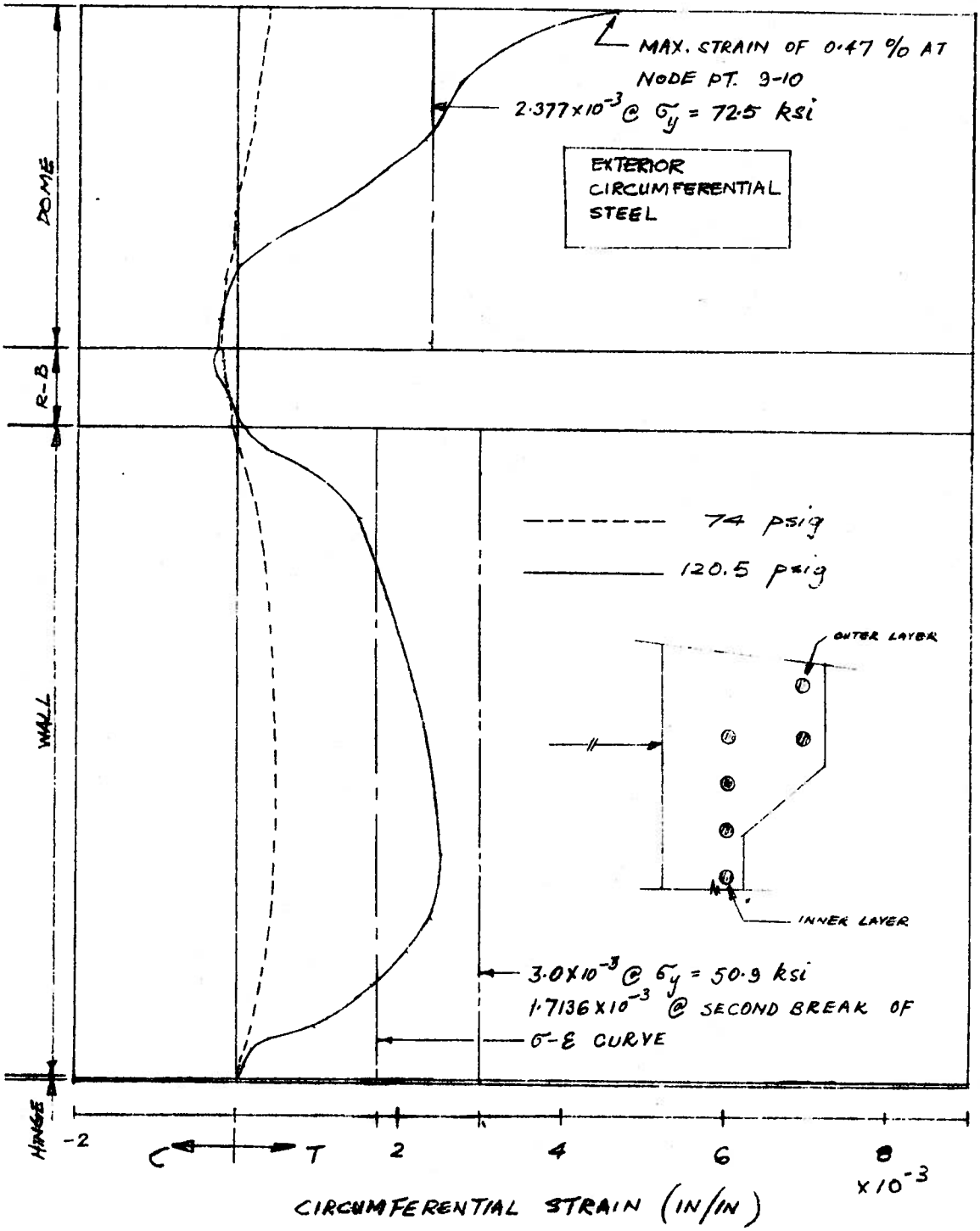

Figure 4.22- Exterior Circumferential Steel Strain (Second Model)

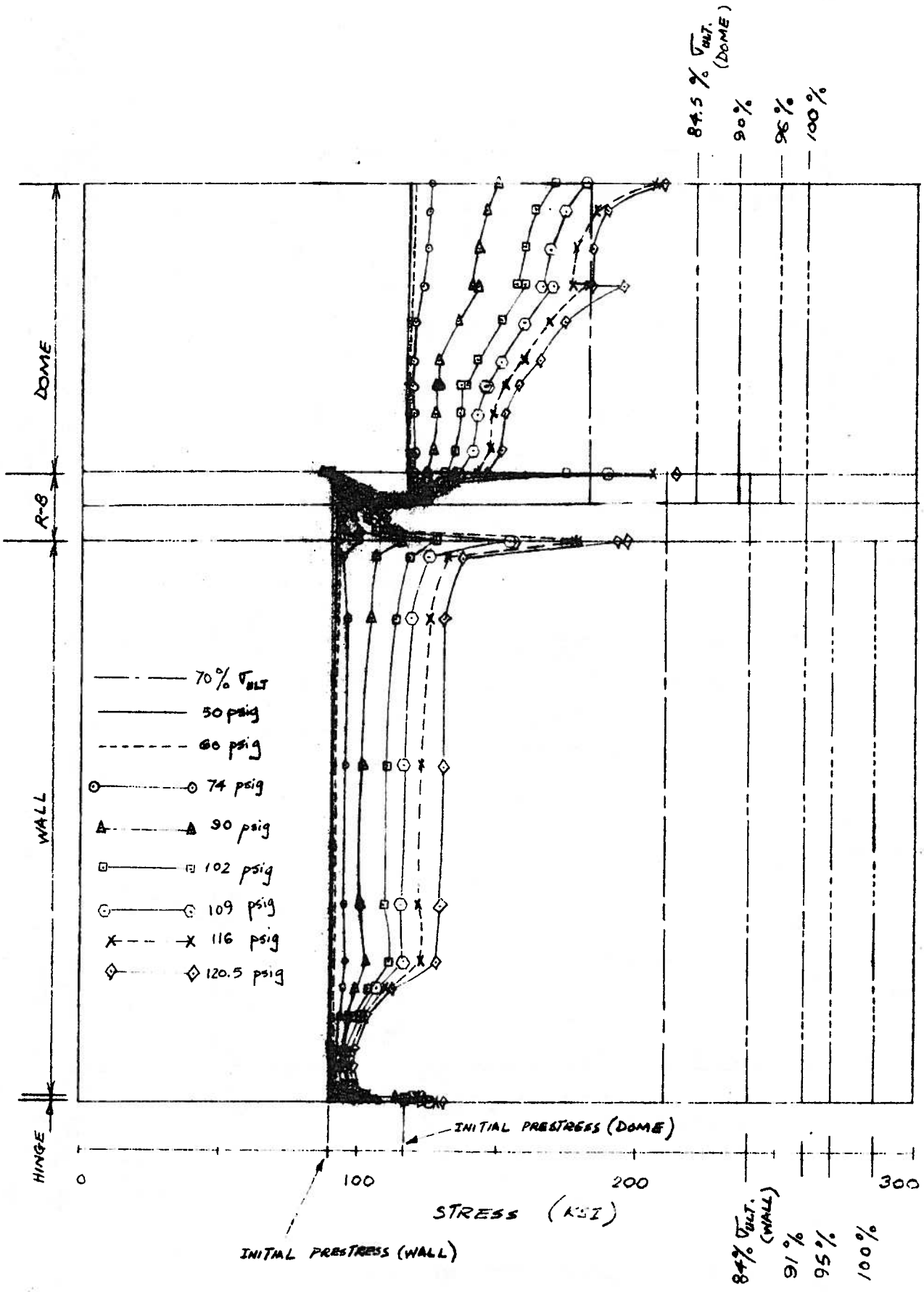

Figure 4.23 - Meridional Tendon Stresses (Second Model)

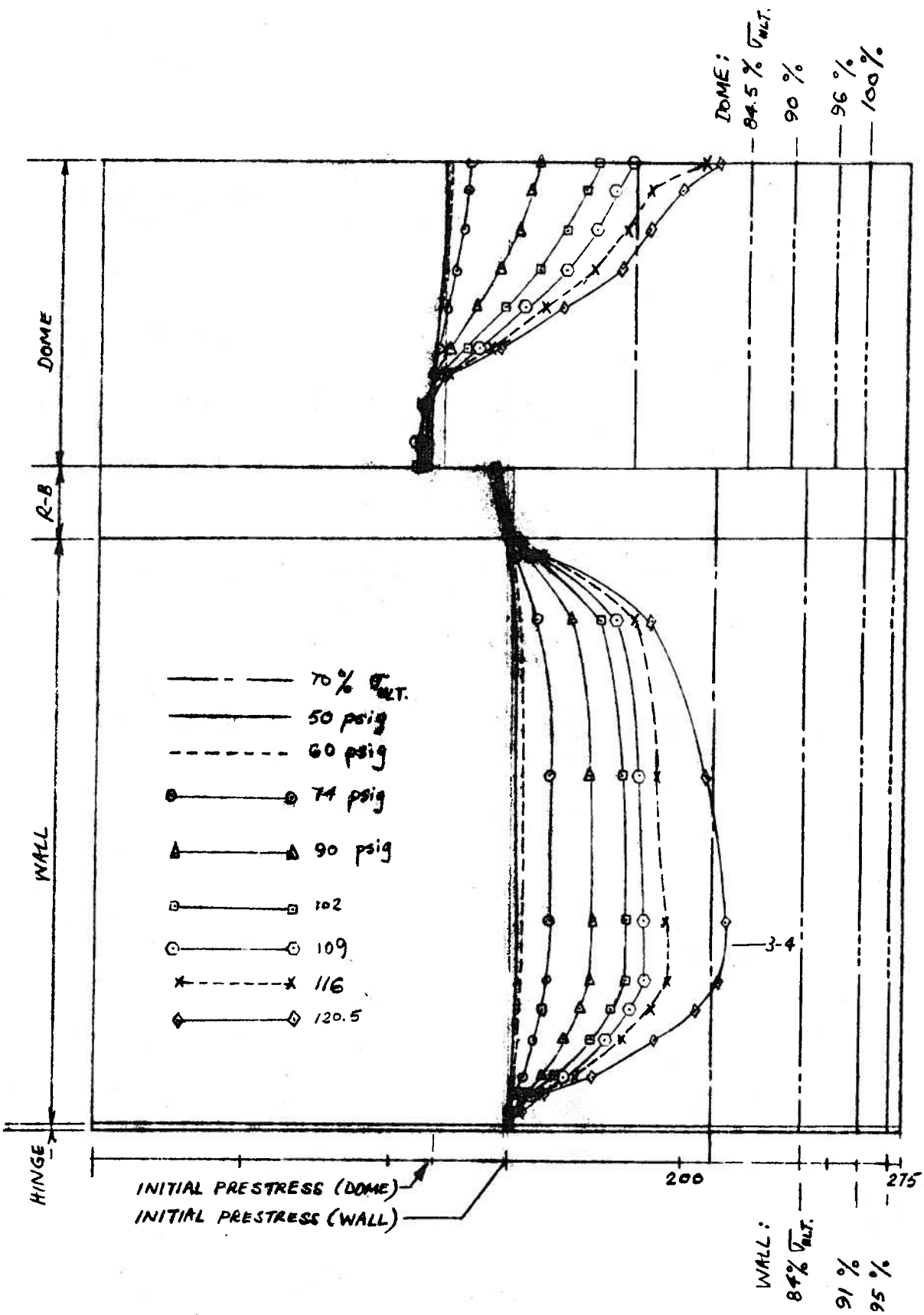

Figure 4.24 - Circumferential Tendon Stresses (Second Model)

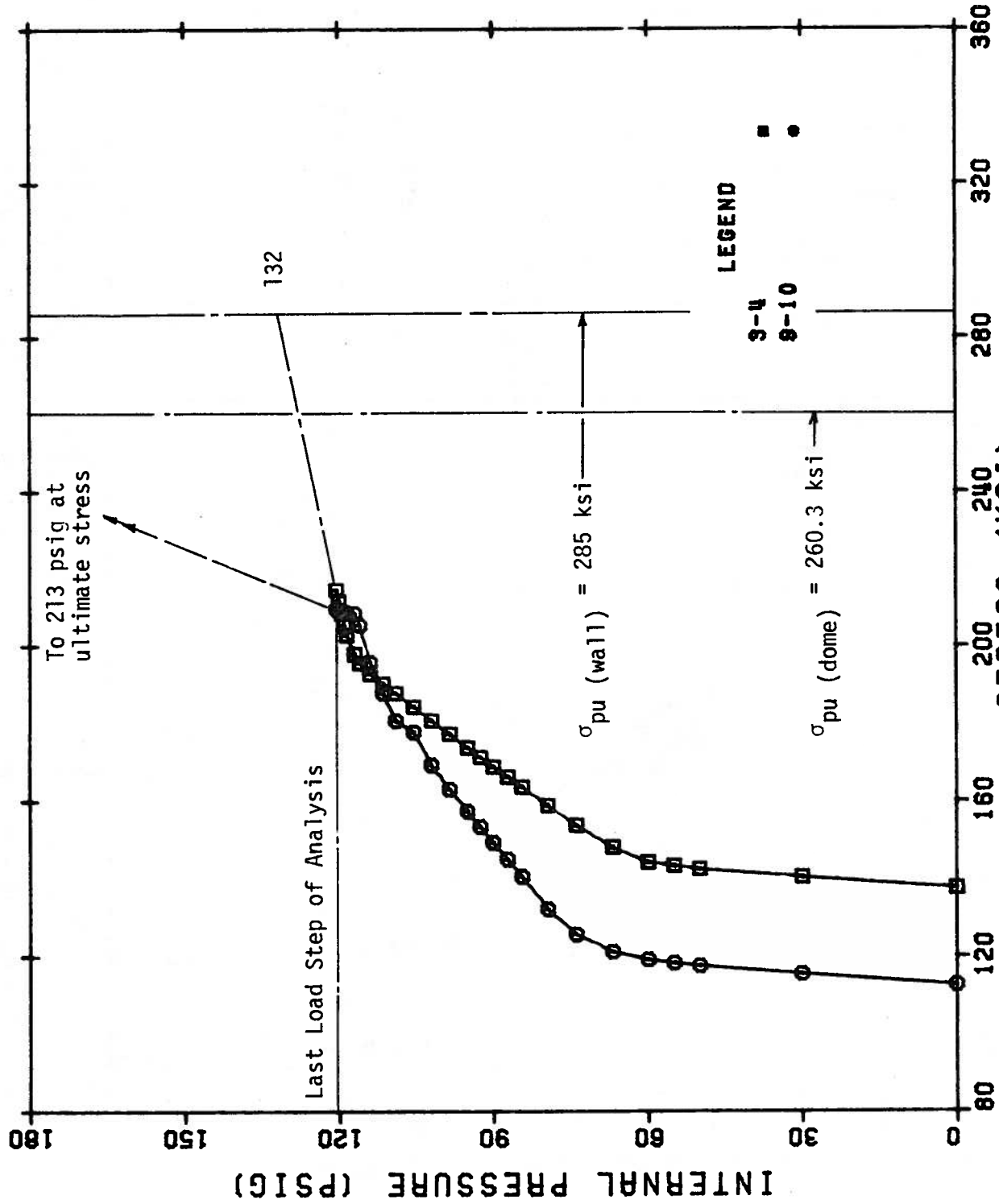

FIGURE 4.25 - Extrapolation of Circumferential Tendon Stress (Second Model)

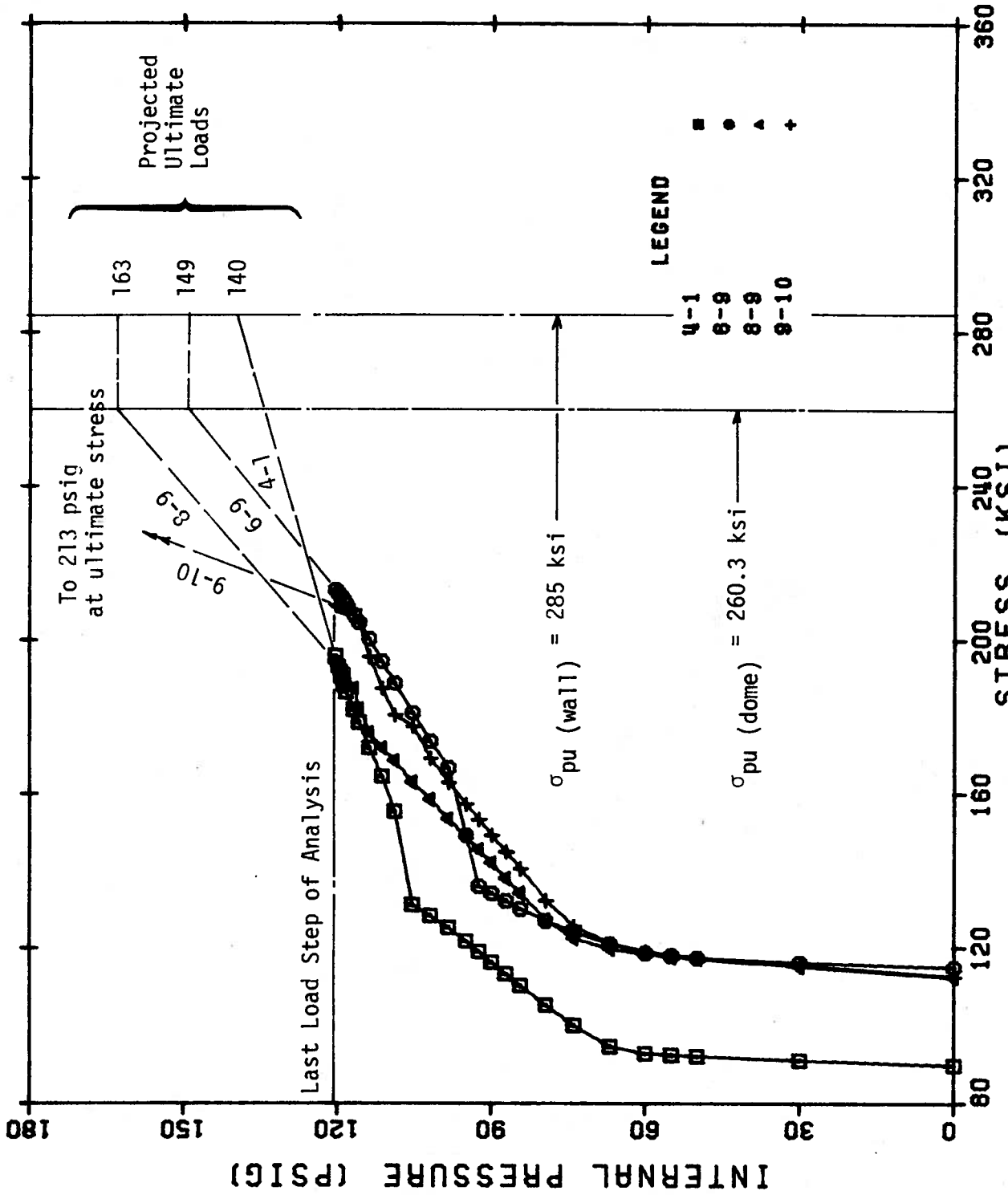

FIGURE 4.26 - Extrapolation of Meridional Tendon Stresses (Second Model)

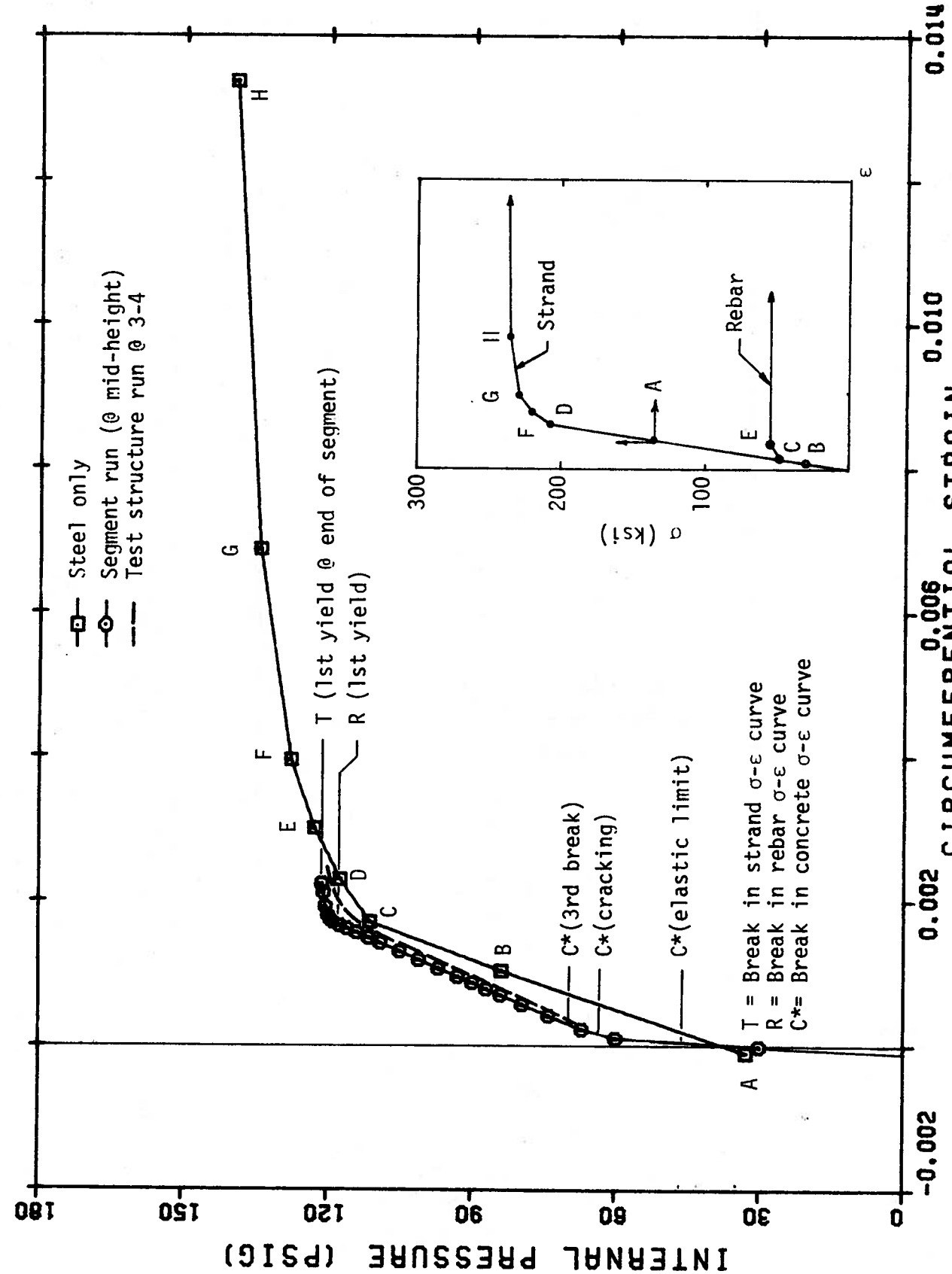

FIGURE 4.27 - Segment Response at Point 3-4 (Second Model)

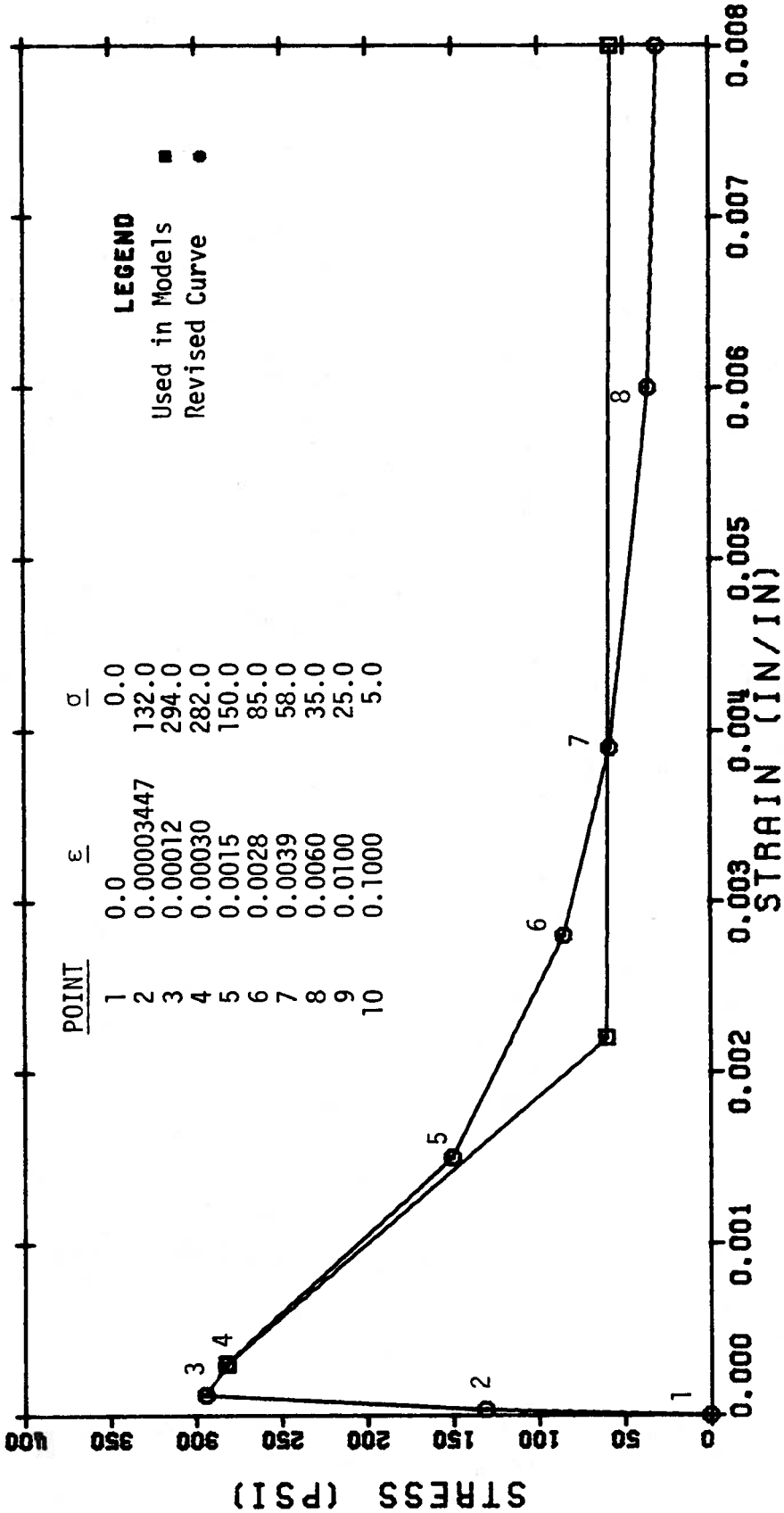

FIGURE 4.28 - Revised Tensile Stress-Strain Curve

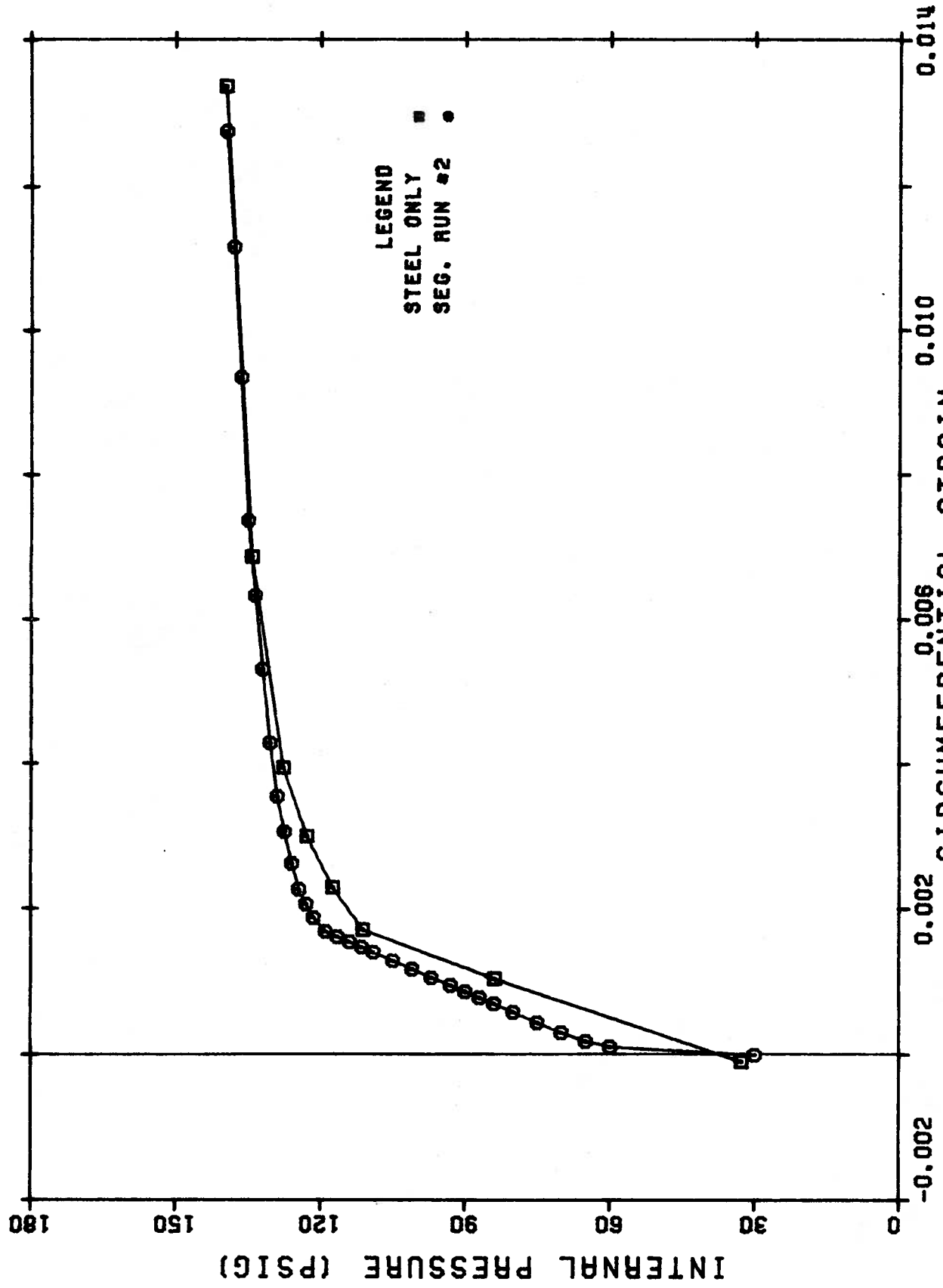

FIGURE 4.29 - Revised Segment Response at Point 3-4 (Second Model)

APPENDIX A

APPENDIX A - DESCRIPTION OF BOSOR5 PROGRAM

A.1 Organization and Capability of BOSOR5

The purpose of this appendix is to present a brief introduction to the general organization and capability of BOSOR5 relative to the problems considered in this report. The theoretical background and numerical techniques are not covered, and the reader is referred directly to the work of Bushnell [11] for these aspects of the program.

BOSOR5 is a program for the analysis of prebuckling and buckling of elastic-plastic complex shells of revolution including large deflections, and creep. It can handle segmented and branched shells with discrete ring stiffeners, meridional discontinuities, and multi-material construction. Axisymmetric behavior is assumed in the pre-buckling analysis.

The original BOSOR5 was written for materials whose stress-strain curves in compression and tension are the same. Two alternative plasticity theories are available for analyzing the shell: the deformation theory and the incremental flow theory. However, only the flow theory portion of the program has been debugged and adapted to be usable for the modified flow theory associated with the three-parameter model described in Chapter 2 and Appendix B. In the flow theory, loading is elastic-plastic while unloading is elastic.

The program utilizes auxiliary low-speed devices in addition to the conventional highspeed storage. The low-speed storage is divided into two large line files (named Files 15 and 16). File 15 stores the indices for all the data in File 16 so that such data can be accessed in blocks. The first part of File 16 contains the data of the shell being

analyzed and the remainder contains the results of every time (or load) step. Therefore, only certain data need be transferred to the high-speed storage during any one phase of program execution.

A large portion of the high-speed storage is taken up by a dynamic working vector, B( ), whose size is initially specified by the user. Data from Files 15 and 16 are transferred into this vector during a major phase of the execution. Once this phase is completed, the vector space is cleared for the next phase of execution.

BOSOR5 is divided into three programs: a preprocessor, a main-processor and a post-processor. The post-processor plots the results but has not been made operational at the University of Alberta. The three programs may be run as one job in a runstream or separately. The normal mode of solution for complex nonlinear problems is to run only one load step at a time on the main processor. The data to initialize the run is read from the results of the previously converged load step which have been saved in File 16. After convergence of the present load step, the results are appended to File 16 and form the initial data for any subsequent load step.

A.2 The Preprocessor

This is the input phase of the program in which the control information, geometric and material properties, and load-time functions are read. The input data and the labeled COMMON are stored in File 16. An echo check of the input is provided immediately after a block of data has been processed.

The preprocessor also checks that the high-speed working space required in each phase of the main-processor does not exceed the dynamic working vector size initially specified by the user. A warning message is provided if this condition is violated.

Three types of loadings can be input: temperature, normal pressure and surface traction, and discrete ring line loads. Loads are associated with load-time functions and scaling factors, so that the actual loads on the shell can be varied at any given time. A single time function may be associated with any number of loadings. The characteristics of each type of loading can be summarized as:

(1) Temperature can vary in the meridional direction and through the wall of the shell. Temperature was used to simulate the prestressing effects during the trial runs of the test specimens described in Sect. 2.5.2. It was observed that the results were good until the yielding of the non-prestressing steel, noting that the concrete was already in the degrading part of the stress-strain curve. Upon yielding of the steel, convergence difficulties were encountered. It seems that temperature loading works well for materials like steel but not in combination with a three-parameter material like concrete. Subsequently, prestressing effects were simulated using external pressure.

(2) Normal pressure and surface traction are assumed to be applied to the reference surface of the shell. They may vary non-uniformally in the meridional direction as determined by certain callout points on the reference surface. Values at other meridional stations between callout points are determined by linear interpolation. Originally, the normal pressure and surface traction for any one shell segment were associated with a common load-time function, that is, they were required to vary proportionately with each other. This restriction was removed in the present version.

(3) Line loads must be applied via discrete rings, which may be fictitious if none are physically present in the shell. In such a case, the ring will not contribute any stiffness to the shell.

A.3 The Main-Processor

The input data for this phase is relatively simple, consisting of only a few statements. One statement specifies the type of analysis (prebuckling and/or buckling analysis) and the type of plasticity theory to be used. The number of time (or loads) steps is also specified together with the starting time. A maximum of 99 time steps can be used during any one job run. However, the program has a restart capability which enables an infinite number of accumulated runs to be made. Only the main-processor, together with a few input statements, need be used for a restart. A restart may be initiated at any of the previous time steps and not necessarily at the last step. The new time increment can also be different from the previous runs. For example, consider a fictitious shell whose results for 4 time steps are stored in File 16 as shown in Fig. A.1(a). The load-time function is shown in Fig. A.1(b). Step 2 could be restarted with a time increment of 7 hours as compared to the original increment of 5 hours as shown in Fig. A.1(b). The new results will be stored in the space occupied by the previous time step #2, without disturbing the old results of other time steps. The different time increment will merely mean that the results of the new step #2 and the old step #3 are discontinuous.

The major stages in the main-processor are shown in the flow chart in Fig. A.2. For each run, the following route is followed:

(1) Labeled COMMON data are retrieved from File 16, together with the creation and storage of new labeled COMMON.

(2) Control input data are read.

(3) Loads for the current load step are computed.

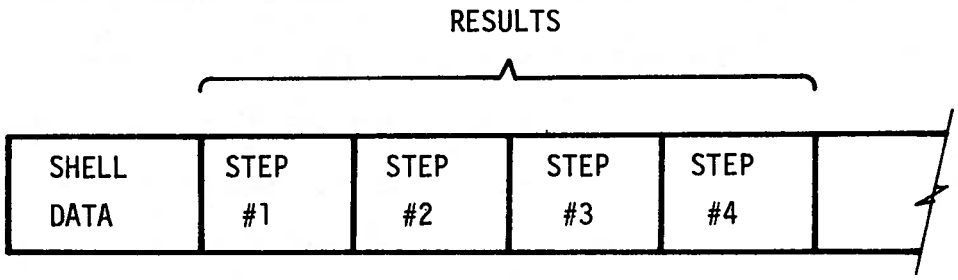

(a) STORAGE SPACES OF FILE 16

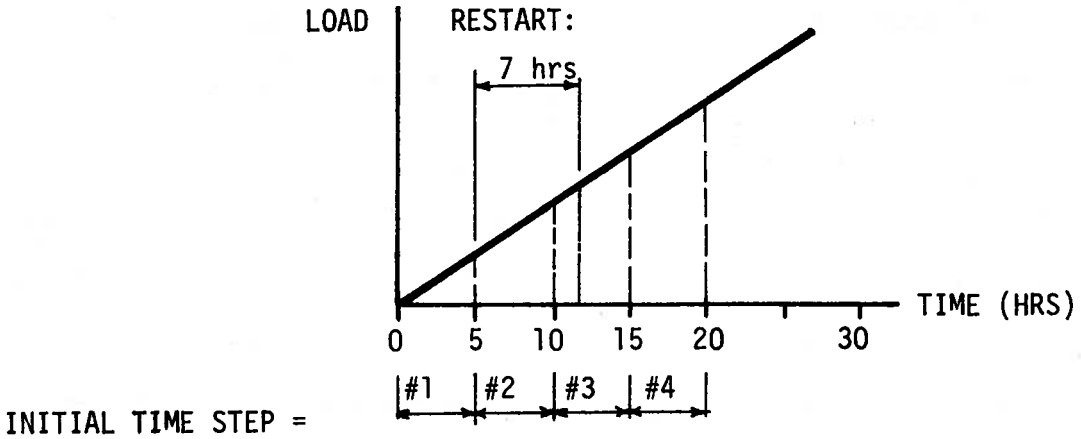

(b) LOAD-TIME FUNCTION

FIGURE A1 - RESTART PROCEDURE FOR A FICTITIOUS EXAMPLE

(4) The non-linear algebraic equations (Eq. 4 of [11]) are set up using the displacement vector, {q}, plastic strains, and the incremental stiffness matrix computed at the end of the previous load step or previous 'trial' (see (7) for the definition of 'trial'). The equations are solved using the Newton-Raphson method of iteration, keeping the stiffness matrix and plastic strains fixed. Iterations are assumed to have converged when each of the displacement corrections, Δq, satisfies:

$$\left|\frac{\Delta q}{q}\right| < 0.001$$

One complete set of Newton-Raphson iterations is termed a completion of the 'inner' loop. The inner loop establishes nonlinear geometric effects only.

(5) The total strains are computed from the latest displacement vector.

(6) The incremental flow theory is used to compute the plastic - strain increments, and the current yield parameters. The stiffness matrix and the 'thermal load vector' are also updated.

(7) Steps (4) to (6) constitute a 'trial' which is one pass through the 'outer loop'. A check is now performed to see if the displacement q resulting from this trial correspond to those from the previous trial. The solution for the load step is assumed to have converged when

$$\left|\frac{\Delta q}{q}\right| < 0.001$$

This means that the material properties have stopped changing between the current and previous trials, and the solution may proceed to the next load step.

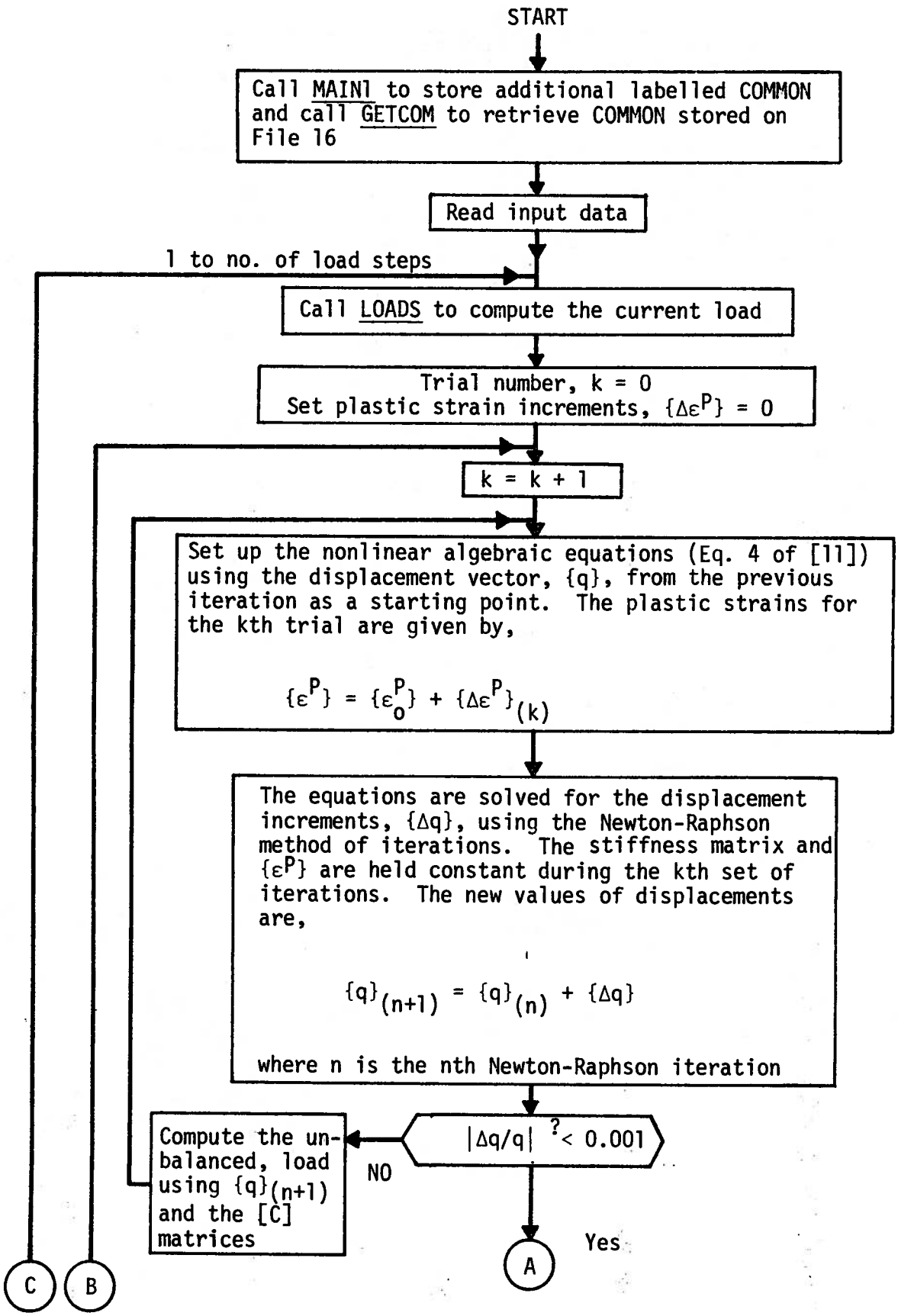

FIG. A.2 - (page 1 of 2)

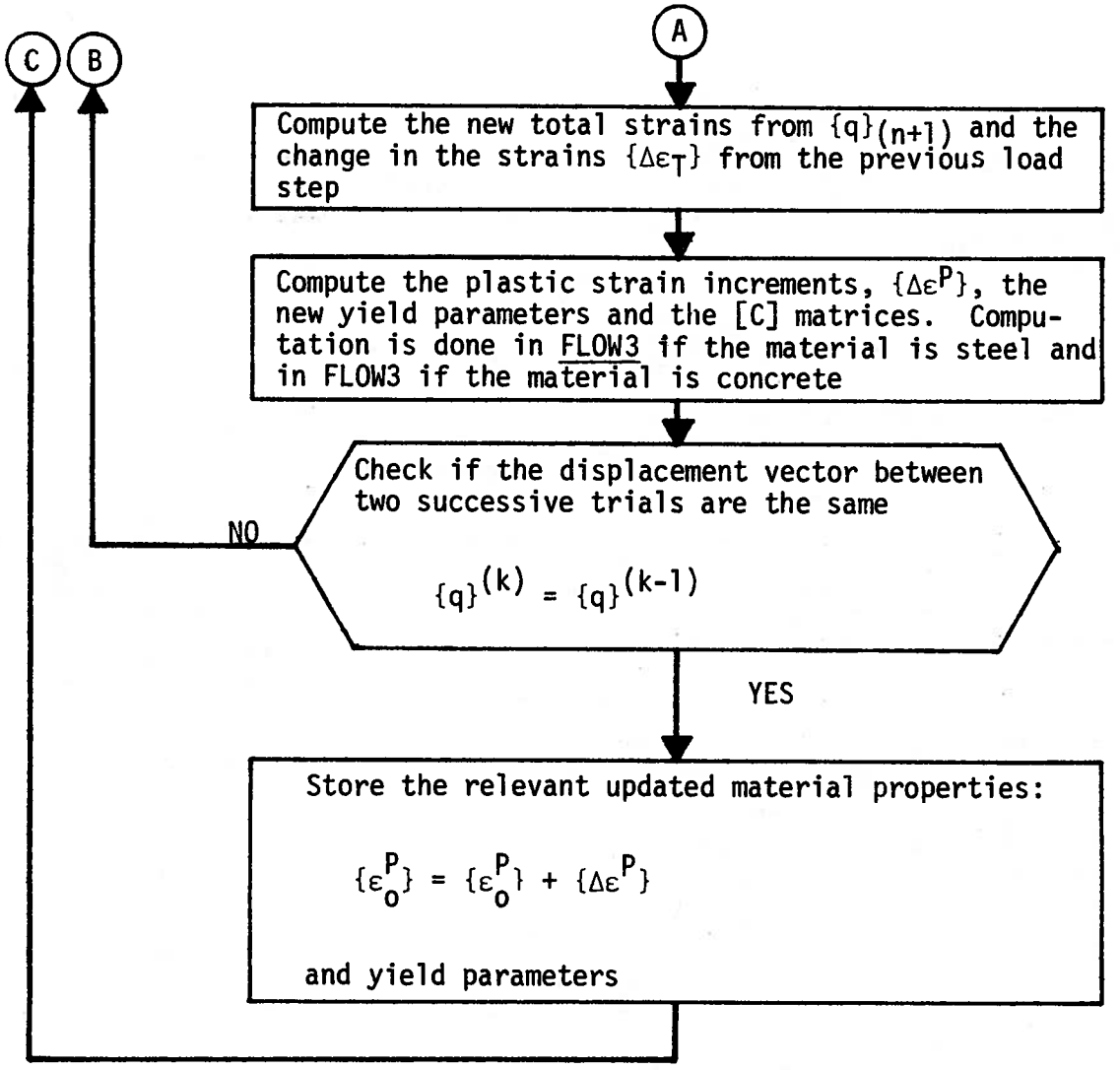

FIGURE A.2 - Flow Chart for Main-Processor of BOSOR5

APPENDIX B

APPENDIX B - DESCRIPTION OF PROGRAM CODING FOR THE THREE-PARAMETER THEORY

B.1 The Subroutine FLOW3

The coding required for the implementation of the three-parameter theory for concrete, as derived in Chapter 2, is contained in the subroutine FLOW3 together with other subroutines called by FLOW3. Basically, the strain increments (meridional and cirumferential) corresponding to the current trial are divided into a number of subincrements. For each subincrement, the corresponding increments of stresses and plastic strains, and current yield parameters are calculated. The subroutine also passes out the updated [C] matrix to the calling subroutine after the subincrement procedure is completed.

FLOW3 can either be implemented directly in the BOSOR5 program or be used to study the stress-strain response of a concrete element under biaxial loading. In the former case, FLOW3 is called by subroutine FLOW whenever the material of the shell layer being analyzed is concrete. The [C] matrices that are passed out are then used in the subsequent trial of the Newton-Raphson iteration. In the latter case, FLOW3 is called by a small MAIN program (Test Program) which primarily generates a pair of strain increments, $\Delta\varepsilon_1$ and $\Delta\varepsilon_2$ (= $\{\Delta\varepsilon\}$), that can be used in the subincrement procedure. The generation of $\{\Delta\varepsilon\}$ is based on the rationale that a concrete element under biaxial stresses (or loads) will undergo strain changes that are proportional to the stress ratio (SRATIO) and the current elastic-plastic constitutive matrix $[D_{EP}]$, as given by Eq. 2.2.17a. That is,

$$\{\Delta\sigma\} = [D_{EP}]\ \{\Delta\varepsilon\} \tag{B.1}$$

Expanding the above and defining $\Delta\sigma_2/\Delta\sigma_1$ = SRATIO, one obtains,

$$\Delta\varepsilon_2 = \left(\frac{\text{SRATIO} * D_{EP11} - D_{EP21}}{D_{EP22} - \text{SRATIO} * D_{EP12}}\right) \Delta\varepsilon_1 \tag{B.2}$$

Therefore, $\Delta\varepsilon_2$ is automatically generated if $\Delta\varepsilon_1$ and SRATIO are read by the MAIN program as input, whereas the $[D_{EP}]$ matrix is calculated from the updated [C] matrix of the previous load step. In this manner, it is possible to obtain the stress-strain response for different applied stress ratios and to compare the results with those of Kupfer, Hilsdorf and Rüsch [19].

A flow chart of FLOW3 is shown in Fig. B.1 and a complete listing of the Test Program is included in Appendix D. The basic steps in FLOW3 are as follows:

(1) Auxiliary storage for λ, μ_1, μ_2, σ_c, σ_{t1}, σ_{t2}, $\{\varepsilon^P\}$, and $\{\sigma_o\}$ is created to save the initial values, which are required for each subincrement solution.

(2) A check is carried out to determine whether the current load step will produce an elastic or a plastic response. The yield function, F, using the fictitious elastic stresses caused by the current load is computed. If $F < 0$, loading is completely elastic and execution of the program leaves FLOW3 with a null [C] matrix. The fictitious elastic stresses thus become the final stresses.

(3) If $F \geq 0$, a plastic analysis is required. The applied strain

increments, $\{\Delta\varepsilon_T\}$, and the fictitious elastic stress increments, $\{\Delta\sigma_T\}$, are first obtained. A check is required to identify the stress path since part of the $\{\Delta\varepsilon_T\}$ could be elastic loading. The portion of the elastic loading is represented by $\mu\{\Delta\varepsilon_T\}$ where μ will vary between 0 and 1.0. The value of μ is determined by examining the dot product of $<\Delta\sigma_T>$ and $\{B\}$, and the yield function, in the subroutine FFMU.

(4) Once all the elastic loading has been taken care of, the remainder of the strain increment $((1-\mu)\{\Delta\varepsilon_T\})$ is divided into subincrements for the plastic analysis. The division is performed in the subroutine SUBDIV, and is based on the criterion that each subincrement of strains results in a limited change of the current yield surface and a limited increase of the equivalent plastic strains.

(5) The subincrement solution is performed at this stage. At the start of each subincrement, the stress path is again identified so that any elastic loading can be removed from the plastic analysis. The incremental stresses and plastic strains are generally computed in the subroutine DELTAS, except when the initial stress point lies on the axes of the CC-zone in the biaxial stress space. In that case, the incremental stresses and plastic strains are calculated in the subroutine CORNER. The subroutine DELTAS also determines if the subincrement encounters a break in the uniaxial stress-strain curves, and if the stress path changes zones. Analysis is performed up to such a break and the remainder of the total strain increments is subdivided in SUBDIV.

(6) Theoretically, the stresses and the hardening parameters updated at the end of each subincrement should satisfy the condition that F = 0. That is, the updated stress point is on the updated yield curve. Any error should be small and the stresses are adjusted in the subroutine DRIFT.

(7) At least two subincrement solutions are carried out for each $\{\Delta\varepsilon_T\}$, so that the results of two successive solutions can be compared for convergence. Convergence is satisfied when,

$$\text{DSIG}/\sqrt{\sigma_1^2 + \sigma_2^2} < 0.06$$

or

$$\text{DSIG} < 5.0 \text{ psi}$$

where DSIG = the change in the stress point between two successive solutions; and, $\{\sigma\}$ = the final stress point of the present subincrement solution. If convergence is not satisfied, the number of subincrements is increased in geometric progression and the subincrement procedure (steps (5) to (7)) is repeated.

(8) On convergence, the updated values of λ, μ_1, μ_2, σ_c, σ_{t1}, σ_{t2}, and $\{\varepsilon^P\}$ are stored.

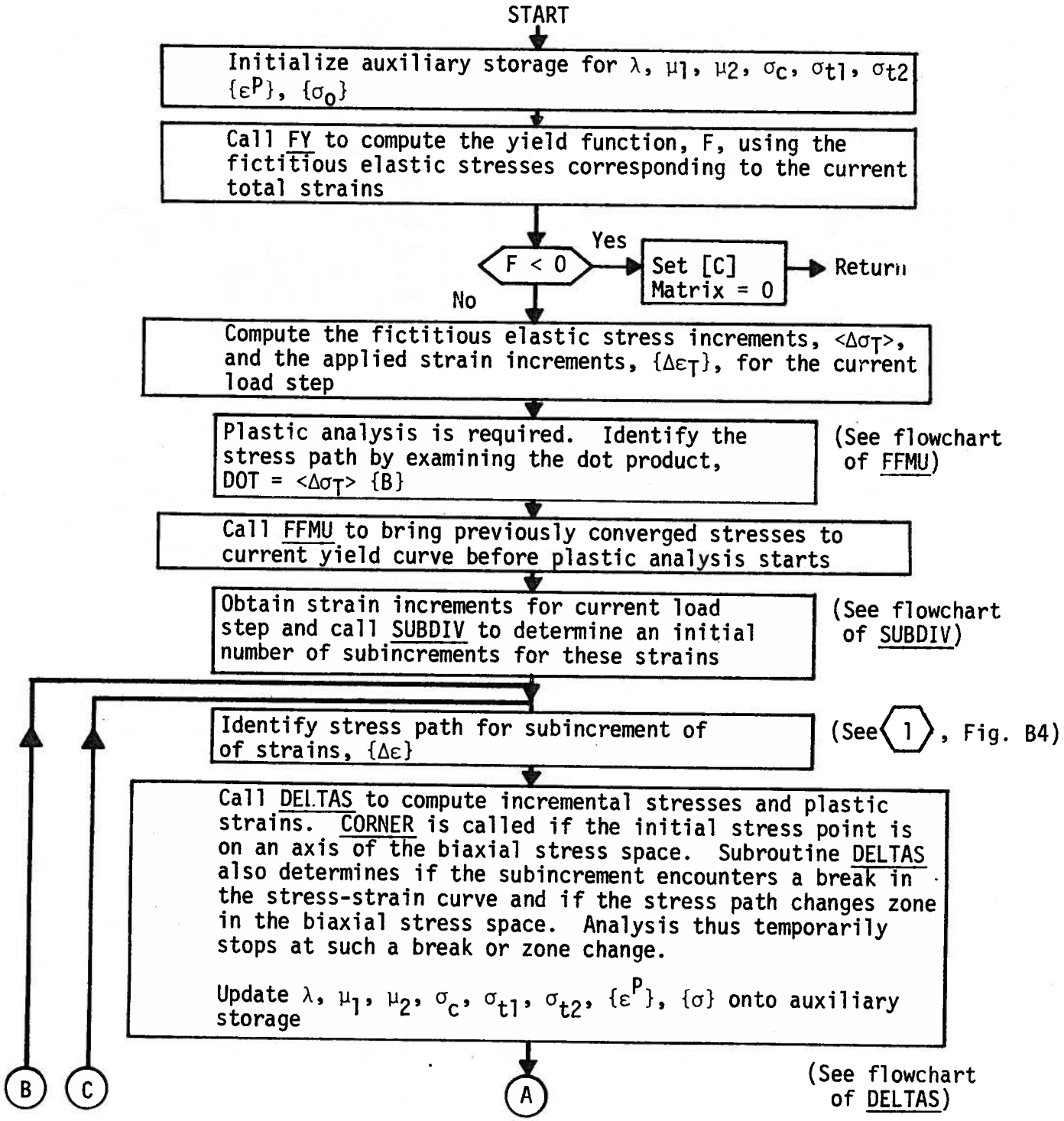

FIGURE B.1 (Page 1 of 2)

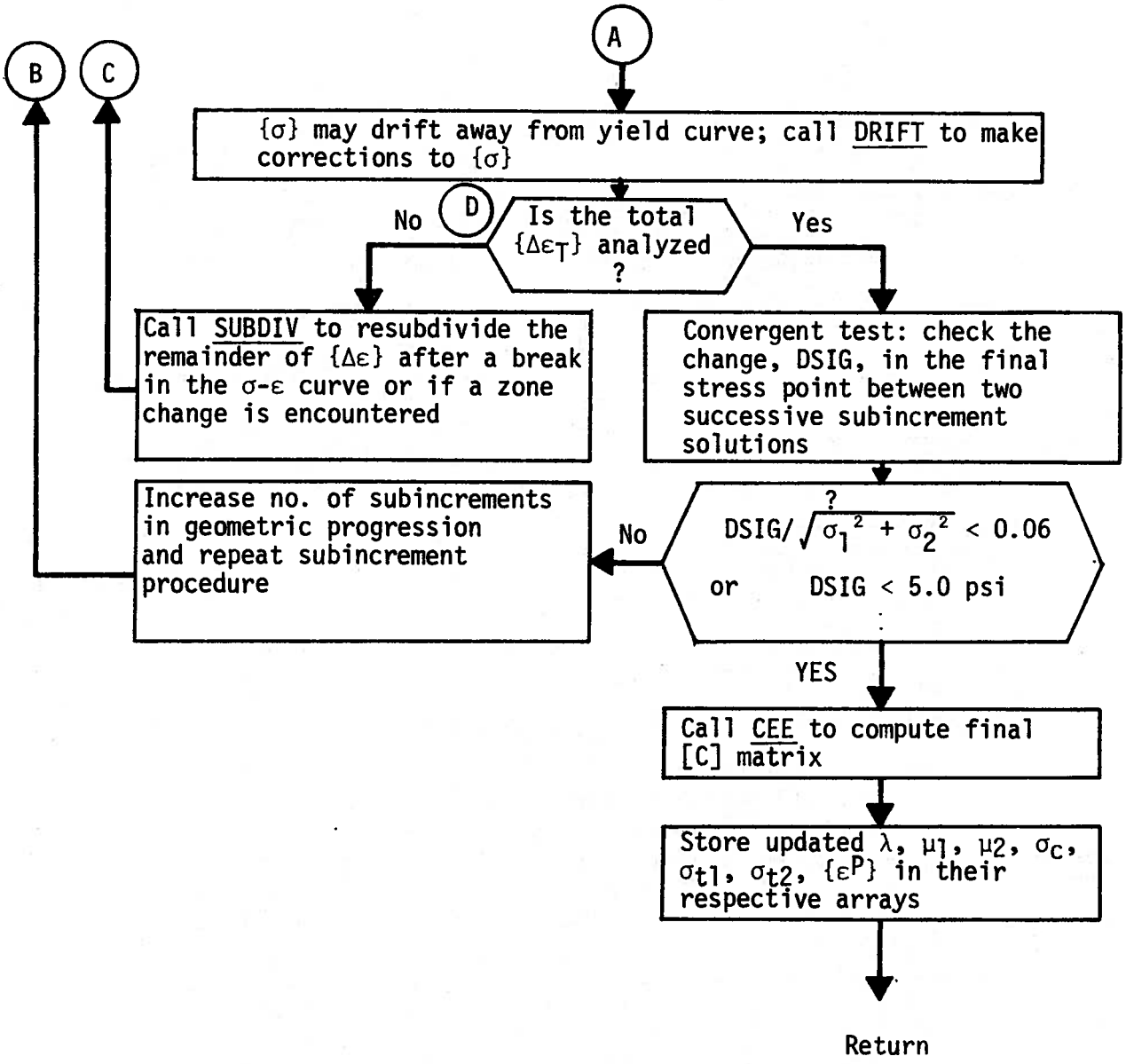

FIGURE B.1 - Flowchart for Subroutine FLOW3

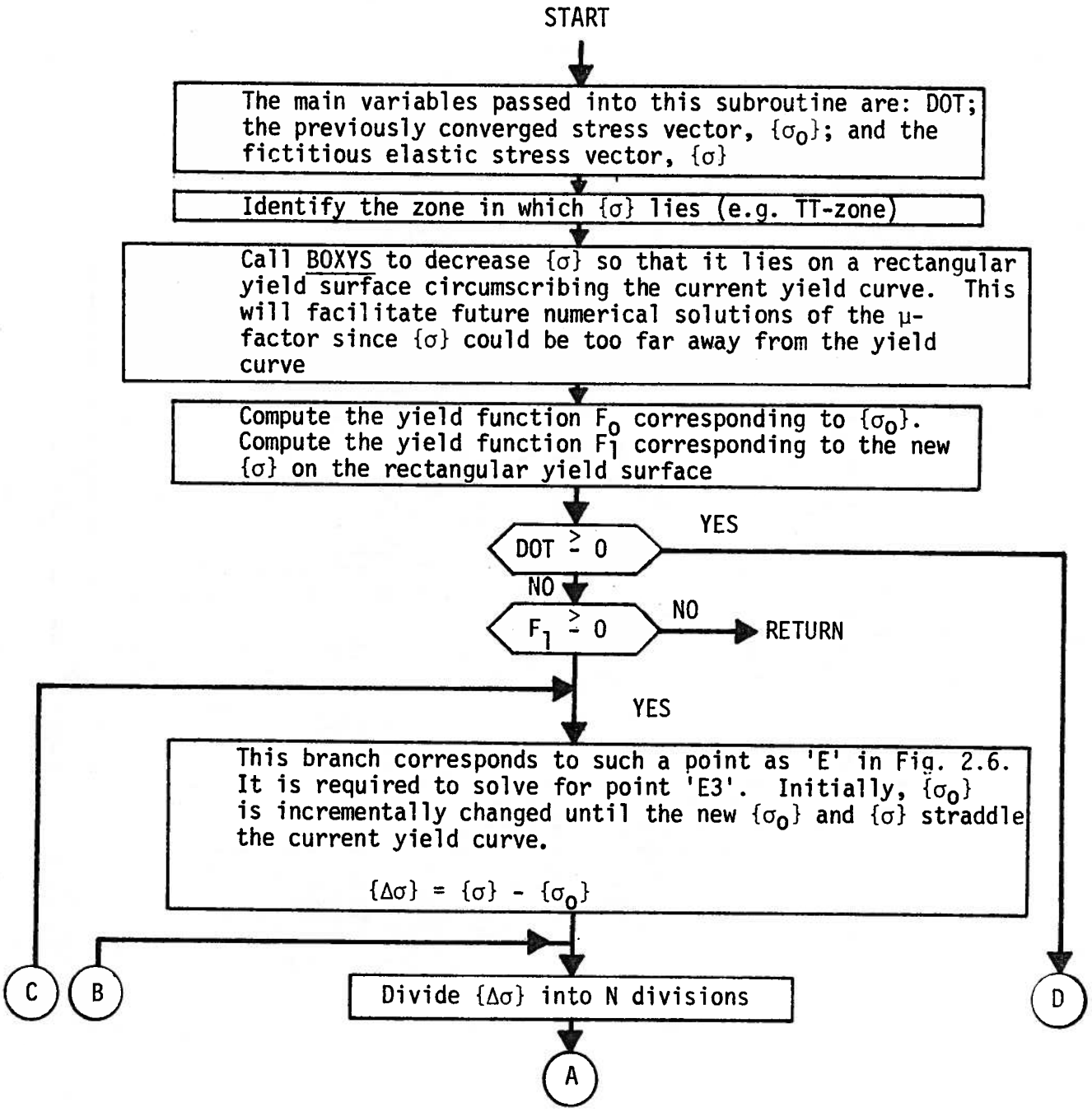

FIGURE B.2 (Page 1 of 3)

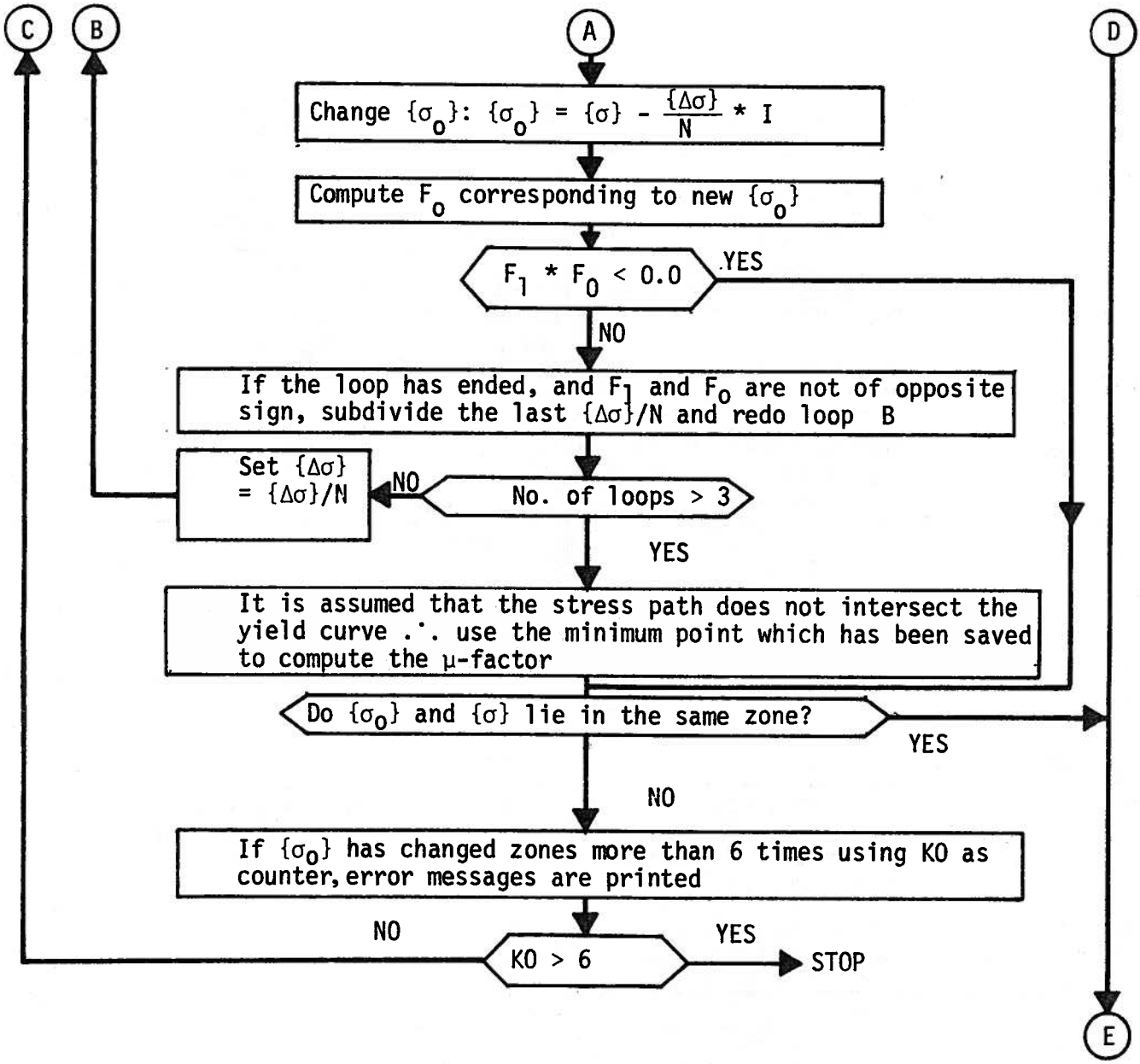

FIGURE B.2 (Page 2 of 3)

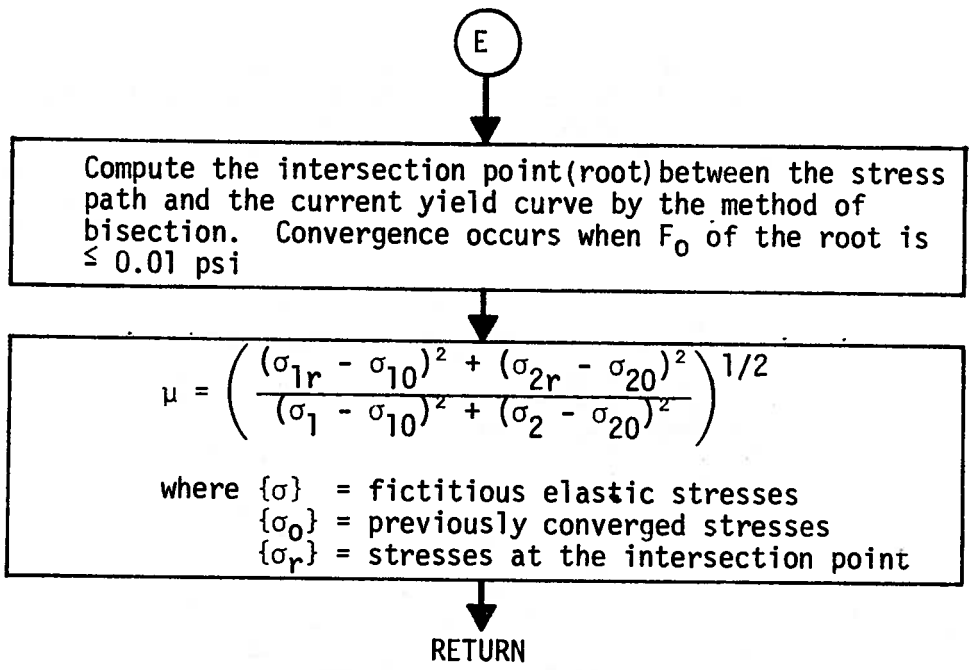

FIGURE B.2 - Flowchart for Subroutine FFMU

The subroutine SUBDIV determines the initial number of subincrements, NOSUB, required for the plastic analysis, using certain criteria as shown in the flow chart.

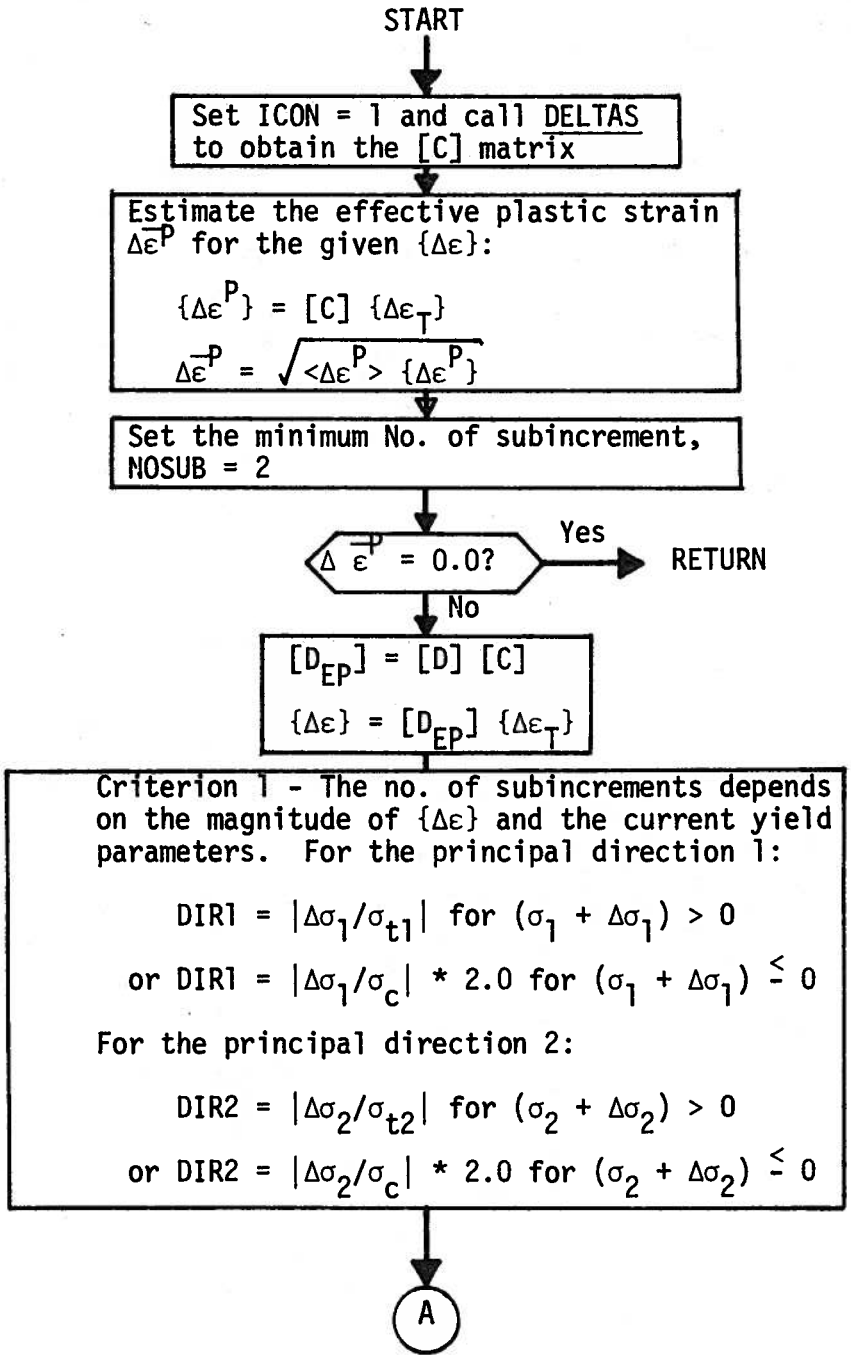

FIGURE B.3 (Page 1 of 2)

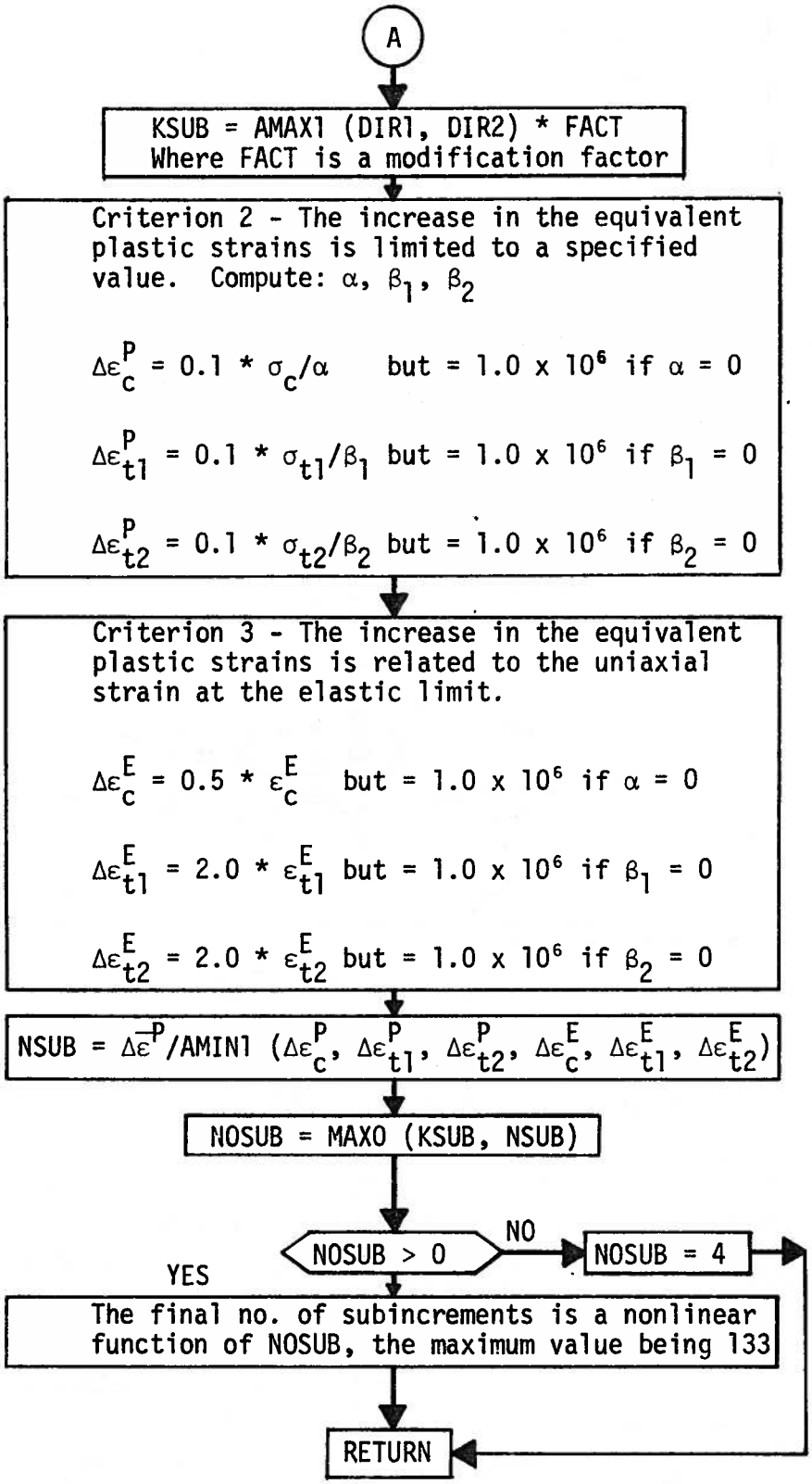

FIGURE B.3 - Flowchart for Subroutine SUBDIV

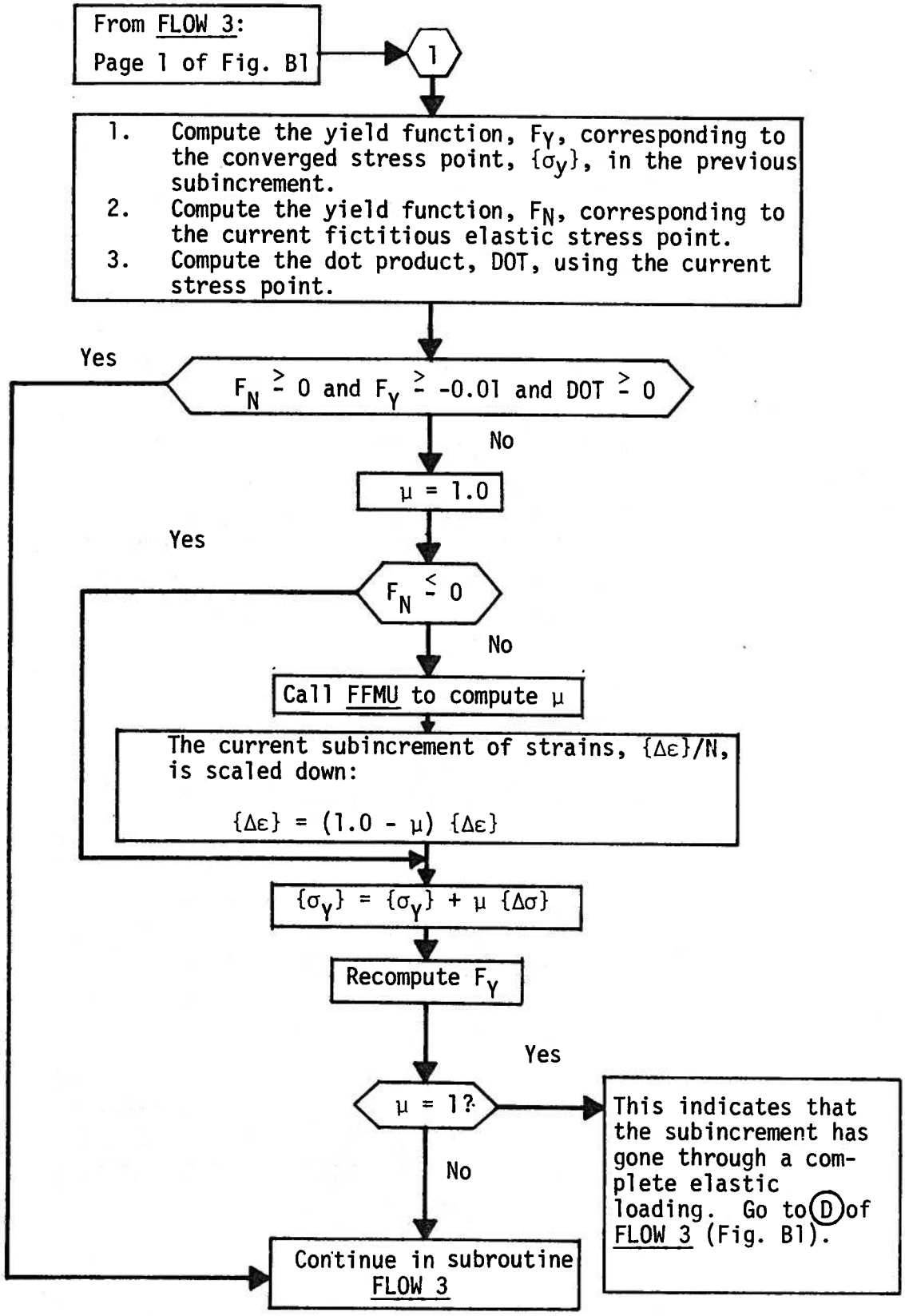

FIGURE B.4 - Flowchart to Determine a Stress Path Response

The subroutine DELTAS either computes the increments of plastic strains and stresses, or the [C] matrix.

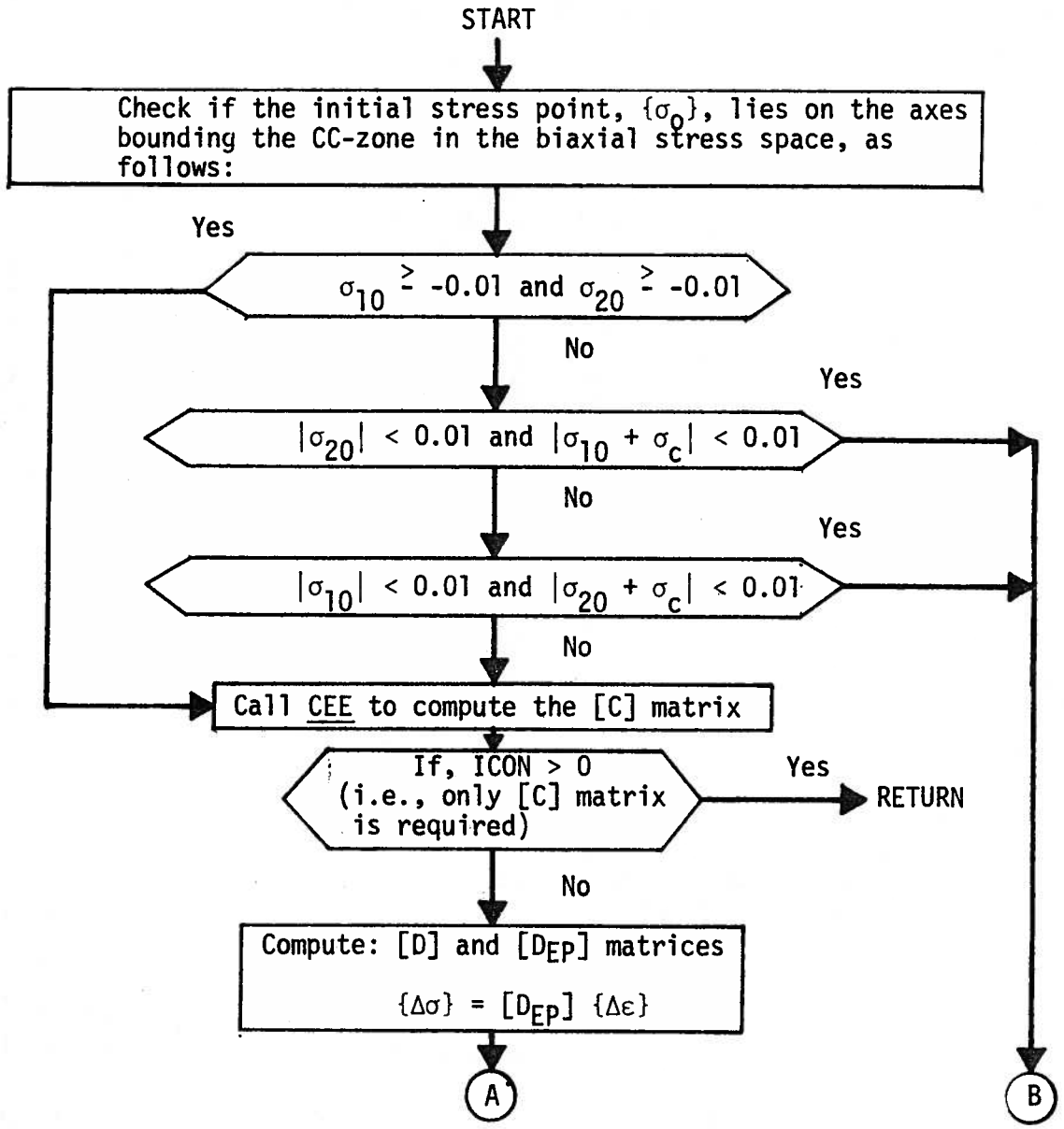

FIGURE B.5 (Page 1 of 3)

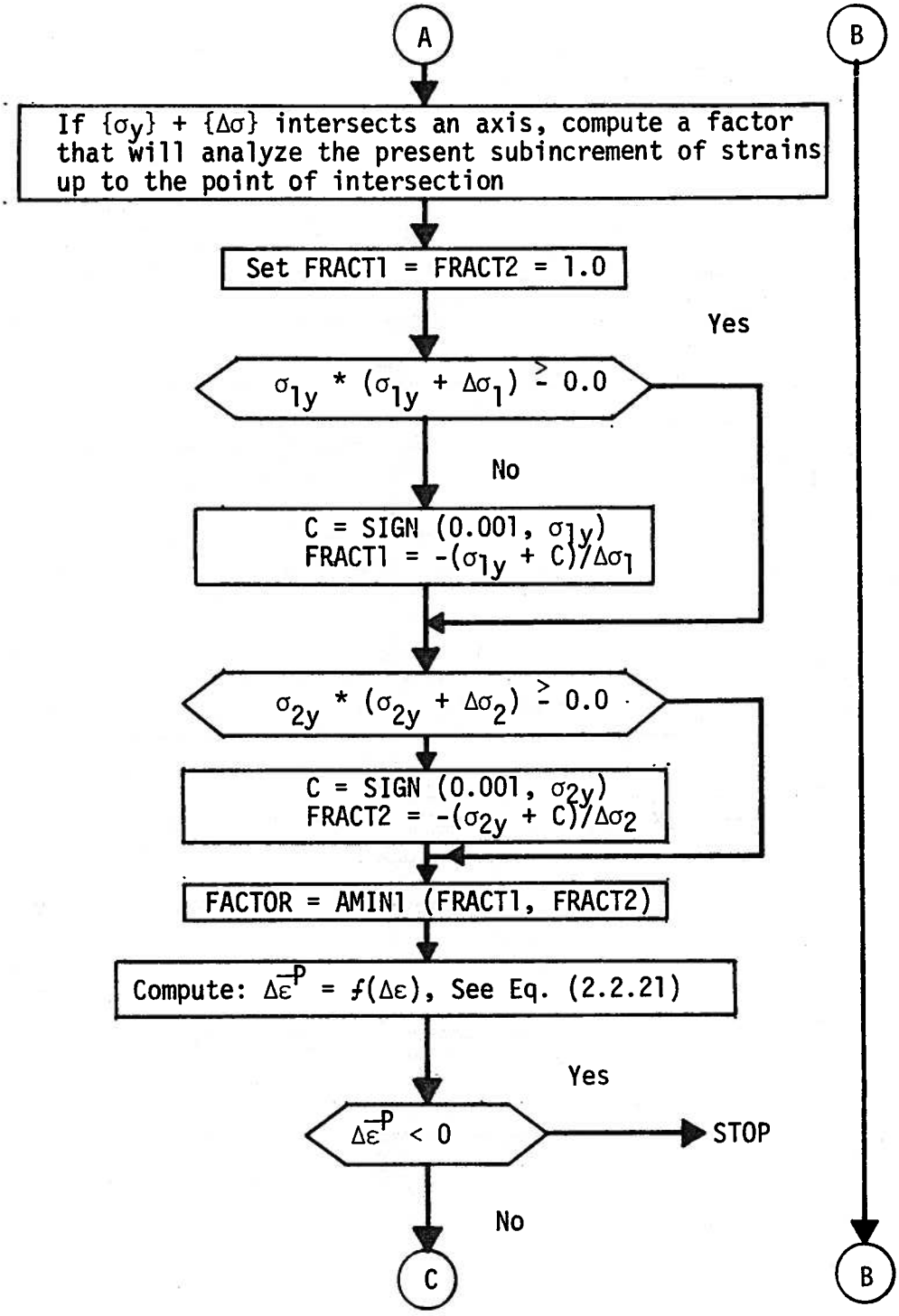

FIGURE B.5 (Page 2 of 3)

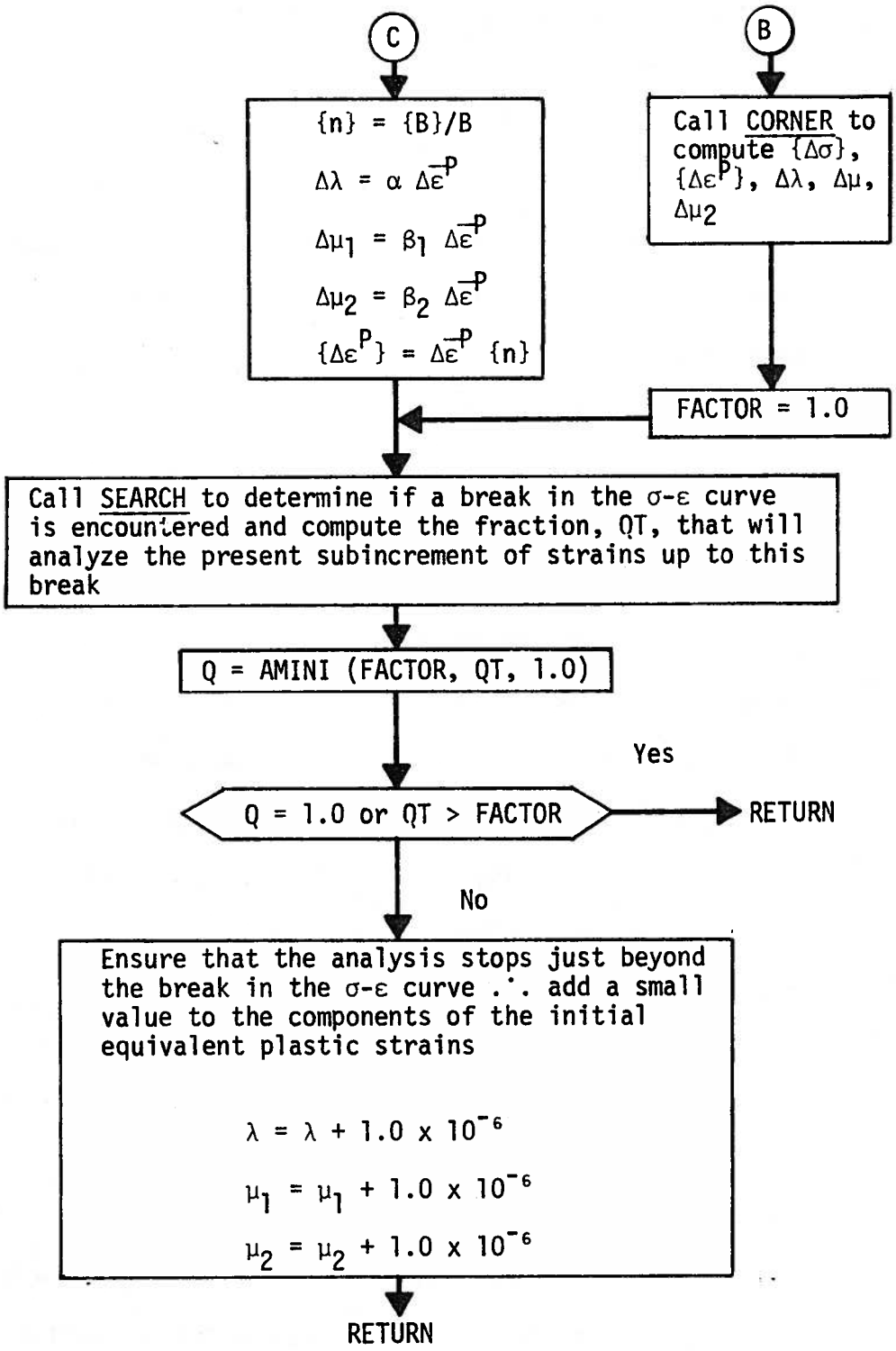

FIGURE B.5 - Flowchart for Subroutine DELTAS

B.2 Subroutines and Functions Associated with FLOW3

BOXYS: called by FFMU.

This brings the temporary stress point, evaluated by assuming linear elastic response, to a rectangular yield surface which circumscribes the current yield surface. This procedure facilitates the determination of the μ-factor which is described in Sect. 2.3.2.

CEE: called by DELTAS and CORNER.

The [C] matrix in Eq. 2.2.23 is computed here.

CORNER: called by DELTAS.

This subroutine is called if the previously converged stress point lies on an axis of the biaxial stress space. At such a location, the yield surface is not smooth and, hence, the direction of plastic strain is not uniquely defined. This subroutine will then calculate the 'preferred' direction and determine the corresponding increments of stresses and plastic strains (see Sect. 2.3.3 for more details).

DELTAS: called by FLOW3 and SUBIDV.

This subroutine computes the increment of stresses (Eq. 2.2.17a), plastic strains (Eq. 2.2.23) and uniaxial plastic strains (Eq. 2.2.6).

DFDCT: called by CORNER and CEE.

The derivatives of the current yield function with respect to the yield parameters are evaluated here and are used for the formation of the [C] matrix (see Eq. 2.2.23).

DFDS: called by FLOW3, CORNER and FFMU.

The derivatives of the current yield function with respect to the stress, i.e. - the {B} vector, are evaluated (see Sect. 2.2.3).

DG: called by CORNER and CEE.

Evaluates the derivatives of the uniaxial compressive hardening function $g(\lambda)$ as given by Eq. 2.3.7.

DK: called by CORNER and CEE.

Evaluates the derivative of the uniaxial tensile function $h(\mu)$.

DRIFT: called by FLOW3

This subroutine brings the updated stresses to the updated yield surface if the stress point drifts away from the yield surface at the end of each subincrement (see Sect. 2.3.2).

FFMU: called by FLOW3

FFMU determines the μ-factor required to bring the initial stress point up to a point on the current yield surface. This point is found by the method of bisection for iterating for roots.

FG: called by FLOW3

The yield parameter in uniaxial compression is determined in this function subroutine (see Eq. 2.3.13a).

FK: called by FLOW3

The yield parameter in uniaxial tension is determined in this function subroutine (see Eq. 2.3.13b and c).

FY: called by FLOW3, DRIFT and FFMU

The yield function is evaluated in this function subroutine.

IZONE: called by FY, DRIFT, BOXYS and FFMU

This function subroutine determines which zone of the yield surface is applicable to a stress point. For example, if both the principal stresses are positive, the stress point is in the tension-tension zone.

PARA: called by CEE

This subroutine computes the parameters α, β_1 and β_2 which are used in the decomposition of the effective plastic strain increment into the equivalent compressive and tensile plastic strain increments, as defined by Eq. 2.2.6.

SAMEL: called by SEARCH

Checks if a break in the uniaxial compression stress-strain curve is encountered (see last paragraph of Sect. 2.3.2).

SAMEM: called by SEARCH

Checks if a break in the uniaxial tensile stress-strain curve is encountered.

SEARCH: called by DELTAS

This subroutine calls SAMEL and/or SAMEM.

SUBDIV: called by FLOW3

This subroutine computes the number of subincrements to be used at the current location in the shell wall, in the current trial and in the current load step. The computation is based on the criteria that the expected rates of change of the yield surface and of the effective plastic strain are limited to certain values.

It is to be noted that certain subroutines must be modified for each of the yield function forms (see Sect. 2.4). These subroutines

are: DFDCT, DFDS, DG, DRIFT, FG, FY, IZONE and SAMEL. The listings shown in Appendix D are for the FORM4 yield function.

APPENDIX C

APPENDIX C - MODIFICATIONS TO ORIGINAL BOSOR5 PROGRAM

C.1 Description of Modification

A number of modifications were implemented in the BOSOR5 program in order to accommodate the three-parameter model for concrete, to rearrange some storage areas, and to manipulate the two permanent storage files (named 15 and 16) in which the results of evey load step are stored. Only the major modifications are briefly discussed below, although numerous minor ones were also incorporated:

(1) The maximum number of layers in the shell wall was increased from 6 to 15. However, the total number of integration points through the shell thickness remains at 50, implying that, if all the 15 layers are used, the average number of integration points per layer can only be 3 (50/15 = 3.3, i.e. 3).

(2) The number of material types were increased from 6 to 9.

(3) The three-parameter theory requires two stress-strain curves (compression and tension curves) as input, as opposed to the single curve for the von-Mises yield criterion used in the original BOSOR5. The extra space is obtained by storing the compression curve in the first half of the existing one-dimensional array of 20 elements, and the tension curve in the second half of the array. This, therefore, limits the number of points of the compressive or tensile stress-strain curve to 10. It also means that the eleventh element of the array has a zero value for a concrete material and this serves as an indicator for following the three-parameter analysis.

(4) New one-dimensional arrays were created for the uniaxial

plastic strains (λ, μ_1 and μ_2) and yield parameters (σ_c, σ_{t1} and σ_{t2}). They are also written on File 16 at the end of the other data for each load step.

(5) The subroutine GASP was rewritten to transfer data to and from core to auxiliary devices (Files 15 and 16) with greater efficiency than the original version with the U. of A. system.

(6) The original BOSOR5 could only take a layer with uniaxial properties provided that it was the last layer in the shell wall. This limitation has been removed in the updated version.

(7) The routing in the original FLOW subroutine was altered to accommodate the FLOW3 subroutine for the three-parameter theory.

(8) Normal pressure and surface traction on any segment need not be associated with a common load-time function, as was required in the original version of BOSOR5. This alteration was achieved by dividing the load-time function identification array, P(25), into two halves. The first half and second half identify the load-time functions associated with normal pressures and surface tractions respectively. This means that the maximum number of load-time functions has been decreased from 25 to 12.

C.2 Modifications to BOSOR5 User's Manual

Alterations to the input instructions for the BOSOR5 preprocessor [10] were necessary to accommodate the modifications made to the original BOSOR5 program. All the page numbers quoted herein are in Ref. 10 and the alterations are as follows:

(1) The third read statement on pg. P44 is now,

READ: ISTEP1(ISEG), ISTEP2(ISEG)

FORMAT: 2I6

where ISTEP1 and ISTEP2 are the control integers for the time functions to be associated with normal pressure and meridional traction, respectively.

(2) The read statement on pg. P50 is now,

READ: NALRED(ISEG), NPLAST(ISEG), NCREEP(ISEG),
MATCD1(ISEG), MATCD2(ISEG)

FORMAT: 4I6, I9

where MATCD1(ISEG) is the control integer for the type of material for the first 6 layers (counting from the leftmost layer) of the shell and MATCD2(ISEG) is the control integer for the type of material for the remaining layers.

(3) The first read statement on pg. P54 is now,

READ: NPOINT, NITEG, ISSFUN, I3PARM

FORMAT: 4IG

When the additional name, I3PARM,

= 0, the original von-Mises yield surface in BOSOR5 is used,

= 1, the three parameter theory for concrete is used and ISSFUN must be set to 0.

(4) When the three parameter theory option is in effect, the compressive stress-strain curve is read into the first ten elements of the arrays, EPEFF(L) and SGEFF(L), in the third and fourth read statements on pg. P54. The tensile stress-strain is read into the remaining elements of EPEFF(L) and SGEFF(L).

APPENDIX D

```
C  MAIN PROGRAM FOR TESTING FLOW3 ROUTINE ******************
C  ********************************************************
C     THE SIZES OF SYC,SYT1,SYT2,ELAMDA,EMU1,EMU2  COULD BE REDUCED
C     TO 1*1 IN THE TEST PRIGRAM. HOWEVER,LEAVE THEM AS 21*50  FOR
C     FUTURE USE (L.CHITNUYANONDH,22 SEPT.  1977)
C
      DIMENSION SGEFFC(10),EPEFFC(10),SGEFFT(10),EPEFFT(10)
      COMMON/ITERS/ITER
      COMMON/DIC/DIC11,DIC12,DIC21,DIC22,KFLAG
      DO 5 I=7,10
      EPEFFC(I)=10.
      EPEFFT(I)=10.
      SGEFFC(I)=1.
    5 SGEFFT(I)=1.
C
C     INITIAL STRAINS E0 AND E02 MUST BE IN THE ELASTIC RANGE
C
      READ(5,1000)   (EPEFFC(I),I=1,7)
      READ(5,1000)   (SGEFFC(I),I=1,7)
      READ(5,1000)   (EPEFFT(I),I=1,6)
      READ(5,1000)   (SGEFFT(I),I=1,6)
      READ(5,1000)U
      READ(5,1000)E0,E02
      READ(5,1000)SRATIO,DE0,NUM
      E=SGEFFC(2)/EPEFFC(2)
      EX=E/(1.-U*U)
      EY=EX
      XNU=U
      ITER=1
      DIC11=EX
      DIC12=EX*U
      DIC21=DIC12
      DIC22=DIC11
      IQ=1
      Z=1.
      PREE0=E0
      PREE02=E02
      EP1=0.
      EP2=0.
C
      SYC=SGEFFC(2)
      SYT1=SGEFFT(2)
      SYT2=SGEFFT(2)
      ELAMDA=0.
      EMU1=0.
      EMU2=0.
      IF(NUM.LE.0) STOP
      IF(NUM.GE.1000) STOP
      WRITE(6,900)SRATIO,DE0,NUM
      WRITE(6,901) E0,E02
  901 FORMAT(1H0,'   EPS1        =',F18.7,' EPS2        =',F18.7)
  900 FORMAT(1H1,'   STRESS RATIO =',F18.7,' STRAIN INC.=',E12.4,
     1  '  NUMBER OF ITER.=',I6)
C     WRITE(6,3000)
C3000 FORMAT(//15X,'E0',9X,'E02',9X,'SIG1',8X,'SIG2',
```

```
C     16X,'SIG2/SIG1')
  200 FORMAT(1H0,'    EPS 1      EPS 2        S1SC        SIGMA 1'
     *    ,'    SIGMA 2      SRATIO      DIC22    ')
      WRITE(6,200)
      DO 100 I=1,NUM
      IF(E0.EQ.0.)E0=1. E-20
      C11=0.
      C12=0.
      C21=0.
      C22=0.
C
C     FIRST GET STRAINS AT KK-TH STATION THRU THICKNESS
C     CONVERGED STRAINS AT LAST LOAD STEP
      EPS1S=PREE0
      EPS2S=PREE02
C     PLASTIC STRAIN COMPONENTS, CREEP STRAIN COMPONENTS FROM LAST LOAD
      EPNEW1=EP1
      EPNEW2=EP2
C     CALCULATE ELASTIC STRAINS CORRESPONDING TO LAST LOAD STEP
      E1SEL=EPS1S-EP1
      E2SEL=EPS2S-EP2
C
C
C     CURRENT STRAINS
      EPS1=E0
      EPS2=E02
C     NOW CALCULATE ELASTIC STRAINS FOR CURRENT LOAD STEP
      E1ELAS = EPS1 -EPNEW1
      E2ELAS = EPS2 - EPNEW2
C     CALCULATE STRESSES FOR CURRET LOAD STEP
      SIG1 = EX*(E1ELAS + U*E2ELAS)
      SIG2 = EY*(U*E1ELAS + E2ELAS)
C
C     NOW CALCULATE EFFECTIVE STRESS AND STRESS COMPONENTS FOR LAST
C     CONVERGED LOAD STEP
      SIG10 = EX*(E1SEL + U*E2SEL)
      SIG20 = EY*(U*E1SEL + E2SEL)
      SIG1Y = SIG10
      SIG2Y = SIG20
C     ENTER THE SUBINCREMENT PROCEDURE
C
      CALL FLOW3(1,1,1,1,EPS1,EPS2,EPS1S,EPS2S,
     1 EPNEW1,EPNEW2,E1SEL,E2SEL,E1ELAS,E2ELAS,SIG1,SIG2,
     2 SIG10,SIG20,SIG1Y,SIG2Y,XNU,EX,EY,E,SGEFFC,EPEFFC,
     3 SGEFFT,EPEFFT,C11,C12,C21,C22,EP1,EP2,Z
     4  ,SYC,SYT1,SYT2,ELAMDA,EMU1,EMU2)
C
      PREE0=E0
      PREE02=E02
      IF(SIG1.EQ.0.) SIG1=1.00E-20
      S2S1=SIG2/SIG1
      S1SC=SIG1/4650.
      IF(SIG1.EQ.0.) X1=0.
      IF(SIG1.GT.0.) X1=SIG1/SYT1
      IF(SIG1.LT.0.) X1=SIG1/SYC
```

```
      IF(SIG2.EQ.0.) X2=0.
      IF(SIG2.GT.0.) X2=SIG2/SYT2
      IF(SIG2.LT.0.) X2=SIG2/SYC
C     WRITE(6,2000)I, E0,E02,SIG1,SIG2,S2S1
C
      WRITE(6,2000)EPS1,EPS2,S1SC,SIG1,SIG2,S2S1,DIC22
C    *          ,X1,X2,EPNEW1,EPNEW2
 2000 FORMAT(1H ,10E12.4)
      GO TO (43,44,45),IQ
   44 E0=E0*1.0001
      GO TO 43
   45 E02=E02*1.0001
   43 GO TO (30,40), KFLAG
   40 D11=EX
      D12=U*EX
      D21=D12
      D22=D11
      DIC11=D11*(1.-C11)-D12*C21
      DIC12=-D11*C12+D12*(1.-C22)
      DIC21=D21*(1.-C11)-D22*C21
      DIC22=-D21*C12+D22*(1.-C22)
      GO TO 55
   30 DIC11=EX
      DIC12=EX*U
      DIC21=DIC12
      DIC22=DIC11
   55 R=(SRATIO*DIC11-DIC21)/(DIC22-SRATIO*DIC12)
      DE02=DE0*R
      IF(E0)35,36,36
   35 CALL BREAK(E0,DE0,EPEFFC,Q1)
      GO TO 39
   36 CALL BREAK(E0,DE0,EPEFFT,Q1)
   39 IF(E02)37,38,38
   37 CALL BREAK(E02,DE02,EPEFFC,Q2)
      GO TO 1111
   38 CALL BREAK(E02,DE02,EPEFFT,Q2)
C  41 WRITE(6,2500)Q1,Q2
 1111 IF(Q1*Q1+Q2*Q2.EQ.0.) GO TO 31
      IF(Q1.EQ.0.) GO TO 42
      IF(Q2.EQ.0.) GO TO 23
      IF(Q1.LE.Q2) GO TO 23
   42 DE02=DE02*Q2
      E0=E0+DE02/R
      IQ=3
      GO TO 32
   23 E0=E0+DE0*Q1
      DE02=DE0*Q1*R
      IQ=2
      GO TO 32
   31 E0=E0+DE0
      IQ=1
   32 E02=E02+DE02
      DE01=DE02/R
C     WRITE(6,1500)DIC22,DE01,DE02,E0,E02,SRATIO,R
C1500 FORMAT(5X,'DIC22 DE01 DE02 E0 E02 SRATIO R=',5E14.6,F11.7,F11.4/)
```

```
  100 CONTINUE
C
 1000 FORMAT(9G10.0)
C2500 FORMAT(5X,'FRACTION OF STRAIN INPUT TO TAKE ANALYSIS UPTO BREAK IN
C     1 THE STRESS-STRAIN CURVE, DIRECTION 1 & 2 =',2F12.8)
C2000 FORMAT(I4,'----',2E12.4,2F12.4,F12.7,/,'-------------------------
C     1-----------------------------------------------------------')
      STOP
      END
```

```
C
C  ***************************************************************
C*********************************************
      SUBROUTINE BREAK(EPS,DELEPS,EPEFF,QM)
C*********************************************
      DIMENSION EPEFF(1)
C     CHECK IF THE NEXT STRAIN INCREMENT FALLS WITHIN THE NEXT
C       SEGMENT OF THE STRESS-STRAIN CURVE
C
      QM=0.
      ET=ABS(EPS+DELEPS)
      EPP=ABS(EPS)
      IF(ET.EQ.0.) RETURN
      DO 10 I=2,10
      J=I
      IF(EPP.LT.EPEFF(I)) GO TO 20
   10 CONTINUE
   20 DO 15 I=2,10
      K=I
      IF(ET.LT.EPEFF(I)) GO TO 50
   15 CONTINUE
   50 IF(J.EQ.K) RETURN
      QM=(EPEFF(J)-EPP)/ABS(DELEPS)
      RETURN
      END
```

```
C
C  ****************************************************************
      SUBROUTINE BOXYS(YS1,YS2,SIG1,SIG2,SIG10,SIG20,SYC,SYT1,
     1SYT2,IT)
C  ****************************************************************
C
C     THIS SUBROUTINE BRINGS THE CURRENT APPROXIMATE STRESSES
C     BACK TO A RECTANGULAR YIELD SURFACE BEFORE CALCULATING
C     THE FFMU-FACTOR
C
      SQ1=1.02*SYT1
      SQ2=1.02*SYT2
      SQC=-1.285*SYC
      IF(SIG1.GT.SQ1.OR.SIG1.LT.SQC) GO TO 10
      IF(SIG2.GT.SQ2.OR.SIG2.LT.SQC) GO TO 10
      YS1=SIG1
      YS2=SIG2
      RETURN
C
   10 XSMALL=SIG10
      XBIG=SIG1
      IF(SIG1.GE.SIG10) GO TO 20
      XSMALL=SIG1
      XBIG=SIG10
   20 YSMALL=SIG20
      YBIG=SIG2
      IF(SIG2.GE.SIG20) GO TO 30
      YSMALL=SIG2
      YBIG=SIG20
C
C     EQUATION OF STRAIGHT LINE: SIG1=SP*SIG2+C
   30 IF(ABS(SIG1-SIG10).LT.1.0E-16) GO TO 90
      SP=(SIG2-SIG20)/(SIG1-SIG10)
      C=SIG2-SP*SIG1
C
C     SETTING YS1 AS SQ1 AND SQC TO CALCULATE YS2
C
      KK=1
      YS2=SQ1*SP+C
   50 IF(YS2.GT.YBIG.OR.YS2.LT.YSMALL) GO TO 40
      IF(YS2.GT.SQ2.OR.YS2.LT.SQC) GO TO 40
      IF(KK.EQ.1) YS1=SQ1
      IF(KK.EQ.2) YS1=SQC
      GO TO 100
   40 IF(KK.EQ.2) GO TO 60
      YS2=SQC*SP+C
      KK=KK+1
      GO TO 50
C
C     SETTING YS2 AS SQ2 AND SQC TO CALCULATE YS1
C
   60 KC=1
      YS1=(SQ2-C)/SP
   80 IF(YS1.GT.XBIG.OR.YS1.LT.XSMALL) GO TO 70
      IF(YS1.GT.SQ1.OR.YS1.LT.SQC) GO TO 70
```

```
      IF(KC.EQ.1) YS2=SQ2
      IF(KC.EQ.2) YS2=SQC
      GO TO 100
   70 IF(KC.EQ.2) GO TO 999
      YS1=(SQC-C)/SP
      KC=KC+1
      GO TO 80
C
C     THIS ROUTE IS FOR A STRESS PATH PARALLEL TO THE SIG2-AXIS
C
   90 YS1=SIG1
      YS2=SQ2
      IF(YS2.GT.YBIG.OR.YS2.LT.YSMALL) GO TO 91
      GO TO 100
   91 YS2=SQC
      IF(YS2.GT.YBIG.OR.YS2.GT.YSMALL) GO TO 995
C     DETERMINE THE ZONE FOR THE TEMPORARY STRESSES ON THE RECTANGULAR
C     YIELD SURFACE
C
  100 IT=IZONE(YS1,YS2,SYC,SYT1,SYT2)
      RETURN
C
  999 WRITE(6,1000)
 1000 FORMAT('***** PROGRAM SHOULD NOT COME THIS ROUTE *****')
      YS1=SIG1
      YS2=SIG2
      RETURN
  995 WRITE(6,1100)SIG10,SIG20,SIG1,SIG2
 1100 FORMAT('***** CANNOT FIND STRESSES ON BOX SURFACE=',4E12.5)
      STOP
      END
```

```
C
C  ****************************************************
      SUBROUTINE CEE(SIG1Y,SIG2Y,SYC,SYT1,SYT2,B1,B2,
     1  EX,EY,U,ELAMDA,EMU1,EMU2,SGEFFC,EPEFFC,SGEFFT,EPEFFT,
     2  C11,C12,C21,C22,DENOM,ALFA,BET1,BET2,DGG,DK1,DK2)
C ****************************************************
C  THIS SUBROUTINE CALCULATES C MATRIX
C  CALLED BY SUBROUTINE DELTAS AND CORNER
      DIMENSION SGEFFC(1),EPEFFC(1),SGEFFT(1),EPEFFT(1)
      D11=EX
      D12=U*EX
      D21=U*EY
      D22=EY
      BMOD=SQRT(B1*B1+B2*B2)
      DENOM1=D11*B1*B1+2.*D12*B1*B2+D22*B2*B2
C
      CALL PARA(SIG1Y,SIG2Y,SYC,SYT1,SYT2,ALFA,BET1,BET2,B1,B2)
      CALL DFDCT(SIG1Y,SIG2Y,SYC,SYT1,SYT2,DC,DT1,DT2)
C
      DGG=DG(ELAMDA,SGEFFC,EPEFFC)
      DK1=DK(EMU1,SGEFFT,EPEFFT)
      DK2=DK(EMU2,SGEFFT,EPEFFT)
      DENOM=DENOM1-BMOD*(ALFA*DC*DGG+BET1*DT1*DK1+BET2*DT2*DK2)
C
      C11=(D11*B1*B1+D21*B2*B1)/DENOM
      C12=(D21*B1*B1+D22*B1*B2)/DENOM
      C21=(D11*B1*B2+D21*B2*B2)/DENOM
      C22=(D12*B1*B2+D22*B2*B2)/DENOM
      RETURN
      END
```

```
      C
      C*************************************************************
            SUBROUTINE CORNER(S1,S2,DEBAR,DEL,DEM1,DEM2,EX,EY,U,ELAMDA,
           1   EMU1,EMU2,SGEFFC,EPEFFC,SGEFFT,EPEFFT,DS1,DS2,C1,C2,
           2      SYC,SYT1,SYT2,DEP1,DEP2,DIC21,DIC22,
           3  DIC11,DIC12,C11,C12,C21,C22,ICON,ALFA,BETA1,BETA2,DGG,
           4  DK1,DK2,B1,B2)
      C*************************************************************
      C
      C   INDC=1, CORNER IS LOCATED ON THE VERTICAL AXIS
      C   INDC=2, CORNER IS LOCATED ON THE HORIZONTAL AXIS
      C
            DIMENSION SGEFFC(1),EPEFFC(1),SGEFFT(1),EPEFFT(1)
            ALFA=0.0
            BETA1=0.0
            BETA2=0.0
            D11=EX
            D12=U*EX
            D21=U*EY
            D22=EY
            DET=D11*D22-D12*D21
            INDC=1
            IF(ABS(S2).LT.0.01) INDC=2
            GO TO (10,20), INDC
         10 SS1=0.001
            SS2=S2
            GO TO 30
         20 SS1=S1
            SS2=0.001
         30 CONTINUE
      C
      C   COMPUTE DERIVATIVES AND OTHER PROPERTIES ON THE POSITIVE SIDE
      C   OF THE AXIS OF YIELD SURFACE
      C
            CALL DFDS(SS1,SS2,SYC,SYT1,SYT2,B1P,B2P)
            CALL DFDCT(SS1,SS2,SYC,SYT1,SYT2,DCP,DT1P,DT2P)
      C
            GO TO (40,50), INDC
         40 SS1=-0.001
            GO TO 60
         50 SS2=-0.001
         60 CONTINUE
      C
      C   COMPUTE DERIVATIVES AND OTHER PROPERTIES ON THE ENGATIVE SIDE
      C   OF THE AXIS OF YIELD SURFACE
      C
            CALL DFDS(SS1,SS2,SYC,SYT1,SYT2,B1M,B2M)
            CALL DFDCT(SS1,SS2,SYC,SYT1,SYT2,DCM,DT1M,DT2M)
      C
            BPMOD=SQRT(B1P*B1P+B2P*B2P)
            BMMOD=SQRT(B1M*B1M+B2M*B2M)
      C
      C   COMPUTE THE NUMERATORS, XPLUS AND XMINUS, USING THE POSITIVE
      C   AND NEGATIVE PROPERTIES, RESPECTIVELY
      C
```

```
      GO TO (70,80) , INDC
   70 IF(SS2)72,72,74
   72 RHS=DG(ELAMDA,SGEFFC,EPEFFC)*(D11*C1+D12*C2)/(B2M*DET)
      XPLUS=B2M*DET*(RHS+(C1*B2P-C2*B1P)/BPMOD)
      XMINUS=B2M*DET*(RHS+(C1*B2M-C2*B1M)/BMMOD)
      A1=C2
      A2=-C1
      ICORN=3
      GO TO 90
   74 RHS=DK(EMU2,SGEFFT,EPEFFT)*(D11*C1+D12*C2)/(B2P*DET)
      XPLUS=B2P*DET*(RHS+(C1*B2P-C2*B1P)/BPMOD)
      XMINUS=B2P*DET*(RHS+(C1*B2M-C2*B1M)/BMMOD)
      A1=C2
      A2=-C1
      ICORN=1
      GO TO 90
   80 IF(SS1) 82,82,84
   82 RHS=DG(ELAMDA,SGEFFC,EPEFFC)*(D21*C1+D22*C2)/(B1M*DET)
      XPLUS=B1M*DET*(RHS+(C2*B1P-C1*B2P)/BPMOD)
      XMINUS=B1M*DET*(RHS+(C2*B1M-C1*B2M)/BMMOD)
      A1=-C2
      A2=C1
      ICORN=2
      GO TO 90
   84 RHS=DK(EMU1,SGEFFT,EPEFFT)*(D21*C1+D22*C2)/(B1P*DET)
      XPLUS=B1P*DET*(RHS+(C2*B1P-C1*B2P)/BPMOD)
      XMINUS=B1P*DET*(RHS+(C2*B1M-C1*B2M)/BMMOD)
      A1=-C2
      A2=C1
      ICORN=4
   90 CONTINUE
      IF(XPLUS*XMINUS)  94,94,91
C
C   THIS BRANCH IS FOLLOWED WHEN THE NUMERATORS ARE OF THE
C   SAME SIGN. NOTE THAT BETA IS DIFFERENT FROM BETA1 OR BETA2
C
   91 IF(XPLUS) 92,92,93
   92 BETA=1.
      GO TO 290
   93 BETA=0.
  290 CONTINUE
C
      CALL CEE(SS1,SS2,SYC,SYT1,SYT2,B1P,B2P,
     1  EX,EY,U,ELAMDA,EMU1,EMU2,SGEFFC,EPEFFC,SGEFFT,EPEFFT,
     2  C11P,C12P,C21P,C22P,DENOMP,AP,BET1P,BET2P,DGG,DK1,DK2)
      CALL CEE(SS1,SS2,SYC,SYT1,SYT2,B1M,B2M,
     1  EX,EY,U,ELAMDA,EMU1,EMU2,SGEFFC,EPEFFC,SGEFFT,EPEFFT,
     2  C11M,C12M,C21M,C22M,DENOMM,AM,BET1M,BET2M,DGG,DK1,DK2)
C
      C11=BETA*C11M+(1.-BETA)*C11P
      C12=BETA*C12M+(1.-BETA)*C12P
      C21=BETA*C21M+(1.-BETA)*C21P
      C22=BETA*C22M+(1.-BETA)*C22P
      IF(ICON.NE.0)  RETURN
C
```

```
      B1=BETA*B1M+(1.-BETA)*B1P
      B2=BETA*B2M+(1.-BETA)*B2P
      BBMOD=SQRT(B1*B1+B2*B2)
      XN1=B1/BBMOD
      XN2=B2/BBMOD
      DIC11P=D11*(1.-C11P)-D12*C21P
      DIC12P=-D11*C12P+D12*(1.-C22P)
      DIC21P=D21*(1.-C11P)-D22*C21P
      DIC22P=-D21*C12P+D22*(1.-C22P)
      DIC11M=D11*(1.-C11M)-D12*C21M
      DIC12M=-D11*C12M+D12*(1.-C22M)
      DIC21M=D21*(1.-C11M)-D22*C21M
      DIC22M=-D21*C12M+D22*(1.-C22M)
      DS1=(DIC11M*C1+DIC12M*C2)*BETA
     1  +(DIC11P*C1+DIC12P*C2)*(1.-BETA)
      DS2=(DIC21M*C1+DIC22M*C2)*BETA
     1  +(DIC21P*C1+DIC22P*C2)*(1.-BETA)
      ALFA=BETA*AM+(1.-BETA)*AP
      BETA1=BETA*BET1M+(1.-BETA)*BET1P
      BETA2=BETA*BET2M+(1.-BETA)*BET2P
      DCPM=BETA*DCM+(1.-BETA)*DCP
      DT1PM=BETA*DT1M+(1.-BETA)*DT1P
      DT2PM=BETA*DT2M+(1.-BETA)*DT2P
      DENOM1=BETA*DENOMM+(1.-BETA)*DENOMP
      DEBAR=((D11*C1+D12*C2)*B1+(D21*C1+D22*C2)*B2)*BBMOD/DENOM1
      DEL=ALFA*DEBAR
      DEM1=BETA1*DEBAR
      DEM2=BETA2*DEBAR
      DEP1=DEBAR*B1/BBMOD
      DEP2=DEBAR*B2/BBMOD
      RETURN
C
C   THIS BRANCH IS FOLLOWED WHEN THE NUMERATORS ARE OF OPPOSITE
C   SIGN. NEED TO FIND AN INTERMEDIATE NORMAL BY SOLVING
C   A QUADRATIC EQUATION
C
   94 DISCR=A1*A1+A2*A2-RHS*RHS
      IF(DISCR) 999,95,95
  999 WRITE(6,9876)
 9876 FORMAT(1H0,'IN CORNER, DISCR.LT.0. AND CANNOT BE SQUARE-ROOTED')
      STOP
   95 R1N2=(A2*RHS+ABS(A1)*SQRT(DISCR))/(A1*A1+A2*A2)
      R2N2=(A2*RHS-ABS(A1)*SQRT(DISCR))/(A1*A1+A2*A2)
      IF(ABS(A1).EQ.0.) A1=1.0E-30
      R1N1=(RHS-A2*R1N2)/A1
      R2N1=(RHS-A2*R2N2)/A1
      XNP1=B1P/BPMOD
      XNP2=B2P/BPMOD
      XNM1=B1M/BMMOD
      XNM2=B2M/BMMOD
      XN1B=XNP1
      XN1S=XNM1
      IF(XN1B.GT.XN1S) GO TO 105
      XN1B=XNM1
      XN1S=XNP1
```

```
      105 XN2B=XNP2
          XN2S=XNM2
          IF(XN2B.GT.XN2S) GO TO 110
          XN2B=XNM2
          XN2S=XNP2
      110 IF(R1N1.GE.XN1S.AND.R1N1.LE.XN1B.AND.
         1   R1N2.GE.XN2S.AND.R1N2.LE.XN2B) GO TO 120
          IF(R2N1.LT.XN1S.OR.R2N1.GT.XN1B.OR.
         1   R2N2.LT.XN2S.OR.R2N2.GT.XN2B)  STOP 999
          XN1=R2N1
          XN2=R2N2
          GO TO 125
      120 XN1=R1N1
          XN2=R1N2
      125 GO TO (131,132,133,134) , ICORN
      131 DEL=0.
          DGK=DK(EMU2,SGEFFT,EPEFFT)
          DEM2=B2P*(D21*C1+D22*C2)/(B2P*(D21*XN1+D22*XN2)+DGK)
          DEP1=DEM2*XN1
          DEP2=DEM2*XN2
          DEBAR=DEM2
          BETA2=1.0
          DS1=0.
          DS2=D21*(C1-DEP1)+D22*(C2-DEP2)
          B1=B1P
          B2=B2P
          GO TO 160
      C
      132 DEM1=0.
          DEM2=0.
          DGK=DG(ELAMDA,SGEFFC,EPEFFC)
          DEL=B1M*(D11*C1+D12*C2)/(B1M*(D11*XN1+D12*XN2)+DGK)
          DEP1=DEL*XN1
          DEP2=DEL*XN2
          DEBAR=DEL
          ALFA=1.0
          DS1=D11*(C1-DEP1)+D12*(C2-DEP2)
          DS2=0.
          B1=B1M
          B2=B2M
          GO TO 160
      C
      133 DEM1=0.
          DEM2=0.
          DGK=DG(ELAMDA,SGEFFC,EPEFFC)
          DEL=B2M*(D21*C1+D22*C2)/(B2M*(D21*XN1+D22*XN2)+DGK)
          DEP1=DEL*XN1
          DEP2=DEL*XN2
          DEBAR=DEL
          ALFA=1.0
          DS1=0.
          DS2=D21*(C1-DEP1)+D22*(C2-DEP2)
          B1=B1M
          B2=B2M
          GO TO 160
```

```
      C
  134 DEL=0.
      DGK=DK(EMU1,SGEFFT,EPEFFT)
      DEM1=B1P*(D11*C1+D12*C2)/(B1P*(D11*XN1+D12*XN2)+DGK)
      DEP1=DEM1*XN1
      DEP2=DEM1*XN2
      DEBAR=DEM1
      BETA1=1.0
      DS1=D11*(C1-DEP1)+D12*(C2-DEP2)
      DS2=0.
      B1=B1P
      B2=B2P
  160 DENOM=XN1*(B1*D11+B2*D21)+XN2*(B1*D12+B2*D22)+DGK
      YX1=B1*D11+B2*D21
      YX2=B1*D12+B2*D22
      C11=XN1*YX1/DENOM
      C12=XN1*YX2/DENOM
      C21=XN2*YX1/DENOM
      C22=XN2*YX2/DENOM
      RETURN
      END
```

```
C
C  ********************************************************
      SUBROUTINE DELTAS(SIG1Y,SIG2Y,SYC,SYT1,SYT2,B1,B2,C1,C2,
     1      DS1,DS2,EX,EY,U,ELAMDA,EMU1,EMU2,SGEFFC,EPEFFC,
     2      SGEFFT,EPEFFT,DEBAR,DEL,DEM1,DEM2,DEP1,DEP2,
     3      DIC21,DIC22,DIC11,DIC12,Q,C11,C12,C21,C22,
     4     ICON,ALFA,BETA1,BETA2,DGG,DK1,DK2)
C  ********************************************************
C   CALCULATES VECTOR DELTA SIGMA
C   ALSO DELTA OF EBARP,LAMBDA AND MU1  MU2
C   ALSO DELTA OF EPNEW1 AND EPNEW2
C   IF ICON>0 IT RETUTRNS THE MATRIX-C
      DIMENSION SGEFFC(1), EPEFFC(1),SGEFFT(1),EPEFFT(1)
      COMMON/IDTY/ISGT,IMPT,ILY,INPT
      DATA CST/1.0E-6/
      Q=0.
      DS1=0.
      DS2=0.
      DEBAR=0.
      DEP1=0.
      DEP2=0.
      DEL=0.
      DEM1=0.
      DEM2=0.
      SYCC=SYC
      SYTT1=SYT1
      SYTT2=SYT2
      IF(SIG1Y.GE.-0.01.AND.SIG2Y.GE.-0.01) GO TO 10
      IF(ABS(SIG2Y).LT.0.01.AND.ABS(SIG1Y+SYC).LT.0.01)
     1   GO TO 150
      IF(ABS(SIG1Y).LT.0.01.AND.ABS(SIG2Y+SYC).LT.0.01)
     1   GO TO 150
C
C     THIS BRANCH COMPUTES DELTAS WHEN THE INITIAL POINT
C     IS NOT AT A CORNER
C
   10 CALL CEE(SIG1Y,SIG2Y,SYC,SYT1,SYT2,B1,B2,
     1  EX,EY,U,ELAMDA,EMU1,EMU2,SGEFFC,EPEFFC,SGEFFT,EPEFFT,
     2  C11,C12,C21,C22,DENOM,ALFA,BETA1,BETA2,DGG,DK1,DK2)
      IF(ICON.NE.0) RETURN
C
C   GET MATRIX D
      D11=EX
      D12=U*EX
      D21=U*EY
      D22=EY
      BMOD=SQRT(B1*B1+B2*B2)
C   GET MATRIX D*(I-C)
      DIC11=D11*(1.-C11)-D12*C21
      DIC12=-D11*C12+D12*(1.-C22)
      DIC21=D21*(1.-C11)-D22*C21
      DIC22=-D21*C12+D22*(1.-C22)
C   GET VECTOR DS
      DS1=DIC11*C1+DIC12*C2
      DS2=DIC21*C1+DIC22*C2
```

```
      FRACT1=1.0
      FRACT2=1.0
      IF(SIG1Y*(SIG1Y+DS1).GE.0.)  GO TO 100
      C=SIGN(0.001,SIG1Y)
      FRACT1=-((SIG1Y+C)/DS1)
  100 IF(SIG2Y*(SIG2Y+DS2).GE.0.)   GO TO 110
      C=SIGN(0.001,SIG2Y)
      FRACT2=-((SIG2Y+C)/DS2)
  110 FACTOR=FRACT1
      IF(FRACT1.GT.FRACT2) FACTOR=FRACT2
      DEBAR=((D11*C1+D12*C2)*B1+(D21*C1+D22*C2)*B2)
     1          *BMOD/DENOM
      IF(DEBAR.GE.0.) GO TO 115
      WRITE(6,1000)DEBAR,ISGT,IMPT,ILY,INPT
 1000 FORMAT(//3X,'DEBAR IS NEGATIVE IN SUBROUTINE DELTAS=',E14.6,4I5)
      STOP
  115 XN1=B1/BMOD
      XN2=B2/BMOD
      DEL=ALFA*DEBAR
      DEM1=BETA1*DEBAR
      DEM2=BETA2*DEBAR
      DEP1=DEBAR*XN1
      DEP2=DEBAR*XN2
      CALL SEARCH(SGEFFC,EPEFFC,SGEFFT,EPEFFT,ELAMDA,EMU1,
     1  EMU2,DEL,DEM1,DEM2,QT,IDEN)
      Q=AMIN1(FACTOR,QT,1.0)
      IF(Q.EQ.1.0) RETURN
      IF(QT.GT.FACTOR) RETURN
      GO TO 225
C
C     THIS BRANCH COMPUTES DELTAS WHEN THE INITIAL POINT IS A CORNER
C
  150 CONTINUE
      CALL CORNER(SIG1Y,SIG2Y,DEBAR,DEL,DEM1,DEM2,EX,EY,U,ELAMDA,EMU1,
     1  EMU2,SGEFFC,EPEFFC,SGEFFT,EPEFFT,DS1,DS2,C1,C2,SYCC,SYTT1,
     2  SYTT2,DEP1,DEP2,DIC21,DIC22,DIC11,DIC12,
     3  C11,C12,C21,C22,ICON,ALFA,BETA1,BETA2,DGG,DK1,DK2,B1,B2)
      IF(ICON.NE.0) RETURN
      CALL SEARCH(SGEFFC,EPEFFC,SGEFFT,EPEFFT,ELAMDA,EMU1,
     1  EMU2,DEL,DEM1,DEM2,QT,IDEN)
      Q=AMIN1(QT,1.0)
      IF(Q.EQ.1.0) RETURN
C
  225 GO TO (240,245,260,270),IDEN
  240 RETURN
  245 ELAMDA=ELAMDA+CST
      RETURN
  260 EMU1=EMU1+CST
      RETURN
  270 EMU2=EMU2+CST
      RETURN
      END
```

```
C
C
C  ************************************************************
      SUBROUTINE DFDCT(S1,S2,SYC,SYT1,SYT2,DC,DT1,DT2)
C  ************************************************************
C  THIS SUBROUTINE COMPUTES DF/DSYC DF/DSYT1 DF/DSYT2
C  DC DT1 DT2 ARE RETURNED TO FORM C MATRIX
C
C
      IF(S1) 10,30,30
   10 IF(S2) 70,70,80
   30 IF(S2) 40,60,60
C
C     ***** TT FOLLOWS *****
   60 DC=0.
      X1=S1/SYT1
      X2=S2/SYT2
      X98=0.0098*X1*X2
      X10=0.0001*X1*X2
      A=1.+X98-0.99*X1
      B=1.+X98-0.99*X2
      D=1.-X10
      Q=SQRT(SYT1*SYT2)
      QP1=0.5*SYT1/Q
      QP2=0.5*SYT2/Q
      ABD=A*B*D
      BDQ=B*D*Q
      ADQ=A*D*Q
      ABQ=-2.*A*B*Q*X10
      DT1=0.01*QP1-(SYT1*ABD*QP1+(1.-A)*BDQ-X98*ADQ+ABQ)/
     1  (SYT1*D**3)
      DT2=0.01*QP2-(SYT2*ABD*QP2-X98*BDQ+(1.-B)*ADQ+ABQ)/
     1  (SYT2*D**3)
      RETURN
C
C     ***** CC FOLLOWS *****
   70 DT1=0.
      DT2=0.
      X1=S1/SYC
      X2=S2/SYC
      IF(S2.EQ.0.) GO TO 71
      R=S1/S2
      IF(R.LT.0.63095074) GO TO 73
      IF(R.GT.1.58490979) GO TO 71
      DC=-1.
      RETURN
   71 DC=-1.-1.46150732*X2*X2-1.2628614*X2**3
      RETURN
   73 DC=-1.-1.46150732*X1*X1-1.2628614*X1**3
      RETURN
C
C     ***** TC FOLLOWS ***** 2ND QUAD. *****
   80 X1=S1/SYC
      X2=S2/SYT2
      Y2=SYT2/SYC
```

```
      DT1=0.
      IF(X2.LT.-2.0*X1) GOTO 8
      DC=-0.8*Y2*X1**2
      DT2=-1.0+0.4*X1**2
      RETURN
8     DC=-Y2*(2.4+5.6*X1)*X1
      DT2=(2.8*X1+2.4)*X1-0.4
      RETURN
C
C     ***** TC FOLLOWS ***** 4TH QUAD. *****
40    X2=S2/SYC
      X1=S1/SYT1
      Y1=SYT1/SYC
      DT2=0.
      IF(X1.LT.-2.0*X2) GOTO 7
      DC=-0.8*Y1*X2**2
      DT1=-1.0+0.4*X2**2
      RETURN
7     DC=-Y1*(2.4+5.6*X2)*X2
      DT1=(2.8*X2+2.4)*X2-0.4
      RETURN
      END
```

```
      C
      C
      C  ***********************************************
            SUBROUTINE DFDS(SIG1,SIG2,SYC,SYT1,SYT2,B1,B2)
      C  ***********************************************
      C   THIS FUNCTION PROVIDES DFY/DSIG1, AND DFY/DSIG2.
      C
            IF((SIG1*SIG1+SIG2*SIG2).EQ.0.0)  GO TO 999
            IF(SIG1) 10,30,30
         10 IF(SIG2) 70,70,80
         30 IF(SIG2) 40,60,60
      C
      C     ***** TT FOLLOWS **********************************
         60 X1=SIG1/SYT1
            X2=SIG2/SYT2
            X98=0.0098*X1*X2
            A=1.-0.99*X1+X98
            B=1.-0.99*X2+X98
            D=1.-0.0001*X1*X2
            Q=SQRT(SYT1*SYT2)
            B1=-Q*(B*D*(-0.99+0.0098*X2)+A*D*0.0098*X2+0.0002*A*B*X2)/
           1  (SYT1*D**3)
            B2=-Q*(B*D*0.0098*X1+A*D*(-0.99+0.0098*X1)+0.0002*A*B*X1)/
           1  (SYT2*D**3)
            RETURN
      C
      C     ***** TC FOLLOWS ***** 4TH QUAD. ***************
         40 X2=SIG2/SYC
            X1=SIG1/SYT1
            Y1=SYT1/SYC
            B1=1.
            IF(X1.LT.-2.0*X2) GOTO 6
            B2=Y1*0.8*X2
            RETURN
      6     B2=Y1*(2.4+5.6*X2)
            RETURN
      C
      C     ***** CC FOLLOWS **********************************
         70 X1=SIG1/SYC
            X2=SIG2/SYC
            IF(ABS(SIG2).LT.1.0E-10) GO TO 71
            R=SIG1/SIG2
            IF(R.LT.0.63095075) GO TO 73
            IF(R.GT.1.58490979) GO TO 71
            DENOM=SQRT(X1*X1+X2*X2-1.23*X1*X2)
            B1=(X1-0.615*X2)/DENOM
            B2=(X2-0.615*X1)/DENOM
            RETURN
         71 B1=-1.
            B2=1.1+2.92301464*X2+1.8942921*X2*X2
            RETURN
         73 B1=1.1+2.92301464*X1+1.8942921*X1*X1
            B2=-1.
            RETURN
      C
```

```
C     ***** TC FOLLOWS ***** 2ND QUAD. ***************
   80 X1=SIG1/SYC
      X2=SIG2/SYT2
      Y2=SYT2/SYC
      B2=1.
      IF(X2.LT.-2.0*X1) GOTO 8
      B1=Y2*0.8*X1
      RETURN
8     B1=Y2*(2.4+5.6*X1)
      RETURN
  999 WRITE(6,1000)
 1000 FORMAT(1H0,'DFYDS WAS CALLED WITH ZERO STRESS VECTOR')
      STOP
      END
```

```
      C
      C
      C  ************************************************
            FUNCTION DG(ELAMDA,SGEFFC,EPEFFC)
      C  ************************************************
            DIMENSION SGEFFC(1),EPEFFC(1)
            COMMON/IDTY/ISGT,IMPT,ILY,INPT
      C    FINDS DSIGMA/DEBARP IN UNIAXIAL COMPRESSION TEST
            E1P=0.67267279*ELAMDA
            IF(E1P.LE.0.)    E1P=1.0 E-21
            E1P=E1P*1.0001
            E=SGEFFC(2)/EPEFFC(2)
            DO 10  I=2,10
            J=I
            IF(E1P.LT.(EPEFFC(I)-SGEFFC(I)/E)) GO TO 50
         10 CONTINUE
            WRITE(6,1000)ELAMDA,ISGT,IMPT,ILY,INPT
       1000 FORMAT(1H0,'IN FUNCTION DG, LAMBDA=',E20.7,
           1        'EXCEEDS RANGE',4I5)
            STOP
         50 ET=(SGEFFC(J)-SGEFFC(J-1))/(EPEFFC(J)-EPEFFC(J-1))
            IF(ET.EQ.0.)    ET=1.0E-06
            DG=0.67267279*ET*E/(E-ET)
            RETURN
            END
```

```
C
C  ****************************************************
      FUNCTION DK(EMU,SGEFFT,EPEFFT)
C  ****************************************************
      DIMENSION SGEFFT(1),EPEFFT(1)
      COMMON/IDTY/ISGT,IMPT,ILY,INPT
C   FINDS DSIGMA/DEBARP IN UNIAXIAL TENSILE TEST
      E1P=EMU
      IF(E1P.LE.0.)    E1P=1.0 E-21
      E1P=E1P*1.0001
      E=SGEFFT(2)/EPEFFT(2)
      DO 10  I=2,10
      J=I
      IF(E1P.LT.(EPEFFT(I)-SGEFFT(I)/E)) GO TO 50
   10 CONTINUE
      WRITE(6,1000) EMU,ISGT,IMPT,ILY,INPT
 1000 FORMAT(1H0,'IN FUNCTION DK, MU=',E20.7,
     1           'EXCEEDS RANGE',4I5)
      STOP
   50 ET=(SGEFFT(J)-SGEFFT(J-1))/(EPEFFT(J)-EPEFFT(J-1))
      IF(ET.EQ.0.)  ET=1.0E-06
      DK=ET*E/(E-ET)
      RETURN
      END
```

```
      C
      C  ************************************************
            SUBROUTINE DRIFT(SIG1Y,SIG2Y,SYC,SYT1,SYT2,DF)
      C  ************************************************
      C
      C THIS SUBROUTINE ATTEMPTS TO CORRECT FOR DRIFT FROM THE YIELD
      C SURFACE BY LOCATING A POINT ON AN APPROXIMATE YIELD LINE
      C AND THEN ITERATING TO THE CURVE(OR UNTIL FY.LT.0.01)
      C
            COMMON/IDTY/ISGT,IMPT,ILY,INPT
            IZ=IZONE(SIG1Y,SIG2Y,SYC,SYT1,SYT2)
            KOUNT=0
      5     KOUNT=KOUNT+1
            GO TO (10,20,20,40,40,40,70,70),IZ
      C
      C **  TT REGION ***
      10    X1=SIG1Y/SYT1
            X2=SIG2Y/SYT2
            IF(X1.GT.X2)  GO TO 15
            S2=SYT2
            S1=SYT2*SIG1Y/SIG2Y
            GO TO 100
      15    S1=SYT1
            S2=SYT1*SIG2Y/SIG1Y
            GO TO 100
      C
      C**  CT REGION ***
      20    X1=SIG1Y/SYC
            X2=SIG2Y/SYT2
            IF(IZ.EQ.3) GO TO 25
      C
      C  ZONE 2
            RS=10./(10.*X2-X1)
            GOTO 90
      C
      C  ZONE 3
      25    RX=X2/X1
            IF(RX.GE.-0.6875) GOTO 30
            RS=3.5/(2.*X2-3.*X1)
            GO TO 90
      C
      30    RS=2.75/(X2-2.75*X1)
            GO TO 90
      C
      C  ***  CC REGION ***
      40    X1=SIG1Y/SYC
            X2=SIG2Y/SYC
            IF(X1.GT.X2)  GO TO 50
      C
            RX=X2/X1
            IF(RX.GT.0.631)  GO TO 48
      C
      C  ZONE 4
            IF(RX.LT.0.246)  GO TO 45
            S1=-1.2672*SYC
```

```
      S2=SIG2Y*S1/SIG1Y
      GO TO 100
C
45    RS=7./(6.*X2-7.*X1)
      GO TO 90
C
C  ZONE 5
48    RS=-4.15603/(X2+2.64692*X1)
      GO TO 90
C
50    RX=X1/X2
      IF(RX.GT.0.631)  GO TO 58
C
C  ZONE 6
      IF(RX.LT.0.246)  GO TO 55
      S2=-1.2672*SYC
      S1=SIG1Y*S2/SIG2Y
      GO TO 100
C
55    RS=7./(6.*X1-7.*X2)
      GO TO 90
C
C  ZONE 5 (AGAIN)
58    RS=-4.15603/(X1+2.64692*X2)
      GO TO 90
C
C  ***  TC REGION ***
70    X1=SIG1Y/SYT1
      X2=SIG2Y/SYC
      IF (IZ.EQ.7)  GO TO 75
C
C  ZONE 8
      RS=10./(10.*X1-X2)
      GOTO 90
C
C  ZONE 7
75    RX=X1/X2
      IF(RX.GE.-0.6875) GOTO 80
      RS=3.5/(2.*X1-3.*X2)
      GO TO 90
80    RS=2.75/(X1-2.75*X2)
C
90    S1=RS*SIG1Y
      S2=RS*SIG2Y
C
C
100   S10=0.95*S1
      S20=0.95*S2
      FO=FY(S10,S20,SYC,SYT1,SYT2,IZ)
C
      DO 150 I=1,100
      F=FY(S1,S2,SYC,SYT1,SYT2,IZ)
      IF(ABS(F).LT.0.009) GOTO 200
      DELTAF=F-FO
      IF(ABS(DELTAF).LT.1.0E-10) GO TO 998
```

```
      S1=S10-FO*(S1-S10)/DELTAF
      S2=S20-FO*(S2-S20)/DELTAF
150   CONTINUE
C
      WRITE(6,1000)ISGT,IMPT,ILT,INPT
1000  FORMAT(//'  **  FAILURE TO CONVERGE IN SUBROUTINE DRIFT',4I5)
C
200   DF=SQRT((S1**2+S2**2)/(SIG1Y**2+SIG2Y**2))
      IT=IZONE(S1,S2,SYC,SYT1,SYT2)
      IF(IT.EQ.IZ) RETURN
      IF(KOUNT.GE.2)  GO TO 999
      IZ=IT
      GO TO 5
C
C
998   WRITE(6,1100)ISGT,IMPT,ILY,INPT
1100  FORMAT(//'    ** ZERO DIVISOR',4I5)
      STOP
C
C
999   WRITE(6,1200) IZ,IT
1200  FORMAT(//' **  ALTERNATING ZONE IN DRIFT  STARTING POINT AT ZONE',
     1         I4,'  CONVERGED POINT AT ZONE',I4)
      STOP
      END
```

```
C ***************************************************************
      FUNCTION FFMU(SIG10,SIG20,SIG1,SIG2,SYC,SYT1,SYT2,DOT)
C ***************************************************************
C  THIS SUBROUTINE FINDS THE FACTOR FMU REQUIRED TO BRING THE
C  INITIAL STATE OF STRESS UP TO A POINT ON THE YIELD LINE, IN
C  A PRESCRIBED DIRECTION. THE POINT IS GENERALLY FOUND BY
C  THE METHOD OF BISECTION FOR ITERATING FOR ROOTS
C
      DIMENSION KNI(6),KINT(6)
      COMMON/IDTY/ISGT,IMPT,ILY,INPT
C  INITIALIZATION
      IZ=IZONE(SIG10,SIG20,SYC,SYT1,SYT2)
      JZ=IZONE(SIG1,SIG2,SYC,SYT1,SYT2)
      CALL BOXYS(YS1,YS2,SIG1,SIG2,SIG10,SIG20,SYC,SYT1,SYT2,JZ)
      JYZ=JZ
      JTZ=JZ
      S1=YS1
      S2=YS2
      S10=SIG10
      S20=SIG20
      F0=FY(SIG10,SIG20,SYC,SYT1,SYT2,IZ)
      F1=FY(YS1,YS2,SYC,SYT1,SYT2,JZ)
C
C  REMOVE ALL 'LOADING'  CASES
      IF(DOT.GE.0.0) GO TO 300
C
C ***************************************************************
C  FOR THE FOLLOWING ,  DOT<0
      FFMU=1.0
      IF(F1.GT.0.01) GO TO 50
      RETURN
C
C  FOR DOT<0 AND F1>0.01 WORK BACKWARDS FROM (SIG1,SIG2) TO FIND A ROOT
C
50    K0=0
60    K0=K0+1
      ILL=2
C  INITIALIZE SAVE VALUES IN CASE  F DOESN'T CHANGE SIGN
      FSAVE=F1
      S1SAVE=YS1
      S2SAVE=YS2
80    DS1=(S1-S10)*0.05
      DS2=(S2-S20)*0.05
      ISS=19
      KK0=(K0+1)/2
      GO TO (81,82,82,84,84,87,87),JYZ
81    DYSCT=0.1*AMIN1(SYT1,SYT2)
      GOTO 89
82    DYSCT=0.1*SYT2
      GOTO 89
84    DYSCT=0.1*SYC
      GOTO 89
87    DYSCT=0.1*SYT1
C
89    DSC=DYSCT/(FLOAT(KK0)**4)
```

```
      IF(DSC.GT.ABS(DS1).AND.DSC.GT.ABS(DS2)) GOTO 90
      ISS=ABS(S1-S10)/DSC + 1
      IF(ABS(S1-S10).LT.ABS(S2-S20)) ISS=ABS(S2-S20)/DSC + 1
      IF(ISS.GT.600) ISS=600
      DS1=(S1-S10)/FLOAT(ISS)
      DS2=(S2-S20)/FLOAT(ISS)
      ISS=ISS-1
C
90    DO 200 I=1,ISS
      S10=S1-FLOAT(I)*DS1
      S20=S2-FLOAT(I)*DS2
      F0=FY(S10,S20,SYC,SYT1,SYT2,JTZ)
      IF(F0.GT.FSAVE) GO TO 180
      FSAVE=F0
      S1SAVE=S10
      S2SAVE=S20
180   K=I
      IF(F1*F0.LT.0.0) GO TO 220
200   CONTINUE
C
C  SINCE A CHANGE IN SIGN HAS NOT OCCURED,SUBDIVIDE THE LAST SECT.
      S1=S10
      S2=S20
      S10=SIG10
      S20=SIG20
      F1=F0
      ILL=ILL+1
      IF(ILL.LT.3)  GO TO 80
C
C  IF THIS POINT IS REACHED IT MUST BE ASSUMED THAT THE STRESS
C  PATH DOES NOT INTERSECT THE YIELD LINE.USE THE MINIMUM POINT
C  WHICH HAS BEEN SAVED  TO ESTABLISH FMU.
      ITZ=IZONE(S1SAVE,S2SAVE,SYC,SYT1,SYT2)
      KNI(K0)=ITZ
      IF(ITZ.EQ.JTZ)  GO TO 210
C  IF ZONES ARE INCOMPATIBLE USE THE NEW ZONE AND REPEAT.
      IF(K0.GE.6)  GO TO 997
      GO TO 230
C
C COMPUTATION OF FMU ON BASIS OF MINIMUM VALUE ON STRESS PATH
210   TS1=S1SAVE
      TS2=S2SAVE
214   K1=0
215   K1=K1+1
      CALL DFDS(TS1,TS2,SYC,SYT1,SYT2,B1,B2)
      DOT=DS1*B1+DS2*B2
      IF(DOT.GT.0.0) GOTO 900
      IF(K1.GE.21) GOTO 996
      TS1=TS1+DS1
      TS2=TS2+DS2
      GOTO 215
C
C  CHECK COMPATIBILITY OF ZONES PRIOR TO GOING FOR ITERATION
C  WHEN F CHANGES SIGNS AND DOT<0
220   ITZ=IZONE(S10,S20,SYC,SYT1,SYT2)
```

```
      KINT(K0)=ITZ
      IF(ITZ.EQ.JTZ) GO TO 590
      IF(K0.GE.6) GO TO 998
C
C  IF ZONES ARE INCOMPATIBLE INITIALIZE FOR  ANOTHER TRY
230   JTZ=ITZ
      S10=SIG10
      S20=SIG20
      S1=YS1
      S2=YS2
      IM=0
      F1=FY(YS1,YS2,SYC,SYT1,SYT2,IM)
      GO TO 60
C
C ***************************************************************
C
C  THE FOLLOWING APPLIES WHEN DOT>0
C
300   FFMU=0.0
      IF(F0.GT.-0.01)  RETURN
      IF(F1*F0.LT.0.0)  GO TO 600
C
C  YOU SHOULD NEVER GET HERE
      WRITE(6,1003)
1003  FORMAT('  **FMU CRITERIA BYPASSED')
      RETURN
C
C  PREPARE FOR ITERATION WHEN DOT<0
  590 S1=S1-FLOAT(K-1)*DS1
      S2=S2-FLOAT(K-1)*DS2
C
C ***************************************************************
C  ITERATION STARTS HERE FOR  DOT<0 AND DOT>0
C
C  THE METHOD OF BISECTION IS USED IN THIS ITERATION
C
600   DD1=S1-S10
      DD2=S2-S20
      DO 700 I=1,80
      TS1=S10+0.5*DD1
      TS2=S20+0.5*DD2
      IM=0
      TF=FY(TS1,TS2,SYC,SYT1,SYT2,IM)
      IF(TF.GT.0.01) GOTO 610
      S10=TS1
      S20=TS2
      F0=TF
610   DD1=0.5*DD1
      DD2=0.5*DD2
      IF(ABS(F0).LE.0.01) GOTO 900
700   CONTINUE
      WRITE(6,1200)ISGT,IMPT,ILY,INPT
1200  FORMAT(' ** FAILURE TO CONVERGE IN FFMU',4I5)
      STOP
C
```

```
C  COMPUTE FFMU
900    FFMU=SQRT(((TS1-SIG10)**2+(TS2-SIG20)**2)/
      *   ((SIG1-SIG10)**2+(SIG2-SIG20)**2))
       RETURN
C
C  SOME OF THE ERROR EXITS
C
996    WRITE(6,1500)
1500   FORMAT('**  CANNOT FIND POINT FOR WHICH DOT>0')
       STOP
997    WRITE(6,1400)(KNI(J),J=1,6)
1400   FORMAT(' **  ALTERNATING ZONES IN FFMU FOR DOT<0',/,
      1 ' AND THE STRESS PATH DOES NOT INTERSECT YIELD SURFACE',/,
      2 5X,'KNI=',6I5)
       STOP
998    WRITE(6,1600)(KINT(J),J=1,6)
1600   FORMAT(' **  ALTERNATING ZONES IN FFMU FOR DOT<0',/,
      1 5X,'KINT=',6I5)
       STOP
C
999    WRITE(6,1002)ISGT,IMPT,ILY,INPT
1002   FORMAT(' ** ZERO DIVISOR (F1-F0) IN FFMU',4I5)
       STOP
       END
```

```
C
C  ****************************************************
      FUNCTION FG(ELAMDA,SGEFFC,EPEFFC)
C  ****************************************************
C   SIGMA VS EBARP IN UNIAXIAL COMPRESSION
      DIMENSION SGEFFC(1),EPEFFC(1)
      COMMON/IDTY/ISGT,IMPT,ILY,INPT
      E1P=0.67267279*ELAMDA
      IF(E1P.LE.0.) E1P=1.0 E-21
      E=SGEFFC(2)/EPEFFC(2)
      DO 10 I=2,10
      J=I
      IF(E1P.LT.EPEFFC(I)-SGEFFC(I)/E) GO TO 50
   10 CONTINUE
      WRITE(6,1000) ELAMDA,ISGT,IMPT,ILY,INPT
 1000 FORMAT(1H ,'IN FUNCTION FG, LAMBDA=',E20.7,
     1       'EXCEEDS RANGF',4I5)
      STOP
   50 ET=(SGEFFC(J)-SGEFFC(J-1))/(EPEFFC(J)-EPEFFC(J-1))
      IF(ET.EQ.0.)  ET=1.0E-06
      EPSPJ1=EPEFFC(J-1)-SGEFFC(J-1)/E
      FG=SGEFFC(J-1)+ET*(E1P-EPSPJ1)*E/(E-ET)
      RETURN
      END
```

```
C
C  ******************************************************
      FUNCTION FK(EMU,SGEFFT,EPEFFT)
C  ******************************************************
C   SIGMA VS EBARP IN UNIAXIAL TENSION
      DIMENSION SGEFFT(1),EPEFFT(1)
      COMMON/IDTY/ISGT,IMPT,ILY,INPT
      E1P=EMU
      IF(E1P.LE.0.)  E1P=1.0 E-21
      E=SGEFFT(2)/EPEFFT(2)
      DO 10 I=2,10
      J=I
      IF(E1P.LT.EPEFFT(I)-SGEFFT(I)/E) GO TO 50
   10 CONTINUE
      WRITE(6,1000) EMU,ISGT,IMPT,ILY,INPT
 1000 FORMAT(1H ,'IN FUNCTION FK, MU=',E20.7,
     1      'EXCEEDS RANGE',4I5)
      STOP
   50 ET=(SGEFFT(J)-SGEFFT(J-1))/(EPEFFT(J)-EPEFFT(J-1))
      IF(ET.EQ.0.)  ET=1.0E-06
      EPSPJ1=EPEFFT(J-1)-SGEFFT(J-1)/E
      FK=SGEFFT(J-1)+ET*(E1P-EPSPJ1)*E/(E-ET)
      RETURN
      END
```

```
C*************************************************************
C     SUBROUTINE FLOW3        ********************************
C*************************************************************
      SUBROUTINE FLOW3(I,J,K,KK,EPS1,EPS2,EPS1S,EPS2S,
     1 EPNEW1,EPNEW2,E1SEL,E2SEL,E1ELAS,E2ELAS,SIG1,SIG2,
     2 SIG10,SIG20,SIG1Y,SIG2Y,XNU,EX,EY,E,SGEFFC,EPEFFC,
     3 SGEFFT,EPEFFT,C11,C12,C21,C22,EP1,EP2,Z
     4  ,SYC,SYT1,SYT2,ELAMDA,EMU1,EMU2)
      DIMENSION SGEFFC(1),EPEFFC(1),SGEFFT(1),EPEFFT(1)
C     COMMON/DIC/DIC11,DIC12,DIC21,DIC22,KFLAG
      COMMON/IDTY/ISGT,IMPT,ILY,INPT
      COMMON/ITERS/ITER
      DATA CONST/1.0E-6/
      DIMENSION NT(8)
C
C ********************************************************************
C ********************************************************************
C *
C *    THE COMMON STATEMENT (1 CARD):COMMON/DIC/DIC11.....TO BE
C *    REMOVED IF THIS SUBROUTINE IS USED IN BOSOR5
C *
C ********************************************************************
C ********************************************************************
C
C   I IS SEGMENT, J IS MESH POINT, K IS LAYER, KK IS INT.  PT.
C     CALCULATES NEW VALUES FOR PLASTIC STRAIN, YIELD
C     SURFACE WITH USE OF THREE-PARAMETER THEORY
      ISGT=I
      IMPT=J
      ILY=K
      INPT=KK
      ILOAD=0
      KPLAST=0
      U=XNU
      XLAMDA=ELAMDA
      XMU1=EMU1
      XMU2=EMU2
      SYCC=SYC
      SYTT1=SYT1
      SYTT2=SYT2
      IF(SYCC.LT.1.   E-08) SYCC=SGEFFC(2)
      IF(SYTT1.LT.1.   E-08) SYTT1=SGEFFT(2)
      IF(SYTT2.LT.1.   E-08) SYTT2=SGEFFT(2)
      ET = E
      ECOEF=E/(1.-U*U)
      C11 = 0.
      C12 = 0.
      C21 = 0.
      C22 = 0.
      EPOLD1=EPNEW1
      EPOLD2=EPNEW2
C     IF FYY<0.0 ,ELASTIC LOADING OR UNLOADING OCCURS
C
      NTOT=0
      ISUB=1
```

```
      NT(ISUB)=1
      DOT=1.
      KFLAG=1
      IZ=0
      FYY=FY(SIG1,SIG2,SYCC,SYTT1,SYTT2,IZ)
      IF(SIG1.GT.1.02*SYTT1.OR.SIG1.LT.-1.285*SYCC)GO TO 15
      IF(SIG2.GT.1.02*SYTT2.OR.SIG2.LT.-1.285*SYCC) GO TO 15
      IF (FYY) 220,15,15
C     NOW FIND FMU, THE FACTOR REQUIRED TO BRING STRESS STATE UP TO
C     THE YIELD SURFACE
   15 DS1 = SIG1 - SIG10
      DS2 = SIG2 - SIG20
      ILOAD=1
      IZ=0
      FYO=FY(SIG10,SIG20,SYCC,SYTT1,SYTT2,IZ)
      CALL DFDS(SIG10,SIG20,SYCC,SYTT1,SYTT2,B1,B2)
      DOT=DS1*B1+DS2*B2
      FMU=FFMU(SIG10,SIG20,SIG1,SIG2,SYCC,SYTT1,SYTT2,DOT)
      KFLAG=2
      SIG1Y = SIG10 + FMU*DS1
      SIG2Y = SIG20 + FMU*DS2
      IZ=0
      FYO=FY(SIG1Y,SIG2Y,SYCC,SYTT1,SYTT2,IZ)
C     THE ELASTIC STRAIN COMPONENTS AT THE YIELD SURFACE ARE . . .
      E1SEL = (SIG1Y - U*SIG2Y)/E
      E2SEL = (SIG2Y - U*SIG1Y)/E
C
C     DE1, DE2 ARE STRAIN INCREMENTS FOR CURRENT LOAD STEP. WE MUST
C              DETERMINE HOW MUCH IS ELASTIC AND HOW MUCH IS PLASTIC.
C
      DE1 =  E1ELAS - E1SEL
      DE2 = E2ELAS - E2SEL
C   BEGIN SUBINCREMENT METHOD
C   SAVE OLD VALUES
      SSYCC=SYCC
      SSYTT1=SYTT1
      SSYTT2=SYTT2
      SLAMDA=XLAMDA
      SMU1=XMU1
      SMU2=XMU2
      SS1=SIG1
      SS2=SIG2
      SS1Y=SIG1Y
      SS2Y=SIG2Y
      SEPNW1=EPNEW1
      SEPNW2=EPNEW2
      CALL DFDS(SIG1Y,SIG2Y,SYCC,SYTT1,SYTT2,B1,B2)
      CALL SUBDIV(SIG1Y,SIG2Y,SYCC,SYTT1,SYTT2,DE1,DE2,NNSUB,B1,
     1            B2,EX,EY,U,XLAMDA,XMU1,XMU2,SGEFFC,EPEFFC,
     2            SGEFFT,EPEFFT)
      DO 12 LN=1,8
   12 NT(LN)=0
      DO 190 ISUB=1,8
C   RESTORE OLD VALUES FOR A NEW SUBINCREMENTAL TRIAL
      NSUB=NNSUB*ISUB
```

```
      SYCC=SSYCC
      SYTT1=SSYTT1
      SYTT2=SSYTT2
      XLAMDA=SLAMDA
      XMU1=SMU1
      XMU2=SMU2
      SIG1=SS1
      SIG2=SS2
      SIG1Y=SS1Y
      SIG2Y=SS2Y
      EPNEW1=SEPNW1
      EPNEW2=SEPNW2
      ADDE1=0.0
      ADDE2=0.0
      C1=DE1/FLOAT(NSUB)
      C2=DE2/FLOAT(NSUB)
      NT(ISUB)=0
C
C  LOOP ON SUBINCREMENTS BEGINS HERE
C
   19 JSUB=0
20    JSUB=JSUB+1
      IF(JSUB.GT.NSUB) GOTO 175
      NTOT=NTOT+1
      NT(ISUB)=NT(ISUB)+1
      Q=1.0
      CC1=C1
      CC2=C2
      IF(ABS(ADDE1+CC1).GT.ABS(DE1)) CC1=DE1-ADDE1
      IF(ABS(ADDE2+CC2).GT.ABS(DE2)) CC2=DE2-ADDE2
      DSE1=EX*(CC1+U*CC2)
      DSE2=EY*(CC2+U*CC1)
      IZ=0
      FYO=FY(SIG1Y,SIG2Y,SYCC,SYTT1,SYTT2,IZ)
      IZ=0
      FYN=FY(SIG1Y+DSE1,SIG2Y+DSE2,SYCC,SYTT1,SYTT2,IZ)
C
C  REMOVE LOADING POINTS ON YIELD SURFACE
C
      KPLAST=1
      CALL DFDS(SIG1Y,SIG2Y,SYCC,SYTT1,SYTT2,B1,B2)
      DOT=DSE1*B1+DSE2*B2
      IF(FYN.GE.0.0.AND.FYO.GE.-0.01.AND.DOT.GE.0.0) GOTO 100
      FMU=1.0
C
C  REMOVE COMPLETELY ELASTIC RESPONSE
C
      IF(FYN.LE.0.0) GOTO 80
C
C  BRING STRESS POINT TO YIELD SURFACE
C
      FMU=FFMU(SIG1Y,SIG2Y,SIG1Y+DSE1,SIG2Y+DSE2,SYCC,SYTT1,SYTT2,DOT)
      ADDE1=ADDE1+FMU*CC1
      ADDE2=ADDE2+FMU*CC2
      CC1=CC1*(1.0-FMU)
```

```
      CC2=CC2*(1.0-FMU)
   80 SIG1Y=SIG1Y+FMU*DSE1
      SIG2Y=SIG2Y+FMU*DSE2
      IZ=0
      FYO=FY(SIG1Y,SIG2Y,SYCC,SYTT1,SYTT2,IZ)
      IF(FMU.NE.1.0) GOTO 100
      KPLAST=0
      WRITE(6,2895)ISUB,JSUB,FYO,I,J,K,KK
 2895 FORMAT(/,8X,'SUBINCR. IS ELASTIC  ISUB,JSUB,FYO =',2I3,E12.4,4I5)
      GOTO 150
C
C  PROCESS PLASTIC PORTION OF SUBINCREMENT STRAIN
C
  100 CALL DFDS(SIG1Y,SIG2Y,SYCC,SYTT1,SYTT2,B1,B2)
      ICON=0
      CALL DELTAS(SIG1Y,SIG2Y,SYCC,SYTT1,SYTT2,B1,B2,CC1,CC2,
     1          DS1,DS2,EX,EY,U,XLAMDA,XMU1,XMU2,SGEFFC,EPEFFC,
     2          SGEFFT,EPEFFT,DEBAR,DEL,DEM1,DEM2,DEP1,DEP2,
     3          DIC21,DIC22,DIC11,DIC12,Q,C11,C12,C21,C22,ICON,
     4          ALFA,BETA1,BETA2,DGG,DK1,DK2)
C
C
C     THE FRACTION Q LOCATES A BREAK IN THE STRESS-STRAIN CURVE
C     OR INDICATES AN INTERSECTION BETWEEN THE STRESS PATH AND AN
C     AXIS OF THE YIELD SURFACE
C
      XLAMDA=XLAMDA+DEL*Q
      XMU1=XMU1+DEM1*Q
      XMU2=XMU2+DEM2*Q
      SYCC=FG(XLAMDA,SGEFFC,EPEFFC)
      SYTT1=FK(XMU1,SGEFFT,EPEFFT)
      SYTT2=FK(XMU2,SGEFFT,EPEFFT)
      EPNEW1=EPNEW1+DEP1*Q
      EPNEW2=EPNEW2+DEP2*Q
      SIG1Y=SIG1Y+DS1*Q
      SIG2Y=SIG2Y+DS2*Q
C
C     BRING STRESSES TO YIELD SURFACE IF DRIFT OCCURS (ONLY FOR THE
C     CASE WHEN THE SUBINCREMENT HAS GONE THRU A PLASTIC ANALYSIS).THEN
C     ADJUST ELASTIC AND PLASTIC STRAINS,KEEPING TOTAL STRAINS CONSTANT
C
      IZ=0
      FYO=FY(SIG1Y,SIG2Y,SYCC,SYTT1,SYTT2,IZ)
      IF(ABS(FYO).LT.0.01) GOTO 150
      CALL DRIFT(SIG1Y,SIG2Y,SYCC,SYTT1,SYTT2,DFAC)
      SIG1Y=SIG1Y*DFAC
      SIG2Y=SIG2Y*DFAC
  150 SIG1 = SIG1Y
      SIG2 = SIG2Y
      ADDE1=ADDE1+CC1*Q
      ADDE2=ADDE2+CC2*Q
      IF(ABS(ADDE1).GE.ABS(DE1)+CONST.OR.ABS(ADDE2).GE.ABS(DE2)+CONST)
     *GOTO 175
      IF(Q.EQ.1.0) GOTO 20
      CALL DFDS(SIG1Y,SIG2Y,SYCC,SYTT1,SYTT2,B1,B2)
```

```
      RDE1=DE1-ADDE1
      RDE2=DE2-ADDE2
      CALL SUBDIV(SIG1Y,SIG2Y,SYCC,SYTT1,SYTT2,RDE1,RDE2,NEWSUB,
     1            B1,B2,EX,EY,U,XLAMDA,XMU1,XMU2,SGEFFC,EPEFFC,
     2            SGEFFT,EPEFFT)
      NSUB=NEWSUB*ISUB
      C1=RDE1/FLOAT(NSUB)
      C2=RDE2/FLOAT(NSUB)
      GOTO 19
  175 CONTINUE
C
C   CONVERGENCE CRITERION
      DSIG=SQRT((SIG1-S1OLD)**2+(SIG2-S2OLD)**2)
      IF(ISUB.EQ.1) DSIG=100000.
      ERR=DSIG/SQRT(SIG1*SIG1+SIG2*SIG2)
      TOLR=0.06
      IF(ERR.LT.TOLR.OR.DSIG.LT.5.0) GO TO 195
      IF(NTOT.GT.1900) GO TO 191
  185 S1OLD=SIG1
      S2OLD=SIG2
  190 CONTINUE
C
  191 WRITE(6,4567)EPS1,EPS2,NTOT,ERR,I,J,K,KK,NNSUB,NT(ISUB)
 4567 FORMAT(1H ,'WARNING: SUBINCREMENT PROCEDURE FAILED TO CONVERGE.
     1 EPS1=',E12.4,'  EPS2=',E12.4,'  NTOT=',I4,/
     12X'REL. ERROR IN LAST TWO SUBINCR. TRIALS:',E10.3,'  SEG.=',I3,
     2'  MESH PT.=',I3,'   LAYER=',I3,'   INT.PT.=',I3,'  NNSUB=',I3,
     3' NT(ISUB)=',I4)
  195 CONTINUE
      IF(KPLAST.EQ.1) GO TO 208
      C11=0.
      C12=0.
      C21=0.
      C22=0.
      GO TO 220
C
C   FORM C AND E MATRICES. SEE ALSO SUBROUTINE DELTAS
C
  208 CALL DFDS(SIG1Y,SIG2Y,SYCC,SYTT1,SYTT2,B1,B2)
      ICON=1
      CALL DELTAS(SIG1Y,SIG2Y,SYCC,SYTT1,SYTT2,B1,B2,CC1,CC2,
     1    DS1,DS2,EX,EY,U,XLAMDA,XMU1,XMU2,SGEFFC,
     2         EPEFFC,SGEFFT,EPEFFT,DEBAR,DEL,DEM1,DEM2,DEP1,DEP2,
     3         DIC21,DIC22,DIC11,DIC12,Q,C11,C12,C21,C22,ICON,
     4         ALFA,BETA1,BETA2,DGG,DK1,DK2)
      EE1=(SIG1Y-U*SIG2Y)/E
      EE2=(SIG2Y-U*SIG1Y)/E
      EPOLD1=EPNEW1
      EPOLD2=EPNEW2
      EPNEW1=EPS1-EE1
      EPNEW2=EPS2-EE2
  220 CONTINUE
      IF(ITER.NE.1) RETURN
      IF(SIG1.EQ.0..AND.SIG2.EQ.0.) GO TO 229
      SYCK=.001*SYCC
```

```
      SYT1K=.001*SYTT1
      SYT2K=.001*SYTT2
      SIG1K=SIG1*.001
      SIG2K=SIG2*.001
      IF(KK.EQ.1) WRITE(6,1214)
 1214 FORMAT(1H )
      WRITE(6,1212)I,J,K,Z, SYCK,SYT1K,SIG1K,SIG2K,
     1       EPS1,EPNEW1,EPS2,EPNEW2,SYT2K
 1212 FORMAT(2I4,I5,F7.3,9E11.4)
      WRITE(6,1213)XLAMDA,XMU1,XMU2,EPOLD1,EPOLD2,ISUB,NT(ISUB),NTOT
 1213 FORMAT(6X,'LAMDA MU1 MU2 EP1 EP2 ISUB NT NTOT ='
     1,4E11.4,11X,E11.4,3X,3I5)
  229 IF(ILOAD.EQ.0) RETURN
C
C     NEW YIELD STRESS
      SYC=SYCC
      SYT1=SYTT1
      SYT2=SYTT2
C
C     NEW EFFECTIVE PLASTIC STRAIN
      ELAMDA=XLAMDA
      EMU1=XMU1
      EMU2=XMU2
C
C
C     NEW PLASTIC STRAIN COMPONENTS
      EP1 = EPNEW1
      EP2 = EPNEW2
      RETURN
      END
```

```
C
C
C  ****************************************************
      FUNCTION FY(SIG1,SIG2,SYC,SYT1,SYT2,IZ0)
C  ****************************************************
C  FY=0 IS YIELDING LOCUS FOR CONCRETE
      IF(IZ0.EQ.0) IZ0=IZONE(SIG1,SIG2,SYC,SYT1,SYT2)
C
      GO TO (60,80,80,70,70,70,40,40),IZ0
C
C
C     ***** TT FOLLOWS **********************************
   60 X1=SIG1/SYT1
      X2=SIG2/SYT2
      IF(X1.GT.0.95.AND.X2.GT.1.02) GO TO 400
      IF(X1.GT.1.02.AND.X2.GT.0.95) GO TO 400
      S=1.0+0.0098*X1*X2
      A=-0.99*X1+S
      B=-0.99*X2+S
      C=(1.-0.0001*X1*X2)**2
      FY=SQRT(SYT1*SYT2)*(0.01-A*B/C)
      RETURN
  400 FY=100.
      RETURN
C
C     ***** TC FOLLOWS ***** 4TH QUAD. ****************
   40 X2=SIG2/SYC
      IF(IZ0.EQ.7) GO TO 47
      FY=SIG1+SYT1*(0.4*X2**2-1.0)
      RETURN
47    FY=SIG1+SYT1*((2.8*X2+2.4)*X2-0.4)
      RETURN
C
C     ***** CC FOLLOWS **********************************
C     THE FY=2.5*SYC IS AN APPROXIMATE BUT REALISTIC VALUE TO INDICATE
C     A PLASTIC OR ELASTIC ANALYSIS (FOR TESTS IN FLOW3-SUBROUTINE)
   70 X1=SIG1/SYC
      X2=SIG2/SYC
      I=IZ0-3
      GO TO(73,72,71),I
   72 FY=SYC*SQRT(X1**2+X2**2-1.23*X1*X2)-SYC
      RETURN
   73 FY=SYC*(((0.6314307*X2+1.46150732)*X2+1.1)*X2-1.0)-SIG1
      IF(X1.LT.-3.5.AND.FY.LT.0.) FY=2.5*SYC
      RETURN
   71 FY=SYC*(((0.6314307*X1+1.46150732)*X1+1.1)*X1-1.0)-SIG2
      IF(X2.LT.-3.5.AND.FY.LT.0.) FY=2.5*SYC
      RETURN
C
C     ***** TC FOLLOWS ***** 2ND QUAD. ***************
   80 X1=SIG1/SYC
      IF(IZ0.EQ.3) GO TO 88
      FY=SIG2+SYT2*(0.4*X1**2-1.0)
      RETURN
88    FY=SIG2+SYT2*((2.8*X1+2.4)*X1-0.4)
```

```
      RETURN
      END
```

```
C
C
C  ************************************************************
      FUNCTION IZONE(S1,S2,SYC,SYT1,SYT2)
C ************************************************************
C  THIS SUBROUTINE DETERMINES WHICH ZONE OF A FORM 4 YIELD
C  FUNCTION IS APPLICABLE TO A STRESS POINT
C
      IF(S1) 10,30,30
10    IF(S2) 70,70,80
30    IF(S2) 40,60,60
C
C ***  TT ZONE  (1ST QUADRANT) ***
60    IZONE=1
      RETURN
C
C ***  TC ZONE  (4TH QUADRANT) ***
   40 X2=S2/SYC
      X1=S1/SYT1
      IF(X1.GE.-2.0*X2) GOTO 48
47    IZONE=7
      RETURN
48    IZONE=8
      RETURN
C
C  ***  CC ZONE  (3RD QUADRANT) ****
70    X1=S1/SYC
      X2=S2/SYC
      IF(ABS(X2).LT.1.0E-10)  GO TO 73
      R=X1/X2
      IF(R.LT.0.63095074)  GO TO 71
      IF(R.GT.1.58490979)  GO TO 73
      IZONE=5
      RETURN
71    IZONE=6
      RETURN
73    IZONE=4
      RETURN
C
C ***  CT ZONE  (2ND QUADRANT) ***
80    X1=S1/SYC
      X2=S2/SYT2
      IF(X2.GE.-2.0*X1) GOTO 88
87    IZONE=3
      RETURN
88    IZONE=2
      RETURN
C
      END
```

```
C
C  ********************************************************
      SUBROUTINE PARA(S1,S2,SYC,SYT1,SYT2,ALFA,BET1,BET2,B1,B2)
C  ********************************************************
C  THIS ROUTINE COMPUTES THE THREE PARAMETERS ALFA, BETA1,
C  BETA2, WHICH ARE  THE FRACTIONS OF PARTICIPATION
C  IN TOTAL PLASTIC STRAIN DEBAR
C
      IF(S1)  10,100,50
   10 IF(S2) 20,20,30
C
C     ****** CC FOLLOWS ******
   20 ALFA=1.
      BET1=0.
      BET2=0.
      RETURN
C
C     ****** TC FOLLOWS (2ND QUAD.)******
   30 ALFA=-S1/SYC
      IF(ALFA.GT.0.999) ALFA=0.999
      BET1=0.
      BET2=1.-ALFA
      RETURN
   50 IF(S2) 60,70,70
C
C     ****** TC FOLLOWS (4TH QUAD.)******
   60 ALFA=-S2/SYC
      IF(ALFA.GT.0.999) ALFA=0.999
      BET1=1.-ALFA
      BET2=0.
      RETURN
C
C     ****** TT FOLLOWS ******
   70 ALFA=0.
      DENOM=B1*B1+B2*B2
      BET1=B1*B1/DENOM
      BET2=B2*B2/DENOM
      RETURN
  100 IF(S2) 110,110,120
C
C     ****** UNIAXIAL COMP. FOLLOWS ******
  110 ALFA=1.
      BET1=0.
      BET2=0.
      RETURN
C
C     ****** UNIAXIAL TENS. FOLLOWS ******
  120 ALFA=0.
      BET1=0.
      BET2=1.
      RETURN
      END
```

```
C
C  ****************************************************
      SUBROUTINE SAMEL(ELAMDA,DEL,SGEFFC,EPEFFC,QL)
C  ****************************************************
C   FINDS WHETHER ELAMDA  AND ELAMDA+DEL BELONG TO THE
C   SAME REGION OF CONST. EQS.
      DIMENSION SGEFFC(1),EPEFFC(1)
      COMMON/IDTY/ISGT,IMPT,ILY,INPT
      QL=1.0
      IF(DEL.EQ.0.)RETURN
C     EUP0=EQUIVALENT UNIAXIAL PLASTIC STRAIN CORRESPONDING
C     TO PREVIOUSLY CONVERGED LOAD STEP
      EUP0=0.67267279*ELAMDA
      E=SGEFFC(2)/EPEFFC(2)
      DO 10 I=2,10
      J=I
      IF(EUP0.LT.EPEFFC(I)-SGEFFC(I)/E) GO TO 20
   10 CONTINUE
      WRITE(6,1200)EUP0,ISGT,IMPT,ILY,INPT
 1200 FORMAT(1H0,'PLASTIC STRAIN EXEEDS RANGE IN SAMEL',E12.4,4I5)
      STOP
   20 ET=(SGEFFC(J)-SGEFFC(J-1))/(EPEFFC(J)-EPEFFC(J-1))
      EET=E/(E-ET)
C     DEU=EQUIVALENT INCREMENT OF TOTAL UNIAXIAL STRAIN
C     FOR A GIVEN DEL
C     EU0=EQUIVALENT TOTAL UNIAXIAL STRAIN CORRESPONDING TO
C     THE PREVIUOLY CONVERGED LOAD STEP
C
      DEU=0.67267279*EET*DEL
      EUPA=EPEFFC(J-1)-SGEFFC(J-1)/E
      EU0=EPEFFC(J-1)+(EUP0-EUPA)*EET
C     CALCULATE THE FRACTION OF SUBINCREMENT TO GET TO BREAK
C
      DELEU=EPEFFC(J)-EU0
      IF(DELEU.GE.DEU) RETURN
      QL=DELEU/DEU
      IF(QL.GT.1.0) QL=1.0
      IF(QL.LE.0.0) GO TO 999
C     WRITE(6,1000)J,ELAMDA,DEL,E
C     WRITE(6,1100)EUP0,EUPA,EU0,DELEU,DEU
 1000 FORMAT(I3,5E20.8)
 1100 FORMAT(6E20.8)
      RETURN
  999 WRITE(6,1300)QL
 1300 FORMAT(/8X,'BREAK FOUND WITH FACTOR OF:',F8.4,'IN SAMEM')
      END
```

```
C  ******************************************************
      SUBROUTINE SAMEM(EMU,DEM,SGEFFT,EPEFFT,QM)
C  ******************************************************
C   FINDS WHETHER EMU  AND EMU+DEM BELONG TO THE
C  SAME REGION OF CONST. EQS.
      DIMENSION SGEFFT(1),EPEFFT(1)
      COMMON/IDTY/ISGT,IMPT,ILY,INPT
      QM=1.
      E1P=EMU
      E1PD=(EMU+DEM)
      IF(E1PD.LE.0.) RETURN
      E=SGEFFT(2)/EPEFFT(2)
      DO 10 I=2,10
      J=I
      IF(E1P.LT.EPEFFT(I)-SGEFFT(I)/E) GO TO 20
   10 CONTINUE
   20 DO 15 I=2,10
      K=I
      IF(E1PD.LT.EPEFFT(I)-SGEFFT(I)/E) GO TO 50
   15 CONTINUE
      WRITE(6,1000)EMU,DEM,ISGT,IMPT,ILY,INPT
 1000 FORMAT(1H0,'ERROR IN SAMEM',2E12.4,4I5)
      STOP
   50 IF(J.EQ.K) RETURN
      EPSPJ=EPEFFT(J)-SGEFFT(J)/E
      QM=(EPSPJ-E1P)/DEM
      IF(QM.GT.1.) QM=1.
      IF(QM.LT.0.0) GO TO 999
      RETURN
  999 WRITE(6,1100)QM
 1100 FORMAT (/8X,'BREAK FOUND WITH FACTOR OF:',F8.4,'IN SAMEM')
      END
```

```
C
C
C  ************************************************************
      SUBROUTINE SEARCH(SGEFFC,EPEFFC,SGEFFT,EPEFFT,XLAMDA,
     1  XMU1,XMU2,DEL,DEM1,DEM2,Q,IDEN)
C  ************************************************************
C  THIS ROUTINE SEARCH FOR PLASTIC DEFORMATION,TO LOACATE THE
C  QUADRANT, THEN SEARCH FOR DISCONTINUITY IN THE EFFECTIVE
C  STRESS STRAIN CURVE, AND COMPUTES THE FACTOR (FAC) NEEDED
C  TO SHIFT THE PLASTIC STRAIN TO THE DISCONTINUITY POINT.
C
      DIMENSION SGEFFC(1),EPEFFC(1),SGEFFT(1),EPEFFT(1)
C
      IDEN=1
      Q1=1.0
      Q2=1.0
      IF(DEM1*DEM1+DEM2*DEM2.EQ.0.) GO TO 70
      IF(DEL.EQ.0.) GO TO 60
      IF(DEM1.EQ.0.) GO TO 80
      GO TO 40
   60 CALL SAMEM(XMU1,DEM1,SGEFFT,EPEFFT,Q1)
      CALL SAMEM(XMU2,DEM2,SGEFFT,EPEFFT,Q2)
      Q=AMIN1(Q1,Q2)
      IF(Q.EQ.1.0) RETURN
      IDEN=3
      IF(Q2.LT.Q1) IDEN=4
      RETURN
C
   70 CALL SAMEL(XLAMDA,DEL,SGEFFC,EPEFFC,Q1)
      Q=AMIN1(Q1,Q2)
      IF(Q.NE.1.0) IDEN=2
      RETURN
C
   80 CALL SAMEL(XLAMDA,DEL,SGEFFC,EPEFFC,Q1)
      CALL SAMEM(XMU2,DEM2,SGEFFT,EPEFFT,Q2)
      Q=AMIN1(Q1,Q2)
      IF(Q.EQ.1.0) RETURN
      IDEN=2
      IF(Q2.LT.Q1) IDEN=4
      RETURN
C
   40 CALL SAMEL(XLAMDA,DEL,SGEFFC,EPEFFC,Q1)
      CALL SAMEM(XMU1,DEM1,SGEFFT,EPEFFT,Q2)
      Q=AMIN1(Q1,Q2)
      IF(Q.EQ.1.0) RETURN
      IDEN=2
      IF(Q2.LT.Q1) IDEN=3
      RETURN
      END
```

```
C
C  ********************************************************
      SUBROUTINE SUBDIV(SIG1,SIG2,SYC,SYT1,SYT2,DE1,DE2,NOSUB,
     1                  B1,B2,EX,EY,U,ELAMDA,EMU1,EMU2,SGEFFC,
     2                  EPEFFC,SGEFFT,EPEFFT)
C  ********************************************************
      DIMENSION SGEFFT(1),SGEFFC(1),EPEFFT(1),EPEFFC(1)
      DATA C/1.0E-6/
      ICON=1
      CALL DELTAS(SIG1,SIG2,SYC,SYT1,SYT2,B1,B2,DE1,DE2,DS1,DS2,
     1            EX,EY,U,ELAMDA+C,EMU1+C,EMU2+C,SGEFFC,EPEFFC,
     2            SGEFFT,EPEFFT,DEBAR,DEL,DEM1,DEM2,DEP1,DEP2,
     3            DIC21,DIC22,DIC11,DIC12,Q,C11,C12,C21,
     4            C22,ICON,ALFA,BETA1,BETA2,DGG,DK1,DK2)
      DEP1=C11*DE1+C12*DE2
      DEP2=C21*DE1+C22*DE2
      DEPB=SQRT(DEP1**2+DEP2**2)
      NOSUB=2
      IF(DEPB.EQ.0.0) RETURN
C
      DIC11=EX*(1.-C11)-U*EX*C21
      DIC12=-EX*C12+U*EX*(1.-C22)
      DIC21=U*EY*(1.-C11)-EY*C21
      DIC22=-U*EY*C12+EY*(1.-C22)
      DES1=DIC11*DE1+DIC12*DE2
      DES2=DIC21*DE1+DIC22*DE2
      DENOM=SQRT((DES1*DES1+DES2*DES2)*(B1*B1+B2*B2))
      COST=4.-4.*(DES1*B1+DES2*B2)/DENOM
      FACT=AMAX1(1.,COST)
      DIR1=ABS(DES1*2.0/SYC)
      IF((SIG1+DES1).GT.0.0) DIR1=ABS(DES1/SYT1)
      DIR2=ABS(DES2*2.0/SYC)
      IF((SIG2+DES2).GT.0.0) DIR2=ABS(DES2/SYT2)
      KSUB=AMAX1(DIR1,DIR2)*FACT
C
      ALFD=ABS(ALFA*DGG)
      BETA1D=ABS(BETA1*DK1)
      BETA2D=ABS(BETA2*DK2)
      DEPC=1.0E6
      DEPT1=1.0E6
      DEPT2=1.0E6
      IF(ALFD.NE.0.0) DEPC=0.1*SYC/ALFD
      IF(BETA1D.NE.0.0) DEPT1=0.1*SYT1/BETA1D
      IF(BETA2D.NE.0.0) DEPT2=0.1*SYT2/BETA2D
      DEEC=1.0E6
      DEET1=1.0E6
      DEET2=1.0E6
      IF(ALFD.NE.0.0) DEEC=EPEFFC(2)*0.5
      IF(BETA1D.NE.0.0) DEET1=EPEFFT(2)*2.0
      IF(BETA2D.NE.0.0) DEET2=EPEFFT(2)*2.0
C
      NSUB=DEPB/AMIN1(DEPC,DEPT1,DEPT2,DEEC,DEET1,DEET2)
      NOSUB=MAX0(KSUB,NSUB)
      IF(NOSUB.GT.4) GO TO 16
      NOSUB=4
```

```
      RETURN
   16 IF(SIG1.LT.0.0.AND.SIG2.LT.0.0) GO TO 15
      IF(NOSUB.GT.200) GO TO 17
      NOSUB=FLOAT(NOSUB)*4./3.-FLOAT(NOSUB)*FLOAT(NOSUB)/300.
      RETURN
   17 NOSUB=133
      RETURN
   15 IF(NOSUB.GT.100) GO TO 18
      NOSUB=FLOAT(NOSUB)*4./3.-FLOAT(NOSUB)*FLOAT(NOSUB)/150.
      RETURN
   18 NOSUB=67
      RETURN
C
C 999 WRITE(6,1000)
C1000 FORMAT('  **  SUBROUTINE SUBDIV INDICATES THAT MORE',
C    1       ' THAT 50 SUBINCREMENTS ARE REQUIRED ')
C     STOP
      END
```